



<https://theses.gla.ac.uk/>

Theses Digitisation:

<https://www.gla.ac.uk/myglasgow/research/enlighten/theses/digitisation/>

This is a digitised version of the original print thesis.

Copyright and moral rights for this work are retained by the author

A copy can be downloaded for personal non-commercial research or study,
without prior permission or charge

This work cannot be reproduced or quoted extensively from without first
obtaining permission in writing from the author

The content must not be changed in any way or sold commercially in any
format or medium without the formal permission of the author

When referring to this work, full bibliographic details including the author,
title, awarding institution and date of the thesis must be given

Enlighten: Theses

<https://theses.gla.ac.uk/>
research-enlighten@glasgow.ac.uk

**SEISMIC VELOCITIES AND DEPTH CONVERSION ACROSS
THE INTISAR "D" FIELD, SIRTE BASIN, LIBYA**

BY

YAHYA AHMED ALI SALEM

**B.Sc. (1983) - Faculty of Petroleum and
Mining Engineering - Tripoli**

Thesis submitted for the degree of Master of Science at the
Department of Geology and Applied Geology, University of Glasgow.

March 1991

ProQuest Number: 11007977

All rights reserved

INFORMATION TO ALL USERS

The quality of this reproduction is dependent upon the quality of the copy submitted.

In the unlikely event that the author did not send a complete manuscript and there are missing pages, these will be noted. Also, if material had to be removed, a note will indicate the deletion.



ProQuest 11007977

Published by ProQuest LLC (2018). Copyright of the Dissertation is held by the Author.

All rights reserved.

This work is protected against unauthorized copying under Title 17, United States Code
Microform Edition © ProQuest LLC.

ProQuest LLC.
789 East Eisenhower Parkway
P.O. Box 1346
Ann Arbor, MI 48106 – 1346

Dedicated to my parents

Acknowledgements

I am indebted to Professor **B. E. Leake**, the head of the department, for admitting me to the department and allowing me the use of the facilities during this research.

I would like to express my thanks to my supervisor Professor **D. K. Smythe**, whose advice and assistance has been available to me throughout the research work, and with his permission this work has been carried out.

My thanks go to Dr. **C. J. R. Braithwaite**, for his careful critical reading of the geological chapter, pointing out some errors, and for giving me new information.

I would like to thank all the geophysical staff in the department who have helped me in different ways. Special thanks go to Mr. **Robert T. Cumberland** for his help on the computer. Mr. **D. McLean** is thanked for his great photographic work to help me to produce the many figures in the thesis.

Najim Ben-Ayad, **Mohamed Boulfoul** and **Fawzi Ahmed** are all thanked for discussions regarding this project at various times. Special thanks go to the geophysicist **M. A. Swedan** in Occidental company of Libya and his colleagues for their help in collecting the data.

Finally, I would like also to express heartfelt appreciation to Dr. **Mustafa Sola** for his help and his encouragement of me in different ways, also to the Petroleum Research Centre and National Oil Corporation, for their financial support and data collection.

II

Contents

Chapter 1 Introduction

1.1 Introduction	2
1.2 Description of Data	9
1.3 The aim of the study	13

Chapter 2 Regional setting and stratigraphy

2.1 Introduction	15
2.2 Regional setting	17
2.2.1 Sirte Basin	17
2.2.2 Stratigraphical succession of the Sirte Basin	23
2.2.3 Concession 103 area.....	26
2.2.4 Geology of the Intisar "D" Field	27
2.3 Stratigraphy of Intisar "D" Field	34
2.4 Summary of Geology	37

Chapter 3 Seismic stratigraphic interpretation

3.1 Well to seismic tie	40
3.1.1 Synthetic seismogram	40
3.1.2 Well to seismic tie	46
3.2 Event identification and selection	47
3.2.1 Preliminary interpretation	52
3.3 Interpretation and mapping	57
3.3.1 Seismic sections	57
3.3.2 Seismic facies analysis	69
3.3.3 Mapping reflection horizons	78
3.3.4 Maps construction	78
(i) Time contour maps	78
(ii) Depth contour maps	86
(iii) Average velocity and depth maps of the top of Kheir Formation	93
3.4 Summary of seismic interpretation	96

Chapter 4 Velocity interpretation

4.1	Velocity interpretation	98
4.1.1	Well velocity survey	101
4.1.2	Seismic velocities	107
4.2	Seismic velocity analysis and mapping	111
4.2.1	Why processing seismic velocities are unsuitable for depth conversion	111
4.2.2	Velocity mapping	121
	(i) Average velocity maps	121
	(ii) Interval velocity maps	126
	(iii) The difference between the well-velocity survey and seismic velocity maps	133
4.3	Summary of velocity interpretation	138

Chapter 5 Data Processing

5.1	Introduction	140
5.1.1	Background	140
5.1.2	Method	140
5.2	Processing procedures	142
5.2.1	Data background	142
5.2.2	Seismic Processing sequence	145
5.3	Pre-stack processing	151
5.3.1	Static and residual static corrections	151
5.3.2	Deconvolution before stack	155
5.3.3	Velocity analysis	156
5.3.4	Normal moveout correction	167
5.3.5	Stacking	171
5.4	Post-stack processing	173
5.4.1	Deconvolution after stack	173
5.4.2	Filtering	175
5.5	Results	178
5.6	Migration	182
5.7	Summary of processing	187

Chapter 6 Conclusions

6.1	Conclusions	190
6.2	Suggestions for further work	194

IV

References	195
Appendix	201

Summary

The Intisar "D" field is one of the oldest fields in the Sirte Basin (Libya), It was discovered by Occidental company in 1966. In 1986 a new 2-D seismic survey was carried out to define the field more accurately, as well as 3-D work being done in the eastern part of the field. This study is concerned mainly with the recent seismic lines and well logs, to produce a new interpretation. The field is situated on the southeast of the Concession 103 area, which lies to the southeast of the Agedabya trough, with the Rakk high to the east and the Zelten platform somewhat farther to the west.

The geology of the Intisar "D" field and the Concession 103 was outlined previously by two papers published. more than ten years ago. One was a study of the geology and the depositional history of Intisar "A" field in the northern part of the Concession, while the second paper described the geology and depositional history of Intisar "D" field, together with the exploration techniques and the production system used.

The main reservoir is an Upper Palaeocene pinnacle reef containing more than one billion bbl (160 million cu m) of recoverable oil.

The reef grew at the same time as the Upper-Sabil platform carbonates were being deposited, At the end of reef growth time near the end of the Palaeocene time, the reefs stopped growing with the introduction of the lower Kheir shales.

Seven seismic lines are available, U-14, U-25, U-51, U-53, U-54, U-6, and U-9, and nineteen wells in the field selected for different purposes lithological information, correlation, and velocity information.

VI

The main aim of this study, new seismic interpretation of important horizons, and velocity interpretation, with a discussion of why the seismic velocities in the area are inaccurate, and the reprocessing part of line U-14.

The tying of well (D1/103) and seismic sections (U14, U25, U51, U53, and U54) are reasonably closely particularly at the Lower Eocene and Upper Palaeocene levels. The other horizons match with small mis-ties approximately (+30 ms). The interpreted horizons are the Upper-Sabil (Upper Palaeocene), Kheir (Upper Palaeocene - Lower Eocene), Gir (top of Lower Eocene), and El-giza (Middle Eocene).

The seismic characteristics indicate strongly contrasting acoustic impedance mostly between the sequences of shales from one side and the limestone from the other.

The reprocessing of part of line U-14 has resulted in a better defined seismic section, displayed both in migrated time and in depth.

VII

List of Figures

Chapter 1

- Fig. 1.1 Geographical location map of the area studied Intisar "D" Field, within the Sirte Basin, Libya. 3
- Fig. 1.2 Line location map showing seismic lines and wells available for the present study. 5
- Fig. 1.3 Field performance curves for Intisar "D" field. (from *Brady, et al.*, 1980). 6

Chapter 2

- Fig. 2.1 Geological map of Libya, simplified from (*Conant and Goudarzi*, 1964). 15
- Fig. 2.2 Tectonic elements map of Sirte Basin, Libya (after *Mouzughi & Taleb*, 1980). 17
- Fig 2.3 Stratigraphic cross-section A-B in Sirte Basin, located on Figure 3.2, datum on top of Upper Cretaceous (Kalash). Lower Palaeocene carbonates wedge out over troughs, independent of location of earlier highs (after *Brady, et al.*, 1980). 19
- Fig. 2.4 Generalized stratigraphic column, Sirte Basin, Libya. (after *Roberts*, 1968). 23
- Fig. 2.5 NW-SE cross-section A-A, in Intisar "D" field. Show the correlations possible within the reef by use of the gamma curves on the left, compensated formation density on the right. Datum on (-2400 m) subsea. 27
- Fig. 2.6 SW-NE cross-section B-B, in Intisar "D" field. Show the correlations possible within the reef by use of the gamma curves on the left, compensated formation density on the right. Datum on (-2400 m) subsea. 28
- Fig. 2.7 W-E cross-section C-C, in Intisar "D" field. Show the correlations possible within the reef by use of the gamma curves on the left, compensated formation density on the right. Datum on (-2400 m) subsea. 29

VIII

Fig. 2.8	Stratigraphy of the East Sirte Basin. Dotted lines are facies variations. Heavy lines are generalized time lines, (after <i>Brady et al.</i> , 1980).	34
----------	---	----

Chapter 3

Fig. 3.1	Synthetic Seismogram displays derived from density and interval velocity logs well D1-103.	42
Fig. 3.2	Acoustic impedance/ Synthetic / Seismic correlation between line U-14 and Well D1-103.	44
Fig. 3.3	Synthetic seismogram steps.	45
Fig. 3.4	Stratigraphic section and main seismic reflectors.	49
Fig. 3.5	Continuous velocity log (CVL) with depth in metres below reference level and the integrated total travel time in milliseconds below datum, (well D1/103).	53
Fig. 3.6	Interpretation of the results : relations of time with depth, average velocity with time, and interval velocity with depth (D1/103).	55
Fig. 3.7	Location map showing seismic sections reproduced (as figures).	58
Fig. 3.8	(a) Seismic line U-14, showing location of wells D1/103, D6/103, D7/103 and D21/103; SPs 110-650.	59
Fig. 3.8	(b) Seismic line U-25, showing location of wells D1/103 and D16/103; SPs 110-610.	60
Fig. 3.8	(c) Seismic line U-51, showing location of wells D1/103, D23/103 and D33/103; SPs 300-720.	61
Fig. 3.8	(d) Seismic line U-53, showing location of wells D1/103 and D5/103; SPs 310-690.	62
Fig. 3.8	(e) Seismic line U-54, showing location of well D1/103; SPs 340-660.	63
Fig. 3.8	(f) Seismic line U-6; SPs 110-650.	64
Fig. 3.8	(g) Seismic line U-9; SPs 110-450.	65
Fig. 3.9	Correlation of seismic horizons (line U-51) and well stratigraphy (D1/103).	70
Fig. 3.10	Diagram showing the geological model, reflection coefficient, and seismic response (normal polarity).	76
Fig. 3.11	Two-way time to Middle Eocene (El-giza) horizon.	80
Fig. 3.12	Two-way time to Lower Eocene (Gir) horizon.	82

IX

Fig. 3.13	Two-way time to Upper Palaeocene (Kheir) horizon.	83
Fig. 3.14	Two-way time to Upper Palaeocene (Upper-Sabil) horizon.	85
Fig. 3.15	El-giza depth contour map.	88
Fig. 3.16	Gir depth contour map.	89
Fig. 3.17	Kheir depth contour map.	91
Fig. 3.18	Upper-Sabil depth contour map.	92
Fig. 3.19	Top Kheir average velocity map	94
Fig. 3.20	Kheir depth contour map	95

Chapter 4

Fig. 4.1	Location map of velocity analyses.	100
Fig. 4.2	Well-velocity survey in well (D1/103).	102
Fig. 4.3	Well correlation showing the lateral variation in interval velocity from sonic logs were generated in D2, D1, and D5/103.	105
Fig. 4.4	Well correlation showing the lateral variation in interval velocity from sonic logs were generated in D16, D1, and D12/103.	106
Fig. 4.5	Interpolated stacking velocity. Velocity analyses are made at locations indicated by V at top (line-U14).	112
Fig. 4.6	Interpolated stacking velocity. Velocity analyses are made at locations indicated by V at top (line-U25).	113
Fig. 4.7	Comparison of interval velocities obtained from sonic log (D1/103) and Dix formula shot point 501 in line U-14.	117
Fig. 4.8	Comparison of interval velocities obtained from sonic log (D1/103) and Dix formula shot point 415 in line U-25.	118
Fig. 4.9	Comparison of interval velocities obtained from sonic log (D1/103) and new seismic velocities in CDP 310 (V.P. 503) in line U-14	119
Fig. 4.9	Top El-giza average velocity map.	123
Fig. 4.10	Top Gir average velocity map.	124
Fig. 4.11	Top Kheir average velocity map.	125
Fig. 4.12	Top Upper-Sabil average velocity map.	127
Fig. 4.13	El-Giza to Gir interval velocity map.	129

Fig. 4.14	Gir to Kheir interval velocity map.	130
Fig. 4.15	Kheir to Upper-Sabil interval velocity map.	132
Fig. 4.16	The difference between the seismic interval velocity and the well velocity survey (D1/103) in the El-giza to Gir interval.	135
Fig. 4.17	The difference between the seismic interval velocity and the well velocity survey (D1/103) in the Gir to Kheir interval.	136
Fig. 4.18	The difference between the seismic interval velocity and the well velocity survey (D1/103) in the Kheir to Upper-Sabil interval.	137

Chapter 5

Fig. 5.1	Receiver array, source array, and the source- receiver configuration for line U-14.	143
Fig. 5.2	The preliminary seismic processing sequence.	145
Fig. 5.3	Shot files equivalent to the selected CMP gathers which used for velocity analysis.	146
Fig. 5.4	Selected CMP gathers corresponding to the same data as in Figure 5.3.	148
Fig. 5.5	Raw stack section using the well velocity survey.	149
Fig. 5.6	Seismic data processing flow-chart.	150
Fig. 5.7	A CMP stack with field static applied.	153
Fig. 5.8	The same section in figure (5.7) after residual statics corrections.	154
Fig. 5.9	(a) Velocity spectra derived from the CMP (160) gathers in Figure 5.4. The display mode is contour.	158
Fig. 5.9	(b) Velocity spectra derived from the CMP (210) gathers in Figure 5.4. The display mode is contour.	159
Fig. 5.9	(c) Velocity spectra derived from the CMP (260) gathers in Figure 5.4. The display mode is contour.	160
Fig. 5.9	(d) Velocity spectra derived from the CMP (310) gathers in Figure 5.4. The display mode is contour.	161
Fig. 5.9	(e) Velocity spectra derived from the CMP (360) gathers in Figure 5.4. The display mode is contour.	162
Fig. 5.9	(f) Velocity spectra derived from the CMP (380) gathers in Figure 5.4. The display mode is contour.	163

XI

Fig. 5.9	(g) Velocity spectra derived from the CMP (450) gathers in Figure 5.4. The display mode is contour.	164
Fig. 5.9	(h) Velocity spectra derived from the CMP (520) gathers in Figure 5.4. The display mode is contour.	165
Fig. 5.10	Definition of Normal move-out (NMO).	168
Fig. 5.11	(a) The CDP gathers of figure 5.4 after NMO correction using the velocity picks derived from the spectra in Figure 5.7.	169
Fig. 5.11	(b) The CMP gathers of Figure 5.9 (a) after muting the stretched zones (the very low frequency zones).	170
Fig. 5.12	Stack section without deconvolution and without filtering.	172
Fig. 5.13	Effect of predictive deconvolution on the stacked data.	174
Fig. 5.14	Frequency analysis in the CMP 309.	176
Fig. 5.15	A sequence of bandpass filter tests. The dataset has been stacked. Low and high frequency cut-offs in Hz are annotated with respective db/octave slopes in parentheses.	177
Fig. 5.16	(a) The original seismic section, processed by western Geophysical Company in 1986.	179
Fig. 5.16	(b) Reprocessed seismic section (final stack section, variable-area and wiggle).	180
Fig. 5.16	(c) The same seismic section in as in Figure 5.16(a) with variable-area display only.	181
Fig. 5.17	(a) Final stack section shown in Fig. (5.16(b)) after Fk migration using velocity lower 10% than the stacking velocity.	183
Fig. 5.17	(b) Final stack section shown in Fig. (5.16(b)) after Fk migration using the stacking velocity.	184
Fig. 5.17	(c) Final stack section shown in Fig. (5.16(b)) after Fk migration using velocity higher 10% than the stacking velocity.	185
Fig. 5.18	Final stack section shown in Fig. (5.16(b)) after depth migration using the velocity shown in Figure 5.18.	186
Fig. 5.19	The summary of seismic processing flow-chart.	188

List of Tables

Chapter 1

Table 1.1	The seismic lines and length, the wells on the lines, the vertical and the horizontal scale.	9
Table 1.2	Well main formations tops and the total depth.	11

Chapter 3

Table 3.1	Two-way time in well D1/103 and in seismic, with mis-ties.	46
Table 3.2	Depth, time, interval velocity, and average velocity well (D1/103).	54
Table 3.3	The main acquisition, processing, and display parameters.	67
Table 3.4	Summary of seismic facies characterized by mounded and draped reflection configurations.	73

Chapter 6

Table 6.1	Summarizing the interval velocity according to the sonic logs in wells D2, D1, and D5.	191
Table 6.2	Summarizing the interval velocity according to the sonic logs in wells D16, D1, and D12.	192

XIII

Appendix

Chapter 3

Tables 3.5 to 3.11	Showing the shot-points, the two-way time in El-giza, Gir, Kheir, and Upper-Sabil horizons, and their depths in the seismic lines (U-14 to U-6) respectively.	203
Tables 3.12 to 3.13	Seismic lines, shot point intersections, and two-way time and mis-tie in the four previous horizons respectively.	210

Chapter 4

Tables 4.1 to 4.7	Seismic interval velocity in the El-giza to Gir, Gir to Kheir, and Kheir to Upper-Sabil, and the average velocity at the top of each horizon in the seismic lines (U-14 to U-6).	212
Tables 4.8 to 4.10	Seismic lines, shot-point intersections, seismic interval velocity and the mis-tie in the interval velocity for the El-giza to Gir, Gir to Kheir, and Kheir to Upper-Sabil intervals.	219
Tables 4.11 to 4.17	The difference between the interval velocity in the well (D1/103), and the seismic velocity through the three intervals, El-giza to Gir, Gir to Kheir, and Kheir to Upper-Sabil (lines U-14, U-25, U-51, U-53, U-54, U-9, and U-6).	222

Chapter 5

Tables 5.1(a) to 5.1(h)	Velocity tables. Two-way traveltime, RMS velocities, average velocities, depth, layer thickness, and interval velocities, in the CMPs where the velocity analysis applied.	229
-------------------------	---	-----

... ..
... ..
... ..
... ..

Chapter 1

1.1 Introduction

1.2 Description of Data

1.3 The aim of the study

... ..
... ..
... ..
... ..

... ..
... ..
... ..
... ..

1.1 Introduction

The geographical location map Fig. 1.1 illustrates the Intisar "D" field, situated on the southeast of the Concession 103 area, which lies to the southeast of Agedabya trough, with the Rakb high to the east and the Zelten platform somewhat farther to the west.

In general the Concession 103 area and the Intisar "D" field which is part from this area, is a flat area, with a very gently rolling topography.

Intisar "D" field was discovered in 1967 by Occidental company. The discovery well was drilled in 1966.

The definition of the Intisar "D" field is based upon 2-D seismic profiles, together with well data provided from exploration, production and injection wells. The first 2-D seismic survey was conducted between 1966 and 1967, providing 6-fold data from a dynamite crew. Recently, a 3-D seismic programme covers essentially the eastern part of the field. Such seismic data allowed a general recognition of the reef bodies on the basis of drape, build-up geometry, associated loss of continuity in the reef mass, and time structural depression beneath the reef due to either velocity sag or differential compaction.

Seismic data were digitally recorded, one of the early uses of the technique in Libya. A 6-fold stack was used in 1966 - 1967. Recently a 48-fold stack survey was recorded in 1986.

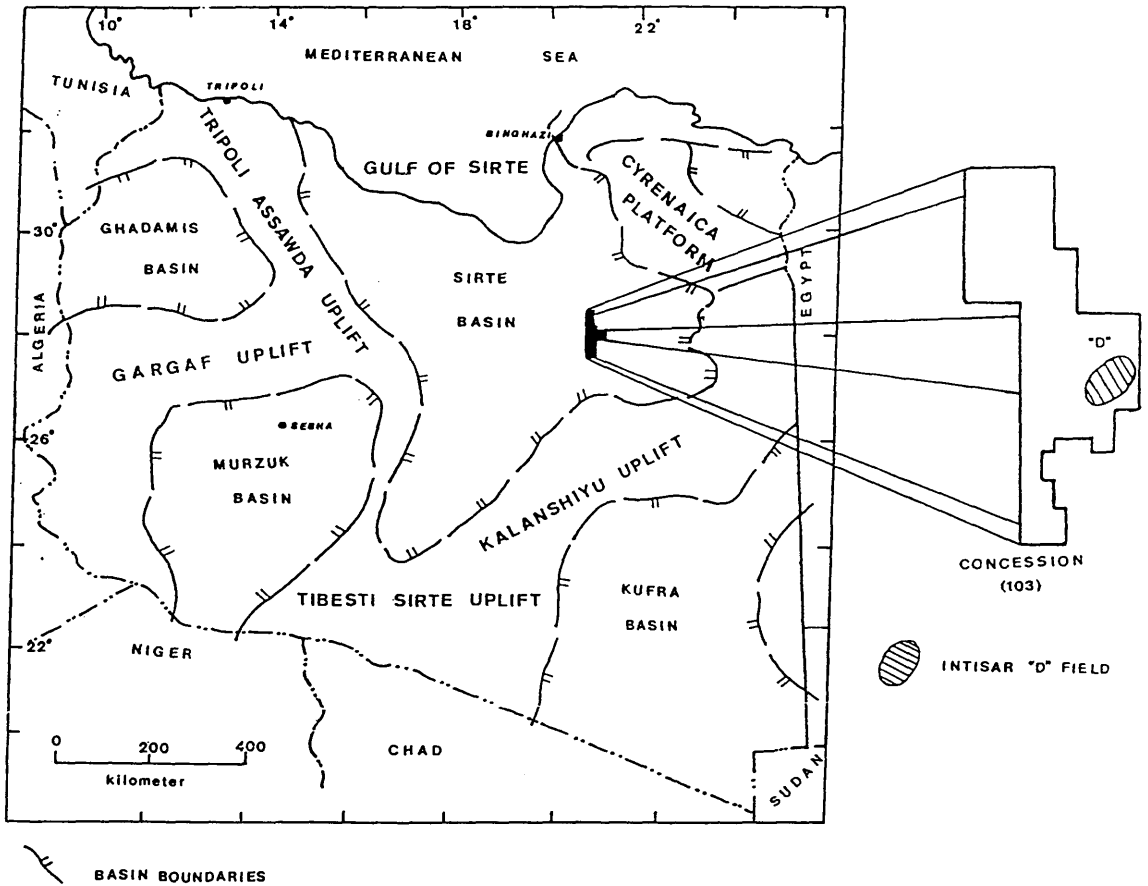


Fig. 1.1 Geographical location map of the area studied
Intisar "D" Field, within, the Sirte Basin, Libya.

The position of the 2-D seismic surveys in relation to each other and the Concession area is shown in Fig. 1.2.

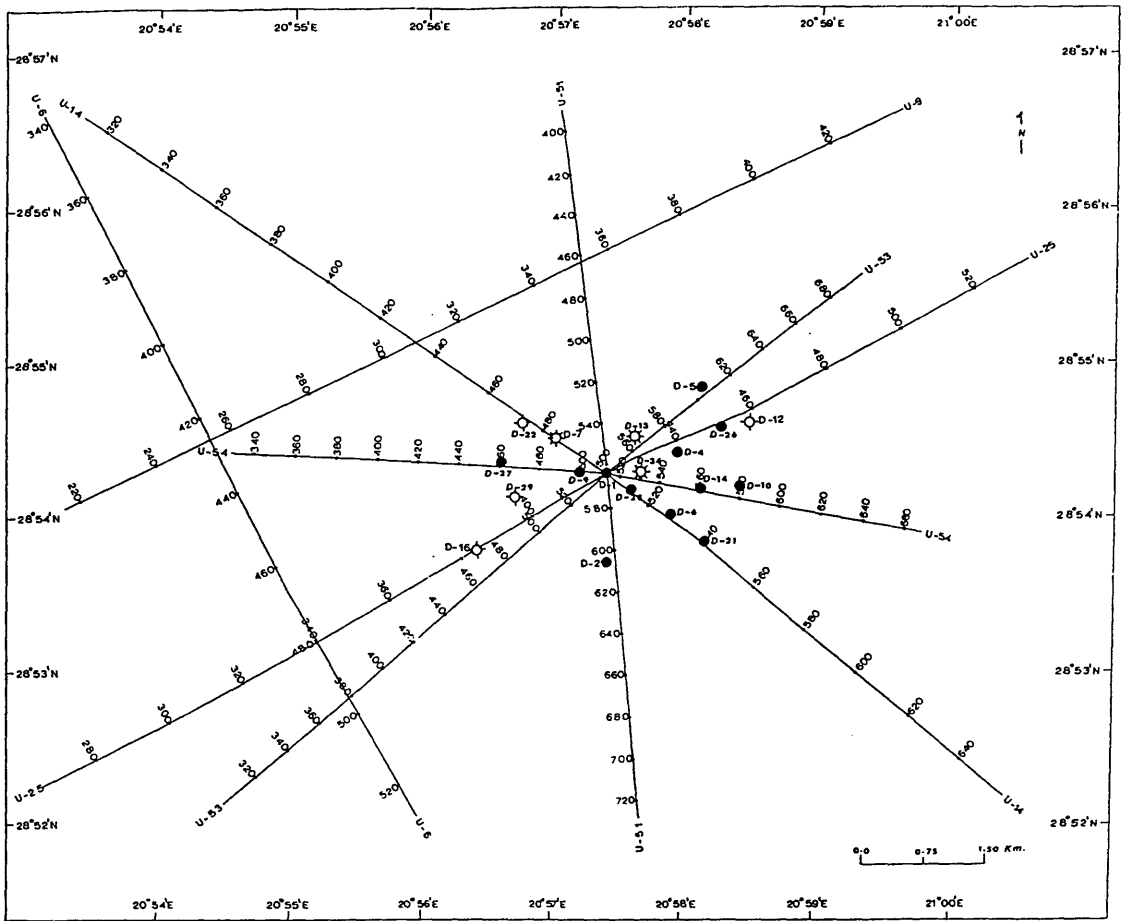
The co-ordinate boundaries of seismic survey are defined as follows :

20° 54 E to 21° 00 E

28° 52 N to 28° 56 N

The geological understanding of the Intisar "D" field was much improved after the drilling of a number of wells by Occidental. With respect to the "D" structure, the field now contains some 46 wells, 36 of which sample the Palaeocene reservoir, while much of the remainder were drilled to develop pay horizons within the El-giza limestone. A total of 19 wells are used in this study for establishing the geological correlations, and for obtaining lithological as well as velocity information.

The main reservoir is an Upper Palaeocene pinnacle reef containing more than one billion bbl (160 million cu m) of recoverable oil. The D1/103 well was drilled to a total depth of 3000 m and encountered oil-bearing carbonate rock from a depth of 2700 m. Wells drilled in the central area of the field penetrated continuous porosity from the top of the pay zone to the oil-water contact and below. The maximum oil column was 220 m, and the reef was full to the apparent spill point. The oil is 40 API gravity, has a paraffinic base and is low in sulphur (*Brady, et al.*, 1980). Field performance curves are presented in Figure 1.3. In January 1979 the field was producing 180,000 b/d (28,000 cu m/d) from 13 wells.



400 420 Seismic line with shot-points

- Oil well
- ☆ Gas well
- ◇ Dry well

Fig. 1.2 Line location map showing seismic lines and wells available for the present study.

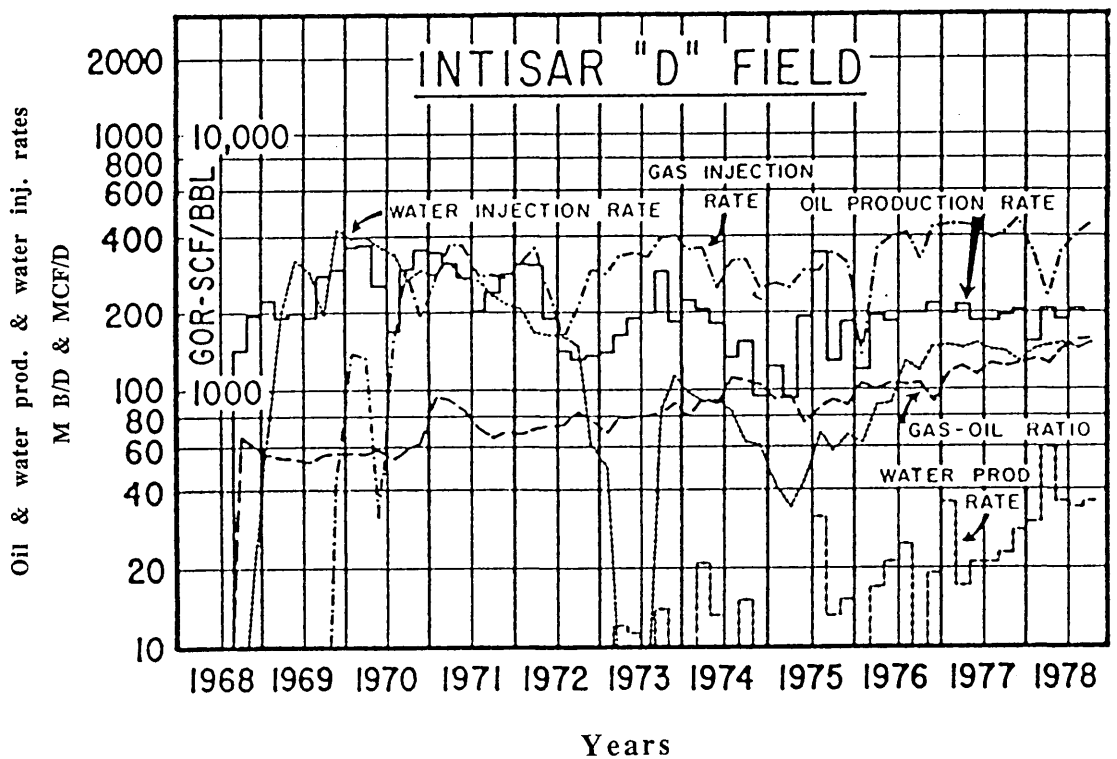


Fig. 1.3 Field performance curves for Intisar "D" field.

From (Brady et al. 1980).

In addition to these producers, 11 water-injection and 7 gas injection wells are used for the input of 150,000 bbl of water (23,900 cu m) and 450 MMcf of gas (13 million cu m) daily. Oil production as of December 31, 1978, was 812 million bbl (129 million cu m). Water and gas injection volumes by the end of 1978, were approximately 600 million bbl (95 million cu m) and 1 Tcf (28 million cu m), respectively.

In 1986 a new 2-D seismic survey was acquired in the field, using advanced reflection techniques. This survey used Vibroseis as a source of energy. The field has been producing at the same rate beginning of the eighties.

Only five wells provide velocity information from sonic logs, D1, D2, D5, D12, and D16 in the 103 area while only well D1/103, contains checkshot data. Synthetic seismograms have been generated for D1/103 well, providing a means to tie the geological depth tops supplied by Occidental, to the seismic data.

The recognition and proper interpretation are important because of variations in reservoir characteristics, of strata within and associated with the build-up.

It is very important that a worthwhile interpretation must be tied to all types of information seismic sections, boreholes, and any other geological information.

This study provides seismic interpreters with :

- (i) Criteria for recognizing carbonate build-up on seismic sections.

- (ii) Two-way time, depth, and interval velocities contour maps for the top Middle Eocene (El-giza) horizon, top Lower Eocene (Gir) horizon, Lower Eocene -Upper Palaeocene (Kheir) horizon, and Upper Palaeocene (Upper-Sabil) horizon.
- (iii) A discussion of why the seismic velocities in the area are poorly determined. Seismic sections U-14, and U-25, selected as examples, show the average interval velocities through the seismic sequences.

1.2 Description of Data

The area under study (Intisar "D" field) consists of the following data:

- (1) Seven seismic lines, U-14, U-25, U-51, U-53, U-54, U-6 and U-9, all obtained in 1986. The following table (1.1) shows their lengths, the vertical and horizontal scales, and the wells through which the seismic lines pass.

Table 1.1 : The seismic lines and length, the wells on the lines, the vertical and the horizontal scales.

Lines	Length of lines (km.)	Wells	V. scale	H. scale
U-14	22.0	D1,D6,D7,D21	1sec :19cm	4cm : 1km
U-25	25.8	D1,D12,D16	"	4cm : 1km
U-51	8.4	D1,D2	"	4cm : 1km
U-53	10.0	D1,D5	"	8cm : 1km
U-54	9.4	D1	"	8cm : 1km
U-6	27.8	-	"	4cm : 1km
U-9	17.8	-	"	4cm : 1km

- (2) The synthetic seismogram which was generated from data collected in well D1/103.
- (3) Nineteen wells in the field selected for different purposes-lithological information, correlation, and velocity information. Table (1.2) shows the names of the wells and the main formation tops; El-giza, Gir, Kheir, and Upper-Sabil, which are selected for the seismic interpretation.

- (4) The sonic logs are available for the wells D1, D2, D5, D12 and D16.
- (5) 2400 feet (730 m) magnetic tape for line (U14-103), containing demultiplexed SEG-Y seismic data for full fold between VPs 409 & 611. This covers Field Files 255 to 363,

The well velocity survey is available only in the well D1/103. With such limited velocity data available it was decided to use this velocity survey for time to depth conversion over the entire field.

The processing seismic velocity information is often unreliable from a geological point of view, as the horizons picked during processing are usually made without reference to a specific geological reflector, but instead are chosen on the basis of reflection strength at each velocity analysis location. Stacking velocity was interpolated without considering the geological information of the area. Wells drilled on the field periphery, particularly on the east flank, encountered one or more significant nonporous, non oil-bearing intervals within the reservoir, and this makes the seismic velocities, as well as the well velocities, increase towards the east and northeast. As mentioned above, the processing seismic velocities in the field are inaccurate, so to generate a new velocity information, it is necessary to reprocess the line U-14 from the VPs 440-580, which crosses the structure, and compare this with the available section.

Table 1.2: Main formation tops measured in the wells, the tops calculated, and the total depth measured.

Wells	Shot-points	Top El-giza (measured) (m)	Top El-giza (calculated) (m)	Top Gir (measured) (m)	Top Gir (calculated) (m)	Top Kheir (measured) (m)	Top Kheir (calculated) (m)	Top U.-Sabil (measured) (m)	Top U.-Sabil (calculated) (m)	Total depth (measured) (m)
D1	503 (U-14)	-1460	-1485	-1982	-2061	-2516	-2537	-2992	-3040	-3017
D2	606 (U-51)	-1475	-1504	-2000	-2080	-2547	-2568	-	-2555	-2988
D4	439 (U-25)	-1467	-1511	-2000	-2090	-2533	-2592	-	-3063	-2908
D5	606 (U-53)	-1473	-1520	-2025	-2108	-2570	-2615	-	-3056	-2800
D6	526 (U-14)	-1470	-1485	-2000	-2068	-2548	-2530	-	-3012	-2907
D7	485 (U-14)	-1455	-1485	-1976	-2046	-2506	-2530	-	-3052	-2907
D9	499 (U-54)	-1460	-1485	-1980	-2090	-2510	-2537	-2980	-3056	-3523
D10	578 (U-54)	-1488	-1522	-2027	-2090	-2524	-2607	-	-3000	-2945
D12	459 (U-25)	-1457	-1550	-1986	-2148	-2600	-2669	-2973	-3071	-3564
D13	565 (U-53)	-1457	-1491	-1986	-2075	-2514	-2553	-	-3040	-3017
D14	560 (U-54)	-1478	-1498	-2010	-2075	-2524	-2553	-2980	-3024	-3171
D16	385 (U-25)	-1485	-1524	-2033	-2097	-2590	-2640	-	-3032	-3010
D21	540 (U-14)	-1484	-1485	-2024	-2090	-2574	-2553	-2950	-2977	-3080
D22	475 (U-14)	-1448	-1485	-1970	-2046	-2512	-2537	-3010	-3040	-3529
D26	450 (U-14)	-1481	-1491	-2016	-2075	-2555	-2623	-2973	-3071	-3088
D27	460 (U-54)	-1457	-1517	-1978	-2090	-2524	-2630	-	-3040	-2934
D28	513 (U-14)	-1465	-1485	-1990	-2061	-2519	-2529	-2985	-3028	-3097
D29	469 (U-54)	-1465	-1511	-1994	-2090	-2510	-2584	-2976	-3056	-3102
D34	528 (U-54)	-1460	-1485	-1987	-2046	-2516	-2537	-	-3040	-2773

1.3 The aims of the study

The objectives of this study include :

- (i) A description of the geology and structural framework of the Sirte Basin in general, including the area of study (Intisar "D" field).
- (ii) Selection of marker horizons which have been mapped giving evidence for stratigraphic identification of these horizons.
- (iii) New seismic interpretation of important horizons. These horizons are the top of middle Eocene (El-giza), the top of Lower Eocene (Gir), the Lower Eocene-Upper Palaeocene (Kheir), and Upper Palaeocene (Upper-Sabil). Two-way time maps and depth maps of each horizon are presented.
- (iv) Velocity interpretation, seismic average and interval velocity maps. Discussion of why the seismic velocities in the area are inaccurate.
- (v) Reprocessing of line U-14 from VPs 409 to 611, with new velocity analysis, using the SierraSEIS package on the Sun computer and comparison the new section with the old one.

Chapter 2

2.0 Regional setting and stratigraphy

2.1 Introduction

2.2 Regional setting

2.2.1 Sirte Basin

2.2.2 Stratigraphical succession of the Sirte Basin

2.2.3 Concession 103 area

2.2.4 Geology of the Intisar "D" Field

2.3 Stratigraphy of Intisar "D" Field

2.4 Summary of Geology

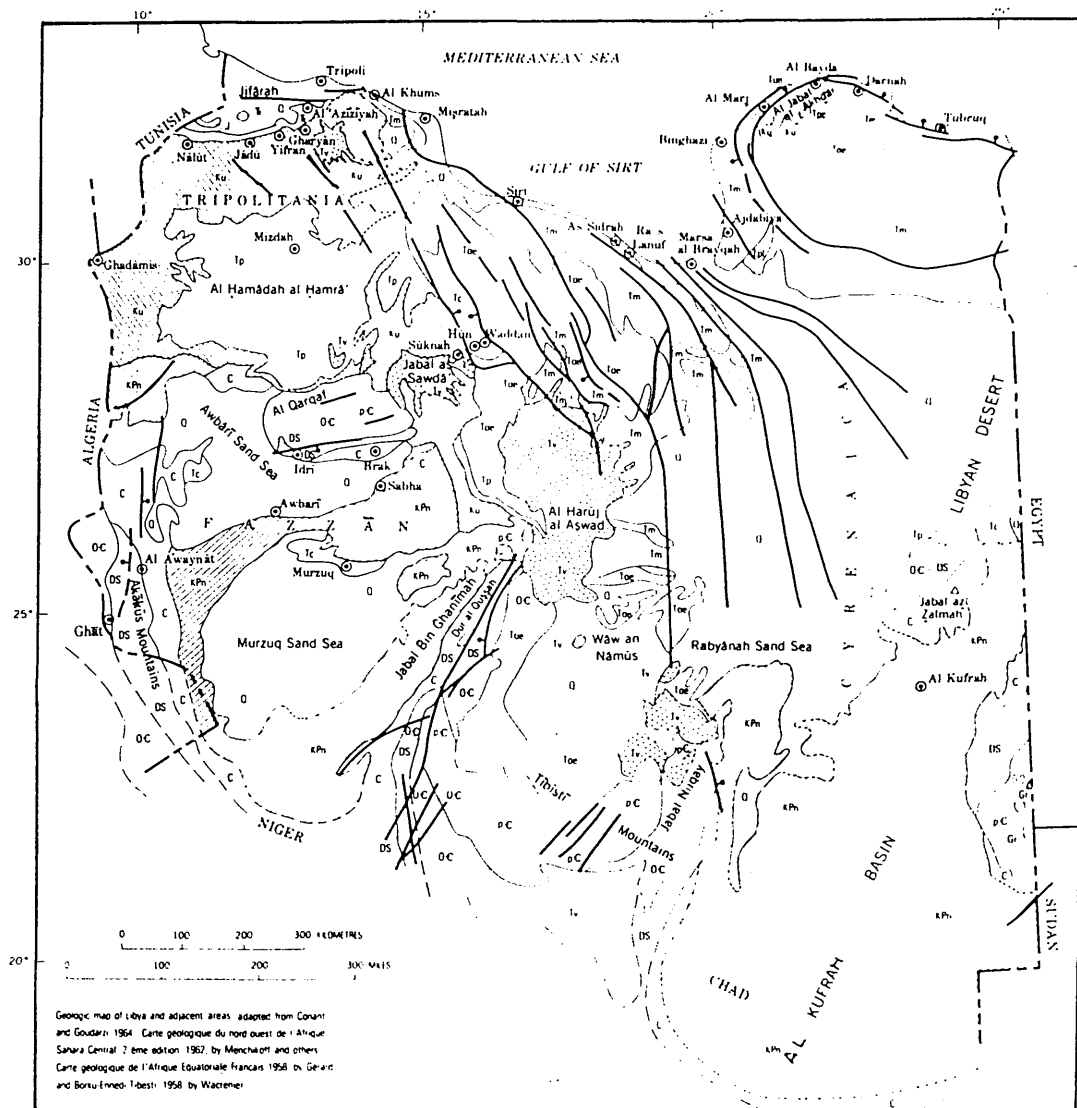
2.0 Regional setting and stratigraphy

2.1 Introduction

Libya is on the Mediterranean coast of North Africa, and has an area of about 1,750,000 square kilometres; the country extends about 950 miles (1,500 kilometres) east and west and as much as 900 miles (1,450 kilometres) north and south. Except for the northern most parts, the country is entirely in the Sahara (*Conant and Goudarzi 1966*).

Libya is bounded on the north by the Mediterranean sea, on the east by Egypt, on the southeast by Sudan, on the west Tunisia and Algeria, and on the south Chad and Niger (Fig. 2.1).

Libya is part of the North African shelf, situated between the stable African craton in the south and the active Mediterranean Tethys area to the north. The cratonic foundation is Precambrian (*Klitzsch 1968*). Since the early Palaeozoic, Libya has lain along the margin of numerous transgressions from the northwest and north. Consequently, the stratigraphic section is mostly complete and mainly of marine origin in the northern and especially north west part of the country, while to the south stratigraphical breaks are more frequent, and continental influences become more important (*Klitzsch 1968*).



EXPLANATION

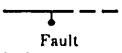
- | | | |
|--------------------------------------|---|----------------------------|
| Q Quaternary |  Tv Volcanic rocks, some of Quaternary age | C Carboniferous |
| Tp1 Pliocene |  Ku Upper Cretaceous | DS Devonian and Silurian |
| Tm Miocene |  KPn Nubian Sandstone including Continental Post-Tassilian (Permian to Lower Cretaceous) | OC Ordovician and Cambrian |
| Toe Oligocene and Eocene | J Jurassic | pC Precambrian |
| Tc Continental beds of uncertain age | Tr Triassic | Gr Granite |
| Tp Palaeocene | | |
- 
 Fault
 Dashed where uncertain; bar and bell on downthrown side

Fig. 2.1 Geologic map of Libya and area on south. Simplified from Conant and Goudarzi (1964).

2.2 Regional setting

2.2.1 Sirte Basin

The Sirte Basin of Libya has an onshore area of approximately 400,000 sq km (155,000 sq mi). It is the youngest of the basins in Libya, and the only one currently producing oil. It contains about 20 giant oil and gas fields.

The Sirte Basin is located in the north central part of Libya, and is defined more or less by the Hon Graben to the west, whilst to the east it is limited by the Cyrenaican platform and the western desert basin. To the north is the Mediterranean sea (Gulf of Sirte), and to the south it is limited by the Tibesti-Sirte Uplift, as shown in Chapter 1, Fig. 1.1.

The structure of the Sirte Basin is complicated, and detailed information is not available. The base consists chiefly of igneous and metamorphic rocks, but locally sedimentary rocks of probable Cambrian or Ordovician, and Silurian ages are known (*Conant & Goudarzi 1966*).

In general, the structure of the Sirte Basin is controlled by four major fracture systems :

The Rift, Atlan, Mediterranean and Meridian systems. The Rift and Atlan systems, respectively with NW and NE alignments are part of the regmatic shear pattern of the African continent. The Meridian system has N-S directions and is probably genetically related to the Rift system. The Mediterranean system has E-W alignments (Fig. 2.2).

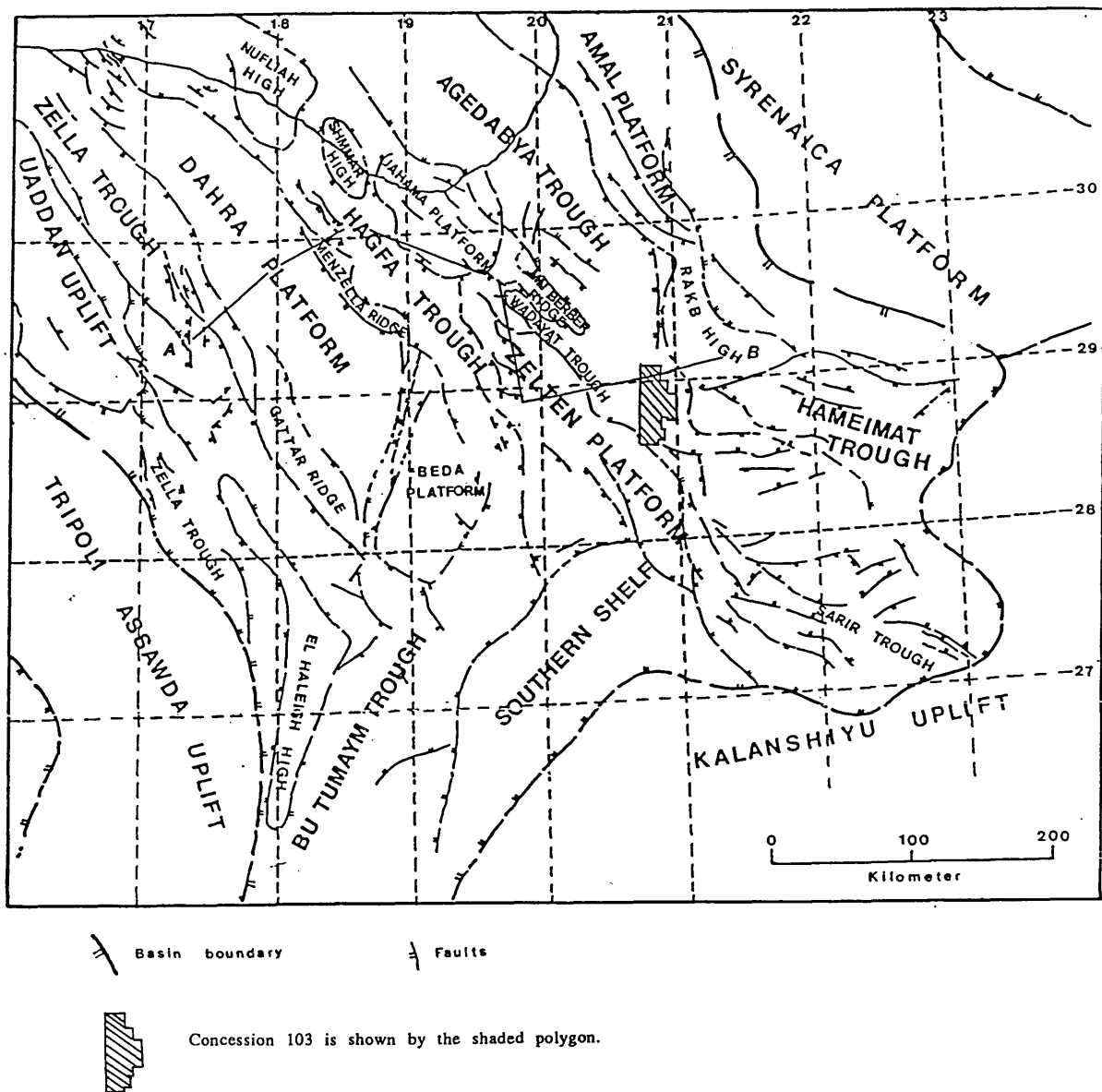


Fig. 2.2 Tectonic elements of Sirte Basin, Libya
(after Mouzughi and Taleb, 1980).

The structural deformation of Libya from the Precambrian to the present is essentially defined by differential uplift, subsidence, block faulting and tilting relative to these fracture systems (*Hea*, 1971). However, the Sirte Basin was formed by large-scale subsidence and block faulting that started in Late Cretaceous time, and continued, at least intermittently, to Miocene time, and perhaps to the present.

Beginning in the Late Cretaceous the northern crest of the Tibesti-Sirte Uplift collapsed to form the Sirte Basin. A number of tilted horsts and grabens of the Rift fracture system were formed (*Hea*, 1971), most of which strike NNW-SSE, approximately parallel to the Zella trough, which is the westernmost element of the Sirte Basin (*Klitzsch*, 1969). The ultimate forces in the formation of the Sirte Basin may be the shear produced by the clockwise rotation of the African craton relative to the Mediterranean (*Klitzsch*, 1969). Subsidence of the Sirte Basin continued from the Late Cretaceous through the Tertiary. The thickness of the Mesozoic-Tertiary section in the parallel troughs between the tilted horsts may attain over 20,000 ft (6100 m) (*Hea*, 1971).

The Sirte Basin is divided into two kinds of provinces : mobile and stable. The mobile provinces are troughs (grabens), whilst the stable provinces are Platforms (highs).

The Upper Cretaceous is generally thin on the platforms. Figure 2.3 showing the thinning of the Upper Cretaceous over the Dahra Platform and also over the Zelten Platform, in contrast to the troughs where the Upper Cretaceous is very thick, the Zella trough, Hagfa trough, and Agedabya trough. The southern Sirte Basin is defined by the outline of the stable province, but

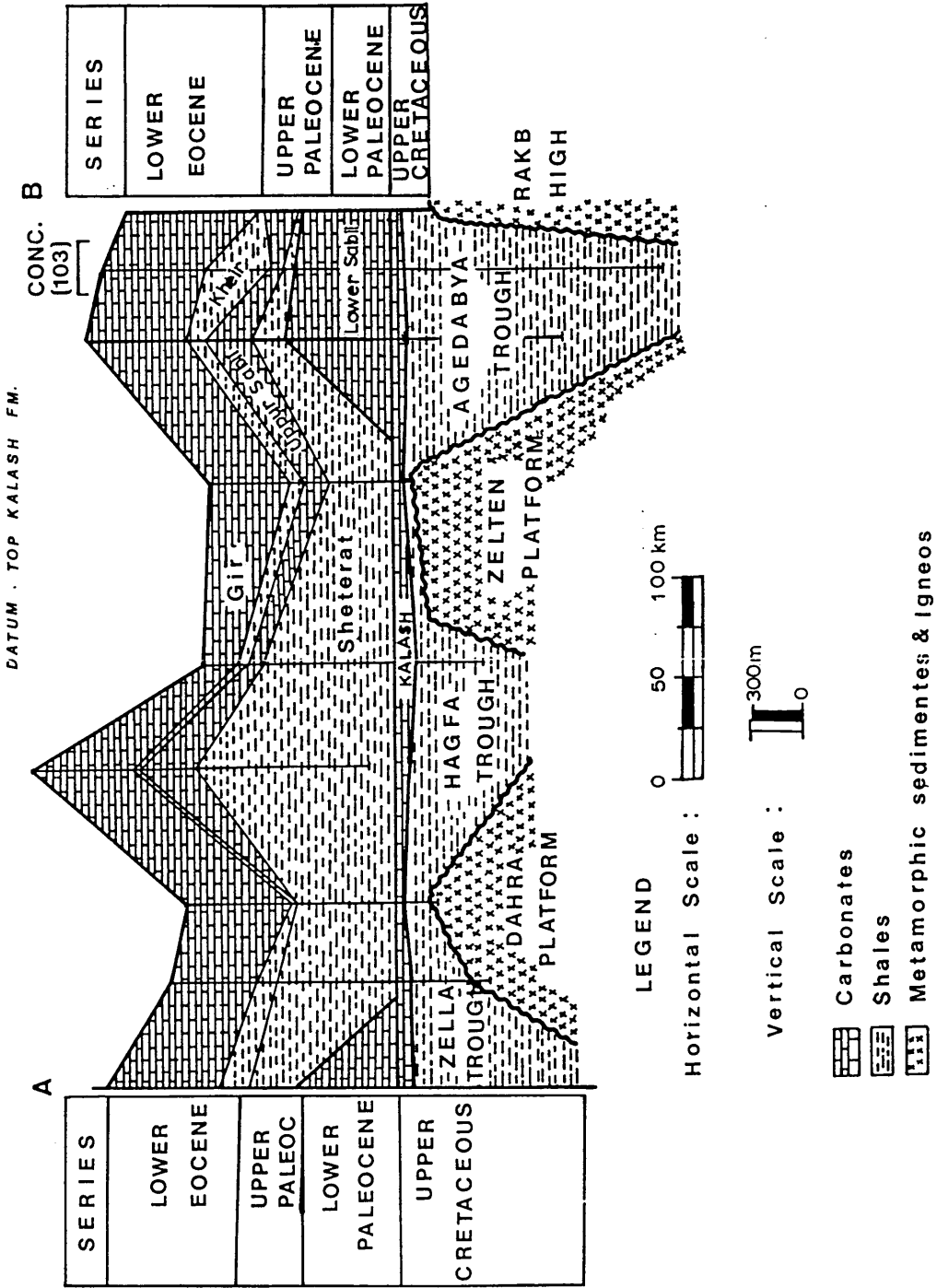


Fig. 2.3 Stratigraphic cross-section A-B in Sirtic Basin, located on Figure 3.2, datum on top of Upper Cretaceous (Kalash). Lower Palaeocene carbonates wedge out over troughs, independent of location of earlier highs (after Brady et al. 1980).

also includes basement promontories and outliers in the mobile province.

Faulting and subsidence started near the beginning of Late Cretaceous time. Large quantities of organic-rich shales, other terrigenous clastic materials and evaporites accumulated on the downfaulted blocks, while in many places the upfaulted horsts were above sea level.

Tertiary strata, chiefly carbonates, are generally continuous over the grabens that were still active. Reef accumulations are present on the flanks and over the crests of the horsts. Toward the south many of the carbonates grade into evaporites and terrigenous clastic rocks. Marine sedimentation continued through the Palaeocene and early to Middle Eocene.

In the central Sirte Basin during Palaeocene time, there were few or no beach deposits. Terrigenous material was possibly introduced from the north and may have been transported for great distances as suspended argillaceous material. Lithologies of Palaeocene age in the Sirte Basin were controlled by transgressions and regressions of an epeiric sea across a broad shelf region that dipped gently into a deep and persistent shale basin. This basin was located north and northwest of Concession 103.

There were two major marine transgressions across the Sirte Basin shelves during Palaeocene time; one occurred midway through the Palaeocene, the second at or near the end. Shale deposits, generally confined to the very low energy zones in the Basin and adjacent re-entrants, blanketed much greater areas during transgressive phases. During normal regressive periods, carbonates were deposited on the shelves (*Terry and Williams, 1969*).

The Palaeocene of the Sirte Basin is characterized by carbonate rocks and shales deposited in an epeiric sea. This heterogeneous series of shales, and carbonates shows considerable variations in formation thickness, which is related to the residual effect of the oil structures rather than renewed tectonic activity. The relatively rigid Precambrian and Palaeozoic highs acted as stable areas in comparison to the synclinal regions, where differential compaction produced local, subtle differences in environment. Not until the Upper Eocene / Lower Oligocene did rejuvenation of the major faults once more have a marked and direct effect on the sedimentation (*Brady et al.*, 1980).

The stratigraphic section with which this study is concerned is shown in Figure 2.3. The terminology used is that proposed by Barr and Weegar (1972). This is at variance with previously published papers, which used terminology developed by individual oil companies. A previous paper on the Concession 103 area (*Terry and Williams*, 1969) utilized slightly different terminology from this presentation.

2.2.2 Stratigraphical succession of the Sirte Basin

The stratigraphical succession of the Sirte Basin is represented by a thick sequence of continental and marine sediments i.e. clastics, carbonates, shales, dolomites, evaporites, etc. (Fig. 2.4). The following section describes in general the stratigraphical succession of the Sirte Basin according to *Klitzsch* (1968).

Precambrian The basement consists of a wide assortment of metamorphic and predominantly granitic igneous rocks. Most of the exposed basement rocks are certainly of Precambrian age, but some of the buried granities in the floor of the Sirte Basin may be of early Palaeozoic age (Fig. 2.4).

Palaeozoic The basal part of coarsely conglomeratic, and most of the succession is coarse-grained, cross-bedded, continental sandstone (Hofra formation).

Rocks of the Silurian system (Tanezzuft shale) indicate the first major transgression of the sea, while in many parts in the basin, marine and non-marine Devonian clastic rocks are found (e.g. in the western part of the basin, Dahra platform and in the eastern part, Amal platform; Fig. 2.2) whereas the Carboniferous and Permian are completely unrepresented. Generally the Palaeozoic in the Sirte Basin has a thickness about 0-1400 m (Fig. 2.4).

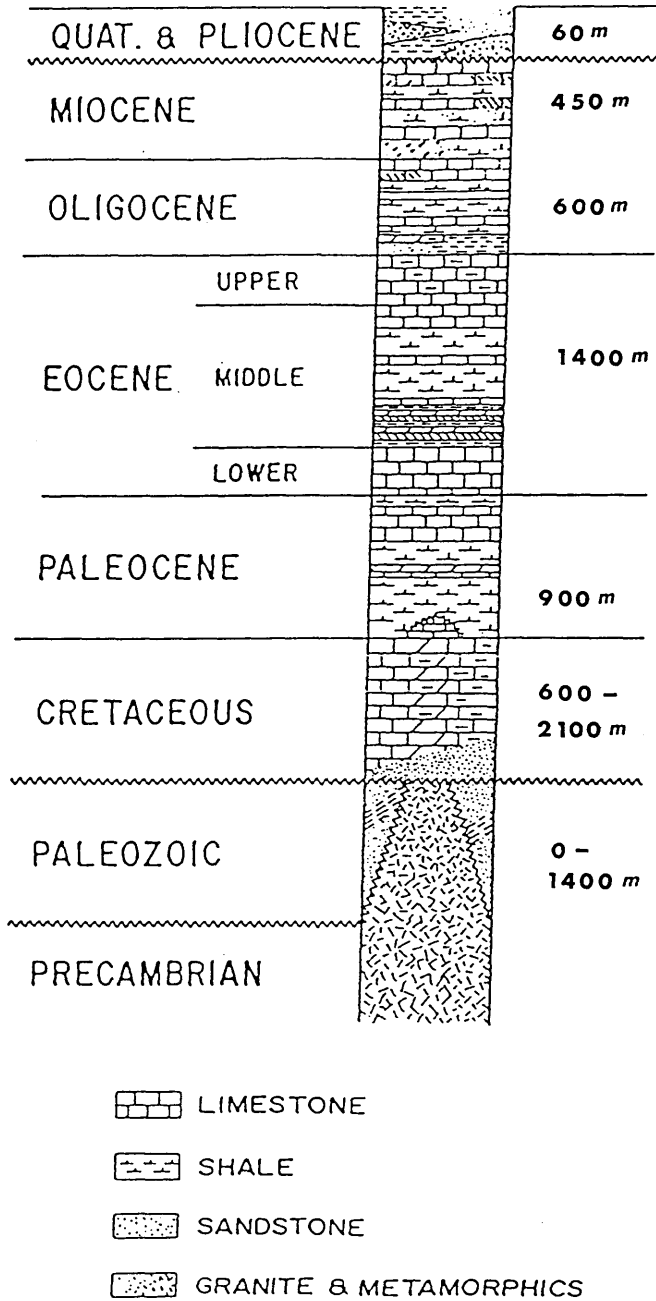


Fig. 2.4 Generalized Stratigraphic column, Sirte Basin, Libya
(after Roberts, 1968).

Mesozoic The oldest Mesozoic (Lower Cretaceous) rocks in the Sirte Basin are represented by continental sandstone (Nubian Formation), in the eastern part of the basin in Sarir trough (Fig. 2.2). The Upper Cretaceous sequence is much more varied as a result of the block faulting that took place during sedimentation.

There are great thickness of dark shales (Sirte shale) in the grabens, which are believed to be important source rocks for oil and gas. The Sheterat shale is the most likely candidate for the origin of the oil in the upper Sabil in Concession 103, though the Kheir marl and Rakh shale may have contributed (*Brady et al.*, 1980). Elsewhere limestone, and dolomite abound and locally serve as oil and gas reservoirs (*Hecht et al.*, 1964, p. 443). The Cretaceous thickness in some parts of the Sirte Basin ranges from 600-2100 m (Fig. 2.4).

Cenozoic Rocks of Tertiary age, chiefly carbonates, are much more varied in the subsurface of Sirte Basin. Lithologies include Palaeocene to Eocene carbonates, and interbedded shaly limestones (marls), limestone, and dolomite. The thickness of Palaeocene and Eocene sequences are about 900 m and 1400 m respectively. In the deepest part of the Basin, extending south-southeast from the head of the Gulf of Sirte, nearly 3000 m of Oligocene to Miocene, but in some parts of the Basin about 1100 m, Fig. (2.4), clastic rocks are known to be present along the axis of a deep trough. Laterally these clastics thin markedly over the marginal highs, where equivalent rocks consist largely of carbonates and evaporites.

Quaternary The Quaternary deposits are principally sand, in some places 50 -100 m thick, and in the others less than 50 m.

2.2.3. Concession 103 area

The Concession 103 area is situated at the southern end of the Agedabya trough (Marsa Brega trough) with the Rakb high to the East and the Zelten platform somewhat further to the West (in the eastern part of the Sirte Basin) with an area of 465,000 acres (1880 sq km) as shown in Fig. (2.2).

Topographically, Concession 103 is a very gently rolling, sandy plain. The surface section is a thin veneer of Quaternary sands and fine gravels overlaying Miocene sandy limestones. Surface elevations range from 140 m above sea level in the south part of the Concession to 80 m above sea level in the north part (*Terry and Williams, 1969*).

After the blanketing by the open-marine, pelagic Kalash Formation, there was a differentiation into one area of continued carbonate deposition and another of nondeposition of carbonates and shales. In the central Concession 103 area was one such area where energies were sufficient to deposit micrite, fine-grained planktonic biomicrite, even during maximum transgression (*Terry and Williams, 1969*).

2.2.4 Geology of the Intisar "D" Field

The first paragraph will describe the reef formation in general.

The term reef is used for bathymetrically positive rigid structures formed by sedentary, intergrowing organisms. A reef is commonly a bioherm, that is, a mound or lens-shaped feature of organic origin which is lithologically discordant with surrounding deposits. Reefs have probably formed in quite shallow water because of the dependence of the constituent organisms upon light (*Bubb & Hatlelid, 1977*). Growth of reefs depend upon many factors, including stability, relative movements of sea level, degree of current action, size and force of local waves, and suitability of local climatic conditions (*Manten, 1971*). Generally the reefs are characterized by growth of corals at or close to sea level.

The Intisar "D" field developed during the Upper Palaeocene in a shelf embayment at the southeast end of the Agedabya trough, one of the numerous grabens within the Sirte Basin. Previous evaluations have concluded that the reef is approximately circular (with a slight NE alignment), up to 5 km diameter and a maximum of 385 m thick. The northeast trend is thought to be the result of the prevailing northwest winds during the Palaeocene (*Terry and Williams, 1969*). Previous well data analysis has suggested that the Intisar "D" field consists of well stratified units which can generally be correlated using down hole logs. Figs. 2.5, 2.6 and 2.7 show SW-NE, NW-SE, and E-W cross sections respectively. The datum was 7800 ft (-2400 m) subsea.

Using well data, previous evaluations have identified two shoals (A and B) which drape over the margins and top of the "D" reef, interfingering with

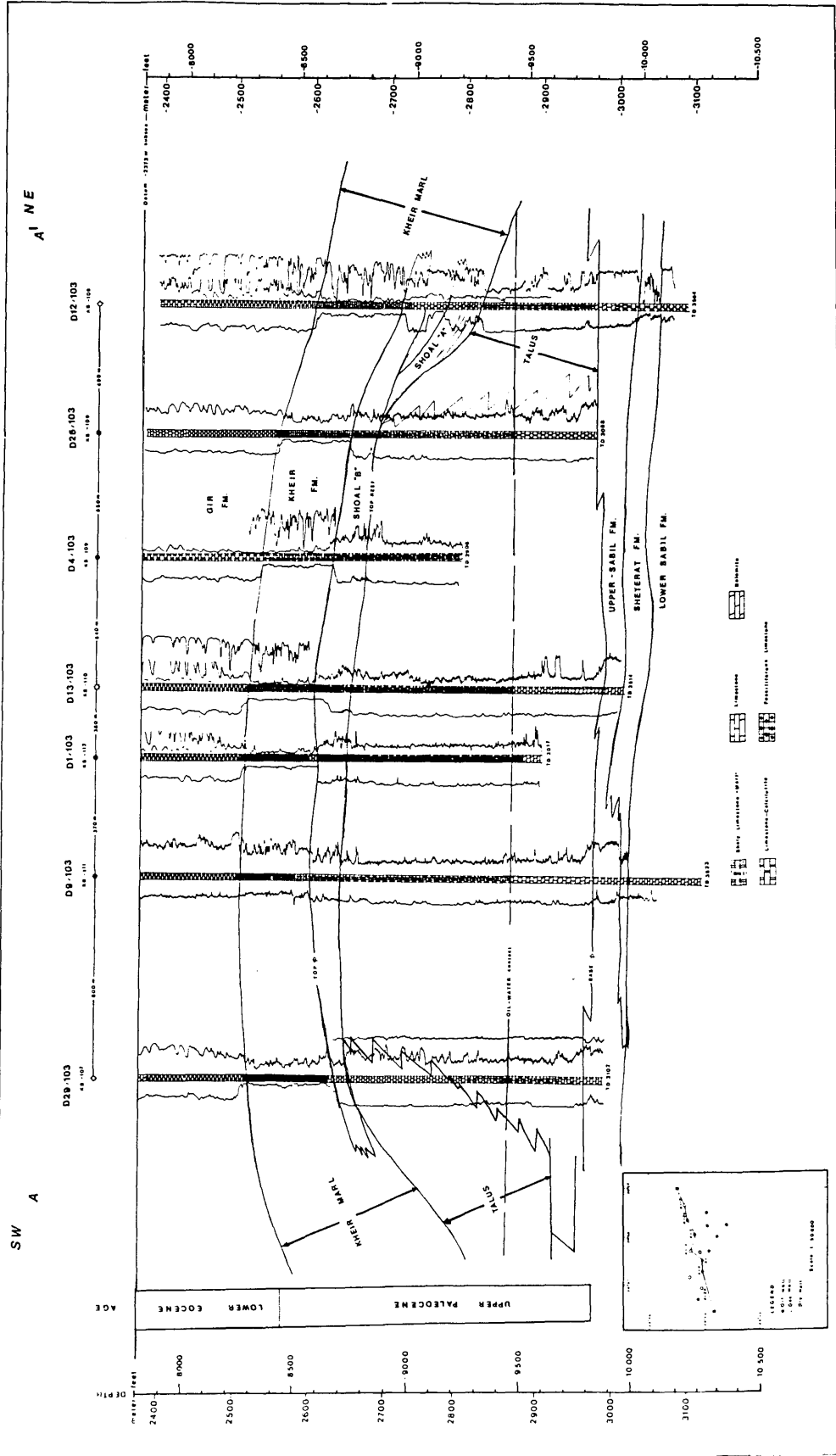


Fig. 2.5 SW-NE cross-section A-A in Intisar "D" field. Show the correlation possible within the reef by use of the gamma curves on the left, compensated formation density on the right. Datum on (-2400 m) subsea.

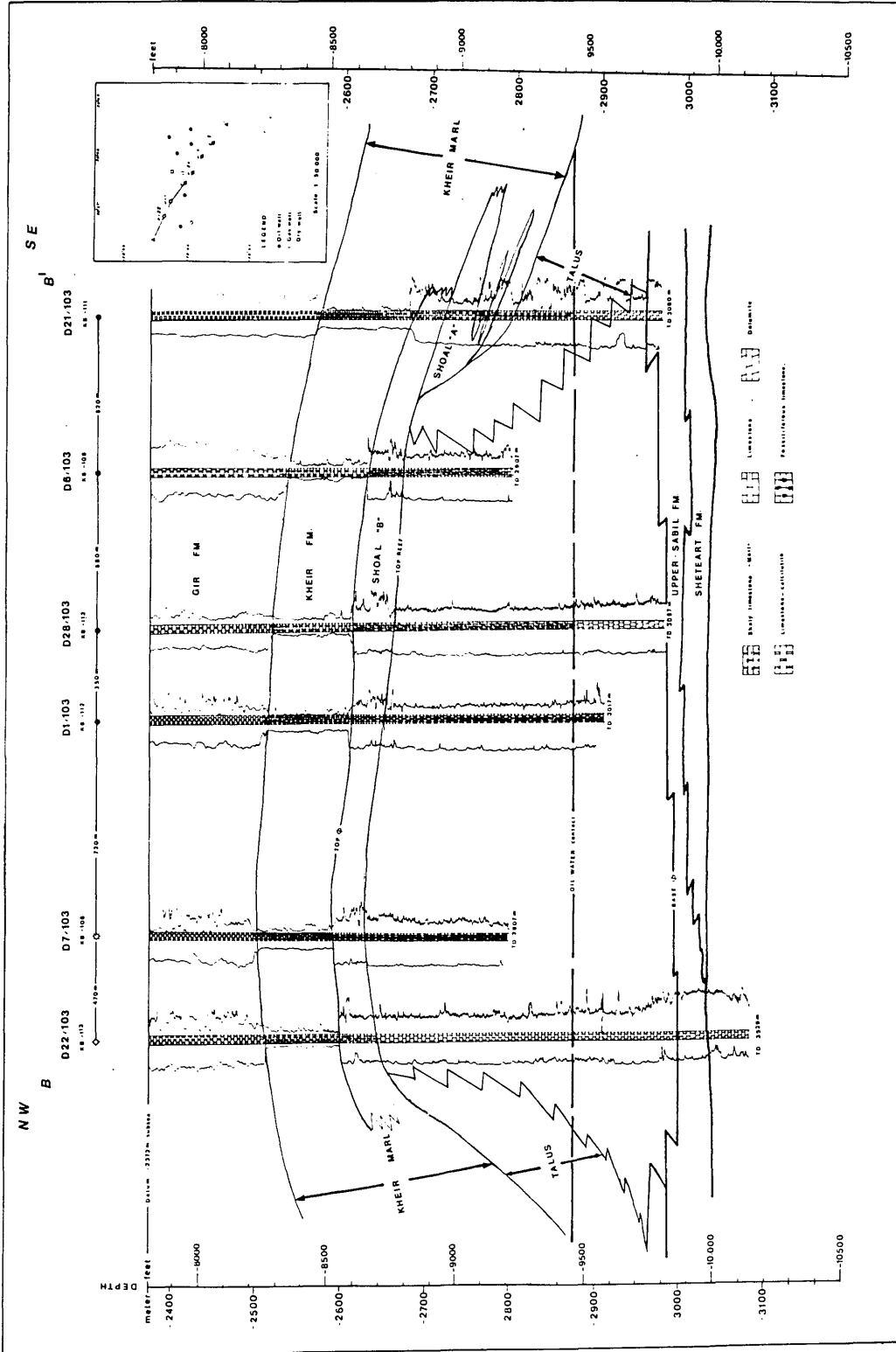


Fig. 2.6 NW-SE cross-section B-B in Intisar "D" field. Show the correlation possible within the reef by use of the gamma curves on the left, compensated formation density on the right. Datum on (-2400 m) subsea.

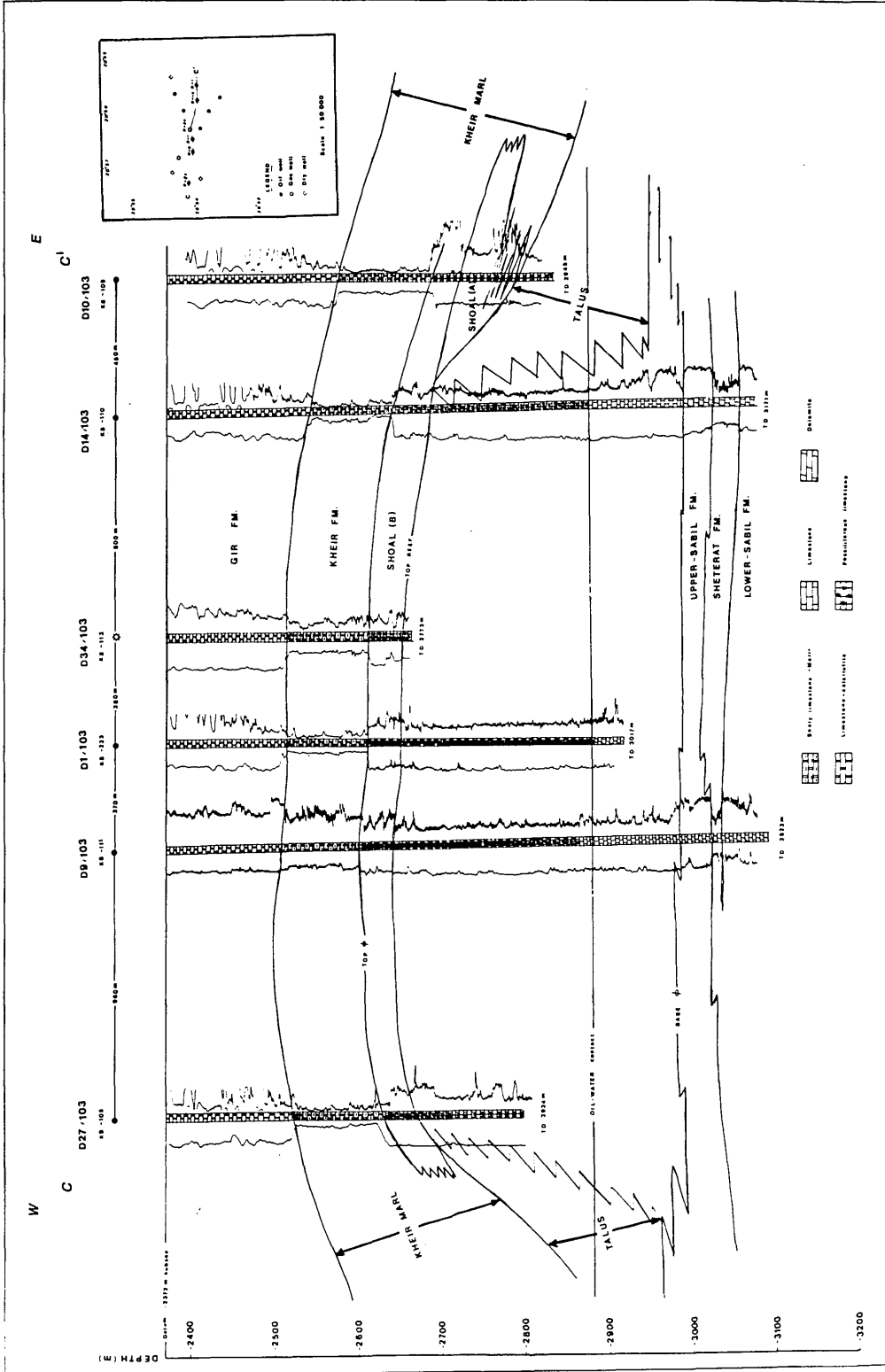


Fig. 2.7 W-E cross-section C-C in Intisar "D" field. Show the correlation possible within the reef by use of the gamma curves on the left, compensated formation density on the right. Datum on (-2400 m) subsea.

the Kheir marl at the reef margins (Figs. 2.5, 2.6, and 2.7), and which can be indirectly correlated with prominent marker horizons within the marl (*Brady et al.*, 1980).

The older, shoal A, is only found around the north, south and east margins of the reef. Its restricted extent has been attributed to an emergent reef top (*Brady et al.*, 1980). Development of shoal A along the western reef flank was probably severely restricted by the steep southwest (and west?) reef margin, where the reef edge dropped rapidly into deep, cold, inhospitable waters (Fig. 2.5).

The wide development of shoal B, across the entire reef top, with limited drape over reef margins, indicates continued subsidence of the shelf, resulting in total reef submergence. These porous limestone shoals are considered to contain at least 17.7% of total oil reserves at Intisar "D" (*Brady et al.*, 1980). The reef is also surrounded by a zone of reef talus which is poorly developed on the steep southwest (and west?) margin Fig. (2.5).

The eastern flanks of the reef body represent a back-reef facies, protected from the higher energy conditions of the western fore-reef facies, which was relatively open to tidal and wave attack from the northwest. The back-reef eastern flanks exhibit gentler slope gradients with an associated greater development of both reef talus deposits (tossed over the main reef during storms and high tides). The following paragraph will discuss the reality of reef talus.

In most text-book models the reef talus is based more on imagination than fact. There are few examples of cross-sections using boreholes through

recent carbonate sequences below reefs. One of these, a section through the Recent reef of Panama shows that this model is far from reality. Recent reefs show that for the most part we are dealing with accretions only 10-15 m thick.

The "fore-reef talus" is one of the most consistent elements in descriptions of fossil reefs, to the point where sediments described as "talus" are often the only part of the association which is preserved. The reef talus is composed of debris eroded from the front of the reef, but in recent systems such material is typically transported landwards rather than down the fore-reef slope (*Braithwaite, 1987*).

The reef flat (back reef) is divided into three separate zones, a near-shore zone of rippled sand, an intermediate zone characterized by marine angiosperms, and an outer zone of sand and cobble ridges constructed from edge-derived material. The edge is made up of an intergrown framework of corals and calcareous algae which forms the wave resistant margin to the structure. In back reef environments, sediments are loose and unconsolidated, and are generally horizontally bedded (*Braithwaite, 1987*).

In Recent reefs, present-day accumulations of both reef framework and associated sediments overlie an older (Pleistocene) basement. This provides much of the relief and, when shelf areas are effectively unable to accommodate further accumulations, excess sediment spills over to form steeply dipping slope deposits (equivalent to "talus" on large scale models).

In Intisar "D", as illustrated by *Brady et al. (1980)*, the maximum thickness of the "reef" is 385 m, although the biolithite (reef framework) is

only 61 m thick. Dips on the flanks are 5-40° in boreholes, but seismic sections and borehole correlation suggests that they are in fact generally low. The steeply dipping beds appear to drape against the reef, which may not have been growing at the same time the adjacent beds were deposited. *Brady et al.* (1980) record the presence of large detached blocks (debris flows?) and slumps within these deposits. The total thickness quoted represents the reef and other sediments as a whole. The thickness of the biolithite is just 61 m, and this is in fact close to the maximum thickness found in recent reefs in different parts of the world today.

On the southwest side of the field, slope angles as high as 32° are recorded, but according to *Brady et al.* (1980), the talus zone is not well-developed. It is thought likely that high energy generated by a prevailing southwest to northeast wind was responsible for promoting talus accumulation on one side only. Strong currents on the west flank of the reef were probably responsible for sweeping mudstones away.

2.3 *Stratigraphy of the Intisar "D" Field*

The stratigraphic sequence in the Intisar "D" field is divided into three major depositional periods, the Miocene-Oligocene, the Eocene, and Palaeocene. The description following is according to the well logs, which were generated in the field by Occidental.

Upper-Sabil Formation

The Upper-Palaeocene (Landenian) carbonates consist predominantly of limestones with lesser dolomite and some shale. The Upper-Sabil carbonates are conformably overlain by the Kheir Formation, and they in turn conformably overlies the Shetrat Formation (Fig. 2.8).

The upper contact is placed below the shale of the Kheir Formation, and the bottom contact is placed at the change from the Upper-Sabil carbonates to the shale of the Shetrat Formation. It has a thickness about 450 feet (140 m).

Kheir Formation

The Lower Eocene-Upper Palaeocene (Ypresian-Landenian) is predominantly shaly limestone (marl); (Fig. 2.8). The Kheir Formation is conformably overlain by the Lower Eocene (Gir Formation), and it, in turn, conformably overlies the Upper Palaeocene (Upper-Sabil) carbonates.

The upper contact is placed at the abrupt change from the limestone to the shale of the Kheir Formation, and the basal contact at the abrupt change from shale to the limestone of the Upper-Sabil carbonate.

The lower Kheir Formation is of Upper Palaeocene age and the upper part is Lower Eocene (Fig. 2.8). The formation has a thickness about 800 feet

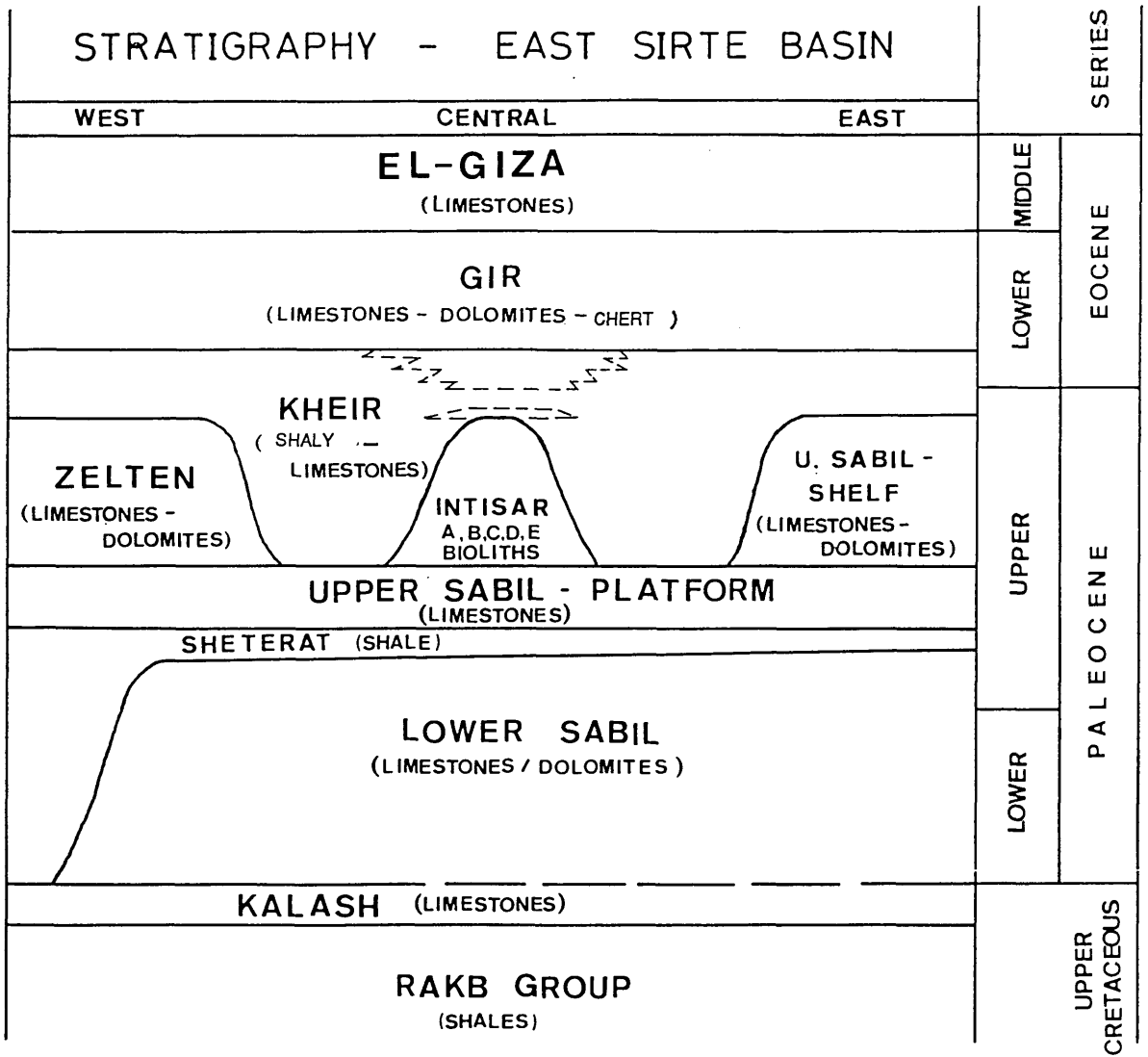


Fig. 2.8 Stratigraphy of the East Sirte Basin. Dotted lines are facies variations. Heavy lines are generalized time lines (after Brady et al. 1980).

(250 m). The Kheir marl has distinctive electric-log characteristics. The top contact occurs at the formation density curves increase, accompanied by a sharp positive deflection in the gamma curve, whereas the bottom contact is at the formation density curve decrease accompanied by a negative deflection in the gamma curve (Fig. 2.5, 2.6 and 2.7).

Gir Formation

The Lower Eocene (Ypresian) Gir Formation is marked by the presence of chert, and is composed dominantly of limestones and occasionally traces of dolomite and dolomitic limestones. The limestones are calcilutite to calcarenite, off-white, light grey and brown, argillaceous, and having fair porosity throughout the section. The uppermost part of the formation has a thickness of approximately 1760 ft (540 m). The Gir Formation occupies a conformable position between both the overlying (El-giza) and underlying (Kheir) units. It has a total thickness about 2100 ft (650 m).

El-giza Formation

The Middle Eocene El-giza consists mainly of limestone. It is calcilutite and occasionally calcarenite, generally off-white to light brown in colour, fair to good porosity, and trace of foraminiferas. It is widespread in the subsurface of the Sirte Basin.

The El-giza limestone overlies the Lower Eocene (Gir Formation) with apparent conformity. This contact is usually placed at the top of the sequence containing common thin limestone and chert beds (Fig. 2.8). It has a thickness of about 1780 ft (550 m), according to the well D1/103, but is more or less the same thickness over all the field, from the seismic interpretation.

2.4 *Summary of geology*

A brief summary of the reef area and the other reefs in the Concession 103 area e.g. "A","B" and "C", is presented to tie together previous ideas and work and to present additional ideas and interpretation which have not been previously discussed.

The reef area is bounded roughly by the east and west boundaries of Concession 103 area. The southern boundary roughly parallels the southern boundary of the Concession. After deposition of the Lower-Sabil carbonates in the Upper Palaeocene time, there was a transgression and the Sheterat shale was deposited over a wide area including the reef area. In those areas sufficiently high a thin Sheterat shale was deposited (Fig 2.8).

In the reef area the reefs grew at the same time as the Upper-Sabil platform carbonates were being deposited, but each reef had its own particular ecological conditions. At the end of reef growth time near the end of the Palaeocene time, the reefs stopped growing with the introduction of the lower Kheir shales.

These lower Kheir shales were overlain by a zone of argillaceous micrites, which developed as shoals over the "D" reef, and "C" reef. In those reefs with sufficiently high energy the lower Kheir sediments were deposited on the flanks of the existing reef as porous shoals (Figs. 2.5, 2.6 and 2.7). This has been established with good reliability, where we have good control in the "D" reef.

The differences between the "D" reef and the other reefs in the Concession 103 area, for example the "A" reef, show that the "A" reef was in a

lower energy zone immediately post-reef time, and that the "D" reef was in a high energy zone. As a result, post reef shoals grew around and over the "D" reef, and to a lesser extent over the "C" reef. The upper Kheir sediments show that the "D" and "E" reefs were in a low energy zone relative to the "A" reef post shoal time. This can be explained by a southeast tilt of the reef area towards the major north south trending fault, which runs a long the east border of the Concession 103 area.

Era	Sub-era Period Sub-period	Epoch	Age	Ma age	Age abbrev.	Ma inter-valts		
Cenozoic	Quaternary or Pleistocene	Holocene		0-0.1	Hol	0.1		
		Pleistocene		2-0	Ple	1-2		
	Neogene	Pliocene	Piacenzian		5-1	Pia	3-1	
			Zanclian		5-1	Zan	5-2	
			Messinian		5-1	Mes	5-2	
		Miocene	Tortonian		14-4	Tor	22-6	
			Serravallian		14-4	Srv	3-1	
			Langhian-Late		14-4	Len	2-2	
			Langhian-Early		14-4	Len1		
		Paleogene	Oligocene	Burdigalian		24-6	Bur	10-2
				Aquitanian		24-6	Aqt	
				Chattian		32-8	Cht	8-2
	Eocene		Rupelian		38-0	Rup	5-2	
			Prriabonian		42-0	Prb	4	
			Bartonian		42-0	Brt	4	
			Lutetian		50-5	Lut	8-5	
	Paleocene	Ypresian		54-9	Ypr	4-4		
		Thanetian		60-2	Tha	5-3		
		Danian		65	Dan	4-8		
	Mesozoic	Cretaceous	Senonian	Maastrichtian		65	Maa	8
Campanian					73	Cmp	10	
Santonian					83	San	4-5	
Coniacian					87-5	Con	1	
Turonian					88-5	Tur	2-5	
Neocomian			Camomanian		91	Cam	5-5	
			Albian		97-5	Alb	5-5	
			Aptian		119	Apt	6	
			Barremian		125	Brm	6	
			Hauterivian		131	Hau	6	
Jurassic		Malm	Valanginian		138	Val	7	
			Berriasian		144	Ber	6	
			Irronian		144	Irh	6	
		Dogger	Kimmeridgian		156	Kim	6	
			Oxfordian		163	Oxf	7	
		Lias	Callovian		169	Clv	6	
			Bathonian		175	Bth	6	
			Bejocian		181	Baj	6	
		Triassic	J2	Aalenian		188	Aal	7
				Toarcian		194	Toa	6
Phiensbachian				194	Pfb	6		
Tr3	Sinemurian			200	Sin	6		
	Hettangian			206	Het	7		
Tr2	Rhaetian			213	Rht	6		
	Nonian			219	Nor	6		
	Camian			225	Cam	6		
	Ladinian			231	Lad	7		
	Anisian			238	Ans	5		
Tr1	Spathian		243	Spa	1 1/2			
	Smithian		248	Smi	1 1/2			
	Dienonian		248	Die	1 1/2			
Permian	P2	Griesbachian		248	Gri	1 1/2		
		Tatarian		253	Tat	5		
		Kazanian		253	Kaz	2-5		
	P1	Ufimian		258	Ufi	2-5		
		Kungurian		263	Kun	5		
		Artinskian		263	Art	5		
		Sakmarian		268	Sak	9		
		Asselian		268	Ass	9		
		Carboniferous	Gzelian	Noginskian		286	Nog	
				Klazminskian		286	Kla	
Dorogomilovsk				286	Dor			
Chamovnichesk				286	Chv			
Krevykinskian				286	Kre			
Moscovian	Myachkovskian			286	Mya			
	Podolskian			286	Pod			
	Kashirskian			286	Ksk			
	Versiskian			286	Vrk			
	Melekesskian			286	Mel			
Bashkirian	Cheremshansk		315	Che				
	Yeadonian		315	Yea				
	Marsdenian		315	Mrd				
	Kinderscoutian		315	Kin				
	Alportian		315	Alp				
Carboniferous	C2	Serpukhovian		320	Ser			
		Chokierian		320	Cho			
	C1			320				
				320				
				320				

Era	Sub-era Period Sub-per.	Epoch	Age	Ma age	Age abbrev.	Ma inter-valts
Paleozoic	Carboniferous	C2	Bashkirian			34
			Marsdenian			
			Kinderscoutian		320	Mrd
			Alportian			Kin
			Serpukhovian			Alp
		C1	Chokierian			13
			Arnsbergian			Cho
			Pendleian			Arn
			Brigantian			Pnd
			Visean			333
	Devonian	D3	Brigantian			19
			Asbian			Bri
			Holkerian			Asb
			Arundian			Hlk
			Chadian			Aru
		D2	Wenlock			8
			Wenlock			360
			Famennian			Ivo
			Frasnian			Has
			Givetian			367
D1	Eifelian			7		
	Emsian			374		
	Siegenian			Fra		
	Gedinnian			Giv		
	Gedinnian			380		
Silurian	S	Emsian			48	
		Siegenian			387	
		Gedinnian			Eif	
		Fridoli			394	
		Ludlow			Ems	
	Ordovician	O3	Gedinnian			7
			Gedinnian			401
			Gedinnian			Stg
			Gedinnian			Ged
			Gedinnian			408
Cambrian	C	Priddian			6	
		Ludlow			414	
		Ludlow			Ldt	
		Ludlow			Gor	
		Ludlow			421	
	Silurian	S	Gleadowian			7
			Gleadowian			Gle
			Whitwell			Whi
			Sheinwoodian			She
			Telychian			428
Ordovician		O2	Froonian			10
			Froonian			Fro
			Idwian			Idw
			Rhuddanian			Rhu
			Hirnantian			438
	Cambrian	C	Hirnantian			10
			Hirnantian			Hir
			Rawleyan			Raw
			Cautleyan			Cau
			Pusgillian			448
Cambrian		C	Onnian			67
			Actonian			Onn
			Marshbrookian			Act
			Longvillian			Mrb
			Soudleyan			Lon
	Cambrian	C	Haragian			10
			Haragian			Sou
			Costonian			Har
			Costonian			458
			Costonian			Cos
Cambrian		C	Llanvillo			10
			Llanvillo			Llv2
			Llanvillo			Llv1
			Llanvillo			468
			Llanvillo			Llv2
	Cambrian	C	Llanvillo			10
			Llanvillo			Llv1
			Llanvillo			478
			Llanvillo			Lln2
			Llanvillo			Lln1
Cambrian		C	Arenig			10
			Arenig			478
			Arenig			Arg
			Tremadoc			488
			Tremadoc			Trt
	Cambrian	C	Merioneth			85
			Merioneth			Dol
			Merioneth			505
			Merioneth			Mnt
			Merioneth			523
Cambrian		C	Merioneth			85
			Merioneth			Men
			Merioneth			540
			Merioneth			Sol
			Merioneth			Len
	Cambrian	C	Merioneth			15
			Merioneth			15
			Merioneth			15
			Merioneth			15
			Merioneth			15
Cambrian		C	Merioneth			20
			Merioneth			20
			Merioneth			20
			Merioneth			20
			Merioneth			20
	Cambrian	C	Merioneth			40
			Merioneth			40
			Merioneth			40
			Merioneth			40
			Merioneth			40
Cambrian		C	Merioneth			60
			Merioneth			60
			Merioneth			60
			Merioneth			60
			Merioneth			60
	Cambrian	C	Merioneth			60
			Merioneth			60
			Merioneth			60
			Merioneth			60
			Merioneth			60
Cambrian		C	Merioneth			60
			Merioneth			60
			Merioneth			60
			Merioneth			60
			Merioneth			60
	Cambrian	C	Merioneth			60
			Merioneth			60
			Merioneth			60
			Merioneth			60
			Merioneth			60
Cambrian		C	Merioneth			60
			Merioneth			60
			Merioneth			60
			Merioneth			60
			Merioneth			60
	Cambrian	C	Merioneth			60
			Merioneth			60
			Merioneth			60
			Merioneth			60
			Merioneth			60
Cambrian		C	Merioneth			60
			Merioneth			60
			Merioneth			60
			Merioneth			60
			Merioneth			60
	Cambrian	C	Merioneth			60
			Merioneth			60
			Merioneth			60
			Merioneth			60
			Merioneth			60
Cambrian		C	Merioneth			60
			Merioneth			60
			Merioneth			60
			Merioneth			60
			Merioneth			60
	Cambrian	C	Merioneth			60
			Merioneth			60
			Merioneth			60
			Merioneth			60
			Merioneth			60
Cambrian		C	Merioneth			60
			Merioneth			60
			Merioneth			60
			Merioneth			60
			Merioneth			60
	Cambrian	C	Merioneth			60
			Merioneth			60
			Merioneth			60
			Merioneth			60
			Merioneth			60
Cambrian		C	Merioneth			60
			Merioneth			60
			Merioneth			60
			Merioneth			60
			Merioneth			60
	Cambrian	C	Merioneth			60
			Merioneth			60
			Merioneth			60
			Merioneth			60
			Merioneth			60
Cambrian		C	Merioneth			60
			Merioneth			60
			Merioneth			60
			Merioneth			60
			Merioneth			60
	Cambrian	C	Merioneth			60
			Merioneth			60
			Merioneth			60
			Merioneth			60
			Merioneth			60
Cambrian		C	Merioneth			60
			Merioneth			60
			Merioneth			60
			Merioneth			60
			Merioneth			60
	Cambrian	C	Merioneth			60
			Merioneth			60
			Merioneth			60
			Merioneth			60
			Merioneth			60
Cambrian		C	Merioneth			60
			Merioneth			60
			Merioneth			60
			Merioneth			60
			Merioneth			60
	Cambrian	C	Merioneth			60
			Merioneth			60
			Merioneth			60
			Merioneth			60
			Merioneth			60
Cambrian		C	Merioneth			60
			Merioneth			60
			Merioneth			60
			Merioneth			60
			Merioneth			60
	Cambrian	C	Merioneth			60
			Merioneth			60
			Merioneth			60
			Merioneth			60
			Merioneth			60
Cambrian		C	Merioneth			60
			Merioneth			

Chapter 3

3.0 Seismic stratigraphic interpretation

3.1 Well to seismic tie

3.1.1 Synthetic seismogram

3.1.2 Well to seismic tie

3.2 Event identification and selection

3.2.1 Preliminary interpretation

3.3 Interpretation and mapping

3.3.1 Seismic sections

3.3.2 Seismic facies analysis

3.3.3 Mapping reflection horizons

3.3.4 Maps construction

(i) Time contour maps

(ii) Depth contour maps

3.4 Summary of seismic interpretation

3.0 Seismic stratigraphic interpretation

3.1 Well to seismic tie

3.1.1 Sonic log calibration

The objective of sonic log calibration is to obtain a time/depth function, as accurately as possible, to be able to compare seismic trace scales with well log scales. The sonic readings should then be recalibrated by check shots which can be obtained with the Well Seismic Tool.

The Well Seismic Tool measures the time required by a seismic pulse generated at the surface to travel down to a geophone positioned at a selected depth in the borehole. Those times are corrected to vertical times and called seismic times. They are used as a reference to calibrate the sonic log through the drift curve corrections.

The drift is the difference, at one depth, between the seismic time and the integrated sonic transit time. Drift is made equal to zero at an arbitrary depth, the tie point.

3.1.2 Synthetic seismogram

In many areas the synthetic seismogram is a reasonable approximation to actual seismic records and is therefore useful in correlating reflection events with particular horizons. Comparison of the actual and synthetic seismograms may also help to determine which events represent primary reflections and which represent multiples (*Telford et al., 1976*). The use of acoustic logs to generate a synthetic section, via the convolution of the earth's

reflectivity series with a wavelet, is a fundamental aid in identifying and predicting how stratigraphic variations may affect a seismic record.

The production of a synthetic seismogram is illustrated in Figure 3.1. Acoustic impedance is calculated by multiplying seismic velocity and density, and reflection coefficients are calculated from impedance changes. The reflectivity coefficients are convolved with a suitable zero or minimum-phase wavelet (*Badley, 1985*). In this synthetic which is created by Occidental Company, they used a Ricker wavelet with a frequency (30 Hz) in zero and minimum phase and bandwidth, similar to the seismic sections, the low band pass filter and high band pass filter 8-12-60-70 respectively.

Calibration of the sonic data was only possible for the D1/103 well, since the D5/103 well lacked checkshot information. Where density information was absent the *Gardner et al., (1974)* equation can be used :

$$\rho = 0.23 * V^{0.25}$$

where :

ρ : density in gm/cc.

V : velocity in m/s.

This equation relating density (ρ) to velocity (V) is considered adequate for sedimentary sequences. Fig. 3.1 (well D1/103) displays the full suite of plots relevant to the synthetic seismograms (namely the sonic, calibrated sonic, density, acoustic impedance, reflectivity functions for primaries, primaries plus multiples and multiples only. The basic assumption in generating the spikogram is that for plane waves propagating vertically through a horizontally stratified elastic medium, reflectivity is governed solely by acoustic impedance contrasts at the layer interfaces. All theoretically possible

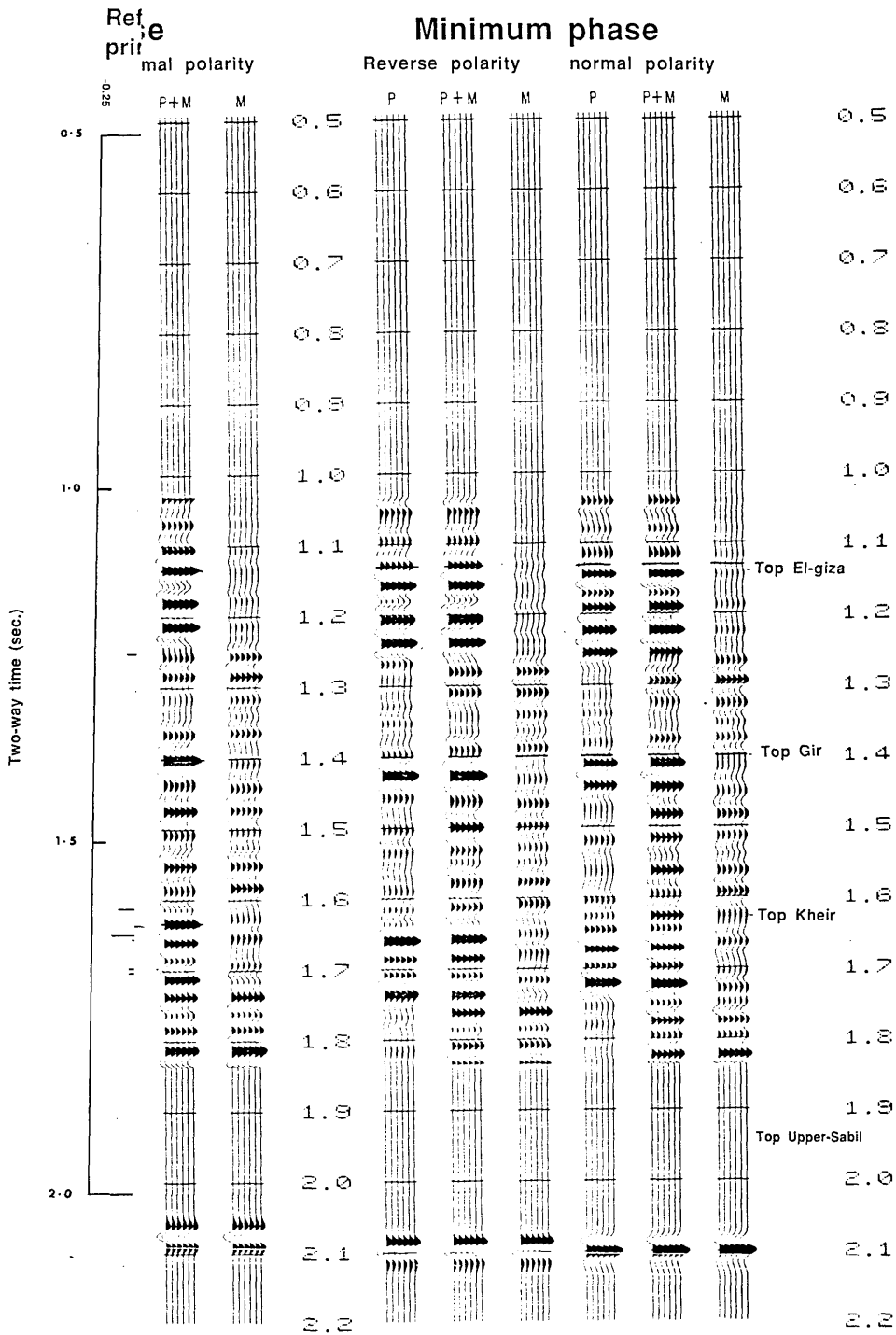
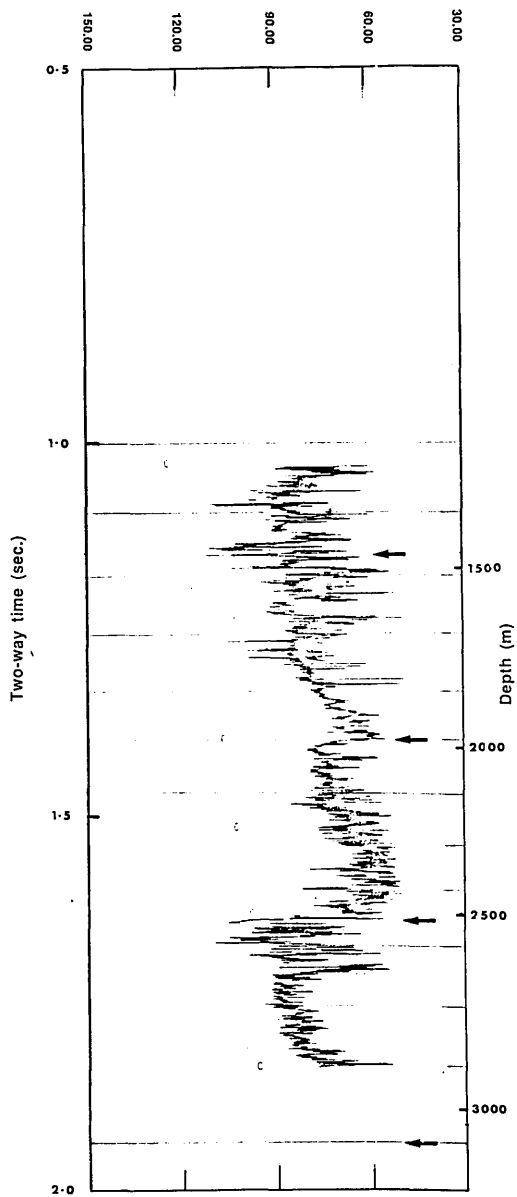
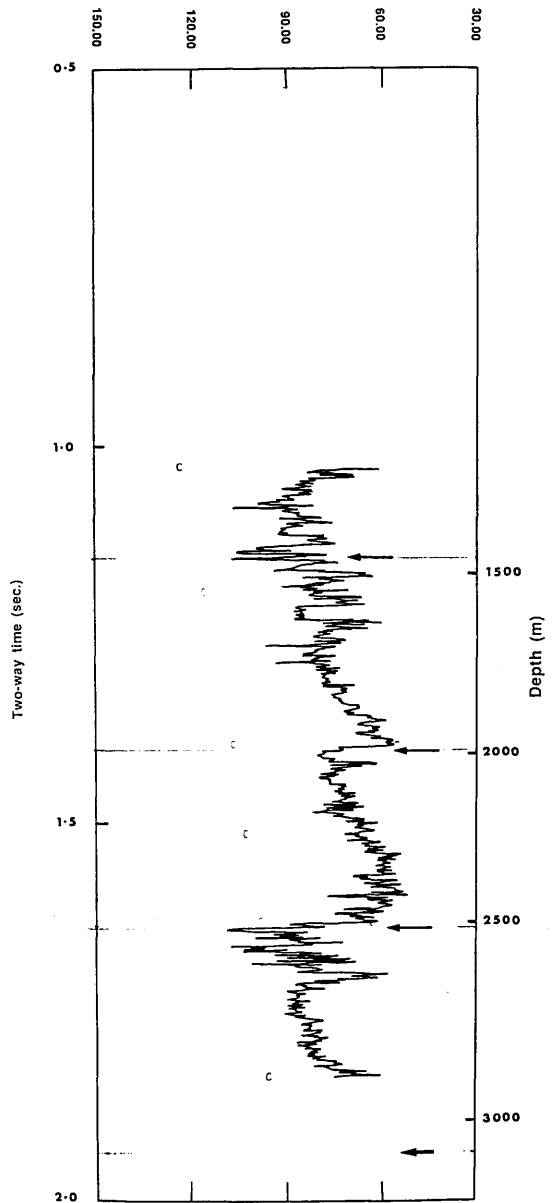


Fig. 3.1 Synthetic seismogram displays derived from density and interval velocity logs (well D1/103)

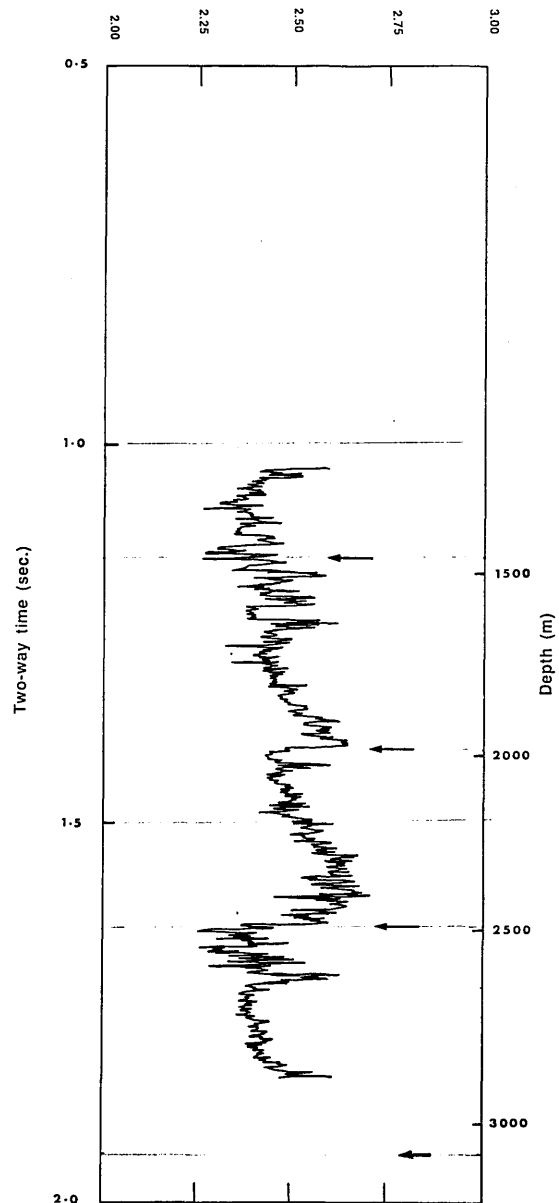
Sonic log in depth
uncalibrated



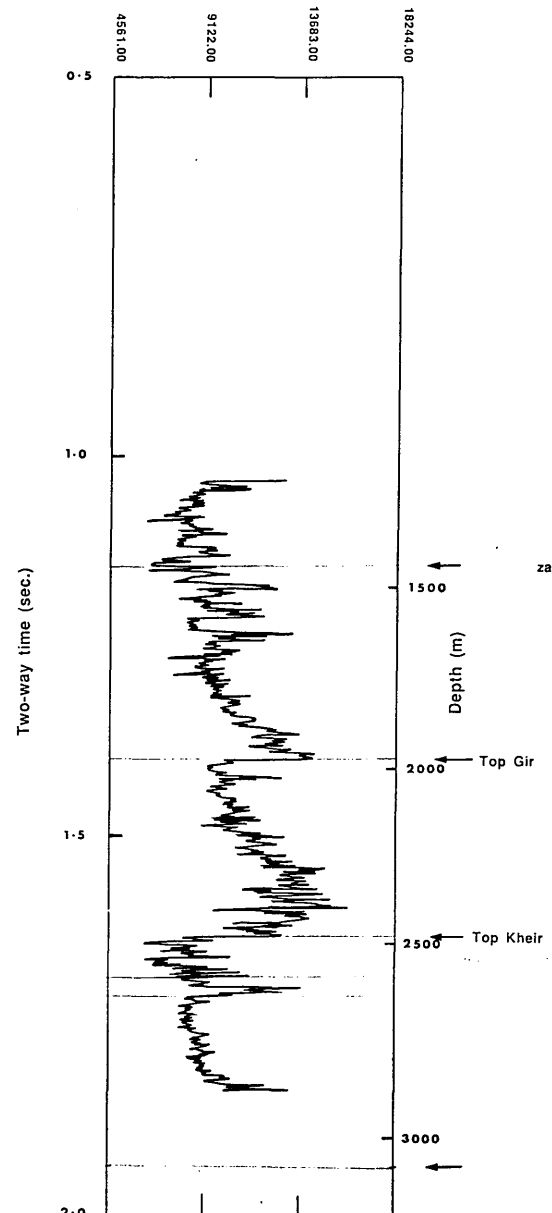
Sonic log in time
calibrated



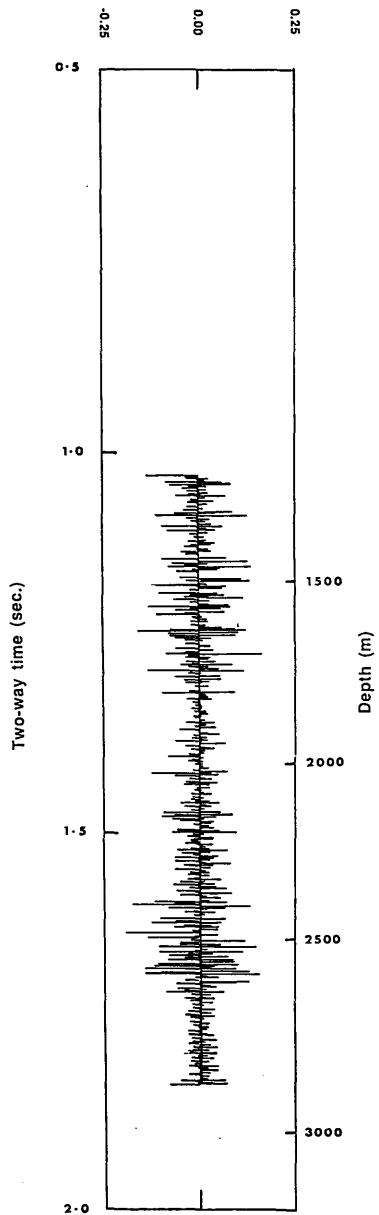
Density log in time
calculated



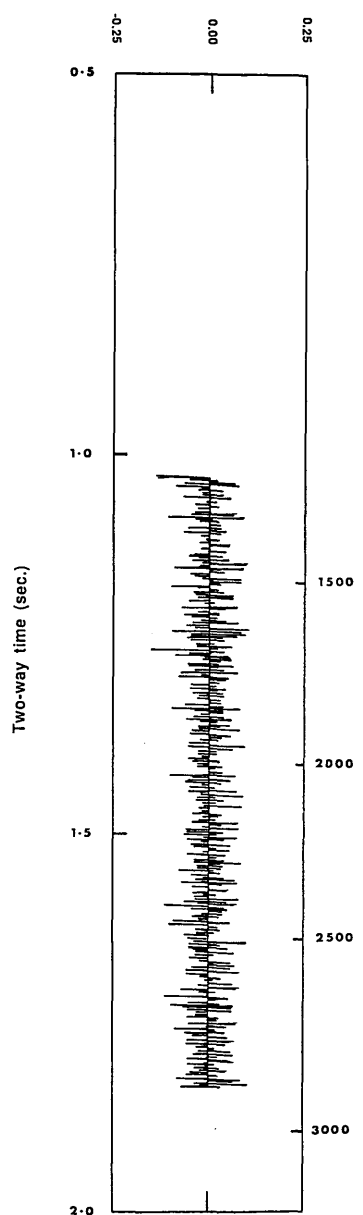
Acoustic impedance
in time



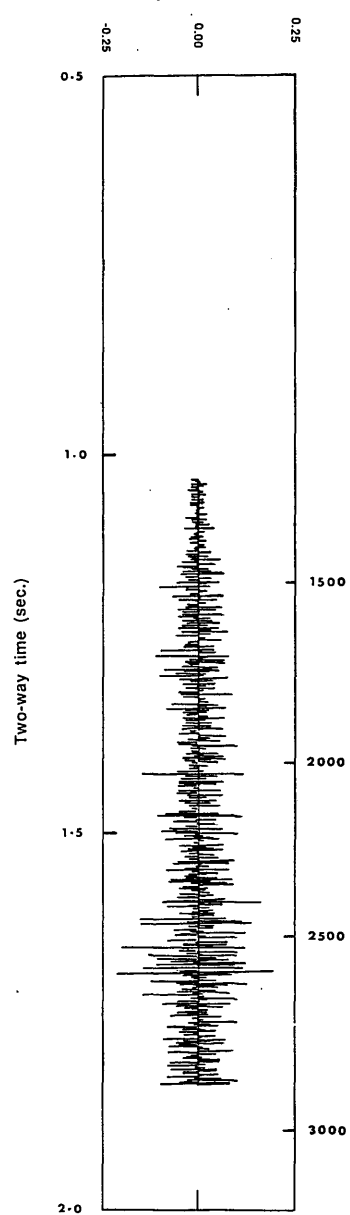
Reflectivity
primaries only



Reflectivity
primaries + multiples



Reflectivity
multiples only



Zero phase

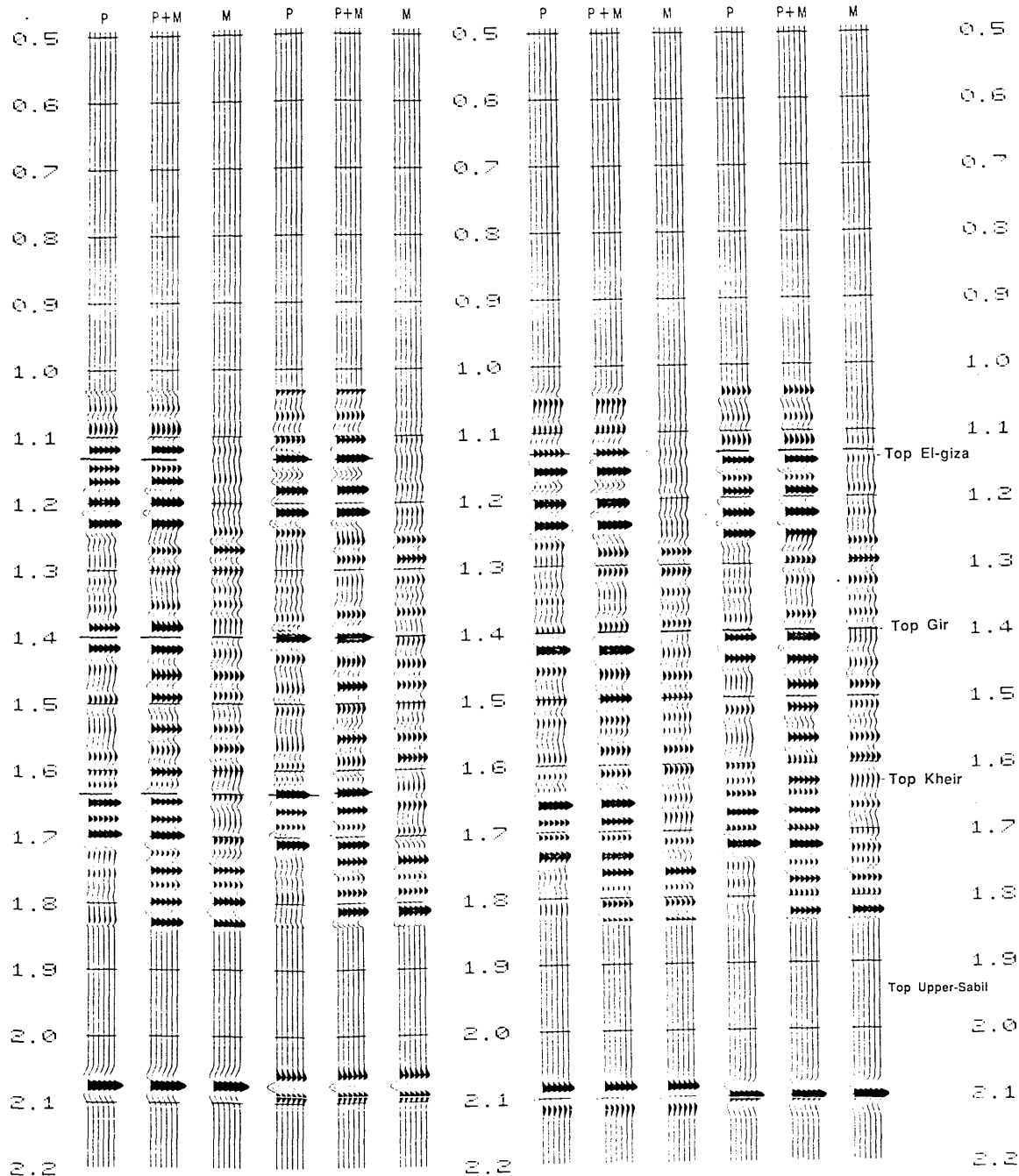
Reverse polarity

normal polarity

Minimum phase

Reverse polarity

normal polarity



multiple combinations that can occur over the duration of the seismic record are included.

Figure 3.1 shows the match of the zero phase, primaries only synthetics generated for the D1/103 well with their respective seismic section. Certainly Figures 3.1 & 3.2 reveal the well to seismic tie to match reasonably closely, particularly at the Lower Eocene and Upper Palaeocene levels. Again the synthetic to surface seismic match is fair in terms of the respective position of the events, together with relative amplitude signature of the key reflectors. The following flow chart (Fig. 3.3) shows the procedures used in generating the synthetic seismograms :

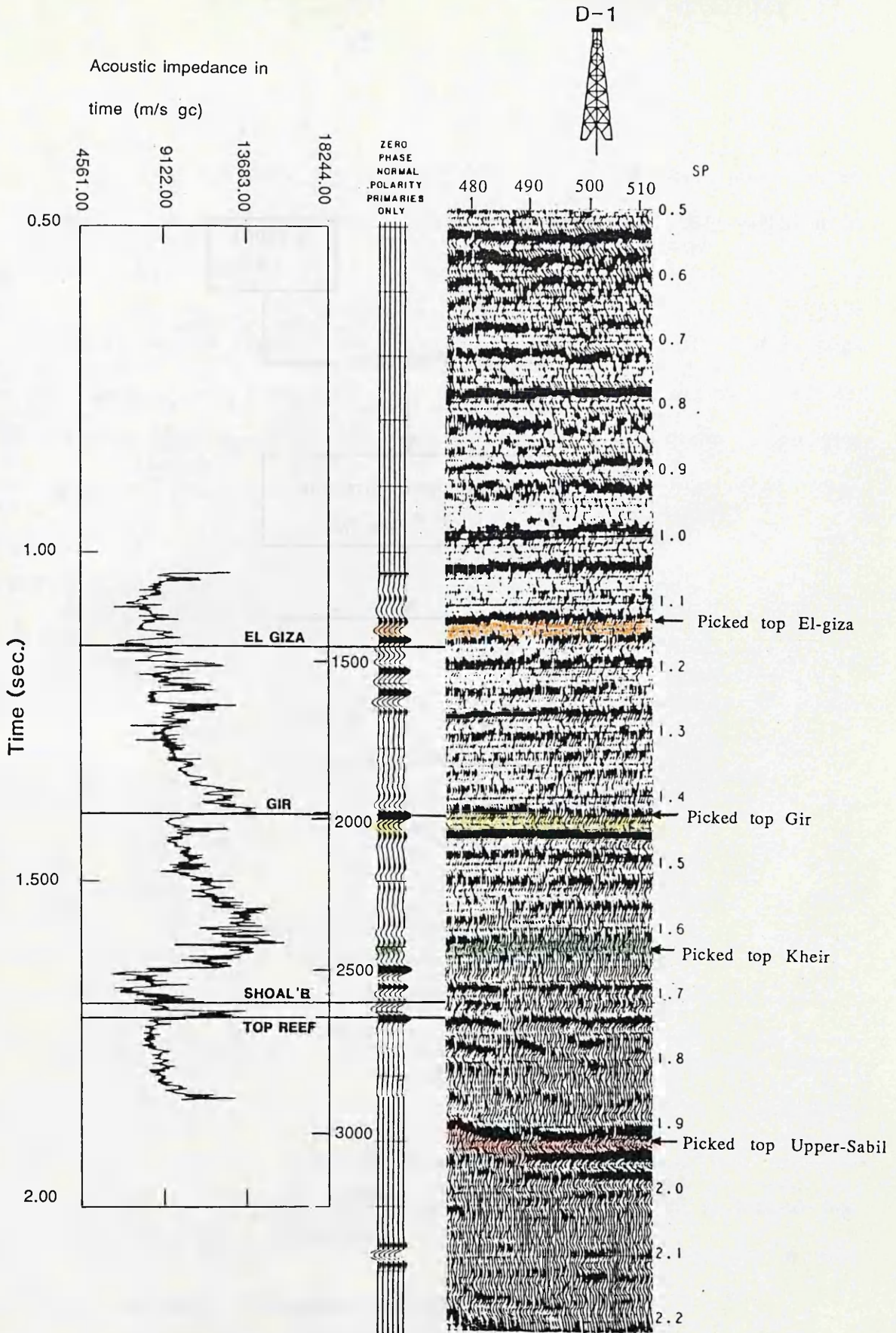


Fig. 3.2 Acoustic impedance / Synthetic / Seismic correlation between line U-14 and well D1/103.

3.1.3 Well to seismic tie

The tying of well and seismic data is an essential step in an interpretation, and the process begins with an analysis of the data collected in the well (*Badley, 1989*).

Comparing the two-way times observed in the well (D1/103) with those in the seismic sections close to the well reveal systematic mis-ties up to 40 ms. The following table shows the difference between the well and the seismic two way times :

Table (3.1) : Two-way time in well D1/103 and in seismic,
with the mis-ties.

Formations	Depth (m)	T.W.T (ms) (well)	T.W.T (ms) (seismic)	Mis-tie (ms) (well-seismic)
El-giza	1460	1144	1140	+4
Gir	1982	1400	1410	-10
Kheir	2516	1634	1630	+4
Upper-Sabil	2992	1920	1930	-10

Figure 3.2 reveals the well to seismic tie to match reasonably closely, particularly at the Lower Eocene and Upper Palaeocene levels, as mentioned in section 3.1. It shows the match of the zero phase, normal polarity synthetic seismogram to the relevant position of seismic line. As D1/103 is located just beyond the survey boundary it has been matched to the nearest in line location, at shot-points 480 to 510 in line U-14.

3.2 Event identification and selection

The following sections discuss the event identification procedures adopted, together with the selection of seismic markers most suited to reveal the stratigraphic detail of the area studied. In addition, the well data are reviewed in terms of log data, synthetic seismogram and time/depth constraints. The location of seismic lines and wells are shown in Chapter 1, Figure 1.2.

The criteria governing seismic event identification has been severalfold, based upon the relation of the well control with the seismic data, together with the evaluation of the seismic boundary conditions according to the principles of seismic stratigraphy.

As common with seismic practice, the time horizons selected for continuous interpretation are those which best facilitate the unravelling of the current geological picture, delineation the structure relief, and historical model of the area. In addition, where depth conversion is necessary, the horizons studied must also reflect comprehension of the velocity variations both spatially and temporally, such that the true structural attitude of the area may be realised. Inspection of the lines through boreholes was the first step in picking the horizons. The well logs not only give the important geological information, but also indicate where good reflections are expected. The picking of horizons was started at line U-14 which passes near the well D1/103. In fact most seismic lines pass through this well. The following events and their ages have been interpreted.

Event	Age
El-giza	Middle Eocene
Gir	Lower Eocene
Kheir	Lower Eocene - Upper Palaeocene
Upper-Sabil	Upper Palaeocene

Figure 3.4 shows the main interesting horizons with their thickness approximately (according to the tops in well D1/103), geological age, lithology, and seismic events.

The horizons have been tied to wells drilled in the area by using the velocity function obtained from the well velocity survey (Fig. 3.7). They are first mapped on a cross-section and then this section is compared with the sections for the cross lines, in order to identify the same horizons on the cross lines, identification is made on the basis of seismic character and arrival times. The horizons are now carried along the cross-lines and ultimately along all lines in the prospect to the extent that the quality of the data permits. The horizons can be carried all the way around a loop (*Telford et. al.*, 1976). The following paragraphs provide a discussion of data quality and event characteristics, and seismic parameters which will be discussed in more detail in Section 3.3.2 as they pertain to each of the horizons interpreted.

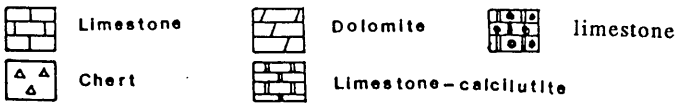
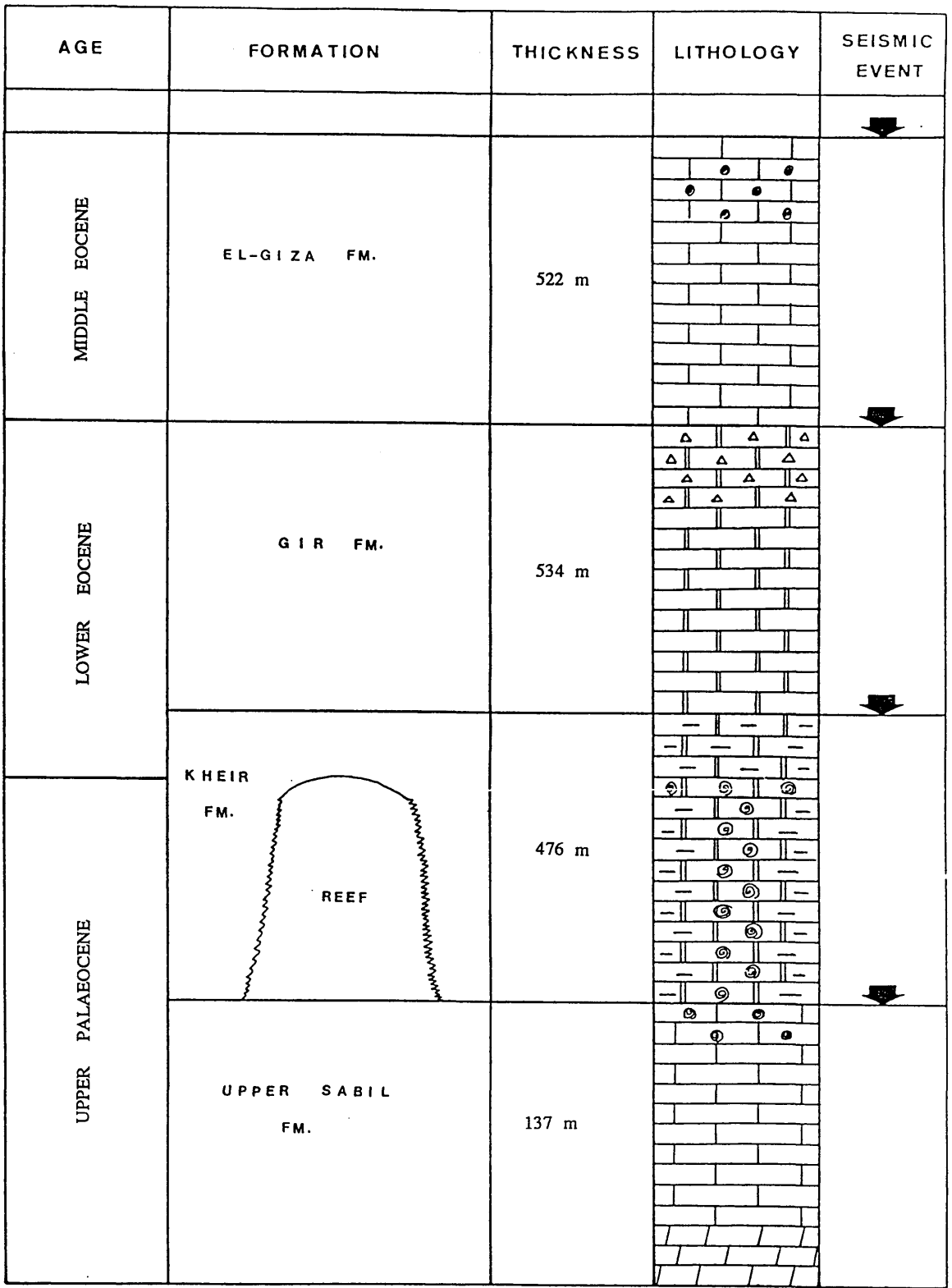


Fig. 3.4 Stratigraphic section and main seismic reflectors.

Top El-giza horizon

The top El-giza (Middle Eocene) is the shallowest event interpreted. It is represented by a conformable, though poorly defined trough with good to fair continuity and high to medium amplitude, which can be carried over the entire area. The El-giza Formation is a relatively homogeneous unit over 275 m thick, for which the two-way travel time is about 1.14 s near the well D1/103, increasing slightly away from the well. The El-giza horizon, together with the Gir, reflect drapes because of differential compaction of strata in the build-up. The effects of drape generally die out stratigraphically upwards.

Top Gir horizon

This reflector marks the top of the Lower Eocene, it has been picked as an single trough immediately above the peak which is representative of the geological tie. Although a low frequency event, good continuity and high to medium amplitude, the data quality was good throughout the survey. As at the El-giza level, the event is conformable and present over the entire survey. Being deeper the dips encountered were also greater due to compactional effects.

Top Kheir horizon

The closest continuous event to the top of the structure is the top Kheir marker. It is represented as a comparatively medium/high frequency continuous peak, with good continuity and medium amplitude. As shown in Figure 3.2 the event does not show a strong reflection in the seismic section. This is because the interference between the seismic responses from closely

spaced acoustic impedance boundaries, which always occur when the reflections from different reflectors overlap.

Top Upper-Sabil horizon

The top Upper-Sabil was the deepest horizon to be interpreted. It is a fairly low frequency event clearly defined by a trough, and was carried across the survey with good certainty. The Upper-Sabil reflection has a high amplitude with a positive reflection coefficient, and high continuity over large area in the field, that is due to the change of the depositional sequence from shale (Kheir) to carbonate (Upper-Sabil) under low energy conditions. This event shows the pull-down beneath the structure, due to low velocity. As we have shown in Figure 3.2, the synthetic does not go as deep as this horizon. The Upper-Sabil represents a deep-water limestone facies characterized by a high amplitude and continuity. No obvious faulting was observed on any of these events.

3.2.1 Preliminary interpretation

In well D1/103 marked velocity breaks occur :

- (i) Top El-giza
- (ii) Top Gir
- (iii) Top Kheir

These are shown in the continuous velocity log, Fig. 3.5. Each of these boundaries should therefore produce a seismic reflection which can be identified on the seismic data.

The second stage in tying in the well data is to calculate the two-way seismic travel time to the reflecting boundaries. For this purpose an integration of the sonic log is performed. This gives (after calibration) the total travel time from datum, which is then doubled to give a two-way time (TWT) for each horizon of interest. From the synthetic seismogram which was generated in D1/103, Fig. 3.1 we can pick the main interesting horizons.

Reflecting horizons were identified on the seismic sections using coloured pencils. Starting from well D1/103, where most of seismic lines intersect, the four reflectors can be followed along all lines. In this way the interpretation gradually moves from the well, eventually to cover the total seismic survey in the area.

Table 3.2 and Figure 3.6 show the depth below the subsea datum, one-way time, interval and average velocities, which were calculated in well D1/103. The interval velocity was obtained by dividing the difference of the two reflector depths on the respective one-way times using the following equation:

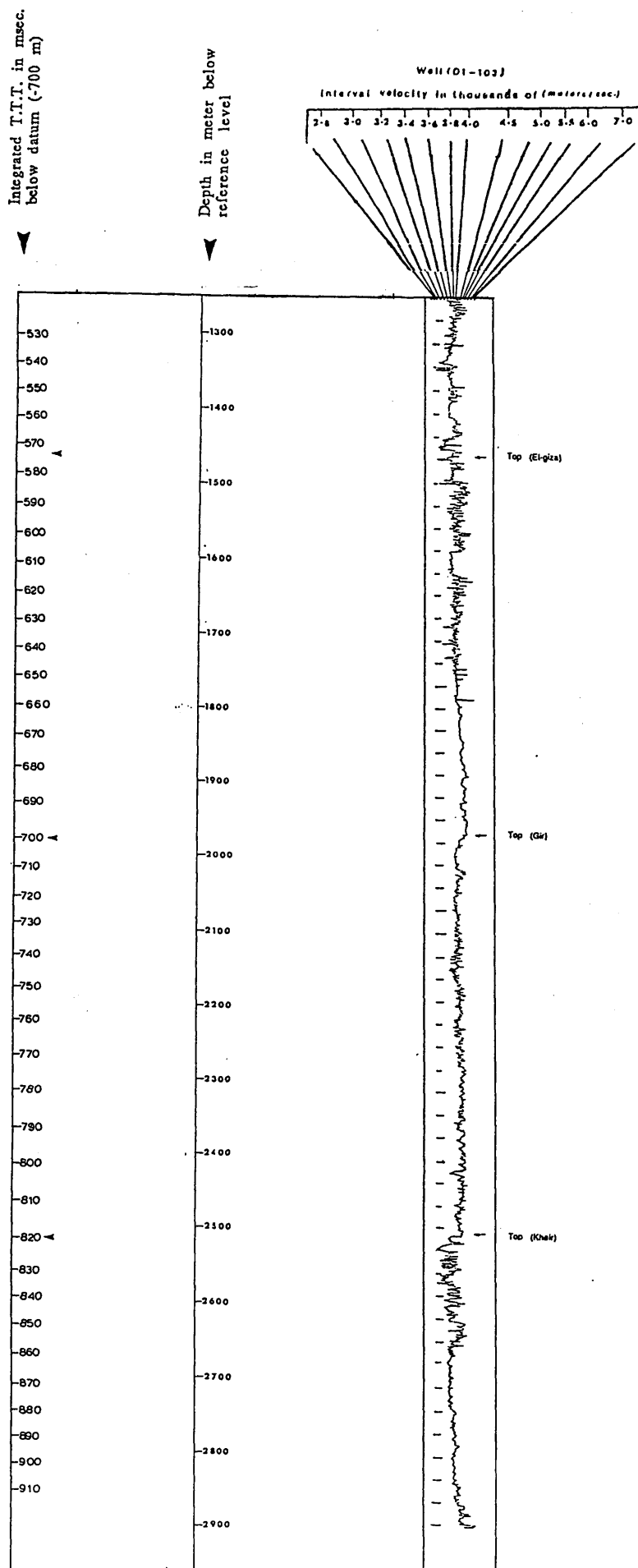


Fig. 3.5 Continuous velocity log (CVL) with depth in meters below reference level and the integrated total travel time in milliseconds below datum (-700 m), well (D1/103).

Table 3.2 : Depth, time, interval velocity, and average velocity in well D1/103.

Depth (m)	One-way time (s)	Interval velocity (m/s)	Average velocity (m/s)
-1257	0.515		2441
-1305	0.530	3200	2462
-1388	0.553	3609	2510
-1415	0.560	3857	2527
-1449	0.569	3778	2547
-1462	0.572	4333	2556
-1479	0.578	2833	2559
-1510	0.585	4429	2581
-1561	0.599	3643	2606
-1692	0.632	3970	2677
-1801	0.660	3893	2729
-1870	0.677	4059	2762
-1980	0.700	4783	2829
-2118	0.733	4182	2889
-2230	0.759	4308	2938
-2242	0.761	6000	2946
-2404	0.794	4909	3028
-2497	0.813	4895	3071
-2516	0.817	4750	3080
-2568	0.831	3714	3090
-2608	0.844	3077	3090
-2781	0.888	3932	3132
-2868	0.912	3625	3145
-2898	0.920	3750	3150

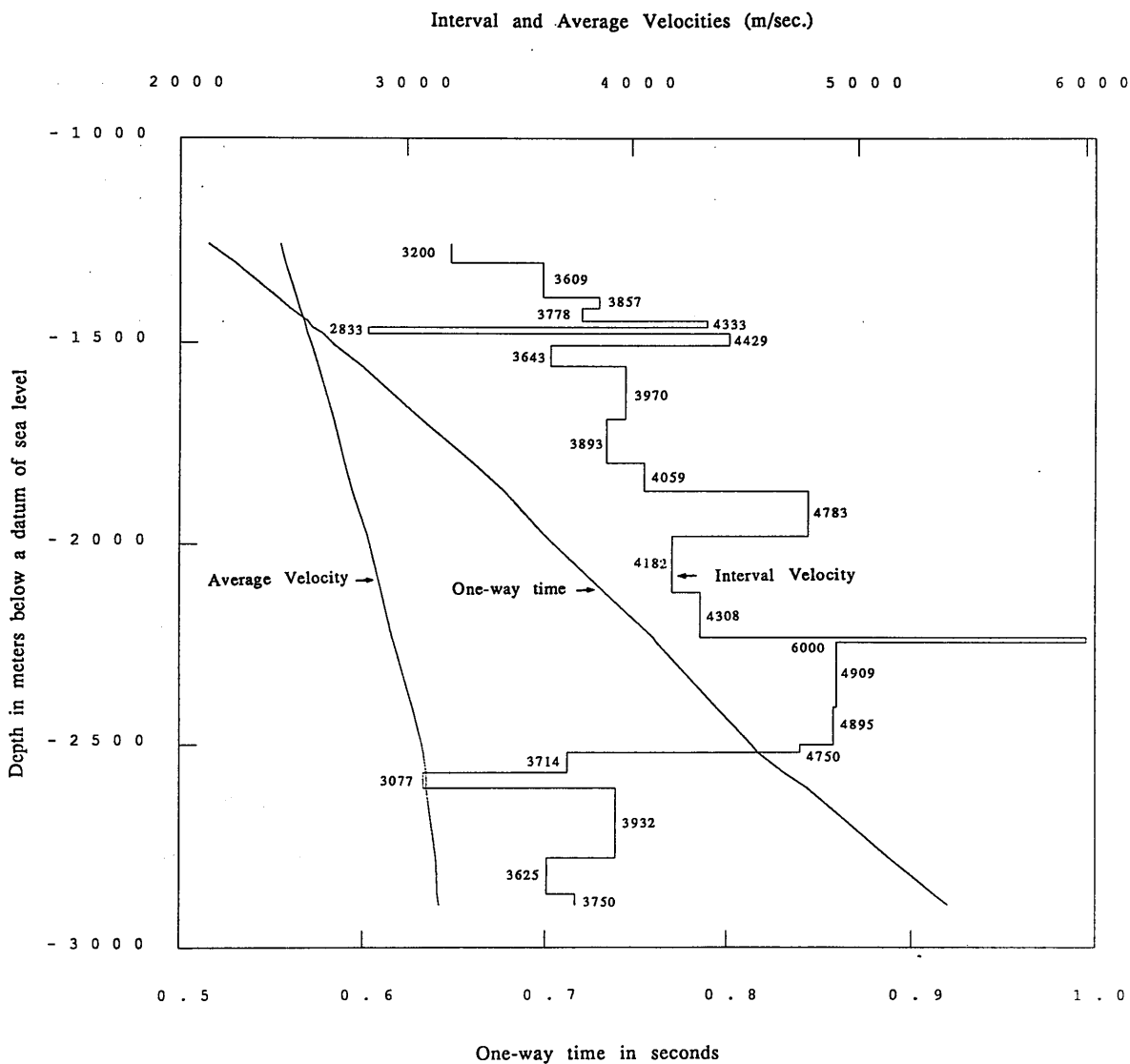


Fig. 3.6 Interpretation of the results : relations of time with depth, average velocity with time, and interval velocity with depth (D1/103). Datum is sea level.

$$V_{\text{int}} = \frac{Z_n - Z_{n-1}}{t_n - t_{n-1}} \dots\dots\dots 3.2$$

where :

V_{int} : Interval velocity (m/s)

Z_n : The lower reflector depth (m)

Z_{n-1} : The upper reflector depth (m)

t_n : One-way time to the lower reflector (s)

t_{n-1} : One-way time to the upper reflector (s)

The average velocity was calculated by dividing the depth (Z) of a reflecting surface below a datum by the observed one-way reflection time (t) from the datum to the surface (*Dobrin, 1976*), using the following equation :

$$V_{\text{av.}} = \frac{Z}{t} \dots\dots\dots 3.3$$

Where :

$V_{\text{av.}}$: Average velocity (m/s)

Z: Reflector depth (m)

t: One-way time of the reflector (s)

3.3 *Interpretation and mapping*

A very important step in the seismic reflection interpretation is the conversion of reflection times to depths, and for this we need to know the velocity distribution in the area. Well velocity surveys are always more accurate than seismic velocities.

The interpretation of seismic data in geological terms is the objective and end product of seismic work. once a final selection of seismic data is made, a new shot-point map was prepared showing only those lines used in the interpretation, (see Chapter 1, Fig. 1.2).

3.3.1 *Seismic sections*

Figure 3.7 shows the locations of seismic lines reproduced as figures, and the boreholes. The seven interpreted seismic sections are shown in Figure 3.8. The lines selected for interpretation are U-14, U-51, U-53, U-54, U-25, U-6 and U-9. The display datum is mean sea level, and all seismic sections are of normal polarity. The final stacked sections represent the seismic response of the subsurface, but in most cases, is not an accurate geological picture.

The previous seismic sections are not migrated. It is well known that most stratigraphic evidence of onlap, reefs and so on, involves angularity between two or more reflections, and hence the reflection elements will not be correctly located with respect to each other unless the data are migrated. So migration is essential, and without it the seismic interpreter is faced with the problem of predicting true subsurface structure from the distorted image seismic time section, especially for complex structures.

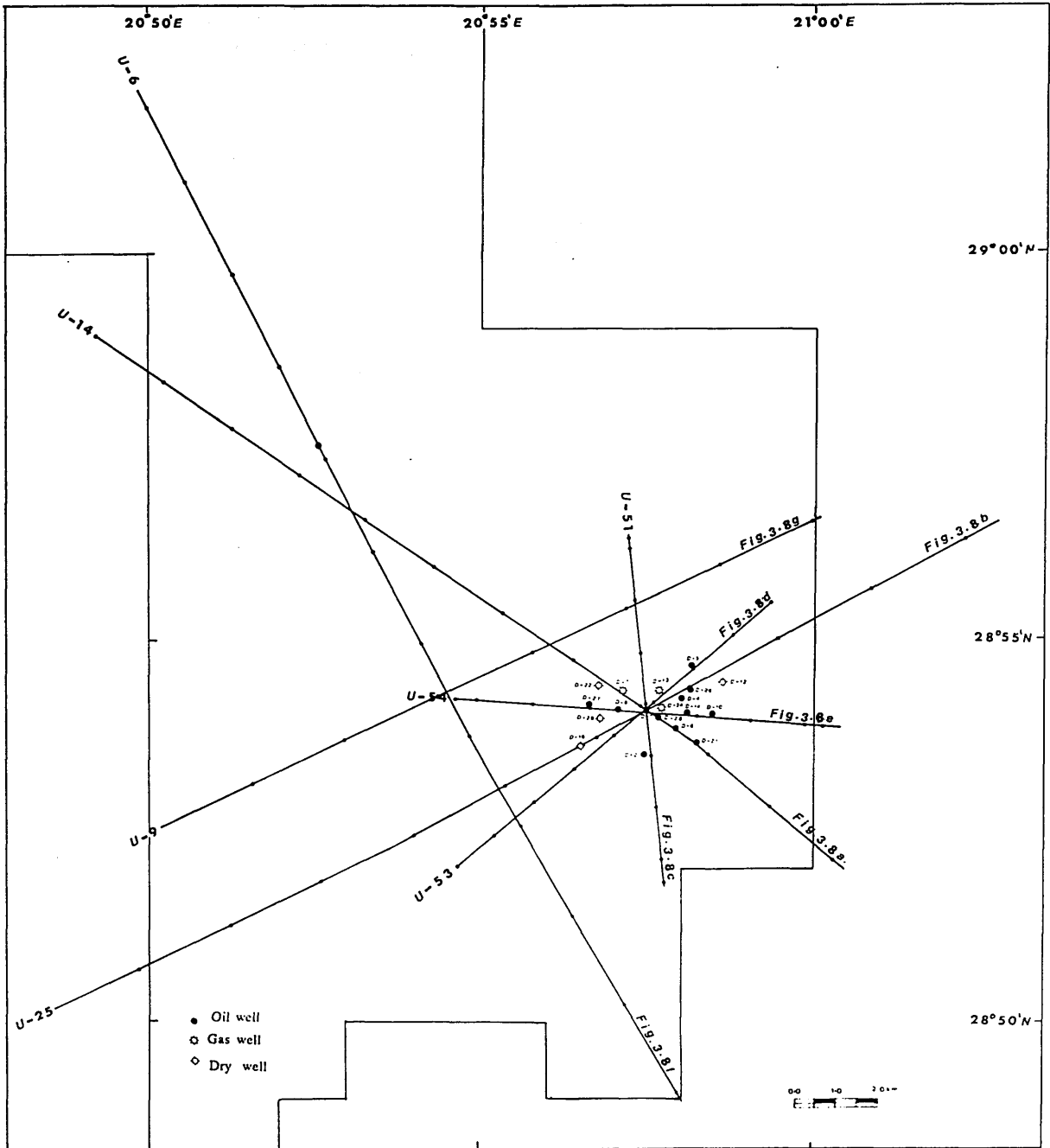


Fig. 3.7 Location map showing seismic sections reproduced (as figures).

Seismic Interpretation

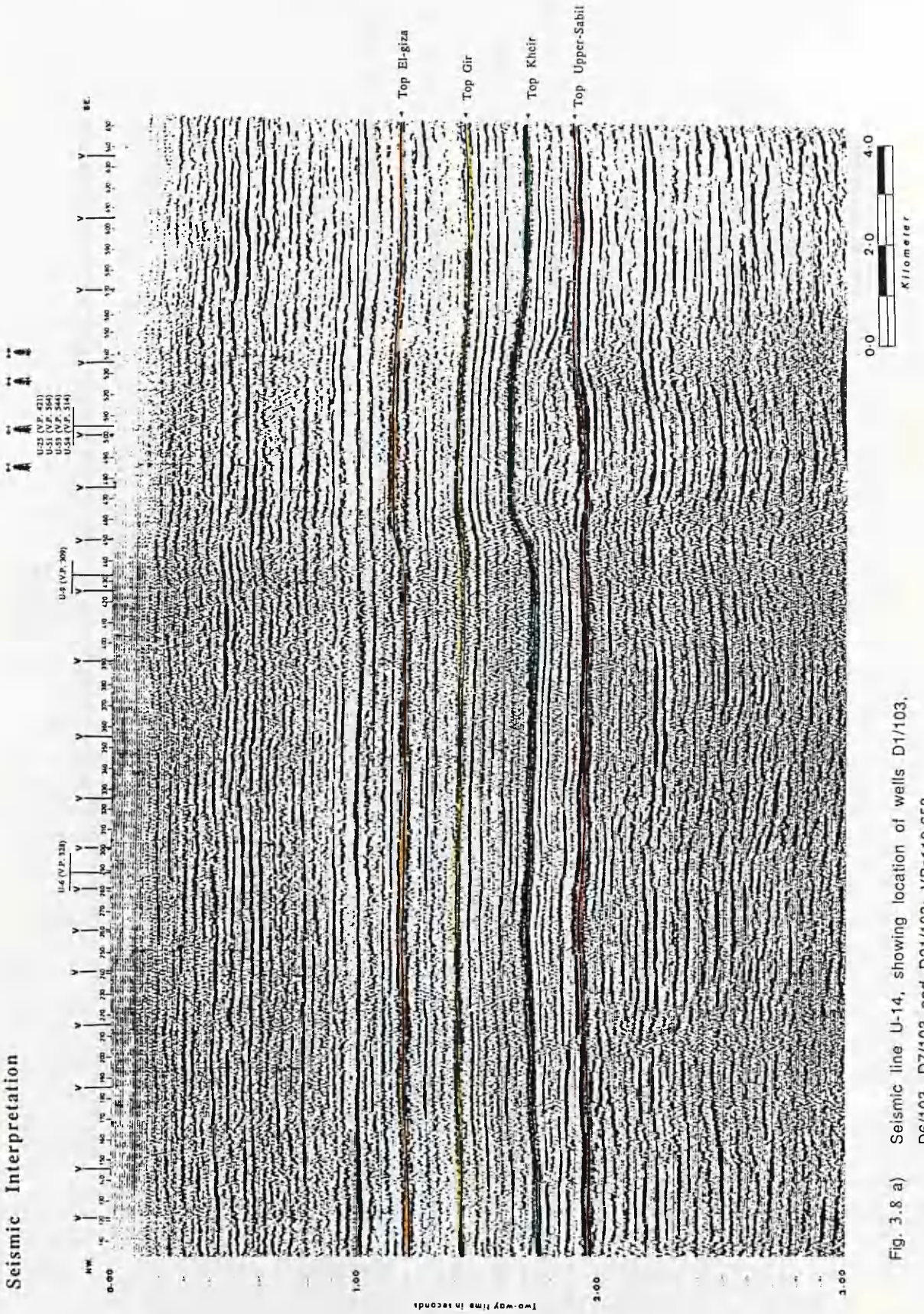


Fig. 3.8 a) Seismic line U-14, showing location of wells D1/103, D6/103, D7/103 and D21/103; VPst110-650.

Seismic Interpretation

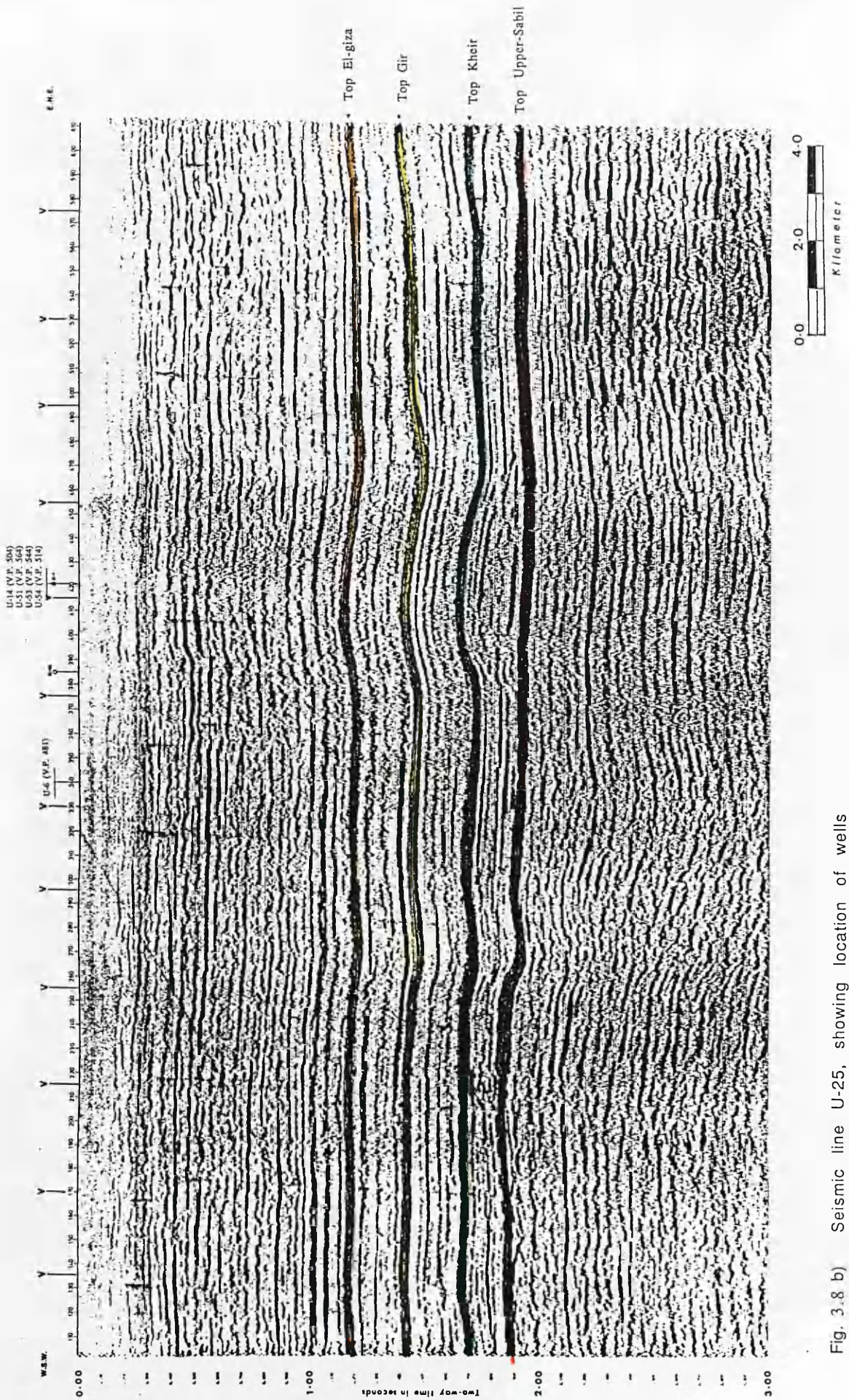


Fig. 3.8 b) Seismic line U-25, showing location of wells D1/103 and D16/103; VPs 110-610.

Seismic Interpretation

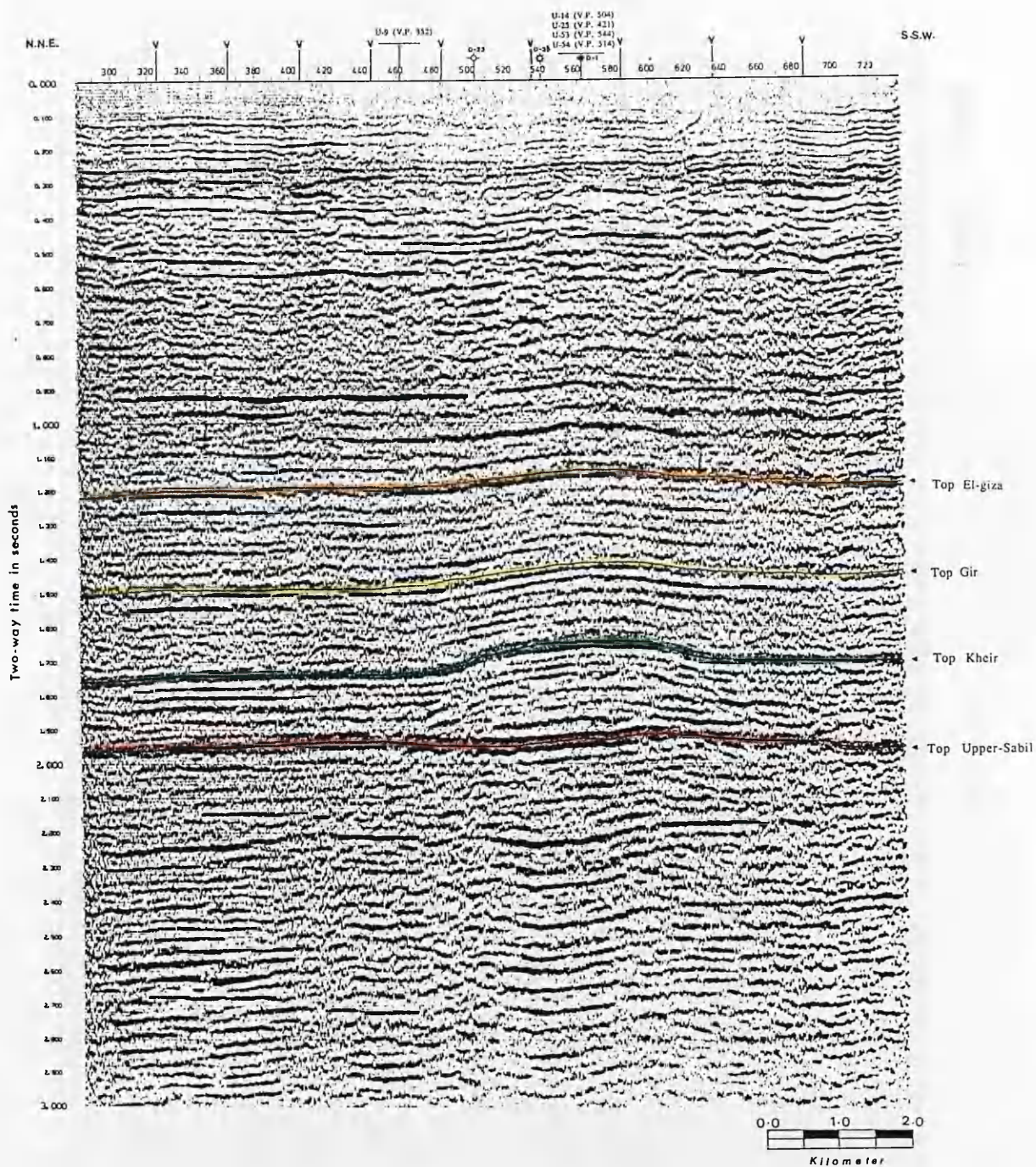


Fig. 3.8 c) Seismic line U-51, showing location of wells D1/103, D23/103 and D33/103; VPs 300-720.

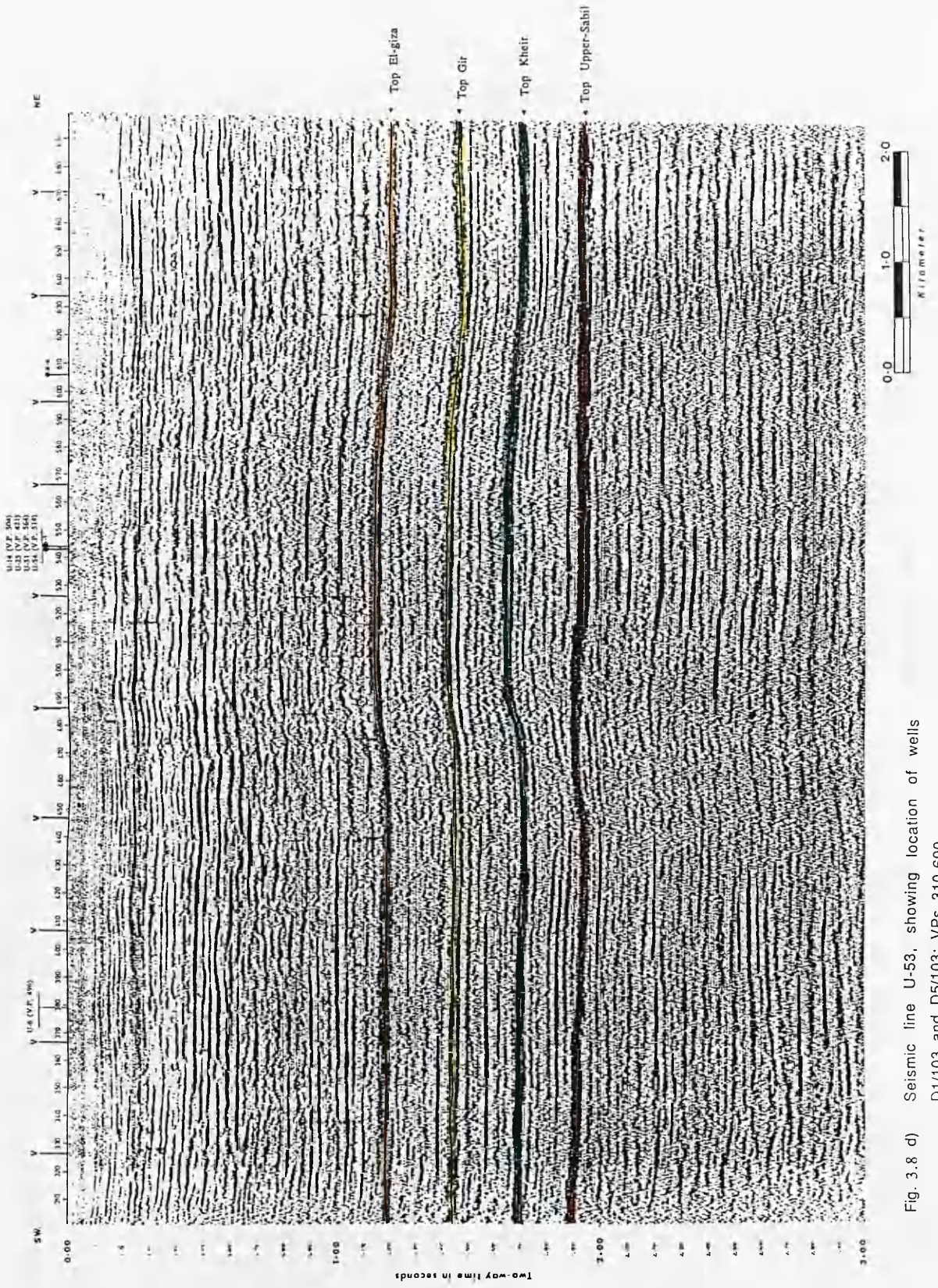


Fig. 3.8 d) Seismic line U-53, showing location of wells D1/103 and D5/103; VPs 310-690.

Seismic Interpretation

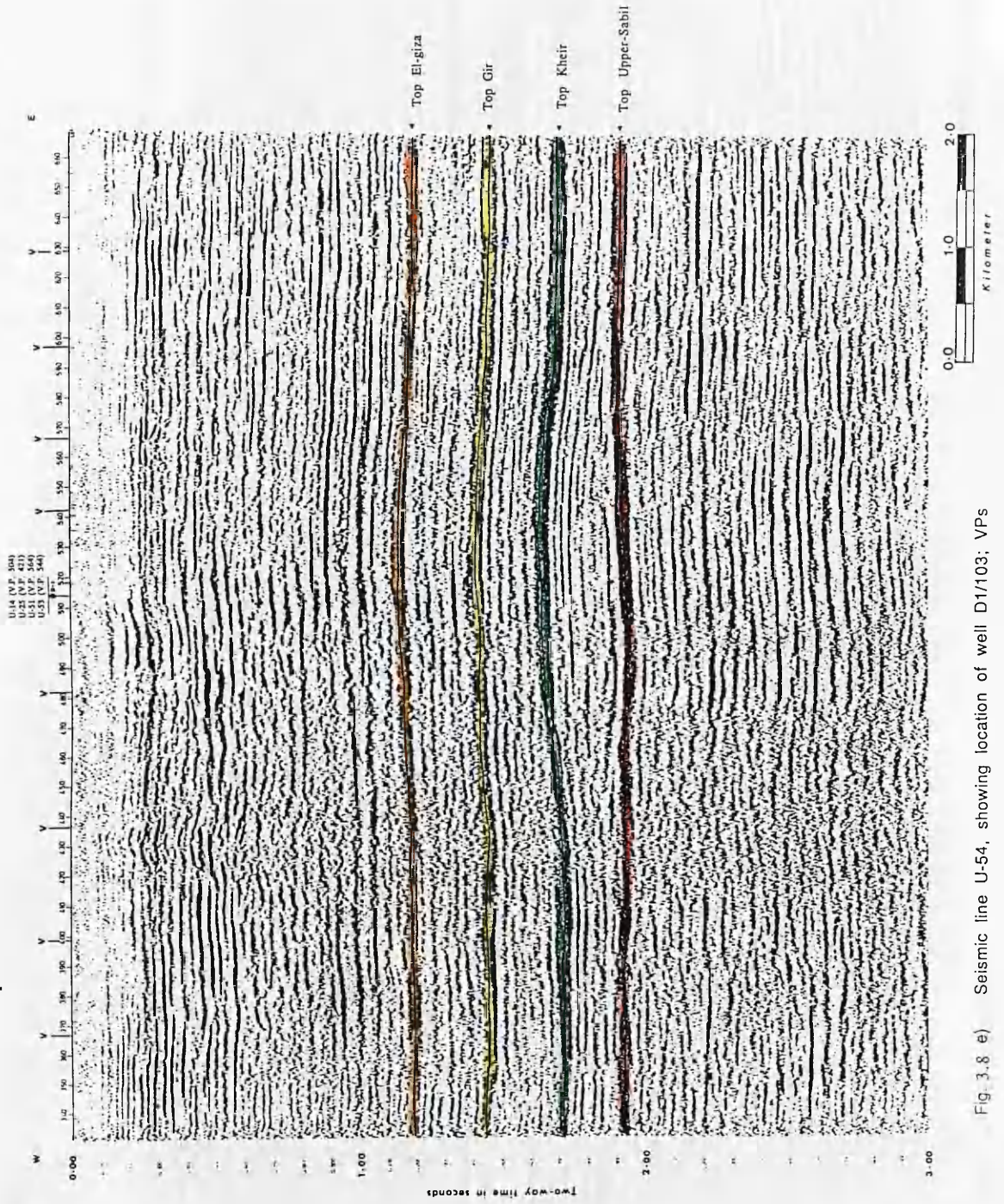


Fig. 3.8 e) Seismic line U-54, showing location of well D1/103; VPs 340-660.

Seismic Interpretation

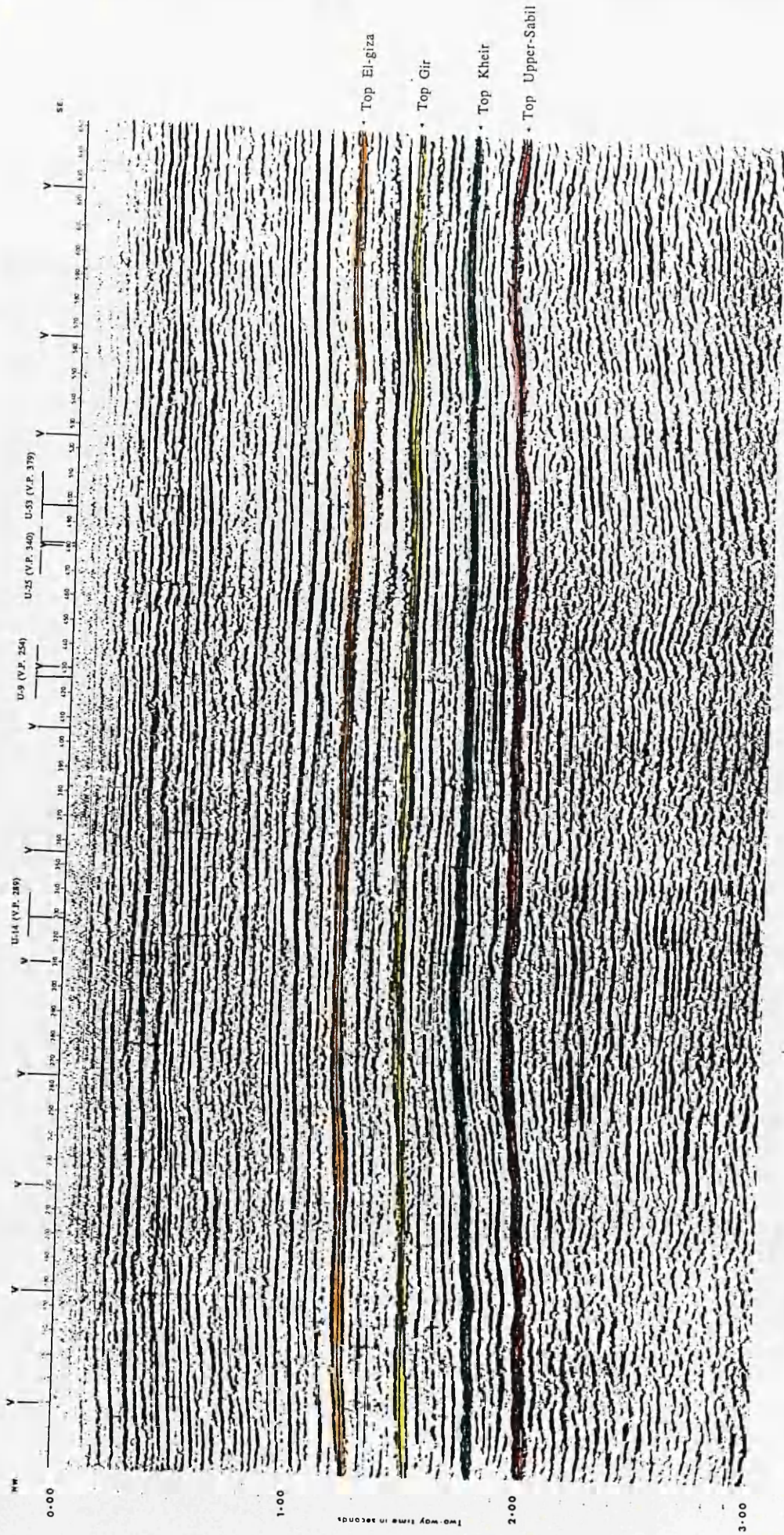


Fig. 3.8 f) Seismic line U-6; VPs 110-650.

Seismic Interpretation

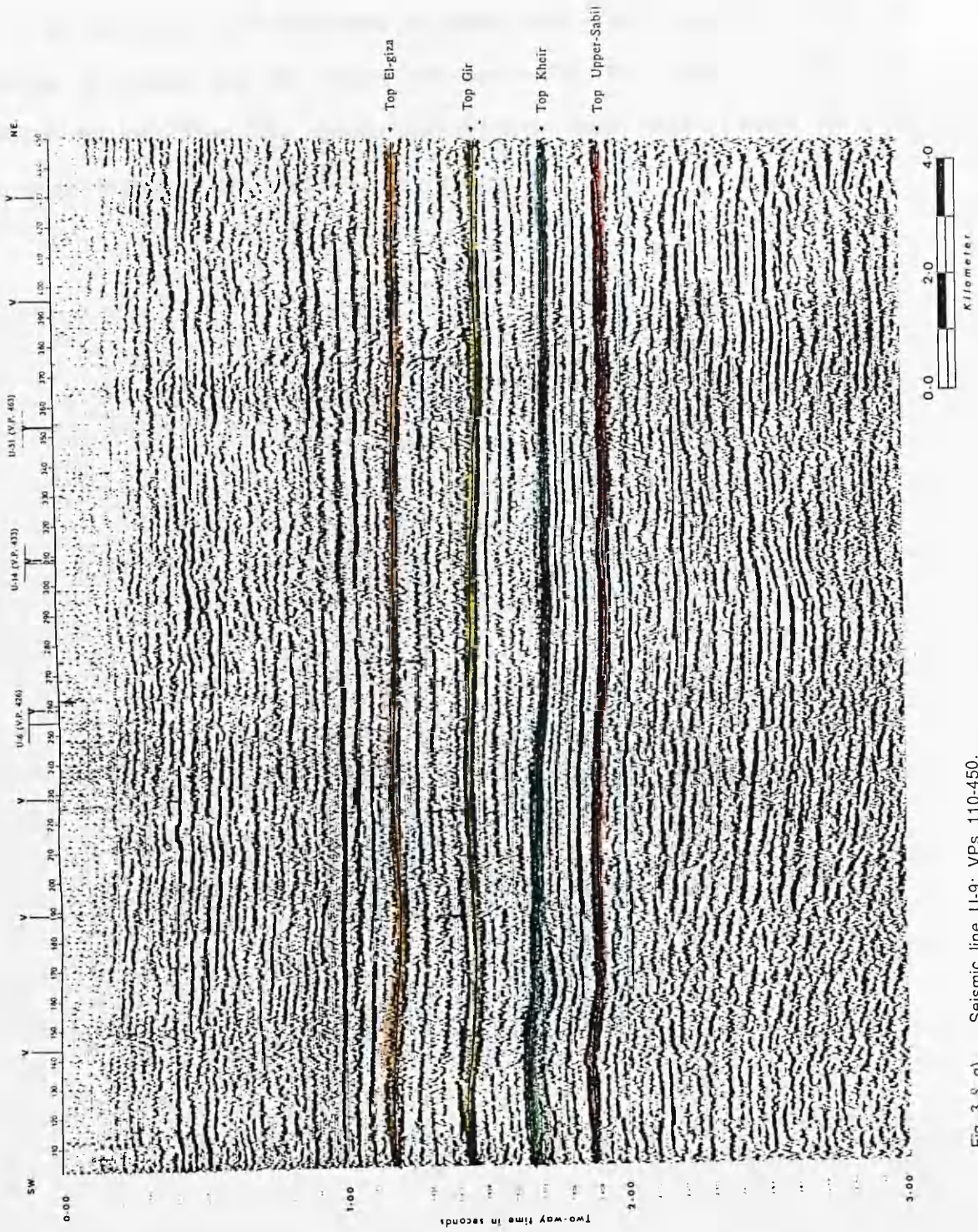


Fig. 3.8 g) Seismic line U-9; VPs 110-450.

In the Intisar "D" field case migration will not be essential, where the structure is simple and the layers are horizontal. It is easy to follow the selected horizons from the unmigrated sections. More details about the time and depth migration are presented in Chapter 5.

Tables 3.3 a, b, and c show the main acquisition, processing and display parameters.

(I) Acquisition

Table (3.3 a): The main acquisition parameters

Acquisition sequence	Parameters
(1) energy source vibroseis	16 s. sweep. 12-72 Hz.
(2) Instrument DFS V.	120 channel
(3) Filters low out high	128 Hz, 70 dB/oct.
(4) Format	SEG B 120 channel
(5) Gain	48 dB.
(6) Sampling rate	2 ms
(7) Record length	4 s
(8) Listening time	20 s
(9) Field spread	160 x 61120 2500 140 0 140 2500 m
(10) Station interval	40 meters
(11) V.P. interval	80 meters
(12) Geophone pattern	2 Rows * 12 geophones 12 m stagger 4 m interval Array length 56 m
(13) Source pattern	4 vibroseis 8 sweeps/record 24 m. stagger 8 m interval Array length 80 m

(II) Processing

Table (3.3 b) : The main processing sequence

Processing sequence	Parameters
(1) Demultiplex	From 9 track SEG B to 9 track SEG Y. Resampled to 4 ms and cross-correlated.
(2) Gain	T** 1.5 Spherical divergence correction from 0 to 4 s.
(3) Edit	Drop noisy traces. Apply line geometry.
(4) Deconvolution	160 ms. operator length : 24 ms Gap. Derived : 500-3000 ms near, 1200-3500 ms far, 3% with noise.
(5) Scale	Single window trace equalisation.
(6) CDP sort	Traces sorted into CDP Gathers.
(7) Static	Correction to near surface floating datum statics derived from intersecting lines.
(8) N.M.O.	Normal moveout correction : velocities picked from constant velocity stack.
(9) Mute	Distance/time muting pairs (meters/ms) (100,0) (200,140) (800,700) (1300,1400) (2500,1900).
(10) Statics	Static corrected to datum of mean sea level. Elevation velocity of 2000 m/s used
(11) Scale	500 ms. Sliding window, 250 ms move up.
(12) Autostatic	Surface consistent automatic residual statics using a 700-2500 ms window and a maximum allowable static of 30 ms.
(13) Stack	Nominal 30 fold stack.
(14) Filter	Band pass filter 8-12-60-70 Hz.
(15) Equalization	Time variant equalization using windows of 0-1600, 1600-3000 ms.

(III) Display

Table (3.3 c) : The display parameters

Display	Parameters
Recording polarity	SEG.
Display polarity	Negative values plotted white
Vertical scale	7.5 in/s
Horizontal scale	12.5 traces/cm 1 : 25,000

3.3.2 Seismic facies analysis

Seismic facies analysis is the description and geological interpretation of seismic reflection parameters, including, configuration, continuity, amplitude, frequency, and interval velocity. Each parameter provides considerable information on the geology of the subsurface. (*Vail et al.*, 1977).

By combining the analysis of stratal relationships with the attributes of the individual reflector, it is often possible to build up quite a detailed picture of the subsurface geology, (*Badley*, 1989).

The objective of seismic facies analysis is to quantify and interpret seismic parameter variations caused by geological changes within seismic sequences and system tracts (*Bally*, 1987).

Figure 3.9 combines the seismic horizons (line U-51) and well stratigraphy (D1/103). Line U-51 is the nearest line to this well (100 m). As we can see, some stratigraphic tops have no seismic response at the well location,

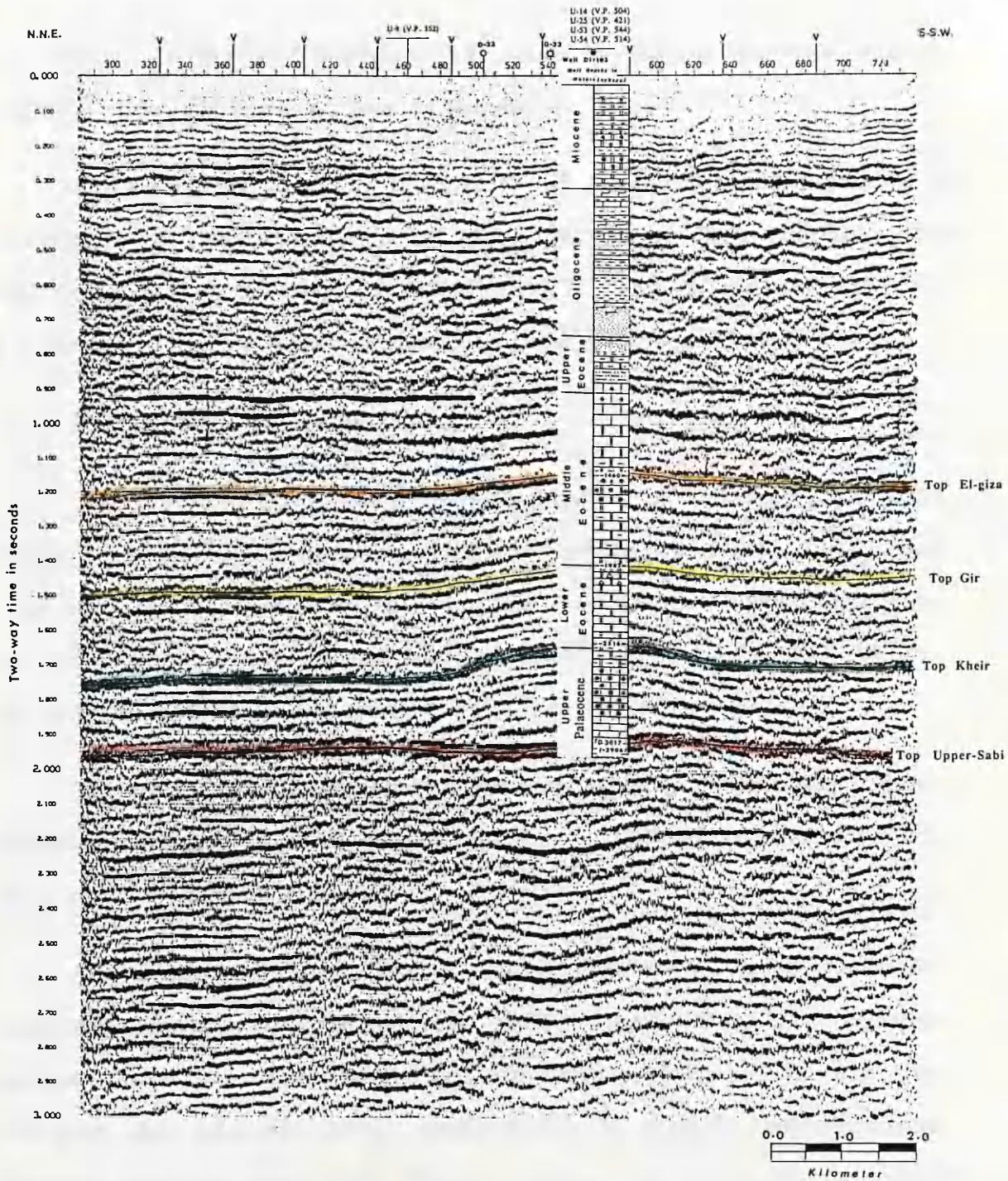


Fig. 3.9 Correlation of seismic horizons (line U-51) and well stratigraphy (D1/103).

for example in the top Oligocene. This may be because the two seismic sequences have the same acoustic impedance.

The seismic sections will be divided into three major parts according to the strength of reflections; the upper part (Miocene to Upper Eocene) from zero time to 1 s, the middle part (Middle Eocene to Upper Palaeocene) from 1 s to 2 s and the lower part (Upper Palaeocene to Lower Palaeocene) from 2 s to 3 s.

(i) Reflection configuration

The reflection configuration is the shape of a reflection or surface (Badley, 1989). The reflection configuration reveals the gross stratification patterns from which depositional processes, erosion, and palaeotopography can be interpreted. The seismic reflection configuration is the most obvious and directly analyzed seismic parameter (*Vail et al.*, 1977).

The upper part (Miocene to Oligocene) exhibits a hummocky seismic reflection configuration. This pattern indicates a uniform rate of deposition on a stable basin plain setting.

The middle part (Middle Eocene to Upper Palaeocene), shows the parallel reflection configuration, as in the shallow part. But the reflection configuration is convex upward (drape) and onlap is clear in this part (Fig. 3.9) from shot point 485 to 630, which makes the shape of reflections quite different from the upper part. These reflections are interpreted as strata forming elevations rising above the general level of the surrounding strata (mound shape), as a result of organic growth.

These reflection configurations (draped and mounded) occur in response to facies deposited with carbonate shelf/platform environment

(*Brown & Fisher, 1980*). Table 3.4 shows the summary of seismic facies characterized by mounded and draped reflection configurations (from *Vail et al., 1977*).

The lower part shows parallel reflection configuration. Pull-down is clear in the sections, due to low velocity.

(ii) Reflection continuity

Continuity can be interpreted in geological terms as lateral changes in acoustic impedance and hence in lithology (*Badley, 1989*).

The shallow reflections (Miocene to Upper Eocene) reveal moderate to good continuity.

The middle part (Middle Eocene to Upper Palaeocene) shows good continuity, including the mapped seismic horizons, El-giza, Gir, and Kheir. The top Middle Eocene reveals good continuity, with a very good strong reflection. The discontinuity appears (internal geometry of the structure) from shot-point 485 to 630 (Fig. 3.9). This is clear also in other sections which cross the structure. These continuous reflectors are characteristic of depositional environments where uniform conditions are laterally widespread. The lower part shows high continuity at the top of the Upper-Sabil limestone and good continuity at the top of the Sheterat shale.

Properties of Seismic Facies	Depositional Environments/Settings		
	Reefs and Banks: <i>shelf/platform margin, back shelf patch reefs and pinnacle/barrier reefs</i>	Submarine Canyon and Lower Slope: <i>proximal turbidities, slumped clastics</i>	Hemipelagic Clastics: <i>proximal basin and lower slope</i>
Reflection configuration	Mounded, chaotic, or reflector-free; pull-up or pull-down common	Mounded; complex and variable	Parallel; mirrors underlying surface
Lithofacies and composition	Shallow-water carbonate biogenic buildups; may or may not exhibit reef-forming framework	Sand and shale submarine fans; complex gravity-failure fans or mounds; turbidity flow; other grain flows, submarine landslides/debris flows; clinoform/fondoform deposits	Terrigenous and calcareous clays (commonly alternating); pelagic oozes; deposition from suspension plumes and nepheloid clouds; fondoform deposits
Geometry and structure	Elongate lens-shaped (shelf/platform edge and barrier reefs); elongate to subcircular lens-shaped (patch and pinnacle reefs/banks); form on stable structural elements	Irregular fan-shaped to mounded geometry; common but not restricted to unstable basins	Sheet to blanket geometry exhibiting drape over underlying surface; common in deep, subsiding basins
Lateral relationships	Shelf/platform edge facies grade updip into parallel/divergent shelf/platform facies; grade downdip into talus and sigmoid clinoform facies; patch reef/bank facies grade updip and downdip into parallel/divergent shelf/platform facies; pinnacle and barrier facies grade downdip into talus clinoforms and to basinal plain (fondoform) facies	May grade shelfward into progradational clinoforms (normally oblique), canyon onlap fill, or pinch out against eroded slope; may grade basinward and laterally into basinal plain (fondoform); onlap fills or drapes	Commonly grades laterally or basinward into basinal plain (fondoform) facies; may grade shelfward into submarine canyon onlap fill; may onlap eroded slope
Nature of upper and lower boundaries	Upper surface concordant or may be onlapped by flank reflections; basal surface concordant, baselapping, or may overlie clinoform top; pull-up or pull-down of basal surface common	Upper surface commonly erosional and onlapped, baselapped, or concordant (with drape); basal surface irregularly baselapping; may appear concordant (low resolution), or may onlap (mounded onlap fill)	Upper surface commonly concordant, but may be onlapped or baselapped; basal surface generally concordant but may onlap eroded mound or slope
Amplitude	High along boundaries; may be moderate to low internally; commonly reflector-free	Variable; generally low; some higher internal amplitudes may be thin hemipelagic drapes	Low to moderate; some high amplitude reflections (well defined on high-frequency, shallow data)
Continuity	High along boundaries; internally discontinuous to reflector-free	Discontinuous to chaotic	High
Frequency (cycle breadth)	Broad; cycle may diverge into massively bedded buildup	Highly variable; commonly narrow	Narrow, uniform

*Modified from Vall et al. (1977, pp. 166-168); changes by Brown and Fisher.

Table 3.4: Summary of seismic facies characterized by mounded and draped reflection configurations.

(iii) Reflection amplitude

This parameter contains information on the velocity and density contrasts of individual interfaces and their spacing. It is used to predict lateral bedding changes and hydrocarbon occurrences (*Vail et al.*, 1977). The reflection amplitude is dependent on the reflection coefficient.

The upper part (Miocene to Upper Eocene), exhibits moderate to high amplitude. The middle part (Middle Eocene to Upper Palaeocene) shows high amplitude, in particular at the top of Middle Eocene, as a result of the change in lithology. The upper interval varies from shale with minor sandstone and limestone interbeds and the lower interval is mainly limestone, which has an acoustic impedance higher than the upper interval; that will yield a positive reflection coefficient.

The lower part exhibits a high amplitude. The top of Upper-Sabil has a high amplitude, where the reflection coefficient is strongly positive, due to the lithology change from Kheir shale to Upper-Sabil limestone. The high amplitude is in the top of the Sheterat shale, with a negative reflection coefficient, reflecting the change in lithology from Upper-Sabil limestone to Sheterat shale. High amplitudes are always associated with the shale to carbonate contrast. The following paragraph discusses in detail the reflection coefficient.

The strength of a reflection generated at a boundary can be quantified in terms of the boundary's reflection coefficient (RC).

$$RC = \frac{\rho_2 v_2 - \rho_1 v_1}{\rho_2 v_2 + \rho_1 v_1} \dots \dots \dots 3.4$$

where :

$\rho_1 v_1$: acoustic impedance in the upper layer.

$\rho_2 v_2$: acoustic impedance in the lower layer.

The reflection coefficient can be positive or negative depending upon acoustic impedance of the upper and lower layers.

In the case in which the shale overlies limestone (e.g. Kheir shale and Upper-Sabil limestone), the reflection coefficient is positive, and a reflecting boundary appears as a trough (white) on the seismic section.

In the case in which the limestone overlies shale, (e.g. Upper-Sabil limestone and Sheterat shale) the reflection coefficient is negative, and a reflecting boundary appear as a peak (black) on the seismic section.

The following diagram shows the geological models and the seismic response.

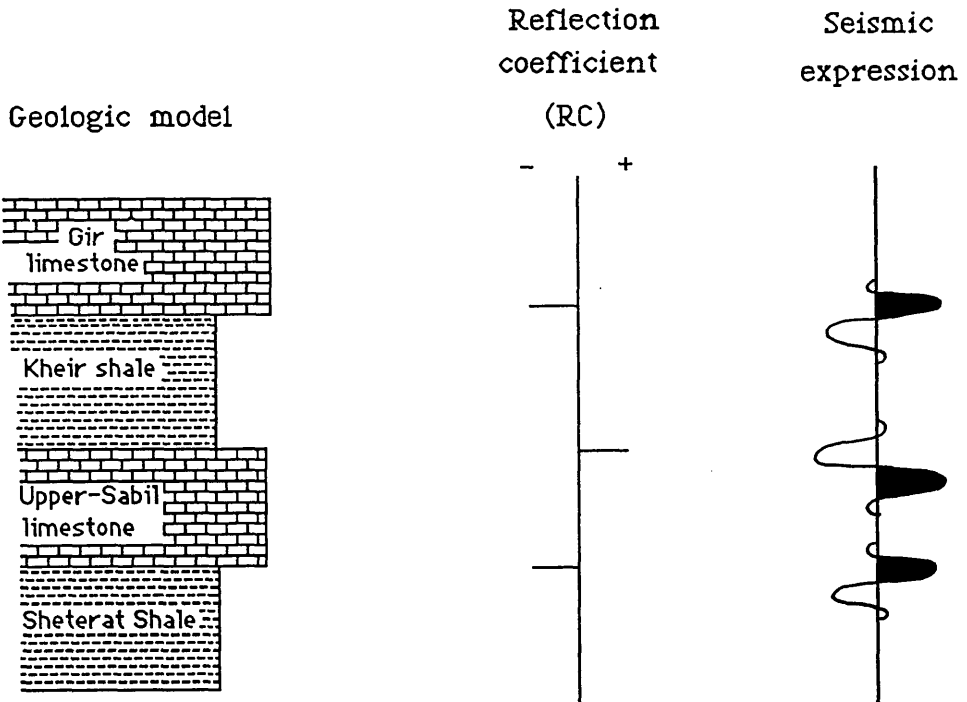


Fig. 3.10 Diagram showing the geological model, reflection coefficient, and seismic response (normal-polarity).

(iv) Reflection frequency

This is a characteristic of the nature of the seismic pulse, but it is also related to such geological factors as the spacing of reflectors or lateral change in interval velocity (*Vail et al.*, 1977). In some areas frequency has been a good indicator of condensate reservoirs; these are associated with a characteristic low frequency anomaly directly underneath them (*Taner & Sheriff*, 1977).

The Earth is a filter for waves are travelling through it. It will attenuate with depth. At shallow depths, where velocities usually are low, the frequencies are high and the wavelength is low. Deeper in the section, where

velocities are higher, the frequencies are lower and the wavelength is therefore high. (Badley, 1985). The relation between the frequency, interval velocity and wavelength is shown by the following :

$$F = \frac{V_{\text{int}}}{\lambda} \dots\dots\dots 3.5$$

where :

F : Frequency in hertz.

V_{int} : Interval velocity in (m/s).

λ : Wavelength in metres.

(v) Interval velocity

This is an important parameter for the estimation of lithology, porosity, and fluid content. A detailed interpretation of the interval velocity derived from the seismic data is presented in Chapter 4.

3.3.3 Mapping reflecting horizons

The horizons which we draw on seismic sections provide us with a two dimensional picture only. A three dimensional picture is necessary to determine whether a structural closure exists. The area within the closing contour is the location of the highest point on the structure. (*Telford et al.*, 1976).

The familiarity of geological setting of the area, type of rocks, and structure expected helps us in choosing the horizons to be mapped.

Once seismic sections have been interpreted, the next objective is to produce contour maps of two-way time and depth to each horizon. We map on a base map (1:10,000) which shows the location of the seismic lines and the wells.

3.3.4 Maps construction

(i) Time contour maps

Values of two-way time are placed on the map (posted) at each shot-point, and the values then contoured. Given maps of two-way time to various horizons and by using average velocities, we can produce depth maps, building up the depth to each horizon (Fig. 3.6 and Table 3.2). These depth values can then be posted and contoured in the same way as the two-way time values. Two-way times are read from the seismic sections, for each 5 ms along each line. The two-way time values are then posted on the base map using

a scale of 1:10,000 at the appropriate shot-points along each seismic traverse (see Chapter 1, Fig. 1.2). The posted value maps are contoured using an interval of 5 ms, which is commonly used in the Sirte Basin. The time values of each horizon are shown in the Appendix (Tables 3.5 - 3.11).

El-giza two-way time contour map

A two-way time contour map for the El-giza horizon was constructed and is shown in Fig. 3.11. The horizon shows smooth and simple contours.

The features and delineation of the structure are precisely shown. The closure contours range from 1145 to 1175 ms, while the contours at the periphery range 1180 to 1200 ms. Away from the closing contours, the contours become broader. In general, the shape of the contours in the central area is equidimensional, and elongated mainly on the flanks.

Nevertheless, there is no geological meaning in the contours at the northeast of the area, where they assume a local N-S trend between shot-points 560-620 and 430-460 on the lines U-53 and U-25 respectively (see Chapter 1, Fig. 1.2). That may be because the two seismic lines are very close in the northeast.

The mis-ties become apparent at the intersections of lines U-53 and U-6, and lines U-25 and U-6, with values between ± 10 ms and ± 15 ms respectively. Other intersections were adjusted, or no mis-ties were found. The intersection shot-points and the adjustment time for the El-giza horizon is shown in the Appendix (Table 3.12).

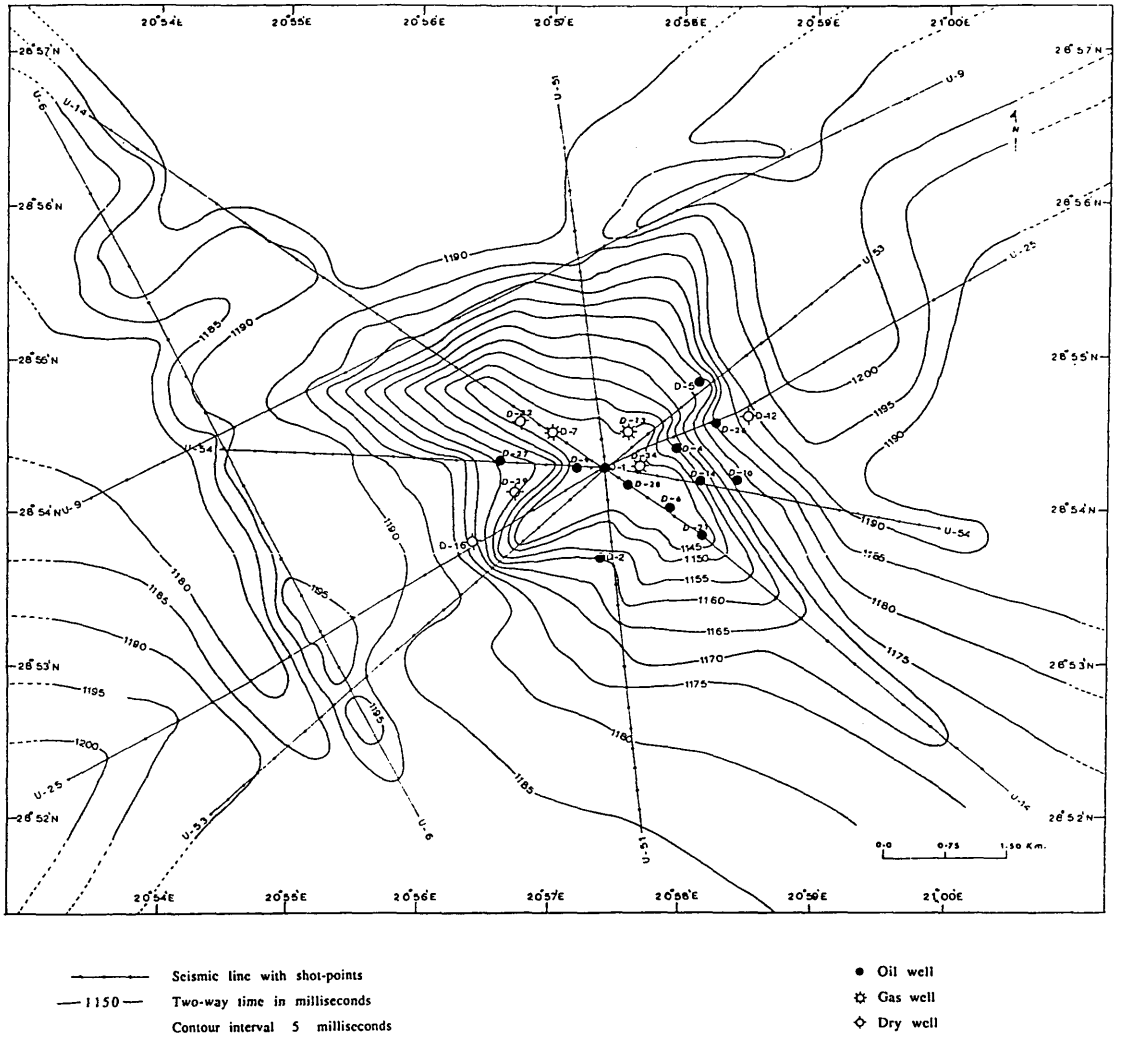


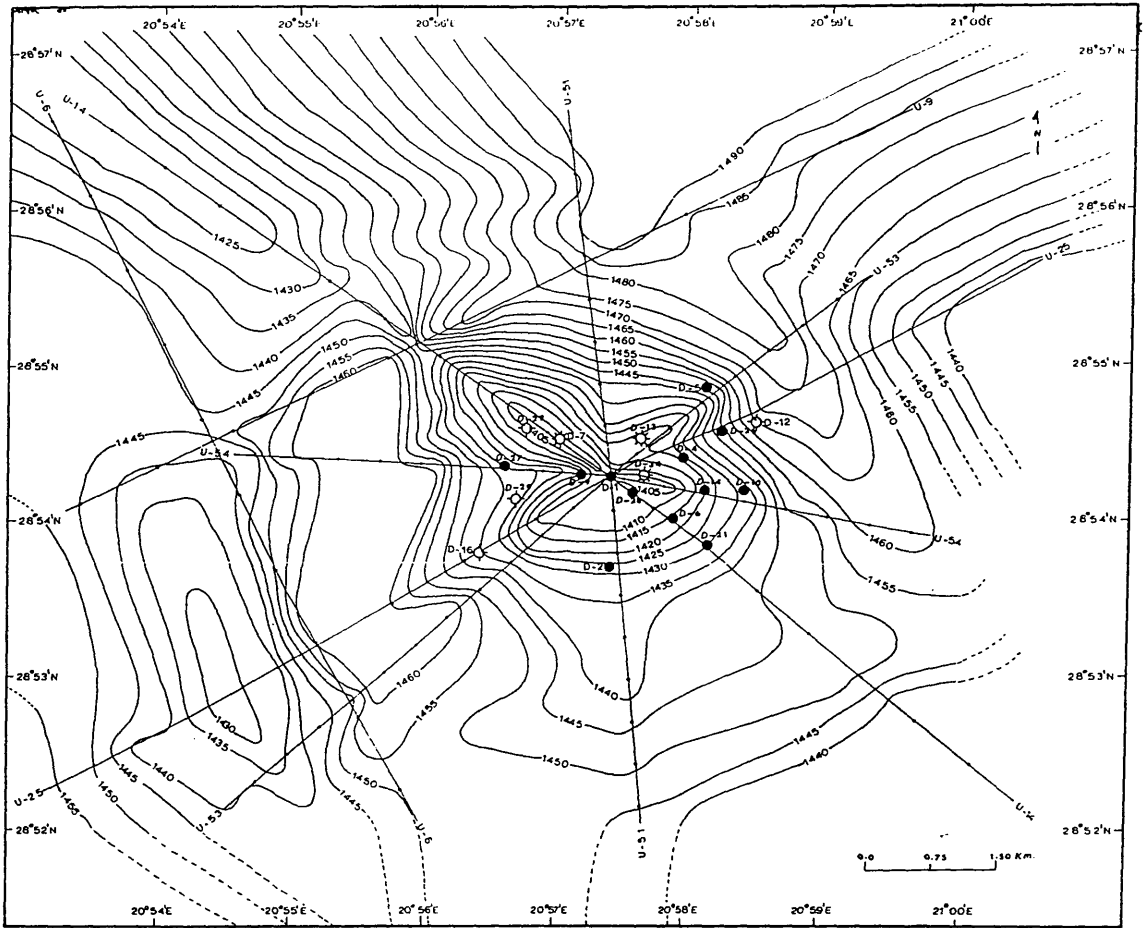
Fig. 3.11 Two-way time to Middle Eocene (El-giza) horizon.

Gir two-way time contour map

The shape of the structure is clearer on the Gir two-way time contour map. As we can see in Fig. 3.12 the Gir seismic time map shows closure from 1450-1410 ms over the field. The difference between the inner closure and the outer is about 40 ms, as a result of the drape in Gir interval. The inner closure contours show nosing in the area above the structure. The Gir seismic time map indicates an anomalous area but, when compared with the highs and lows in the El-giza reflection which is just above the Gir reflection, we see that it results directly from the seismic time "highs" and "lows", due to large velocity contrasts. The intersection shot-points and the adjustment time for the Gir horizon are shown in Appendix (Table 3.12). The mis-ties become high in the lines intersections at this level.

Kheir two-way time contour map

This reflector (Kheir) is very close to the top of the structure (Fig. 3.13). The contours are steep and very dense, just over the structure. The closure of the contour range 1625-1700 ms, about 75 ms. represents the drape which is bigger than it was for the Gir and El-giza reflectors. In fact this seismic horizon represents the external shape of the structure as it is. Figure 3.12 shows that the shape is equidimensional and more nearly circular. As we move towards the northeast in the area the two-way time becomes higher, and the closure is apparent at 1740 ms. The mis-ties in the seismic line intersections found at this horizon are quite high, (Appendix, Table 3.13).



- Seismic line with shot-points
- 1420— Two-way time in milliseconds
- Contour interval 5 milliseconds
- Oil well
- ★ Gas well
- ◇ Dry well

Fig. 3.12 Two-way time to Lower Eocene (Gir) horizon.

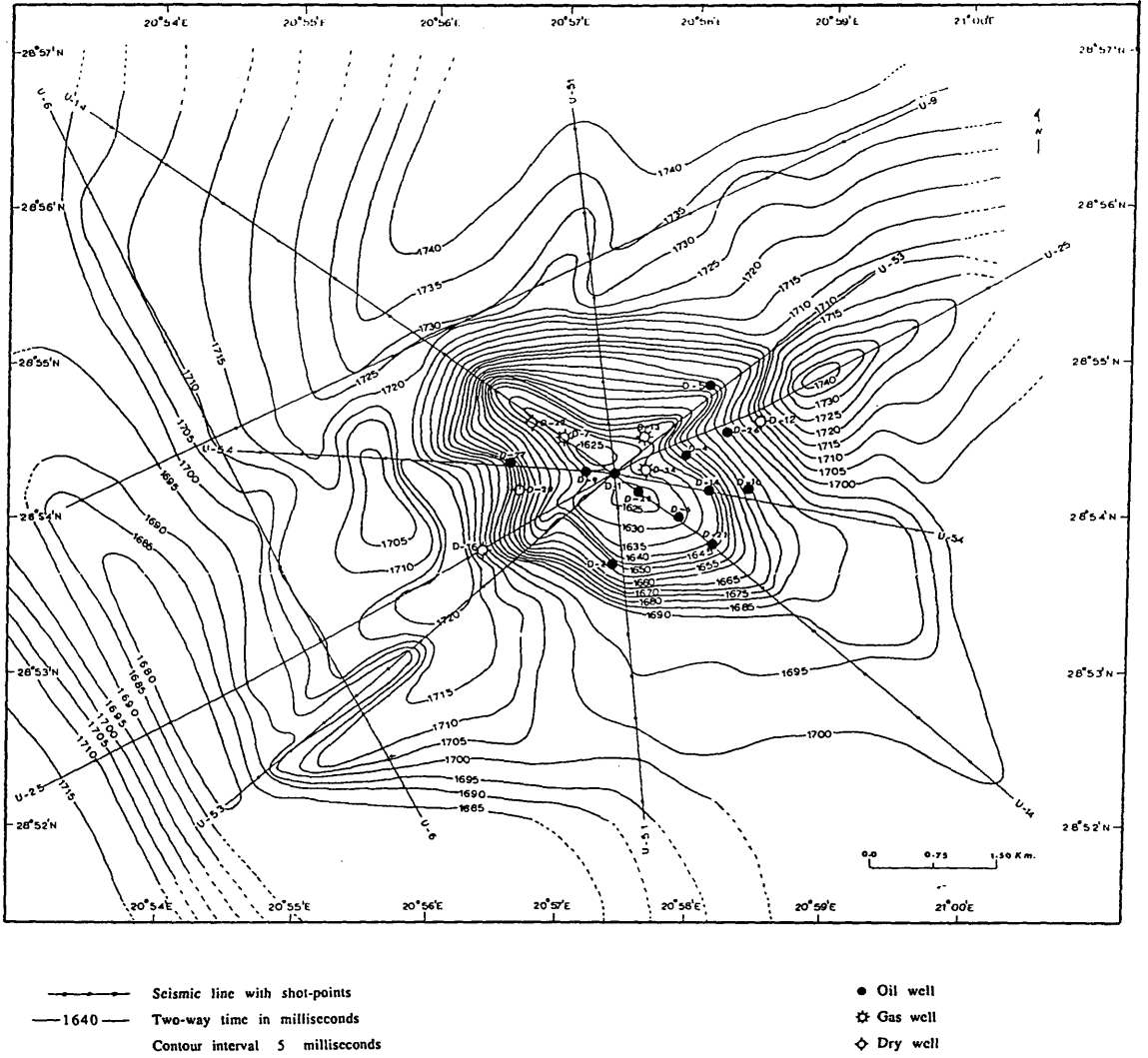


Fig. 3.13 Two-way time to Upper Palaeocene (Kheir) horizon.

Upper-Sabil two-way time contour map

This horizon is at the base of the structure. The area which is underneath it shows a low two-way time of 1935 ms.

The map of the top Upper-Sabil (Fig. 3.14) shows smooth and simple contours, and closure contours which represent high and low two-way times. The mis-ties between the seismic lines have quite high values; at some intersections they are about 20 ms, (Appendix, Table 3.13).

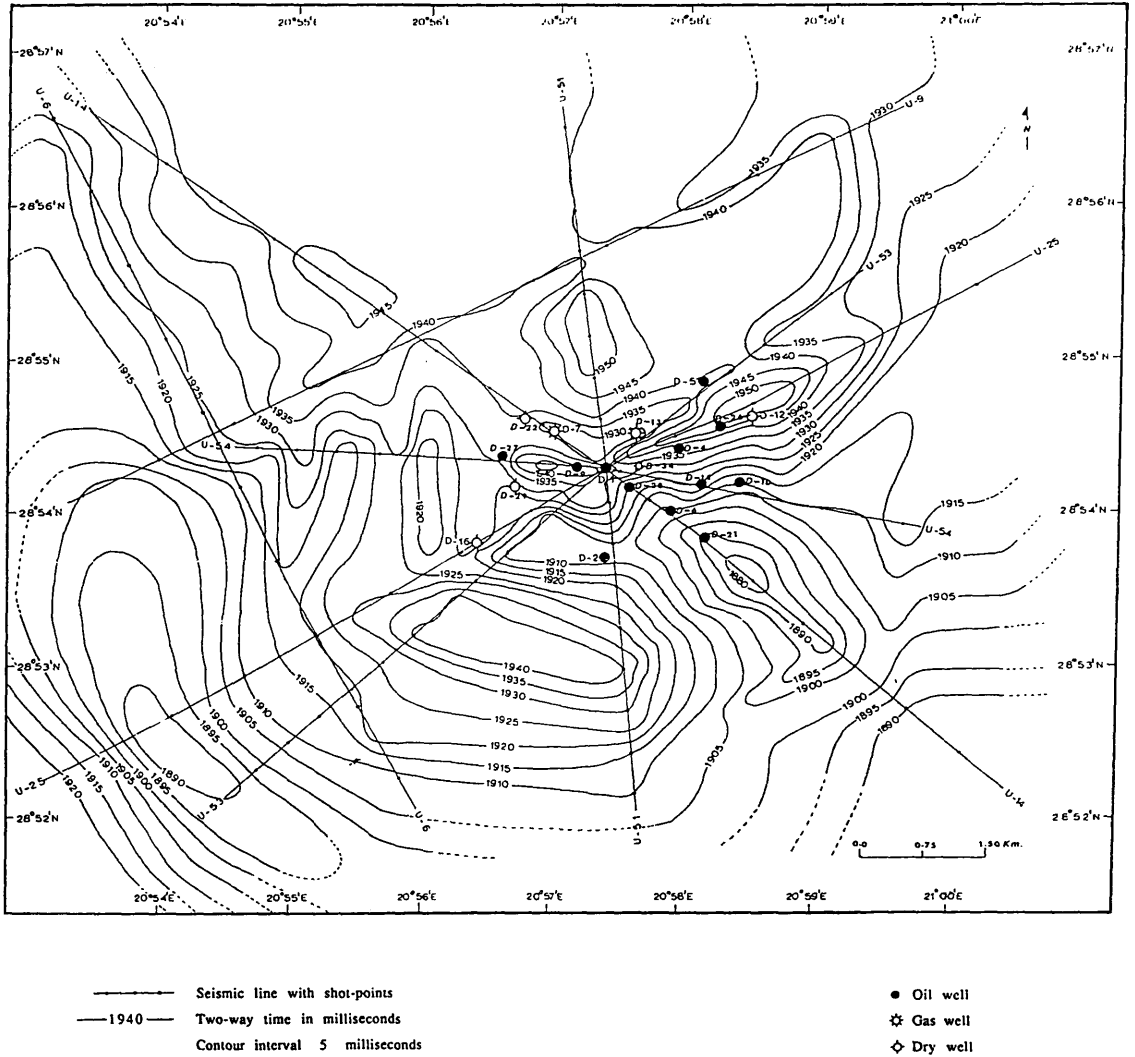


Fig 3.14 Two-way time to Upper Palaeocene (Upper-Sabit) horizon.

(ii) *Depth contour maps*

Seismic time maps in the above section are the result of a seismic surveys in the area. The depth maps become important to seeing clearly the geology of the area. As mentioned before, a velocity survey is available only in the D1/103 well. (Fig. 3.6). The depth contour maps of the selected seismic horizons (El-giza, Gir, Kheir, and Upper-Sabil) are constructed as follows.

The one-way travel time for each horizon along all the seismic lines is multiplied with the top average velocity in the well (D1/103) of each horizon (as shown in Fig. 3.6, and Table 3.2). The depth values using this method have some errors, especially far away from the well control, towards the periphery of the area. This is because we are neglecting lateral variation of velocity, and have used just one value over all the area. The error will be bigger in the regional study. The velocities derived from the seismic processing are unreliable, and will give inaccurate depths, so for the time to depth conversion we use the well velocity surveys (D1/103). The contour interval used in the depth maps is 10 m.

The following section describes in detail the depth contour maps for the four seismic horizons. The depth values of each horizon as mentioned are tabulated in Appendix, Tables 3.5 to 3.11.

El-giza depth contour map

Figure 3.15 shows the top El-giza in depth below sea level. The closure contours vary from 1485 to 1535 m in the centre of the area, in particular over the structure. These show clearly the trend and the shape of the structure, which is northwest to southeast. The closure contours represents a high area (a mound shape), as a result of the drape in the El-giza sediment which rises 70 m. The area become slightly deeper away from the closure contours, especially in the southwest and northeast where depths are 1565 and 1555 m respectively.

In general, the high area is surrounded by the low. Comparison of the well-tops on the centre of the area with this depth map of El-giza, shows that they are very close.

Gir depth contour map

The structure map of Gir horizon (Fig. 3.16) shows that the closure contours from 2065 to 2105 represent the high. As with the El-giza depth contour map, the structure takes the same northwest to southeast trend. While the contours are close in the northeast, they become wider in the southwest. The high is surrounded by small depressions. In the southwest the Gir is high again, in particular between the shot-points 310 and 320 on line U-25.

The structural gradient, or rate of change of depth, is measured by the spacing of the contours; close spacing means, of course, a large gradient. From the interpretation of the depth contour map of this horizon, the area rises to form a high in the northwest (line U-14), and the contours nearly close.

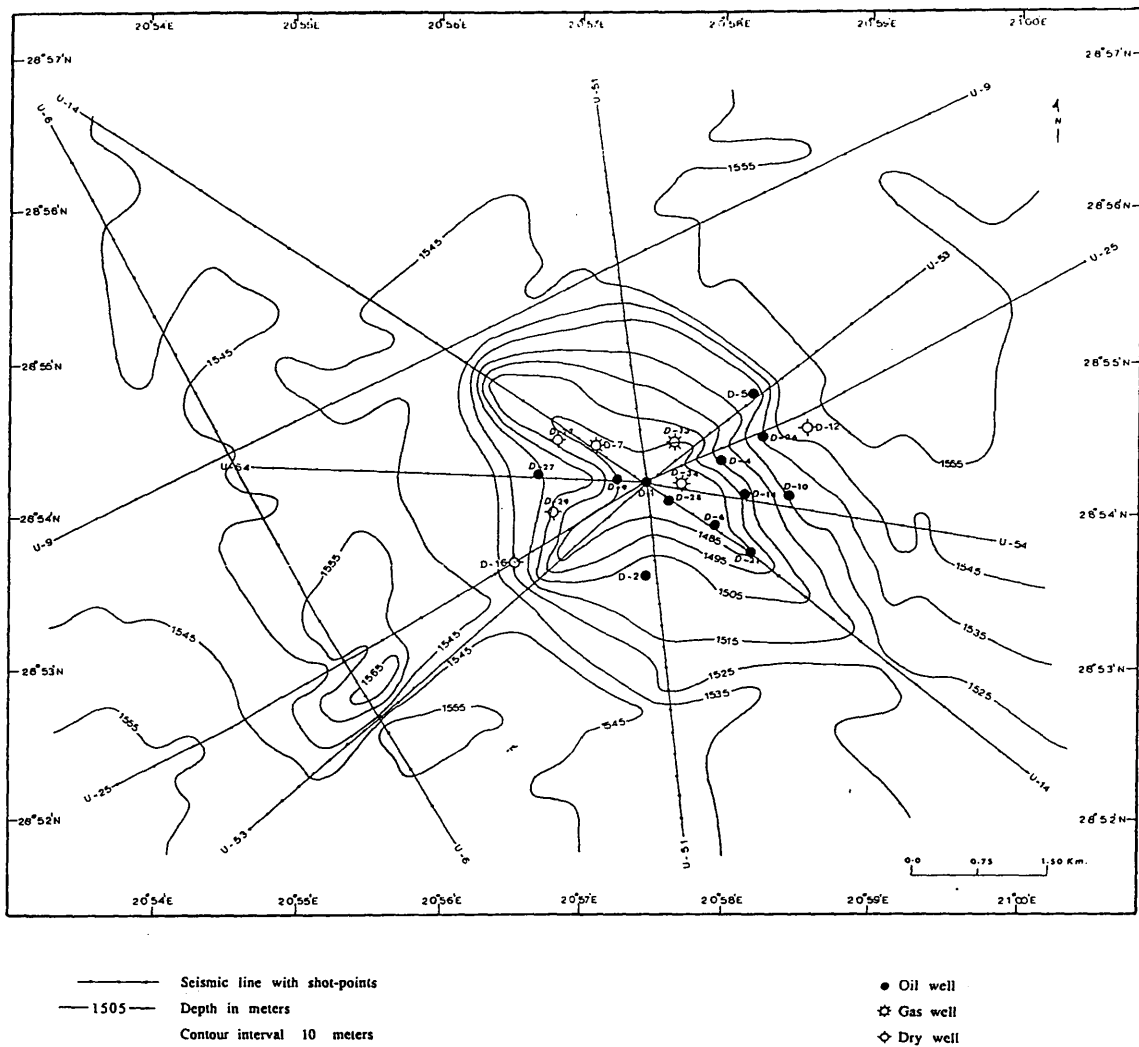
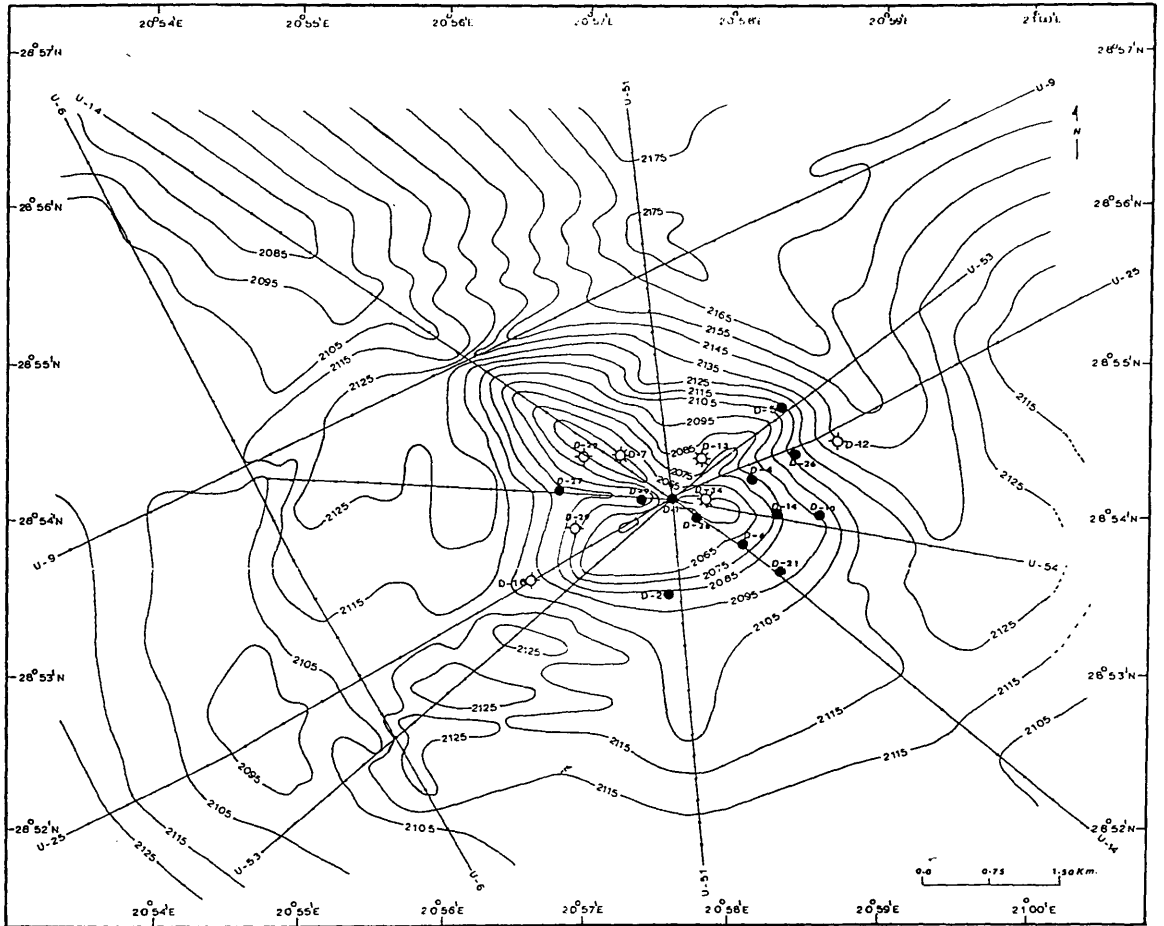


Fig. 3.15 El-giza depth contour map.



- | | | | |
|--------|-------------------------------|---|----------|
| —●— | Seismic line with shot-points | ● | Oil well |
| —2145— | Depth in meters | ☆ | Gas well |
| — | Contour interval 10 meters | ◇ | Dry well |

Fig. 3.16 Gir depth contour map.

Kheir depth contour map

The Kheir horizon is close to the top of the structure, and as we can see in Figure 3.17 the closure contours just over the structure become dense and close together. The closure contours from 2535 m to 2645 m represent the high area of about 110 m in amplitude. Moving towards the northeast the area become slightly deeper (2695 m) between the shot-points 470 and 480 in line U-25, which is about 160 m deeper than the highest point in the closure. Away from the closure contours towards the southwest the depth of the area gradually increase from 2655 m to 2665 m. The structure in this horizon as well as in the other two horizons El-giza and Gir trend in a northwest-southeast direction, which is the same trend of the most troughs and highs in the Sirte Basin, in particular the Agedabya Trough (see Chapter 2, Fig. 2.2).

Upper-Sabil depth contour map

The contour map in Figure 3.18 shows the depth to the top Upper-Sabil, which is different from the contour maps for El-giza, Gir, and Kheir. The contours become broader all over the area. In the periphery the area gradually becomes more deep. In the southwest, and in particular between the shot-points 290 and 300 on line U-25, their depth is 2985 m. Other closure contours (3055 m) are in the centre around the well (D1/103), and in the south at VP. 440 and VP. 640 on lines U-53 and U-51 respectively.

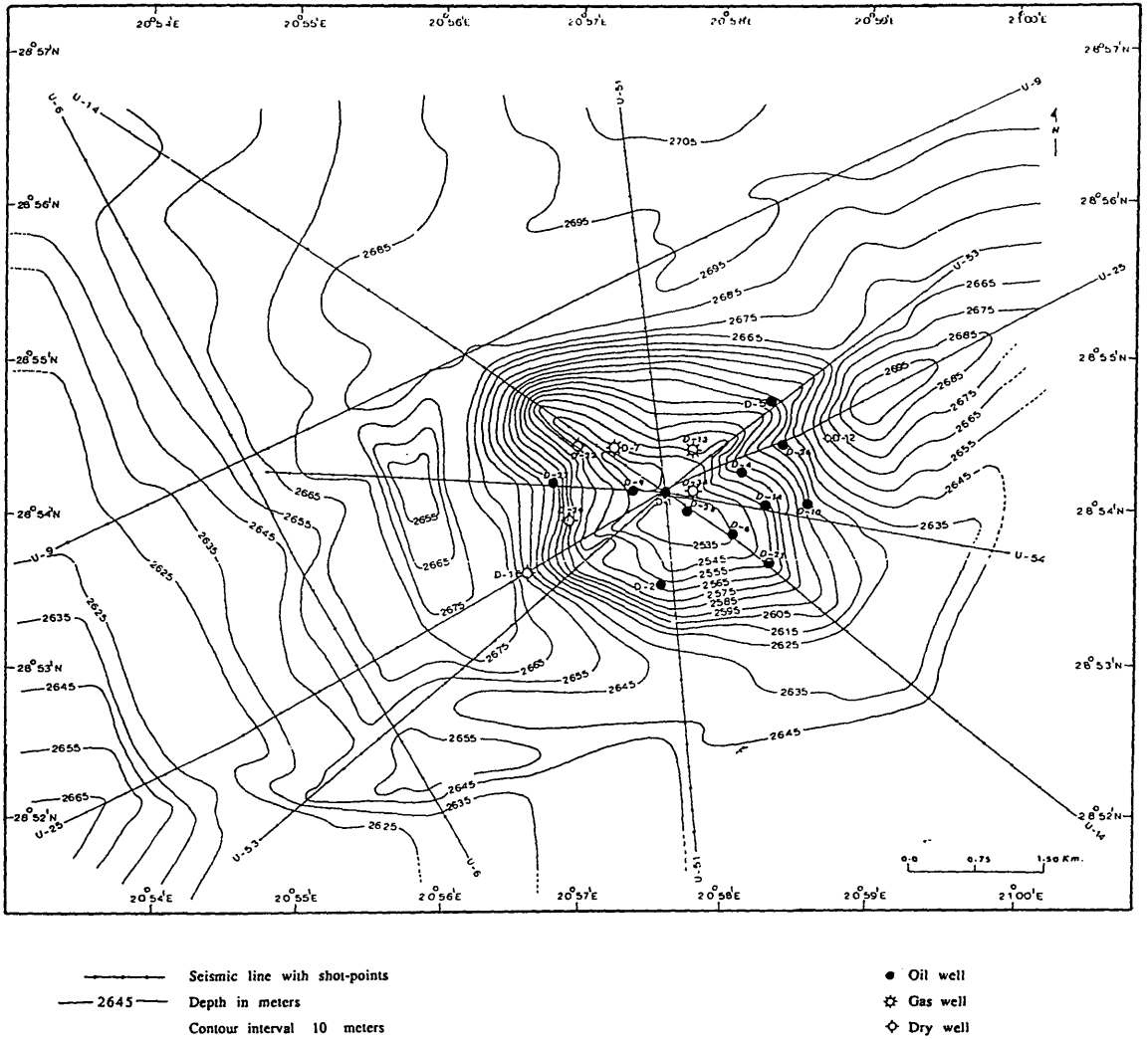


Fig 3.17 Khair depth contour map.

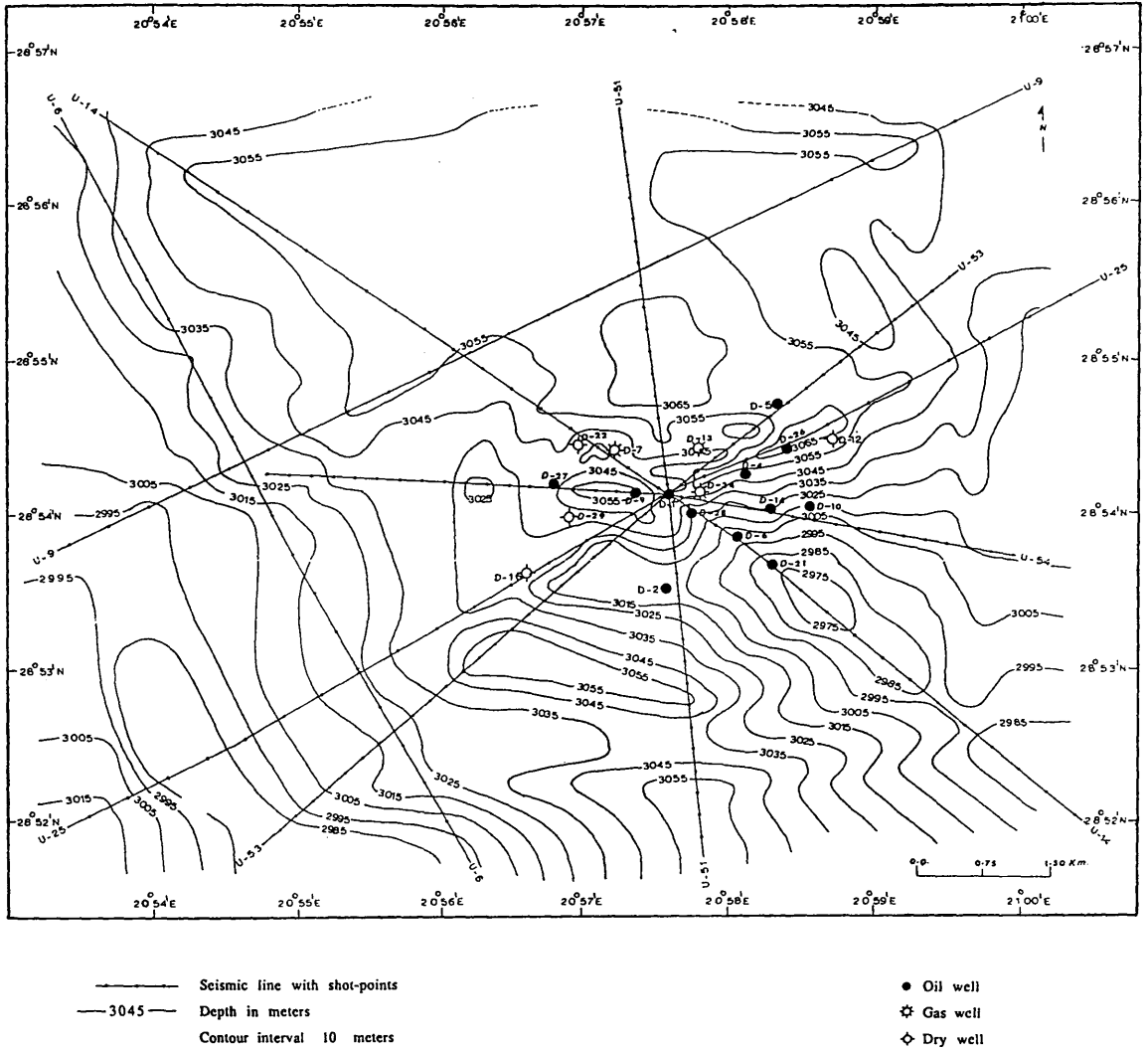


Fig. 3.18 Upper-Sabil depth contour map.

(iii) *Average velocity and depth maps of the top of Kheir Formation*

The Kheir horizon is close to the top of the structure, it is selected to derive average velocity from well depths tied to seismic sections and convert to depth using this velocity function.

(1) Average velocity map

Figure 3.19 shows the average velocity map of the top of Kheir Formation, by using the well tops was shown in table 1.1 and the one-way travel time to the top of Kheir Formation along the seismic lines concentrated in the central zone containing the wells.

The map shows a gentle velocity gradient. The average velocity is graduated from 3000 m/s in the central zone to 3125 m/s away from the centre. It is clear there is no big change in the velocity over the central area, which indicate that is realistic to use the well velocity surveys (D1/103) for the time to depth conversion.

(2) Depth map

The depth of the top of Kheir Formation shows in Figure 3.20, using the previous average velocity was shown in Figure 3.19. The closure contours range from 2450 to 2580 m and reflected the reef shape which is equidimensional and more nearly circular. Comparing this map with the central zone of the depth map of the top of Kheir Formation which was shown in Figure 3.17, where the closure contours range from 2535m to 2645. There is similarity between the two maps. This map shows a few tens of meters less than the map in Figure 3.17.

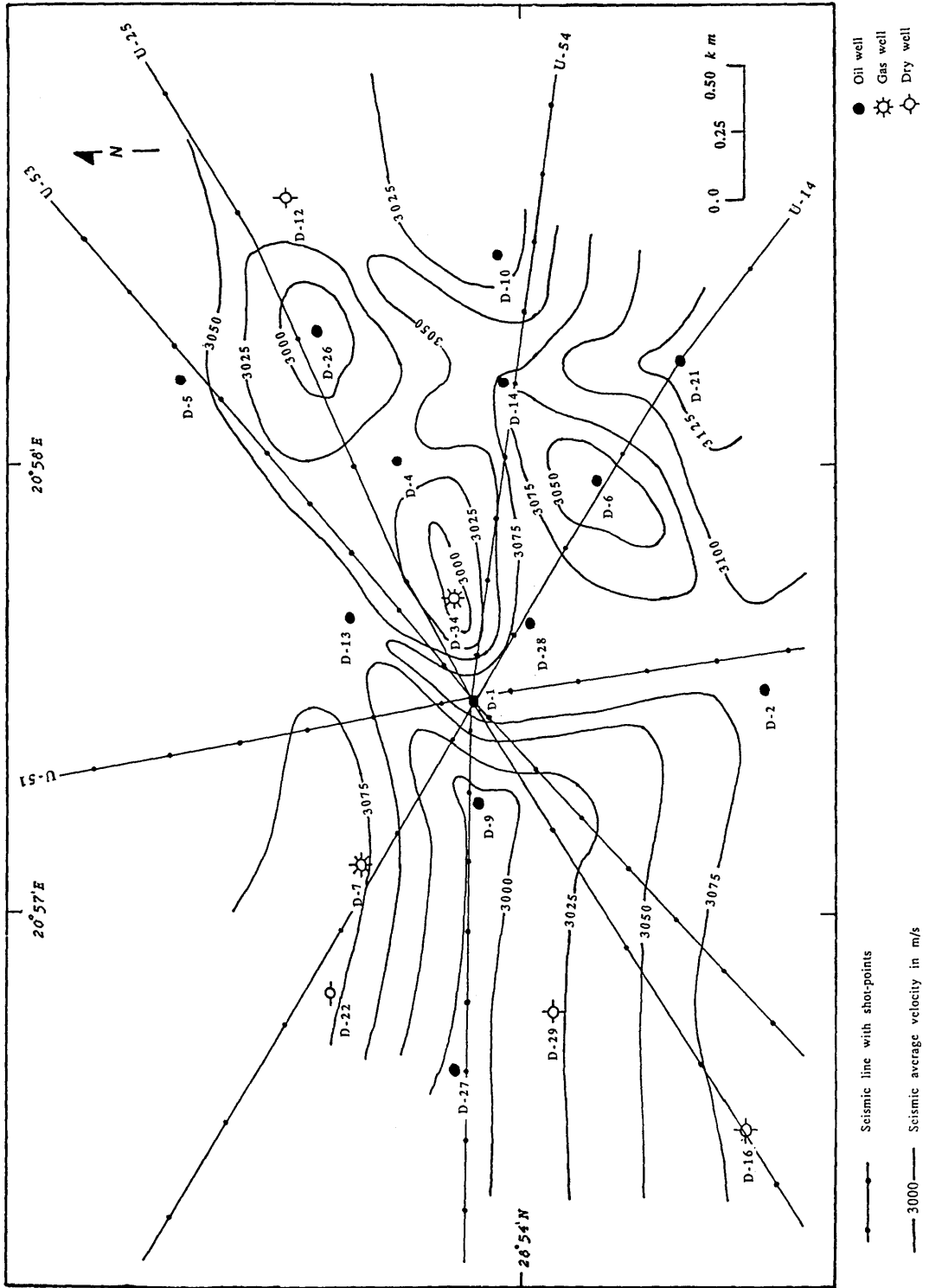


Fig. 3.19 Top Kheir average velocity map.

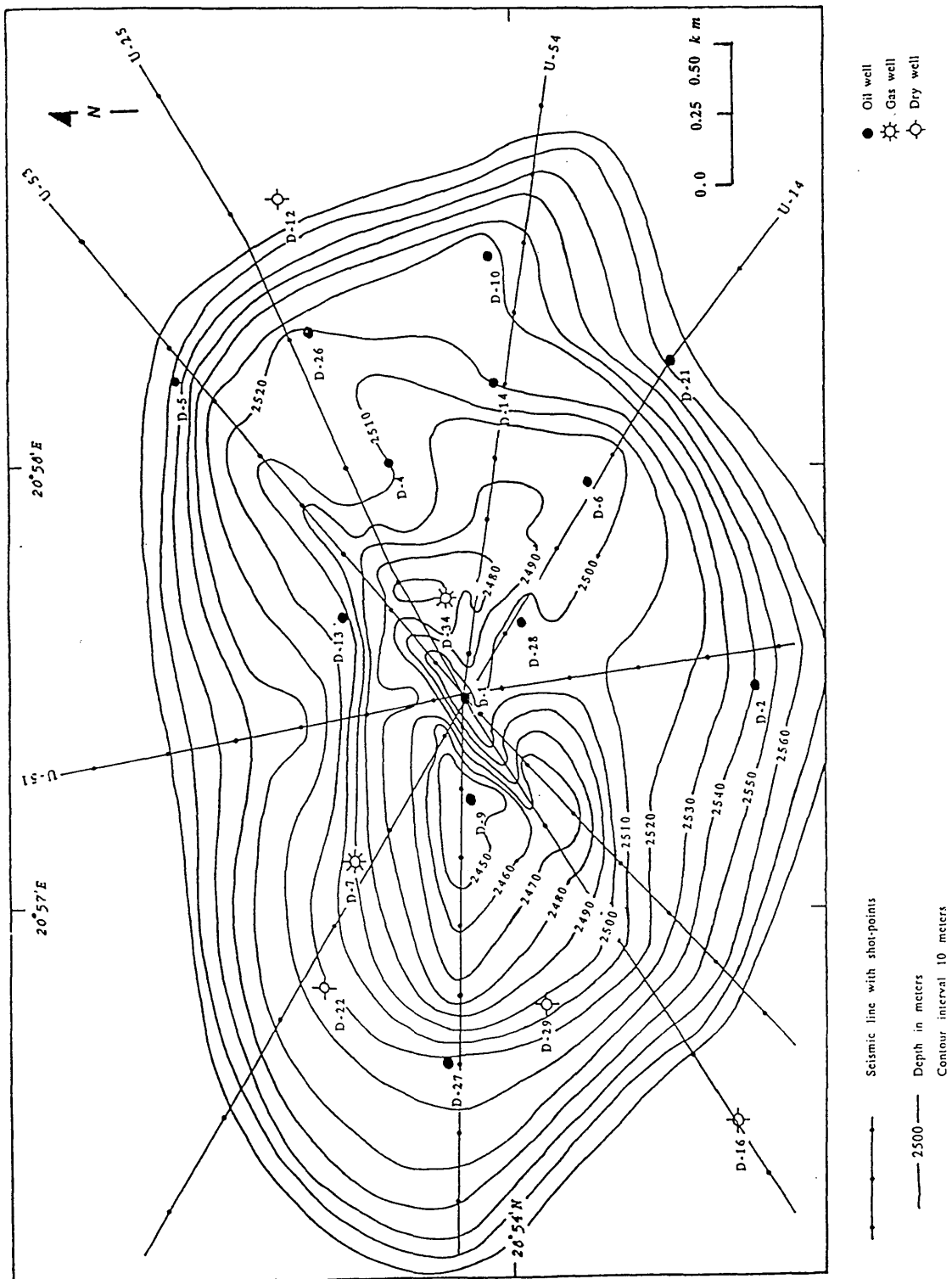


Fig. 3.20 Kheir depth contour map.

3.4 *Summary of seismic interpretation*

- (1) The well and seismic data are in good agreement, with small mis-ties.
- (2) The selected horizons give a clear geological picture of the area, in particular the environment of deposition and the reef build-up.
- (3) Reflectors in sediments are mostly parallel bedded, and vary laterally in intensity and continuity.
- (4) Strong reflectors forms heavy lines or bands on a seismic profile indicating strongly contrasting acoustic impedances between layers.
- (5) Weak reflectors do not stand out and indicate low acoustic impedance contrasts.
- (6) From the seismic facies analysis it is clear that the predominant depositional environment is deep water (300 m). This is also evident from the reflection configuration (parallel reflections).
- (7) Reflections of constant high amplitude and good continuity over large areas, such as the reflections from the top of Middle Eocene, top of Upper-Sabil limestone and top of Sheterat shale, separate shales and carbonates deposited under low energy conditions.
- (8) The depth contour maps are constructed using the single central well velocity survey for the entire area .

Chapter 4

4.1 Velocity interpretation

4.1.1 Well velocity survey

4.1.2 Seismic velocities

4.1.2.1 Background

4.2 Seismic velocity analysis and mapping

4.2.1 Why processing seismic velocities are unsuitable for depth conversion

4.2.2 Velocity mapping

(i) Average velocity maps

(ii) Interval velocity maps

(iii) The difference between the well-velocity
survey and seismic velocity maps

4.3 Summary of velocity interpretation

4.1 Velocity interpretation

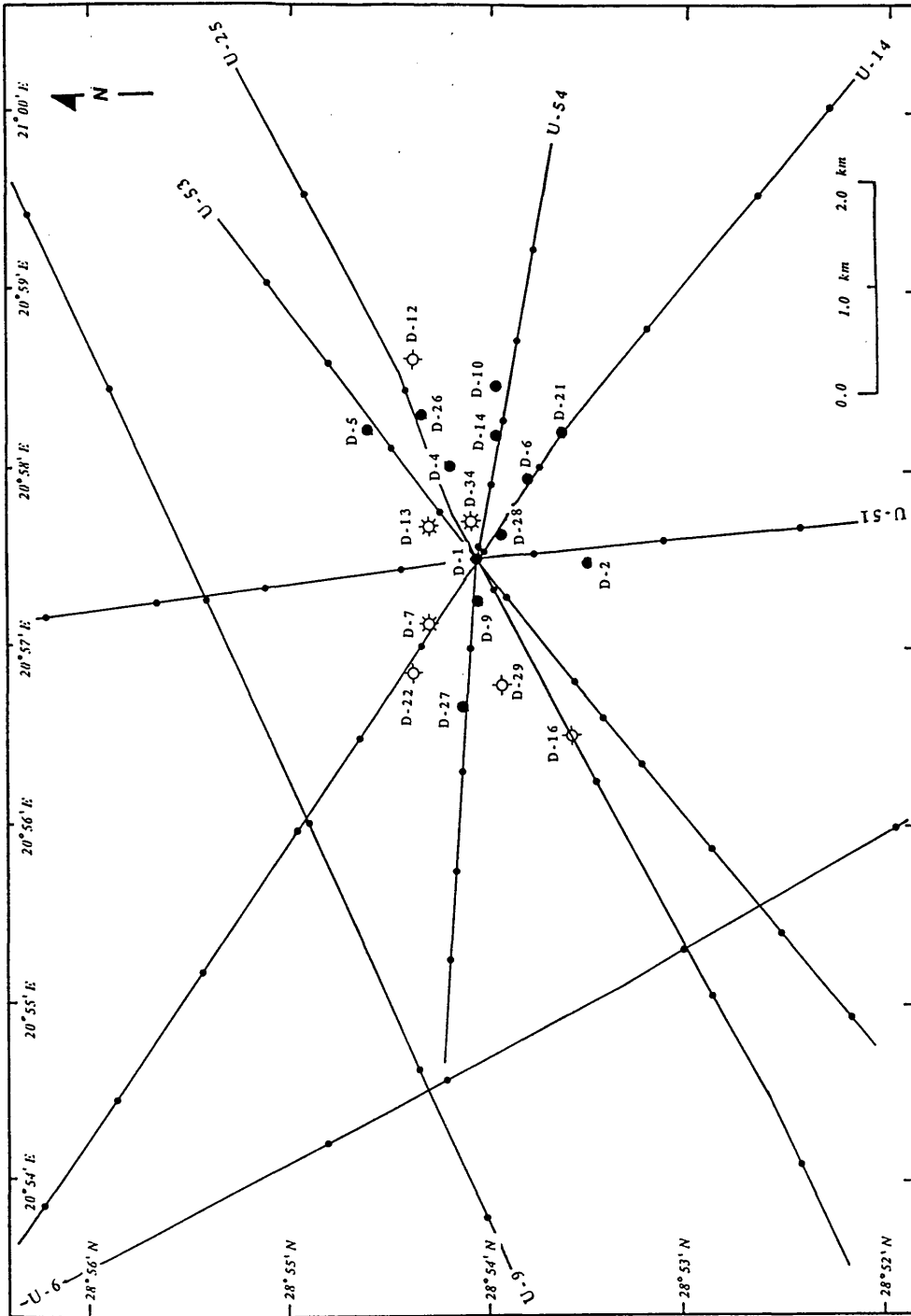
This Chapter discusses the velocity interpretation illustrated with relevant diagrams. Velocity plays a central role in the seismic method. In interpretation we use velocity to help identify lithology and to convert seismic times to depth. Velocity variations happen as a result of change in rock properties, include varying formation thickness, facies change and other rocks physical properties, such as porosity, density, burial pressure, etc. (Badley, 1989).

The main objective of the velocity study carried out here was to produce realistic velocity fields for those horizons selected for stratigraphic interpretation. Naturally the successful transformation from time to depth relies on credible velocity fields. Various techniques were investigated to establish velocity fields suitable for depth conversion. The well velocity surveys which were generated in well D1-103 for time to depth conversion are used because they are more realistic than the seismic velocities, which are inaccurate (see Chapter 3, Table 3.2 and Fig. 3.6).

Naturally a further source of velocity data is the stacking velocities which are provided as a result of the data processing sequence. By definition they are particularly useful in areas where there is no well control. This seismic velocity analysis technique involves interpolating the derived stacking velocity function to a point which corresponds to the relevant interpreted horizon time picked from the data. It is also possible to use a combination of methods, for example, updating an stacking velocity field to tie available well data.

The velocity analysis starts with the formation of CDP velocity gathers at a number of points along the sections. The locations of the velocity analyses over the area are shown in Fig. 4.1.





- Oil well
- ☆ Gas well
- Dry well

—●— Seismic line with shot-points and the locations of the velocity analyses

Fig. 4.1 Location map of velocity analyses.

4.1.1 Well velocity survey

The technique of the well velocity surveys is known, and the principles of this technique are explained in many geophysics texts.

Well-shooting is the most direct procedure for velocity measurements. In this method (Fig. 4.2) we shoot on (or near) the surface and record the arrival times of waves by geophones suspended in the well, gradually change the positions of shots and the geophones. The reciprocal of this transit time (expressed in $\mu\text{sec/ft}$), is the interval velocity in the formation penetrated. The sonic log is automatically integrated to give a total travel time, which is then shown as a function of depth by means of ticks at intervals of 1 ms (Telford *et al.*, 1976).

Generally, a velocity survey is particularly important in each exploration well. Surface seismic velocity profiles, derived from moveout scanning, are of course governed by the assumption of limited lateral variation of facies and by the relative accuracy of the method.

A velocity survey has two main uses:

- (i) To improve the accuracy of the initial interval velocity profile. Time measurement is improved by one way measurements through successive layers, and distance is directly measured by the logging cable.
- (ii) To provide greater detail in the time/depth functions, so that better explanations of all the secondary characters of the seismic trace can be made.

These additional details are derived from the sonic log, which has the advantage of high vertical resolution permitted by a high frequency source (25 KHz) and short spacing (2 feet).

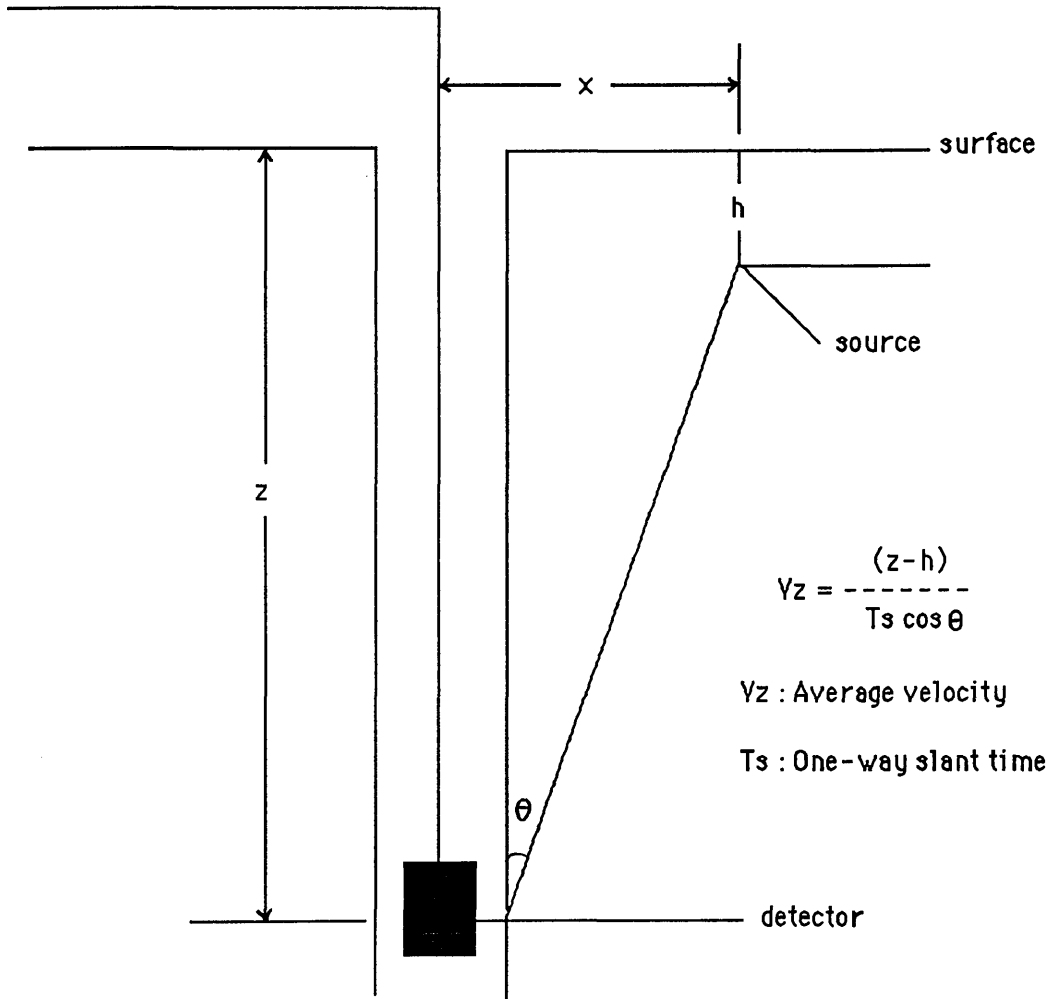


Fig. 4.2: Velocity surveying by well shooting method.

The velocity log (as shown in Chapter 3, Fig. 3.5) shows the interval velocities of the El-giza, Gir, and Kheir Formations penetrated by the well (D1/103) as a function of depth.

Continuous velocity logs have many applications - geological correlation, porosity determination, identification of formations, and synthesis of reflections.

Two types of velocity are calculated from logs and velocity surveys :

Interval velocity is obtained from well velocity surveys or a continuous velocity log, which is influenced by lithology, density, porosity, fluid content, etc. The interval velocity is obtained by the distance between detector positions in the well and dividing it by the difference in arrival times at the two depths, after the arrival times have been corrected.

Average velocity is the weighted average of the component interval velocities of a number of adjacent layers, and is the velocity used in depth conversion (*Badley*, 1989). As was explained in Chapter 3, Section 3.2.1, it is the actual distance from source to receiver, divided by the observed time.

Figures 4.3 & 4.4 show the lateral variations of the interval velocity by sonic logs over the field in south-northeast and west southwest- east northeast respectively. The interval velocity in Figure 4.3 increases from south to the northeast for all the intervals.

Figure 4.4 shows that the interval velocity increases in El-giza to Gir and Gir to Kheir intervals, from west-southwest to the centre around well (D1/103) and decreases towards the east-northeast. In the Kheir to the top of the structure and the top of the structure to the Upper-Sabil intervals, the velocity is high in the west-southwest, low in the centre, and becomes high in east-northeast (Fig. 4.4). The main reason for increasing velocity is the

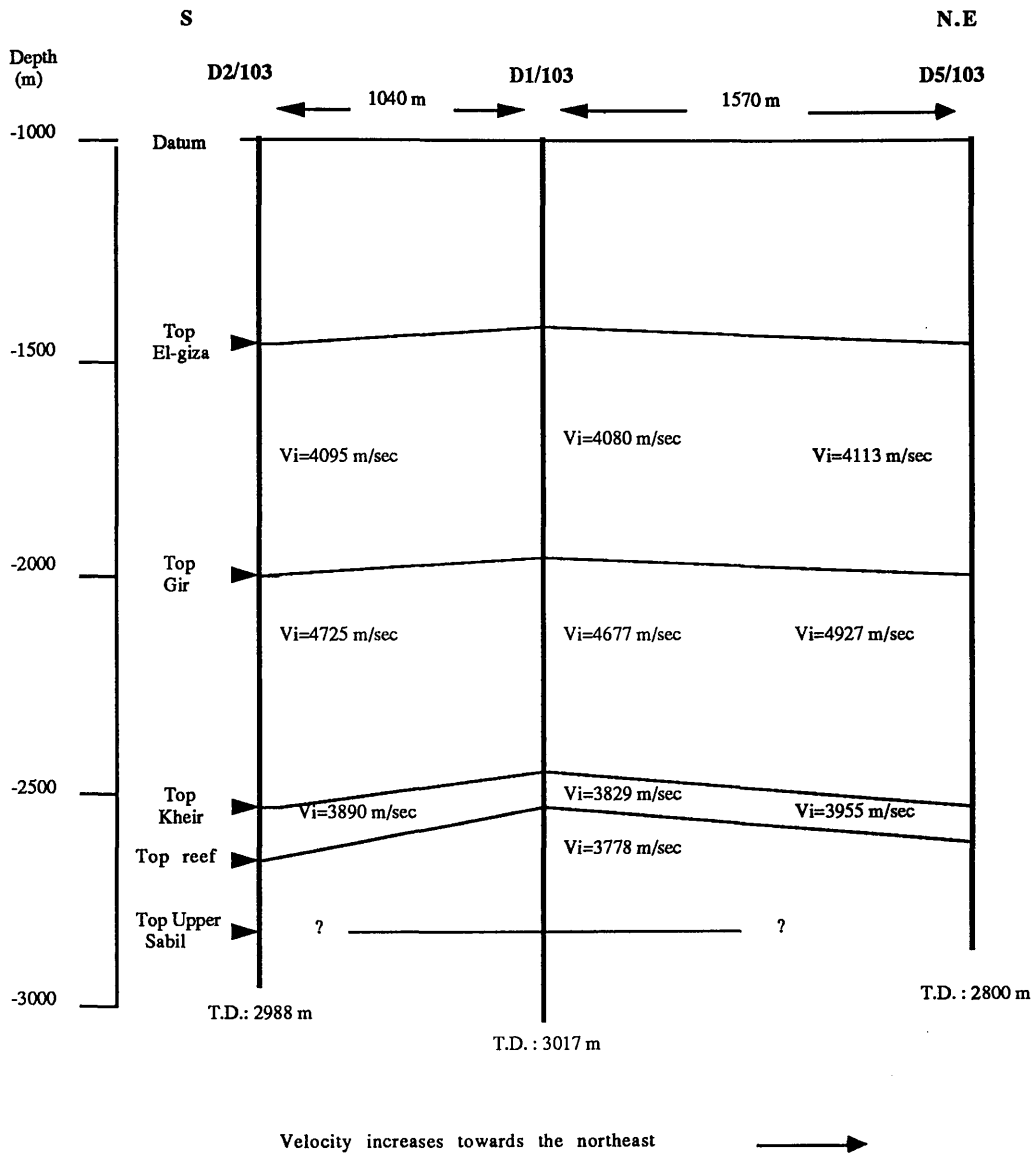


Fig. 4.3 Well correlation showing the average interval velocity in El-giza to Gir, Gir to Kheir and Kheir to Upper-Sabil intervals, from sonic logs generated in D-2, D-1, and D-5/103

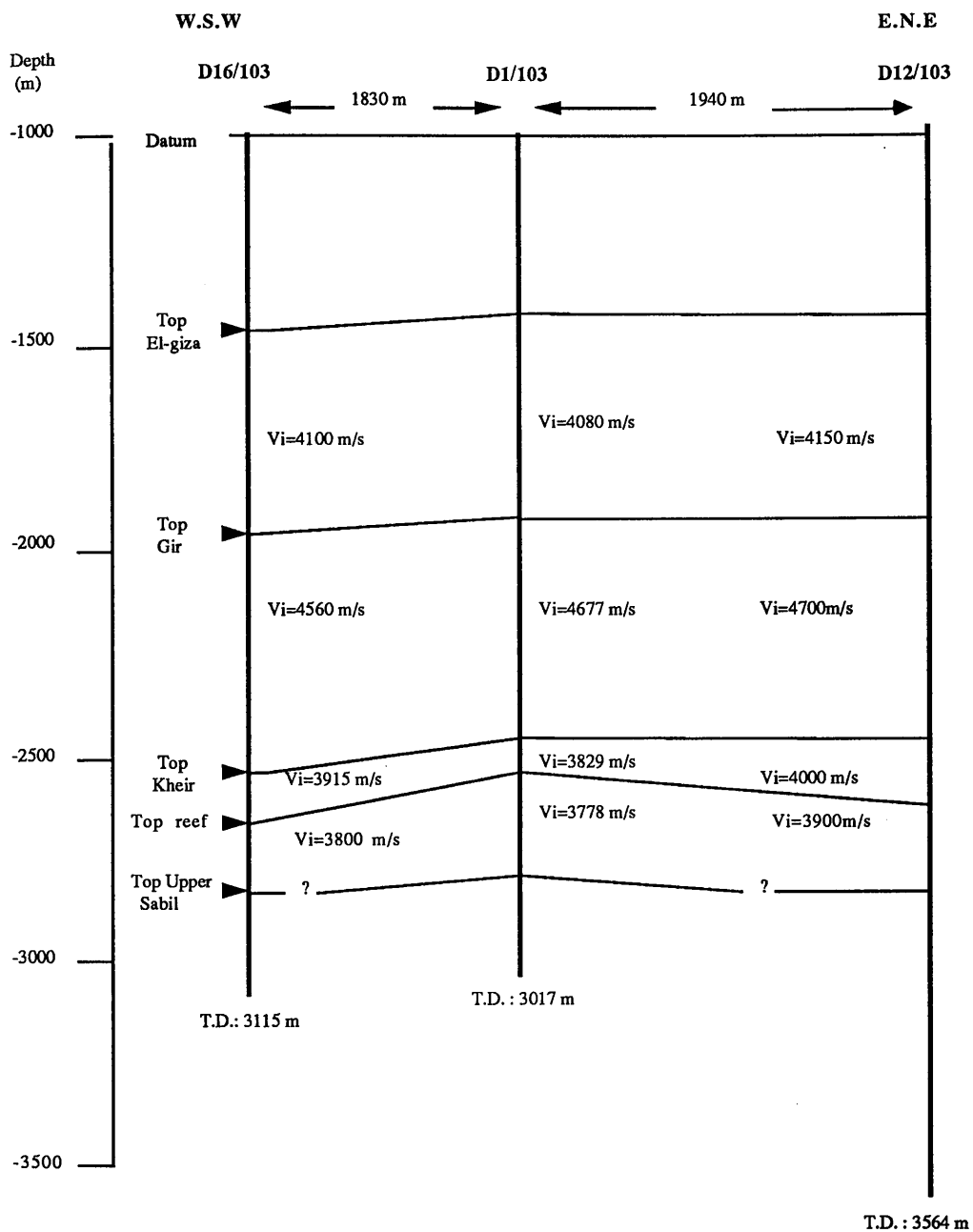


Fig. 4.4 Well correlation showing the lateral variation of interval velocities, from sonic logs generated in D-16, D-1, and D-12/103

porosity, and that is illustrated from the wells drilled in the reef flanks (e.g. D16, D12, and D22/103). These wells encountered one or more significant nonporous, non oil-bearing intervals within the reservoir, and this make the velocity increase towards those directions.

4.1.2 Seismic velocities

4.1.2.1 Background

The following section describes the seismic velocities which are used in this work.

(i) Normal Moveout Velocity (Stacking velocity)

Seismic velocity is important in data processing to correct for the normal moveout (NMO) due to the separation of the source and receiver. This kind of seismic velocity called normal moveout velocity (V_{NMO}), which is obtained from reflection time/distance relationships, is used to stack seismic traces. V_{NMO} is given by the following formula :

$$V_{NMO} \approx \frac{X}{\sqrt{T_x^2 - T_0^2}} \dots\dots\dots 4.1$$

where :

X : source to geophone spacing

V_{NMO} : Normal Moveout Velocity

T_0 : two-way reflection time when $x=0$

T_x : two-way reflection time for any distance x

V_{NMO} varies with offset and also varies with time. V_{NMO} is invariably greater than average velocity, because the ray-paths used in calculating V_{NMO} do not

coincide with the minimum ray-path followed by the sound waves (*Badley*, 1989).

(ii) Root Mean Square velocity (V_{RMS})

V_{RMS} is the weighted root mean square of the component interval velocities, and refers to a specific ray-path, the least-time path through a layered medium, and for small offsets V_{RMS} is obtained from the following relationship :

$$V_{RMS} = \left(\frac{\sum_{i=1}^n V_{I_i}^2 \cdot \Delta t_i}{\sum_{i=1}^n \Delta t_i} \right)^{1/2} \dots\dots\dots 4.2$$

where :

V_{RMS} : root mean square velocity

V_{I_i} : interval velocity for the i'th layer ($1 \leq I \leq n$)

Δt_i : the difference in two-way reflection time for i'th layer.

When we have horizontal velocity layering and horizontal reflectors, V_{RMS} is not same as the V_s . In general the V_{RMS} value is a mathematical quantity and devoid of any physical meaning (*Badley*, 1989). For the availability of interval velocity from a well survey (D1/103) and other velocity informations from sonic logs. Then the RMS velocity can be calculated and can be used for a normal moveout correction (ΔT). The RMS

velocity will always give a better result for ΔT than the average velocity calculated from the same survey.

(iii) Interval velocity (V_{int})

Seismic wave velocity is measured over a depth interval. In sonic log determinations the interval may be 1 to 3 feet. In well shooting it may be as great as 1000 feet or more. This usually implies measurements across the bedding.

The Dix (1955) formula can be used to estimate interval velocity (V_{int}) between any pair of V_{NMO} events.

$$V_{int} = \left(\frac{V_{RMS_n}^2 \cdot T_n - V_{RMS_{n-1}}^2 \cdot T_{n-1}}{T_n - T_{n-1}} \right)^{1/2} \dots\dots\dots 4.3$$

Where :

- V_{int} : interval velocity.
- V_{RMS_n} : Root mean square velocity at the upper level.
- $V_{RMS_{n-1}}$: Root mean square velocity at the lower level.
- T_n : Two-way or one-way time to upper level.
- T_{n-1} : Two-way or one-way time to lower level.

(iv) Average velocity ($V_{av.}$)

The distance traversed by a seismic pulse is divided by the required time, and often corrected to a reference datum plane. The average velocity is used

to convert from travel time to depth, because it is the true vertical velocity in the ground. However the average velocity should never be used for NMO calculations because it gives a ΔT that is too large.

$$V = \frac{\sum_{i=1}^n V I_i \cdot \Delta t_i}{\sum_{i=1}^n \Delta t_i} \dots\dots\dots 4.4$$

where :

V : Average velocity

$V I_i$: Interval velocity for n layers

Δt_i : The difference in two-way reflection time for n layers.

The average velocity is used to convert from travel time to depth.

4.2 *Seismic velocity analysis and mapping*

4.2.1 *Why processing seismic velocities are unsuitable for depth conversion*

In order to assess the suitability of using seismic velocities for depth, a horizon consistent seismic velocity dataset was generated for the El-giza, Gir, Kheir, and Upper-Sabil horizons.

This entailed sampling the stacking velocity functions at times which corresponded to the picked horizon times for the four events. The interval velocities were calculated from the root mean square velocities using equation 4.3. Each velocity dataset was subsequently hand gridded and contoured.

However, the trends apparent from the well datasets, in particular the regional velocity increase towards the northeast, may be a result of the nonporous rock, as shown in Section 4.1.

This knowledge of the velocity distribution over the area is useful but usually is not accurate enough, e.g. the difference between the seismic interval velocity and the well velocity surveys at some shot points approach ± 1000 m/s. For more detail see Appendix, Tables 4.11 to 4.17. By way of example, and to show how the seismic velocities are inaccurate in the area, two seismic sections are selected: U-14 and U-25. These show the average interval velocities through each line and the difference between the well velocities (D1/103) and the seismic interval velocities (Figs. 4.5 & 4.6).

Line U-25, shown in Figure 4.6, passes through wells D16, D1, and D12, illustrated in Figure 4.4. The following table compares the wells and seismic average interval velocities, in particular for the main interval horizons.

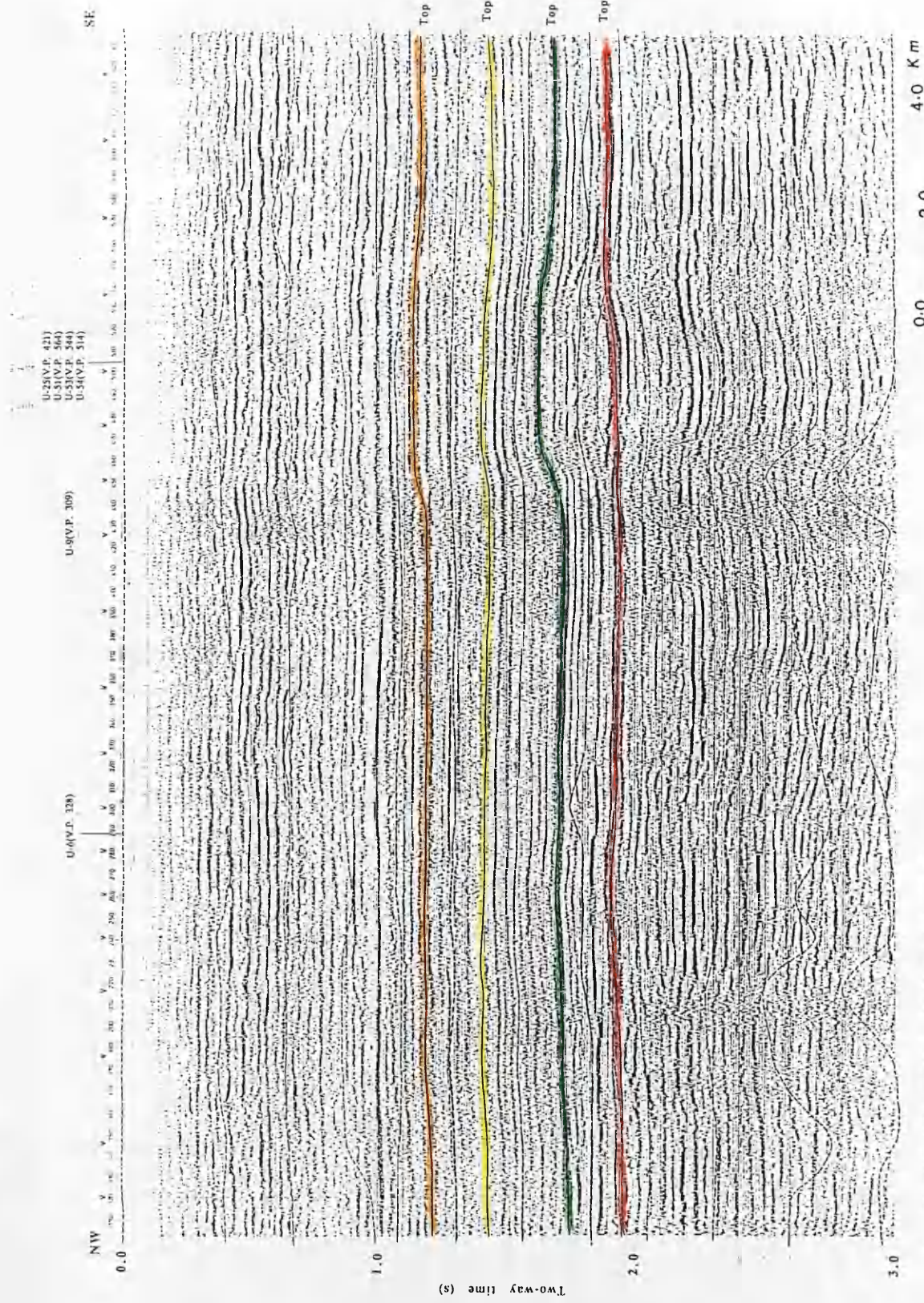
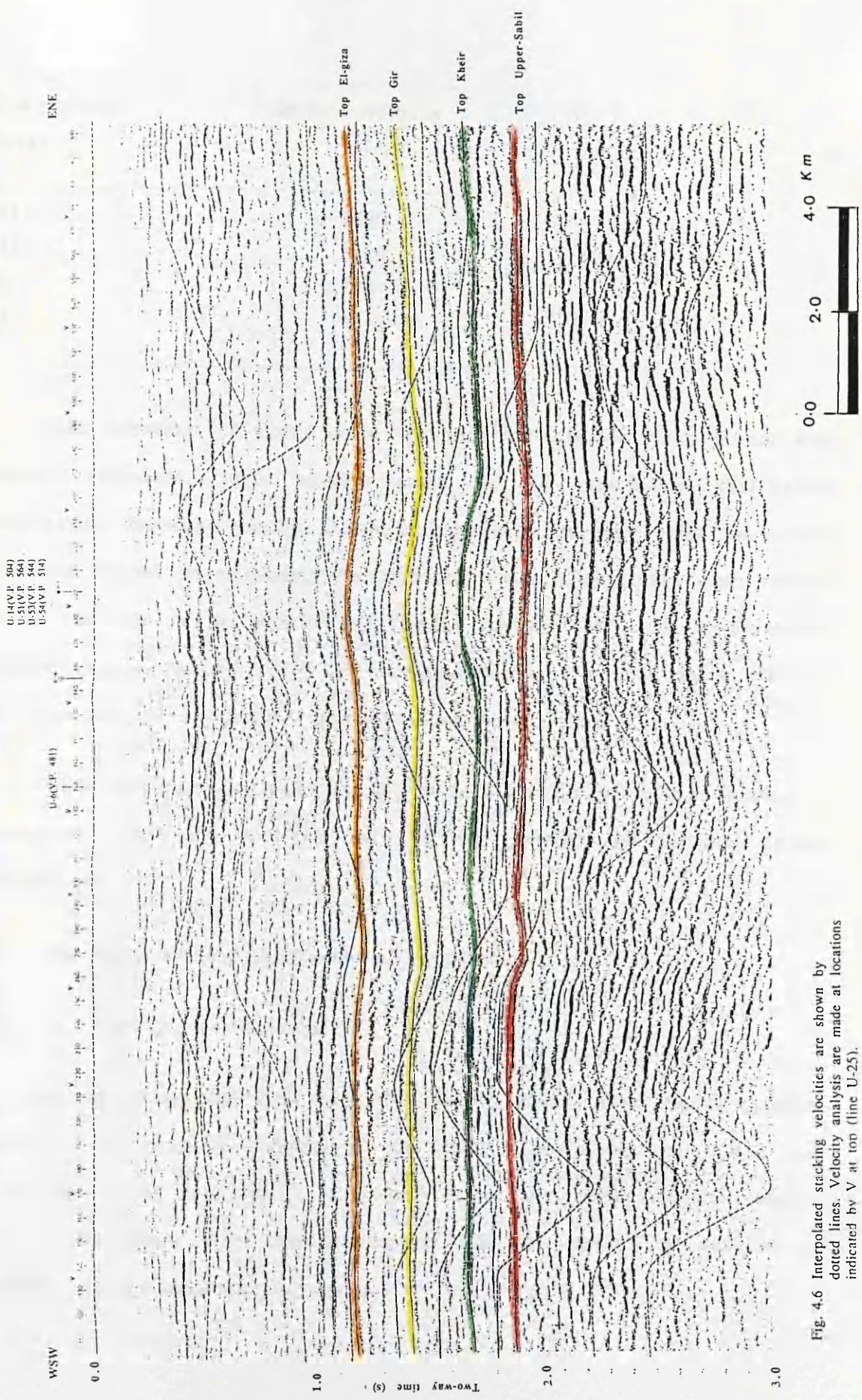


Fig. 4.5 Interpolated stacking velocities are shown by dotted lines. Velocity analysis is made at locations indicated by V at top (line U-14).



U-14(V.P. 564)
 U-15(V.P. 565)
 U-51(V.P. 544)
 U-52(V.P. 543)

U-60(V.P. 481)

WSIV

ENE

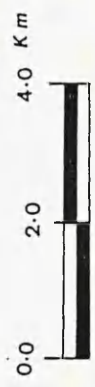


Fig. 4.6 Interpolated stacking velocities are shown by dotted lines. Velocity analysis are made at locations indicated by V at top (line U-25).

Well velocity (m/s)	Seismic velocity (m/s)
3613	2852
4129	3499
4053	3787
4240	5052

The behaviour of elastic wave velocities in carbonate rocks is not well known. Therefore, some authors come to the conclusion that clear relationships between velocity, depth and porosity, as they exist for clastic sediments, cannot be established for carbonate rocks. One of the main reasons for this is seen in the presence of vugular porosity and, to a lesser extent, fracture porosity which affects the compressibility of a rock in a different way from that of intergranular porosity (*Jankowsky, 1969*).

Most carbonate sediments are in reality a mixture of several lithological components. Generally we can say that the velocity of carbonate rocks depends on:

- (i) The type, size and distribution of its porosity.
- (ii) Its lithologic composition.

In the Intisar "D" field case the features which create highly complex conditions are material composition and fabric (principally type, size and distribution of the pore space). It is well known that most computer velocity analysis procedures make the assumption that the subsurface consists of uniform isotropic non dipping layers.

The seismic velocities are therefore inaccurate in the field for the following reasons :

- (1) As a result of the dipping reflectors, in the reef flanks where the dip become steep (about 32° , as illustrated in Chapter 2), this influences the calculated velocity values. To correct the velocity values we divide the values by the cosine of the dip. In practice it is better to avoid this velocity analysis location.
- (2) The interval velocities which represents the physical property of the rocks were calculated by using Dix's equation (1955), (eq. 4.3) which is valid only for horizontal layers.
- (3) Anisotropy, where the stacking velocities are correct, but gave an error in computing true interval velocity and true average velocity (using time to depth conversion).
- (4) Noise, acquisition geometry errors and static errors.
- (5) Errors in picking spectrum.

The pull-down which is revealed in the seismic sections, in particular U-14 and U-51, is a result of the slower interval velocities of the reflections below the reef build-up than those of the surrounding strata, the lower interval velocity being relative to the high porosity limestone.

The inaccuracies in the Dix velocities usually becomes apparent when a check-shot survey is available, for the following reasons (*Badley, 1989*) :

- (i) Difference in the ray-paths; check-shots are near vertical and travel only one-way.

- (ii) Inaccuracies, errors and false geometric assumptions concerning the stacking velocities.
- (iii) Departure from the assumption of horizontal layering for stacking velocities.

In addition to these problems, there are pitfalls in using Dix interval velocities for depth conversion.

Furthermore, the seismic lines U-14 and U-25 pass close to the well D1/103, and to show the difference in interval velocity in the well and in the seismic sections. The comparison of the interval velocities obtained from the sonic log (D1/103), and those from the Dix's (1955) formula at the closest shot points (VP. 501) and (VP. 415) where a velocity analysis is performed in the lines U-14 and U-25 respectively. Figures 4.7 and 4.8 show the difference between well and seismic velocities. On the other hand Figure 4.9 shows the difference between well and new seismic velocities become small.

On the two sections mentioned above, the times picked during processing are usually made without reference to a specific reflection, but instead are chosen on the basis of reflection strength at each velocity analysis location. Stacking velocity (rms velocity) is then interpolated without considering the geological information of the area. The application of good geological sense is often one of the best tools for reconciling anomalous points in a velocity distribution.

A velocity contrast commonly exists between the reef build-up and laterally equivalent strata, resulting in differences in seismic travel time through the strata (*Hatlie et al., 1977*).

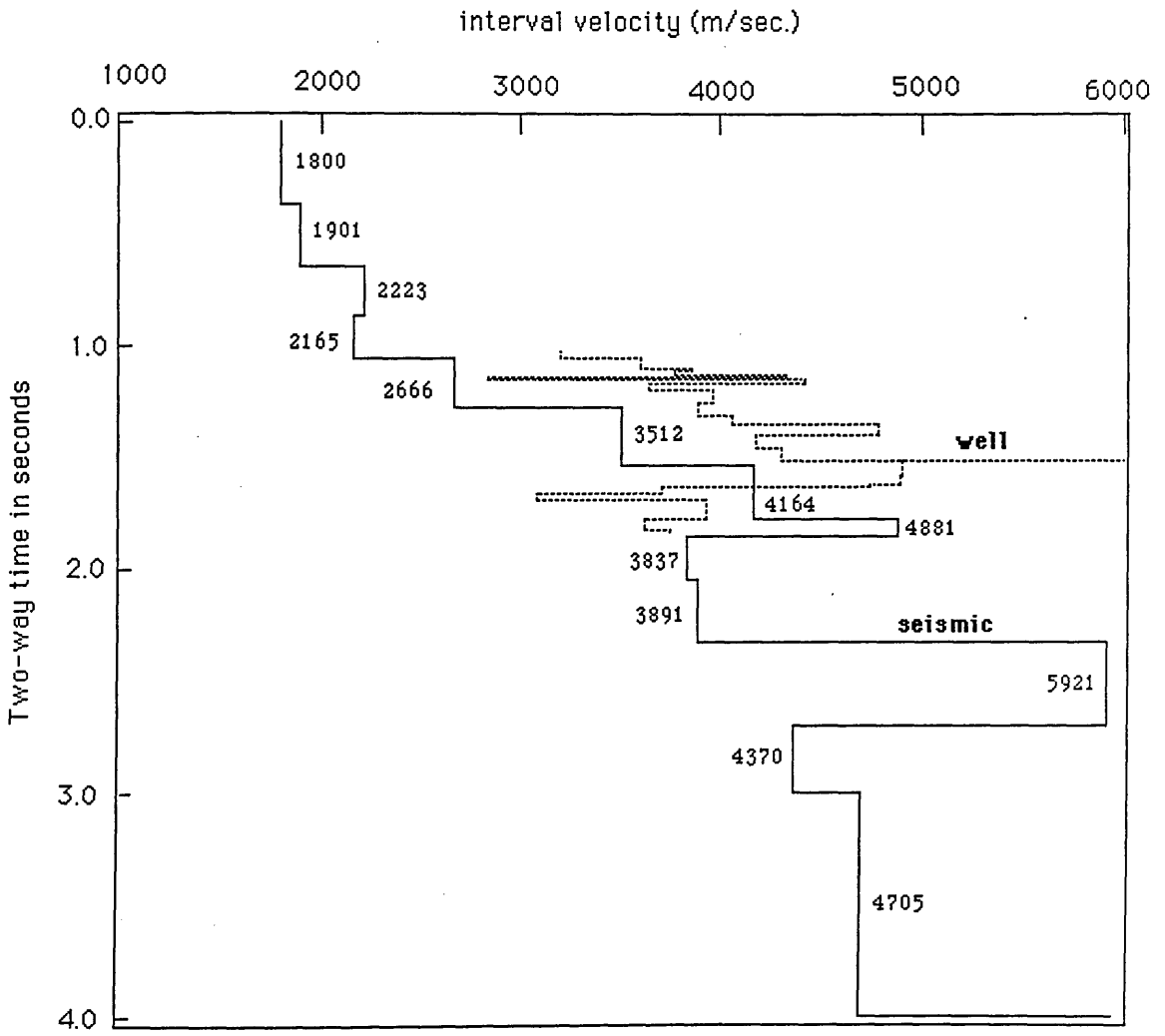


Fig. 4.7 Comparison of interval velocities obtained from sonic log (D1/103) and Dix formula sp. 501 in line U-14.

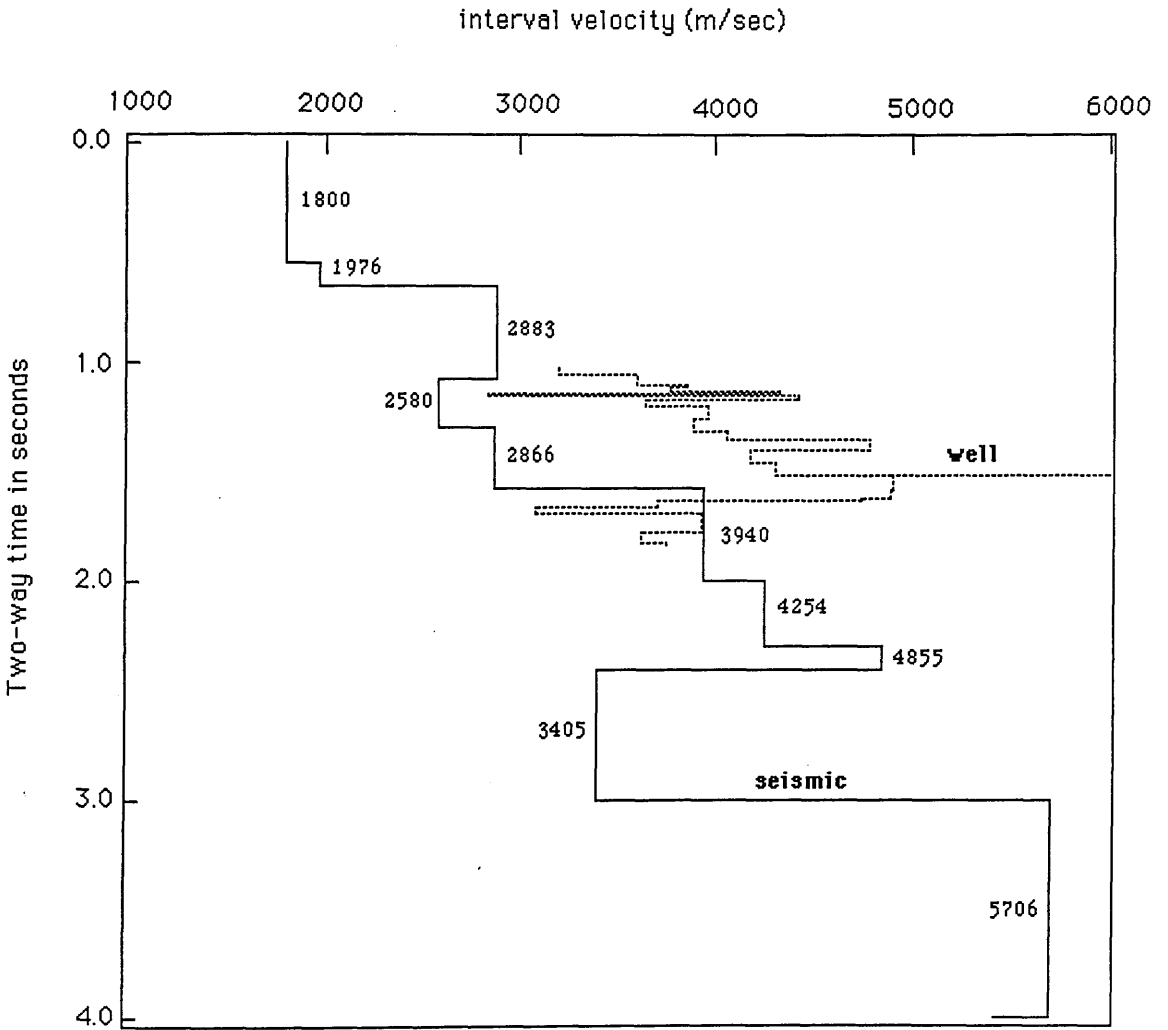


Fig. 4.8 Comparison of interval velocities obtained from sonic log (D1/103) and Dix formula sp. 415 in line U-25.

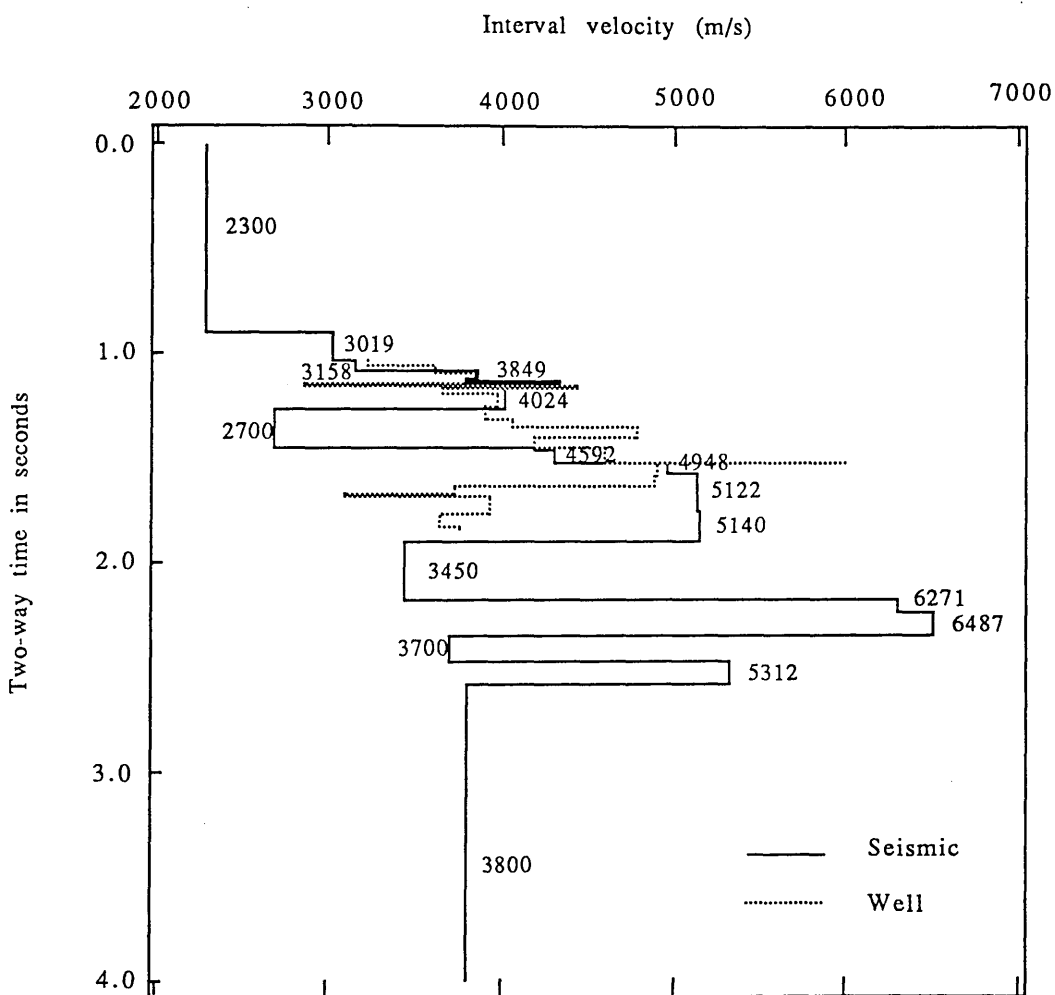


Fig. 4.9

Comparison of interval velocities obtained from sonic log (D1/103) and new seismic velocities in CDP 310 (V.P. 503) in line U-14.

In order to obtain accurate velocity information for performing depth conversion and stratigraphic analysis, the velocity analyses need to be closely spaced and keyed to reflection horizons.

For more accurate velocity estimates, correlating better with the sonic logs in the field, I have reprocessed part of line U-14, which crosses the structure. The new processing sequence, including the essential step (the velocity analyses) is presented in Chapter 5.

4.2.1 *Velocity mapping*

Three types of velocity maps were constructed :

- (i) Average velocity maps.
- (ii) Interval velocity maps.
- (iii) Maps showing the difference between well and seismic velocities.

The three types of velocities including a new velocity analysis for the reprocessed part of line U-14.

The average velocity maps show the lateral variations in the top of each horizon, and the most important influence on velocity is, of course, depth. More detail about the velocity interpretation illustrated with maps will be given in the following sections.

(i) Average velocity maps

The contour patterns on all average velocity maps are sufficiently similar, so that the area can be divided roughly into zones of low, medium, and high velocity. These contours show that the velocities differ by more than 1000 m/s from one side of the area to the other.

The velocity anomalies on the all maps reveal similarity in shape and variations. The average velocity values in the top of each horizon are shown in the Appendix (Tables 4.1 - 4.7).

Top El-giza average velocity map

Figure 4.9 shows the top El-giza average velocity, which is high in southwest and northeast. The anomalous values are 3200 and 3500 m/s. respectively. On the other hand the average velocities are low in northwest and southeast; 2300 and 2500 m/s respectively.

Top Gir average velocity map

The average velocities of the top Gir are illustrated in fig. 4.10. Generally the anomalous zones are similar to those for the top El-giza. The lowest velocity region is 2500 m/s, and the highest region is 3700 m/s. The velocities increase toward the northeast, as mentioned before. The Gir average velocity map shows closely spaced contours, which means a large gradient.

Top Kheir average velocity map

The iso-velocity contours become closer and denser, and the velocity increases to the northeast (Fig. 4.11), where the velocity is 4200 m/s. High velocity occurs around the location of velocity analysis VP. 375 on line U-25, where it is 4700 m/s. Elsewhere, values are about 3500 m/s over all the area at this level.

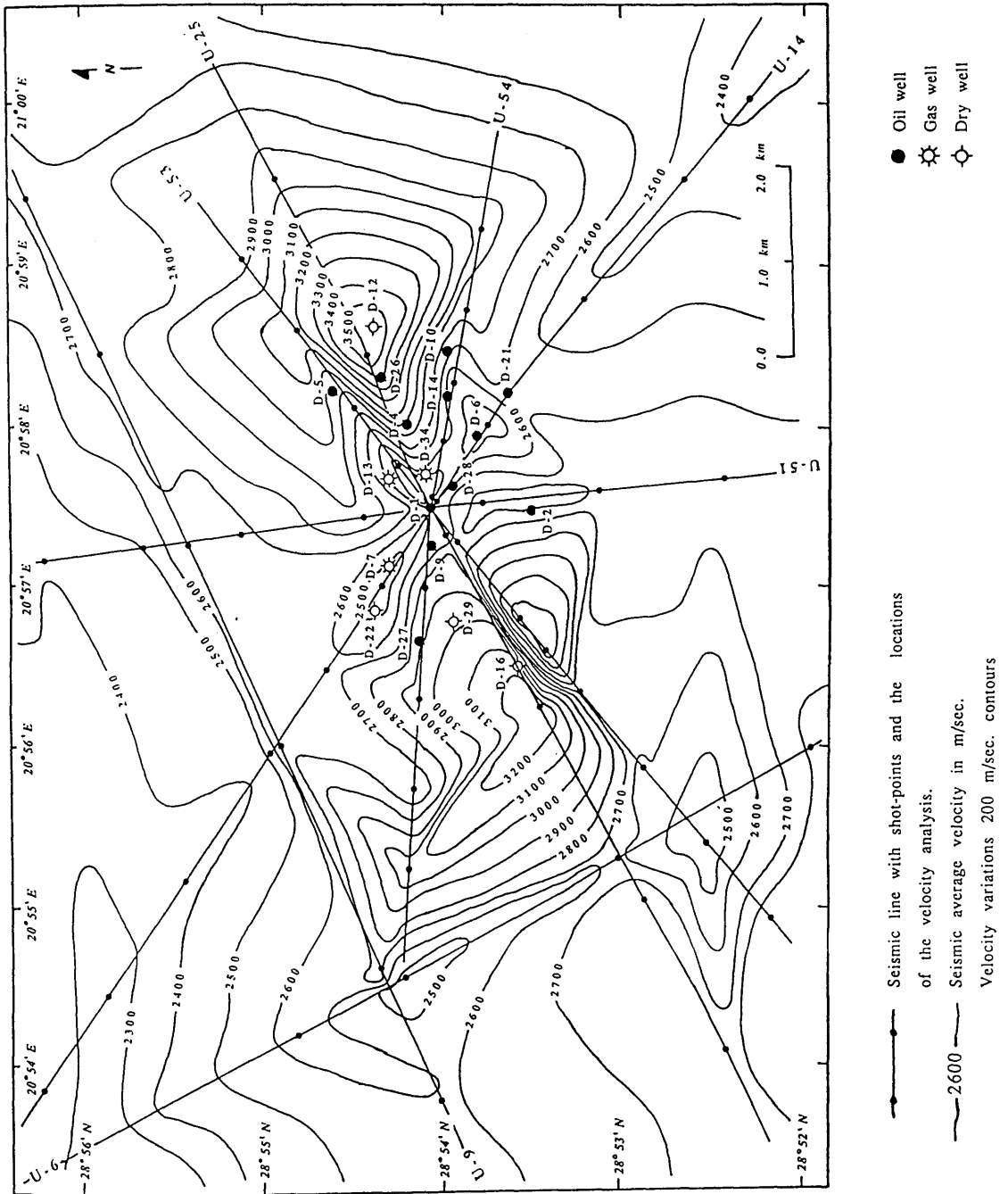


Fig. 4.9 Top El-giza average velocity map.

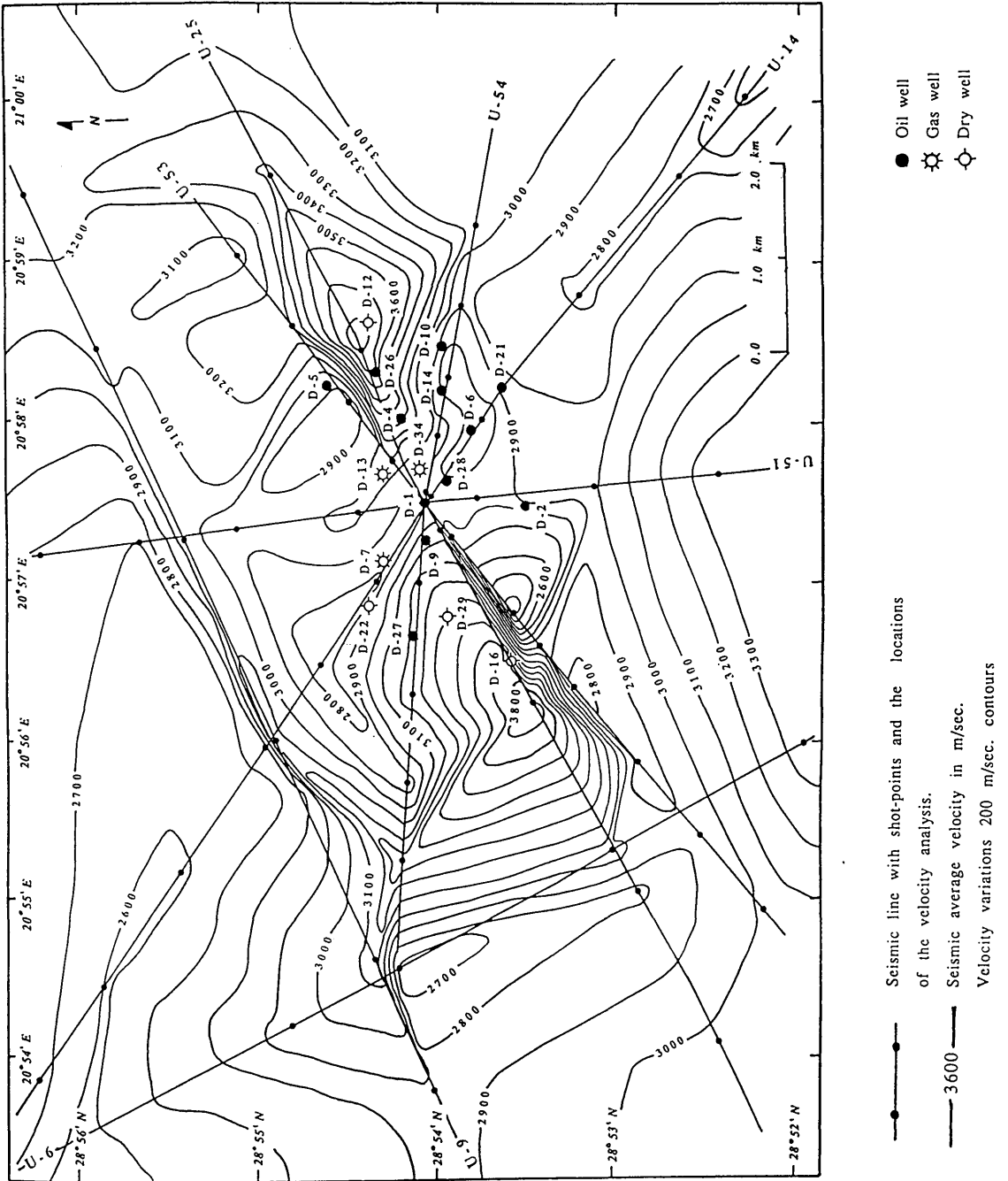


Fig. 4.10 Top Gir average velocity map.

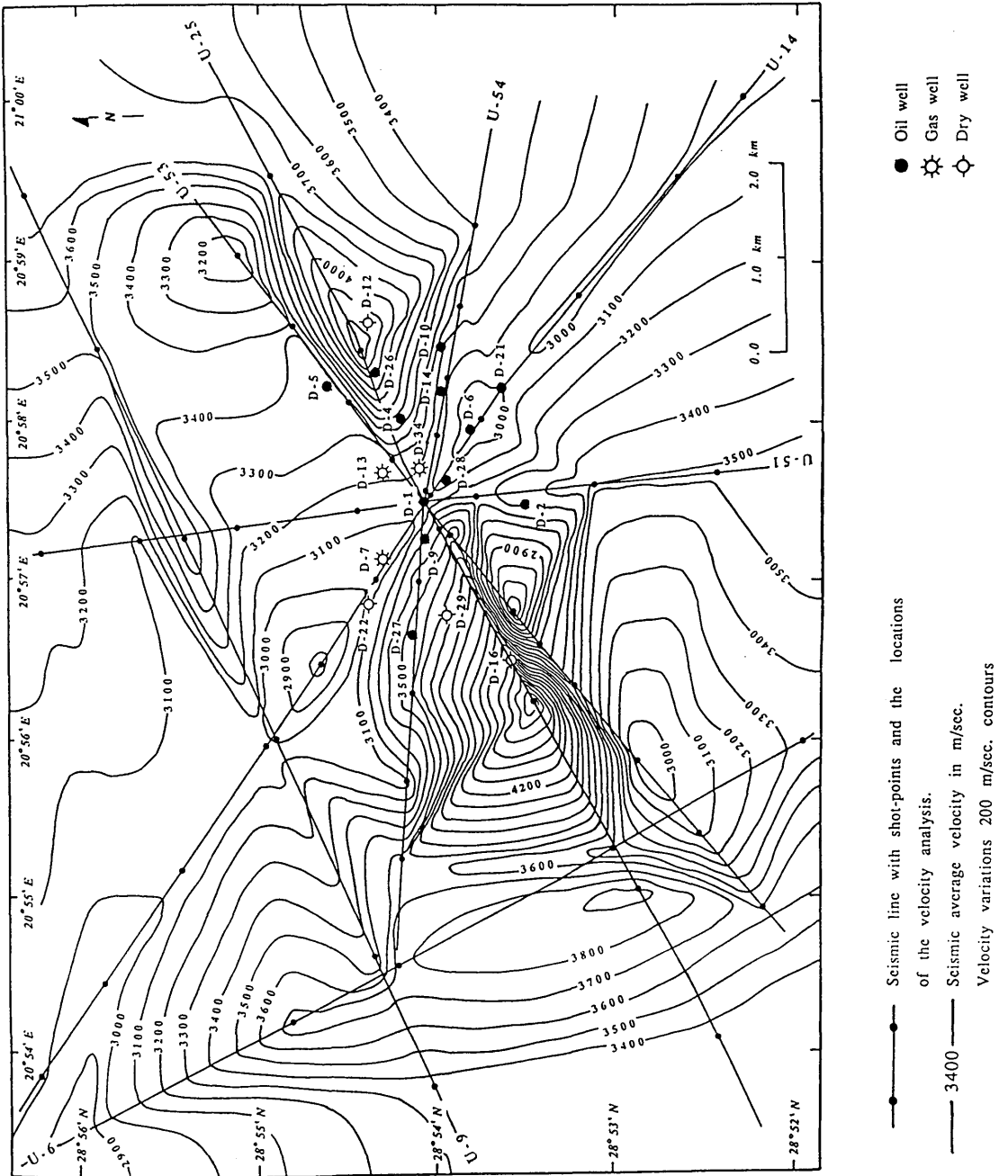


Fig. 4.11 Top Kheir average velocity map.

Top Upper-Sabil average velocity map

Figure 4.12 shows the average velocity contours for the top Upper-Sabil. As above, the velocity is high in the northeast (4200 m/s), but becomes higher in the southwest (5300 m/s) in the location of velocity analysis at VP. 375 on line U-25.

(ii) *Interval velocity maps*

The Dix's (1955) formula is used to estimate interval velocity (V_{int}) between any pair of (V_{NMO}) events.

The interval velocities which are obtained by using the above formula are placed on the base map (1:10,000) were generated approximately every 1600 m on each seismic line. The following paragraph will interpret the interval velocities from the maps in the three sequences El-giza to Gir, Gir to Kheir, and Kheir to Upper-Sabil. The contours illustrates the importance of the lateral changes, the rate of change of the interval velocity take sudden bends at the seismic lines. From the geological point of view the closer contour around one shot point is meaningless. The interval velocity values in the El-giza to Gir, Gir to Kheir, and Kheir to Upper-Sabil intervals are shown in the Appendix (Tables 4.1 - 4.7).

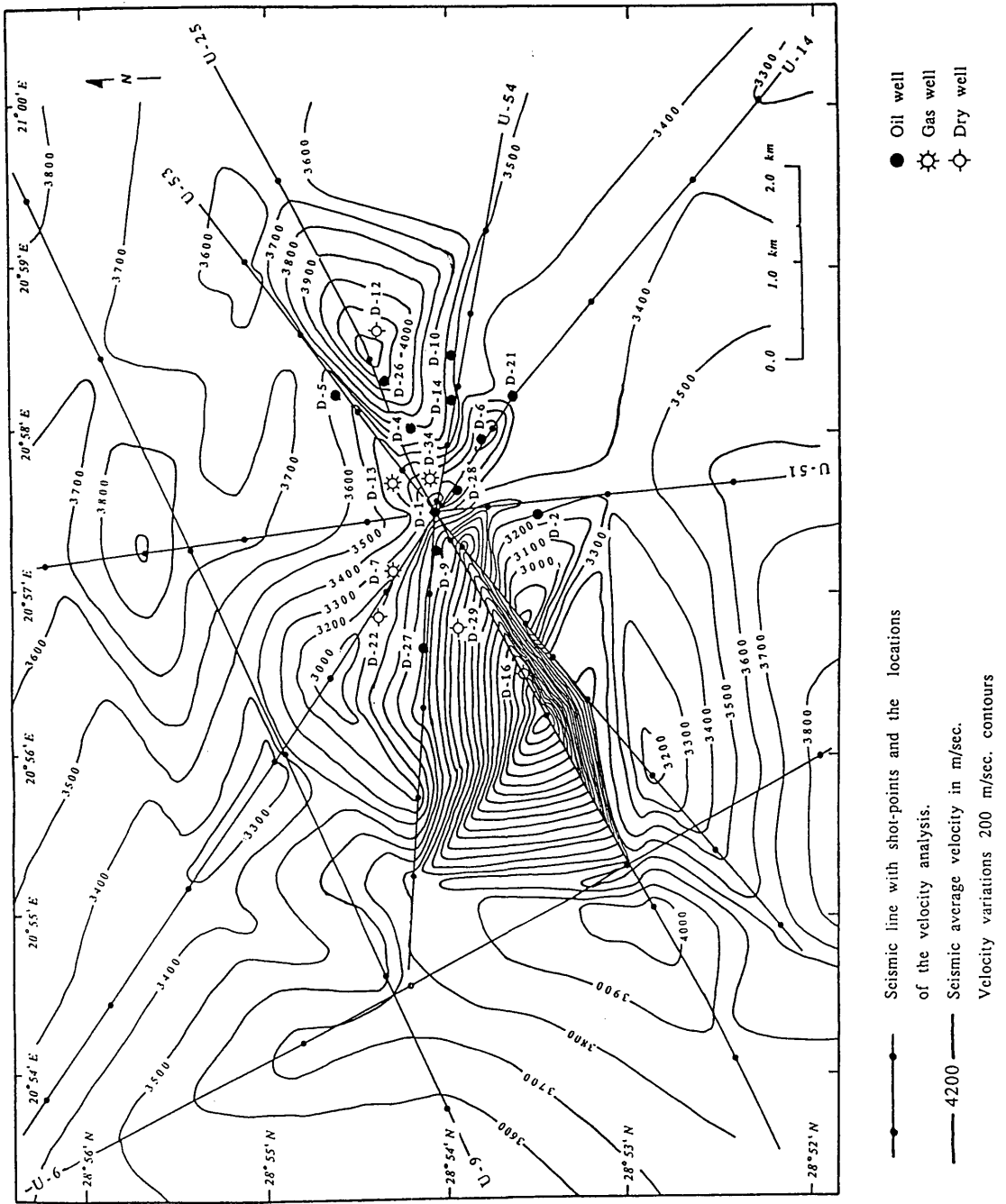


Fig. 4.12 Top Upper-Sabil average velocity map.

El-giza to Gir interval velocity map

The interval velocity contour map (Fig. 4.13) shows the high and low velocity anomaly contours over the El-giza to Gir interval.

High velocities are found at the southwest at the end of seismic lines U-25, U-53, and U-6, in particular at shot-point 326 on line U-53, where it is 4000 m/s. In the northeast the interval velocities increase as well, the closure velocity anomaly contour being 4800 m/s. These two anomalies indicate that the facies changes on both sides of the reef build-up. It is common that at a given depth older or harder rocks have higher velocities. Interval velocities are low in the northeast (2400 m/s), increasing gradually towards the southwest, while in the centre of the area they are 2800 m/s, becoming lower in the southeast (2600 m/s).

Gir to Kheir interval velocity map

The Gir to Kheir velocity map (Fig. 4.14) shows the interval velocity variations over this sequence.

The highest interval velocity is 5200 m/s. The closure contour is around one shot-point (469) on the line U-53, and results from the error in stacking velocity, which is located on the reef flank, where there is a steep dip as at this location. Therefore from a geological point of view, this velocity anomaly is meaningless. The velocities are uniform over this sequence except in the southern area, where they become wide distributed and high-up to 5200 m/s.

In general the interval velocity is high in the south, and low in other areas.

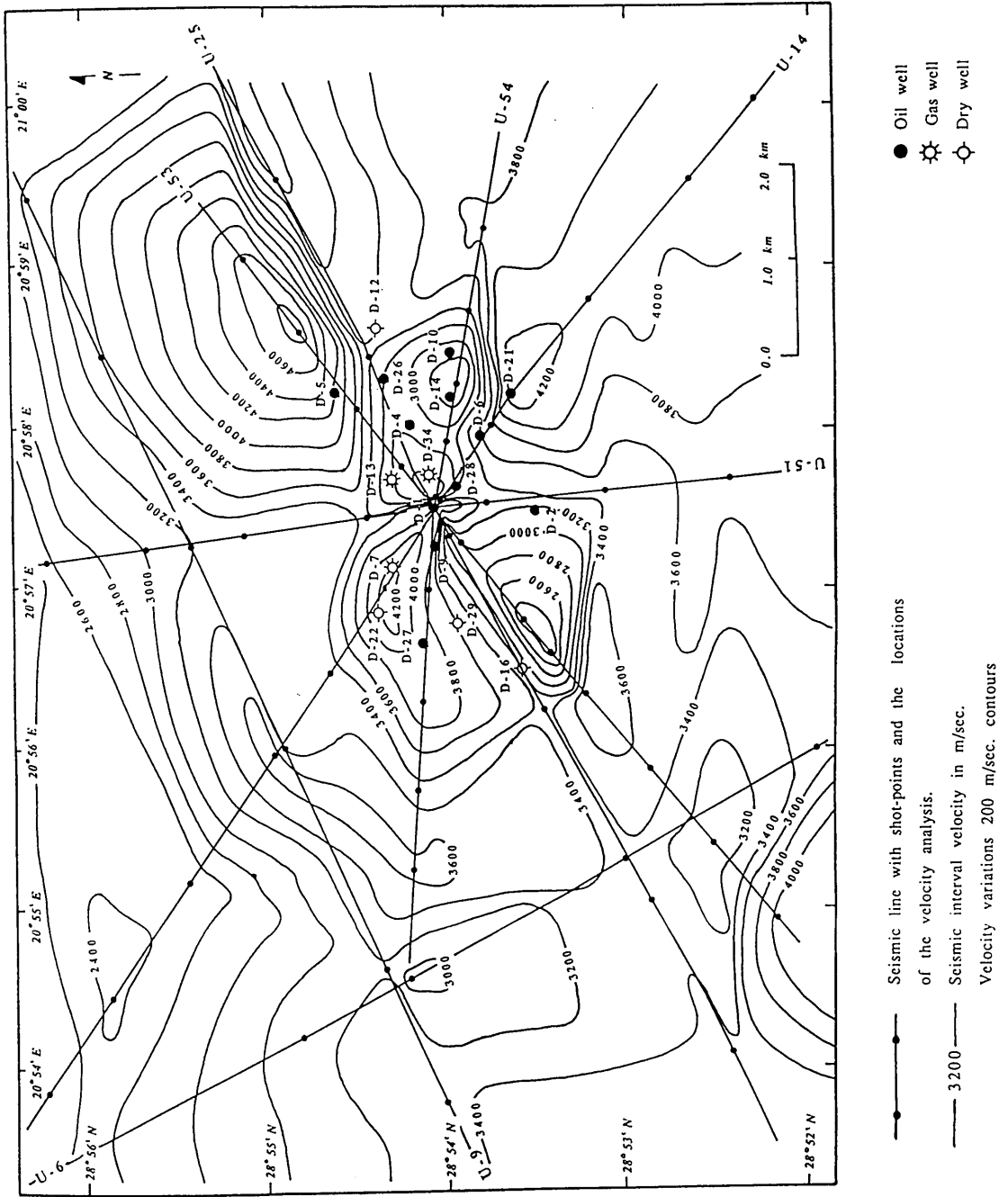


Fig. 4.13 El-giza to Gir interval velocity map.

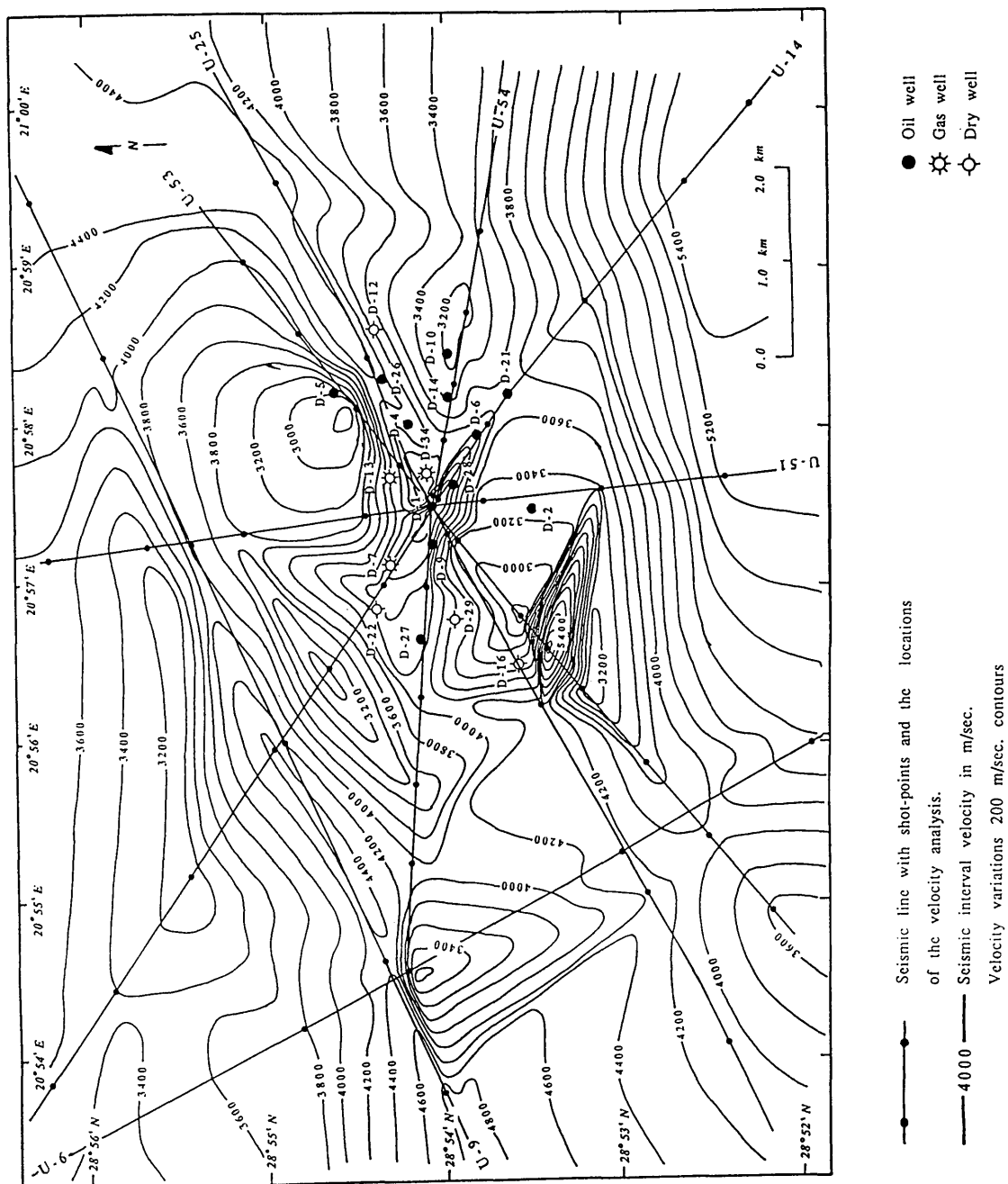


Fig. 4.14 Gir to Kheir interval velocity map.

Kheir to Upper-Sabil interval velocity map

This is the deepest interval interpreted, and it includes the reef structure. Figure 4.15 shows the interval velocity variations; the contours in this interval become more densely spaced, and show high interval velocities over all the area.

The interval velocity contour map illustrates high velocity in the west part of the area (6600 m/s); in the south it is 4800 m/s; in the east 5200 m/s. In the centre of the area it increases from 3400 to 4800 m/s, and in the north it is up to 5000 m/s.

Generally the interval velocity is high on the periphery and low in the centre where the reef grew. The low velocity is over the structure; this may be from the influence of porosity and the fluid content (oil and gas).

The interval velocity maps show similar zones of high, medium, and low velocity. The contours of all the maps tend to take sudden bends at the seismic lines, as shown in the El-giza to Gir interval velocity map, the contours take sudden bends at the seismic lines U-25, and U-53, where the two lines are close in the northeast and in the southwest. The sudden bends increase in the deep sequences (Gir to Kheir interval, and Kheir to Upper-Sabil interval), may be as a result of the mis-tie which is obvious in the seismic lines intersections.

Therefore from a geological point of view, these velocity maps are inaccurate.

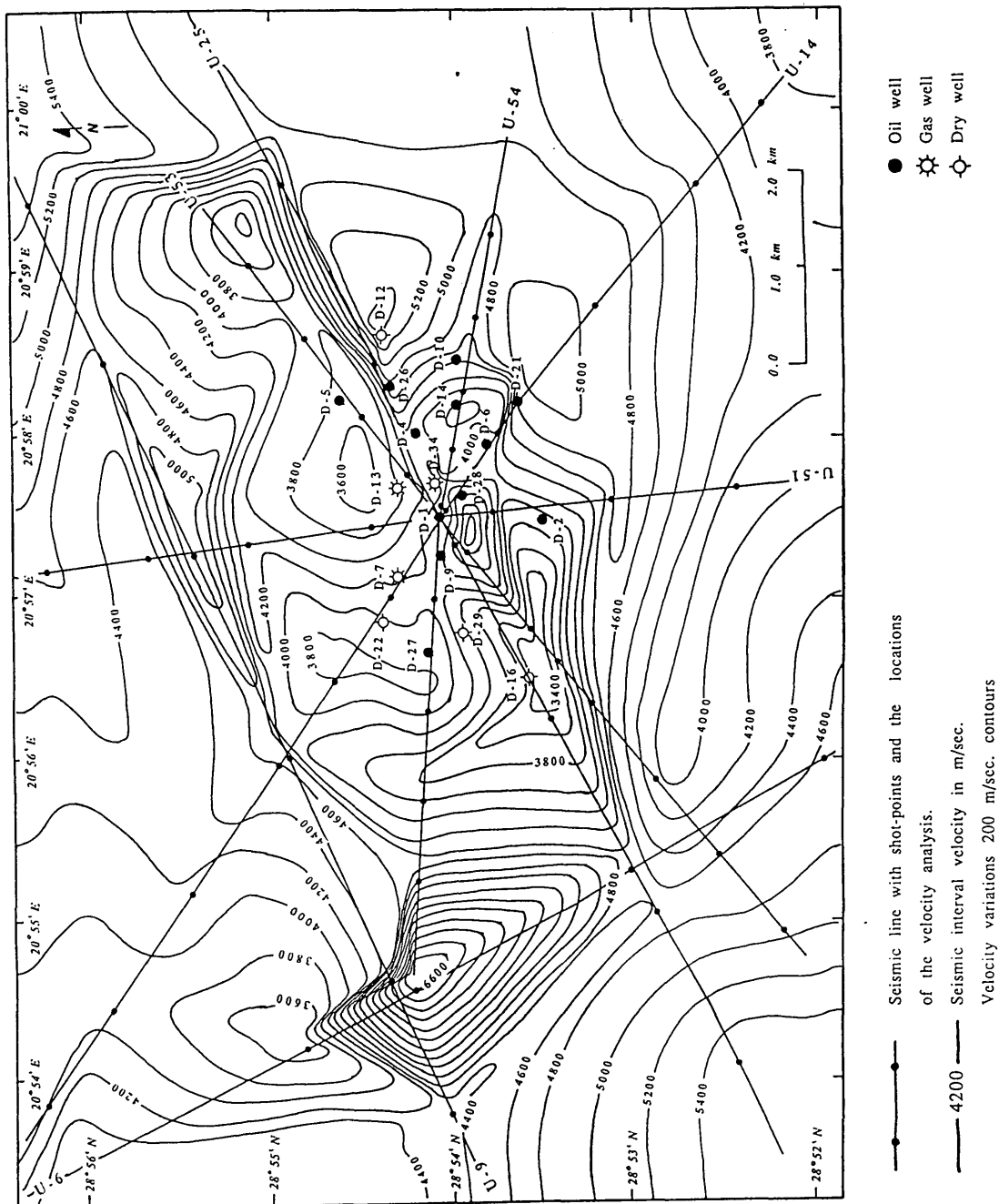


Fig. 4.15 Kheir to Upper-Sabil interval velocity map.

(iii) *The difference between the well velocity survey and seismic velocity maps*

The seismic interval velocity maps values shown in Figures 4.13, 4.14, and 4.15 are simply subtracted from the well velocity survey values in well (D1/103), from the assumption that we have a constant accurate velocity, to show the location where there is a difference between the two kind of velocities.

Figures 4.16, 4.17, and 4.18 show the difference between the well velocity surveys and seismic interval velocity.

In Fig. 4.16 some velocity anomalies are up to ± 1600 m/s in SP.(496), in line U-53, ± 1400 m/s in SP.(571), 1600 m/s in SP.(356), and ± 1200 m/s in SP.(451) in line U-14. Other velocities anomalies show a lower difference range from ± 200 m/s to ± 800 m/s. After changing the velocity along line U-14 and using the new velocity picked from the spectrum, the differences between the well and the seismic velocity for the interpreted horizons become small.

Fig. 4.17 exhibits the difference between the well velocity survey and seismic interval velocities in Gir to Kheir interval. In this interval three anomalies showing high difference ± 2000 m/s in SP.(426) in line U-14, SP.(596) and SP.(486) in line U-53, and ± 1600 m/s in SP.(606) in line U-14. The difference in this interval is high for all over the area.

Fig. 4.18, this map shows the difference in the deep interval Kheir to Upper-Sabil, the velocity anomaly in SP.(340) in line U-6 the difference ± 3000 m/s and ± 1600 m/s in SPs.(375 and 455) in line U-25. Other velocities anomalies have a range of ± 1000 m/s to ± 200 m/s.

The difference maps, apparently apply equally well to the previous interval velocity, where the contours have the same trend, and confirm that the seismic interval velocities are larger than the well-velocity survey.

The difference between the seismic interval velocity and well velocity survey values in the El-giza to Gir, Gir to Kheir, and Kheir to Upper-Sabil intervals are shown in Appendix (Tables 4.11 - 4.17).



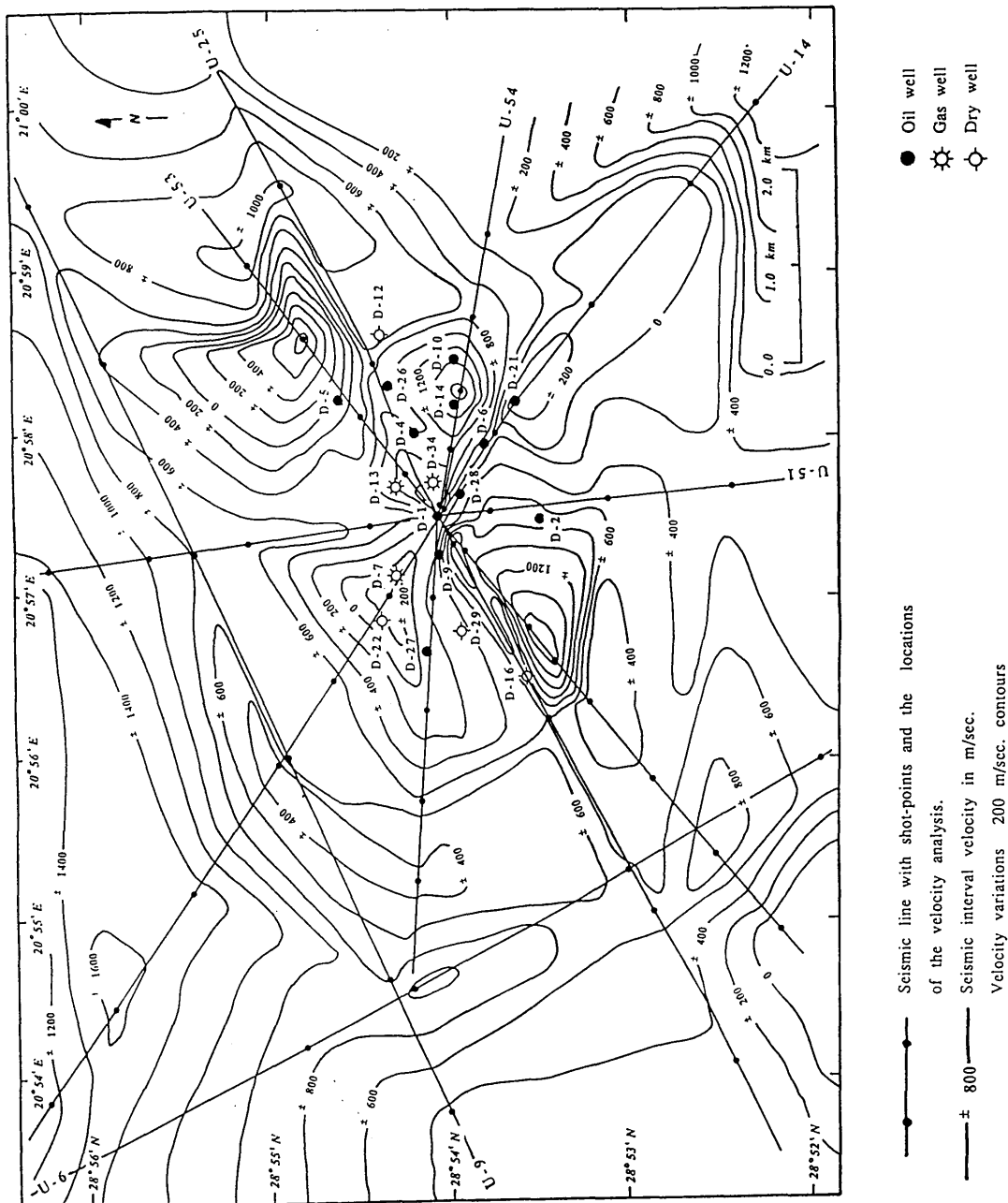


Fig. 4.16 The difference between the seismic interval velocity and the well velocity survey (D1/103) in the El-giza to Gir interval

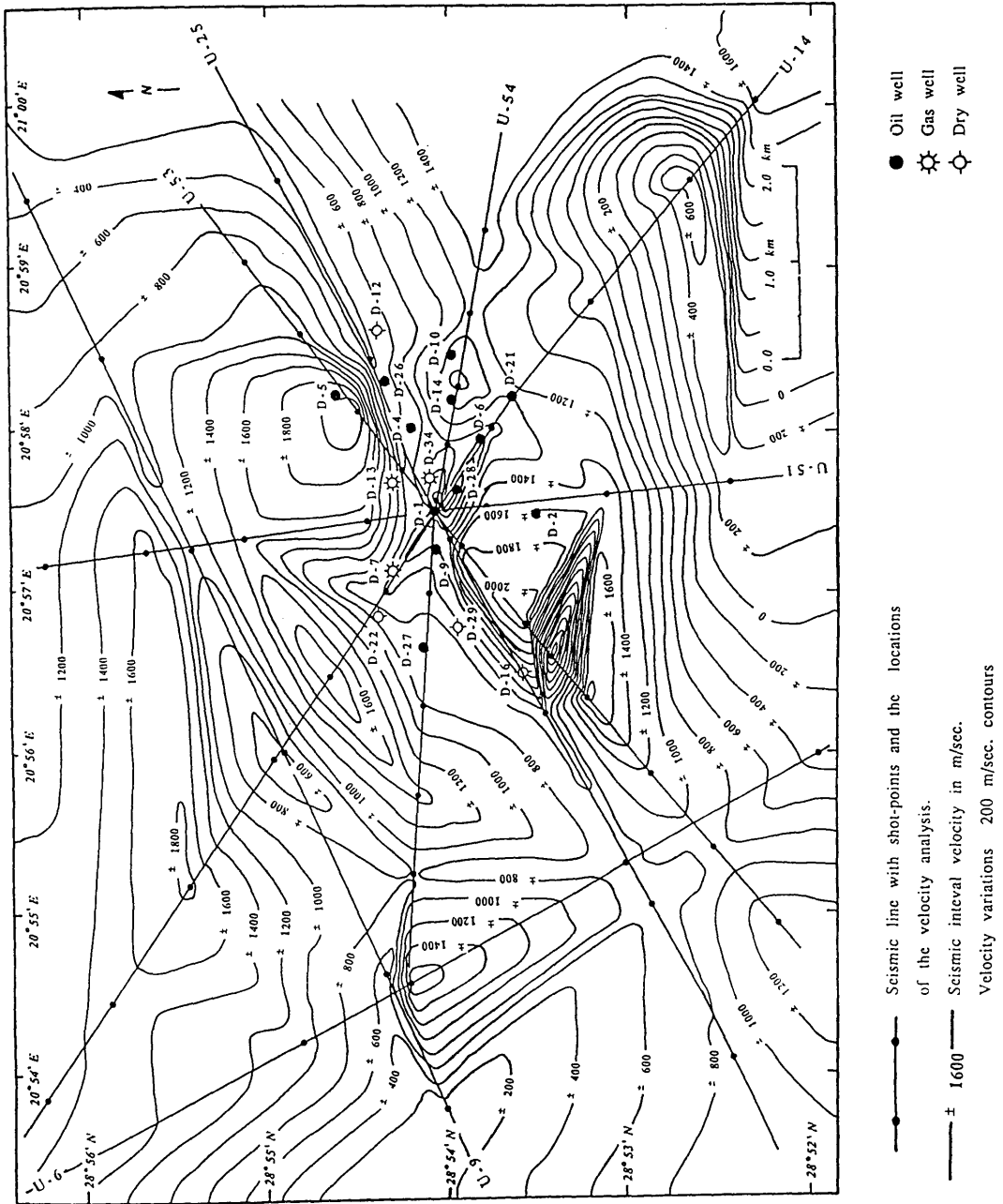


Fig. 4.17 The difference between the seismic interval velocity and the well velocity survey (D1/103) in the Gir to Kheir interval

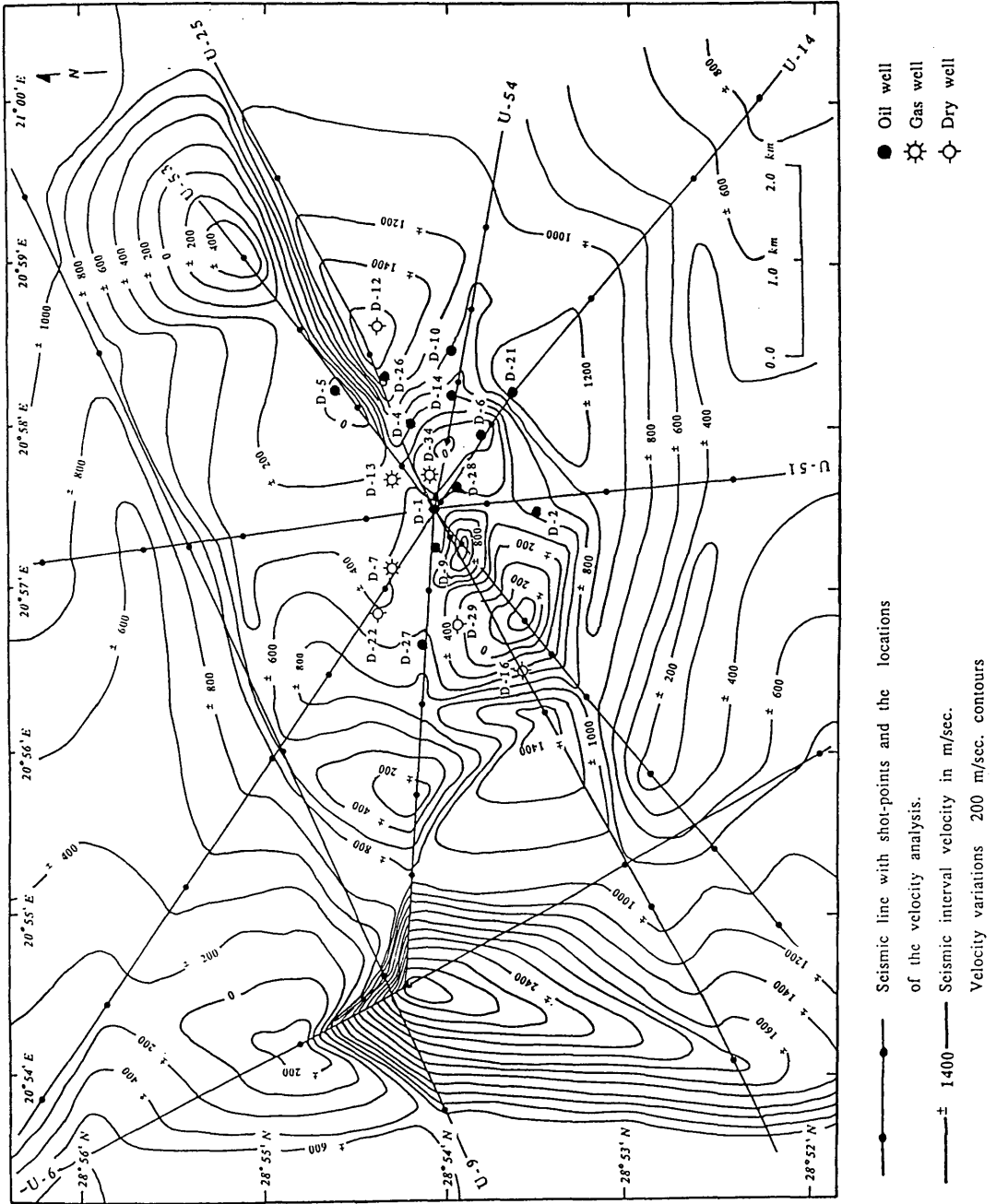


Fig. 4.18 The difference between the seismic interval velocity and the well velocity survey (D1/103) in the Kheir to Upper-Sabil interval

4.3 *Summary of velocity interpretation*

- (1) The errors in normal-moveout corrections can produce sizeable errors in stacking velocities; especially for deep reflections (Fig. 4.3); these in turn cause large errors in the calculation of interval velocities, especially when the interval is small.
- (2) Velocity measurements are sometimes severely distorted by various factors, such as interference effects, noise of various kinds, and distortions produced by shallow velocity anomalies or weathering variations.
- (3) For non-parallel upper and lower boundaries the interval velocity calculations are unreliable.
- (4) Stacking velocities depend on the geophone spread geometry. Long spread lengths show higher velocities and vice versa.
- (5) Well velocity surveys show that lateral velocity variations in the Intisar "D" field are serious enough to require systematic correction of the seismic data.
- (6) The seismic interval velocity maps as shown in Figs. 4.13, 4.14, and 4.15, generally show low interval velocity over the reef structure, in the centre of the area, and high on the boundaries (periphery).

Chapter 5

5.0 Data Processing

5.1 Introduction

5.1.1 Background

5.1.2 Method

5.2 Processing procedures

5.2.1 Data background

5.2.2 Seismic Processing sequence

5.3 Pre-stack processing

5.3.1 Static and residual static corrections

5.3.2 Deconvolution before stack

5.3.3 Velocity analysis

5.3.4 Normal moveout correction

5.3.5 Stacking

5.4 Post-stack processing

5.4.1 Deconvolution after stack

5.4.2 Filtering

5.5 Results

5.6 Migration

5.7 Summary of processing

5.1 Introduction

5.1.1 Background

The seismic data processing involves three basic steps of operation: data correction, data enhancement and data display. It is aimed at producing a final section with an optimum resolution and good velocity estimation. The static correction, noise cancellation, and stacking processes affect the resolution.

In this Chapter we shall describe a sequence for the processing using the SierraSEIS package Part of line U-14 from the SPs 409 to 611 was selected to reprocess. The object of the reprocessing consisted of the application of static and normal moveout corrections through careful control of the seismic velocities, avoidance of picking the multiples, filtering to remove noise, deconvolution.

Velocity analysis is the most important processing step, because it yields the information applied for normal moveout corrections and migration, and the determination of the velocities of the subsurface for interpretation of lithologies.

5.1.2 Method

The processing sequence is started by reading the demultiplexed tape (SEG-Y format) using the SierraSEIS package on the Sun computer network in the Geology and Applied Geology Department of Glasgow University. Geometry information is added and the data are sorted into CMP gathers.

The most important part of the seismic data processing is to describe each recorded trace to the computer. This step involves basically converting the field notes (survey data and operator's report) in to computer instructions. The survey data outlines the coordinates of all shot points and receivers and the operator's (observer) report identifies every shotpoint and the relevant spread geometry.

5.2 *Processing procedures*

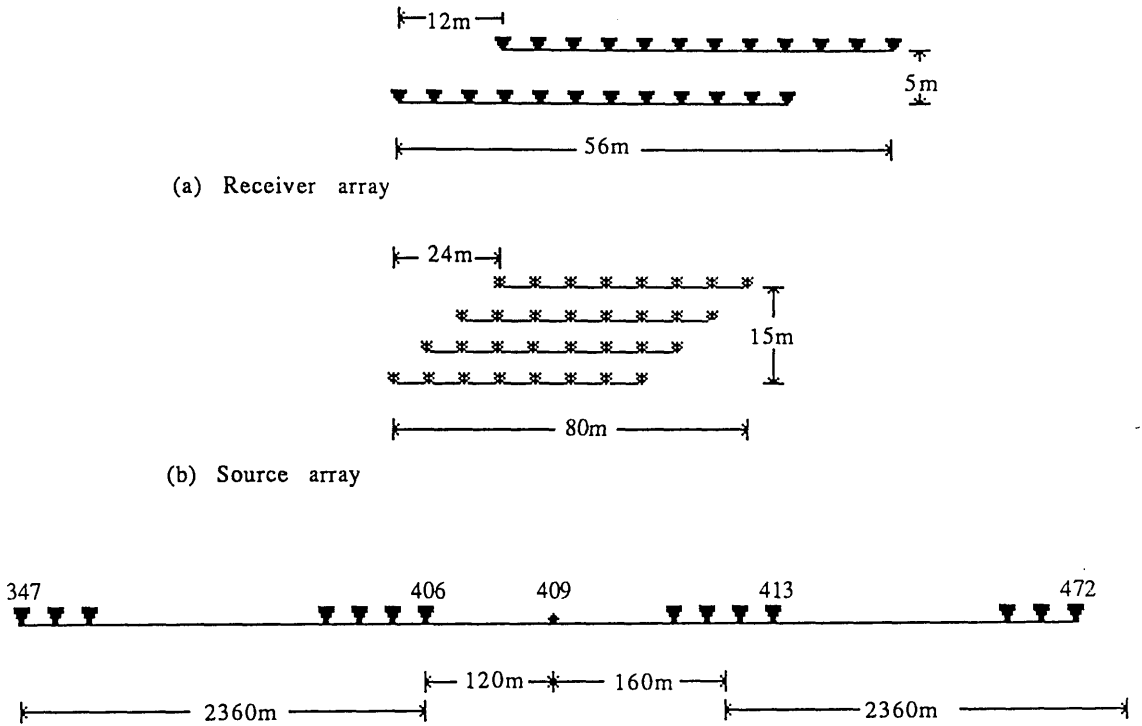
5.2.1 Data background

When the shotpoint location relative to the traces in a given spread is at the mid-point of the spread is called split spread or centre-shooting. The configuration for a 120-trace, split spread is illustrated in Fig. 5.1.

In most situations, it is common to leave a gap between the source and the first receiver station (or even within a spread) to avoid interference from low velocity noise train. In our case the gap is 120 m on one side and 160 m on the other side. The distance between shotpoints is 80 m and the distance between receivers is 40 m. The distance from source to farthest spread stations is 2360 m in the both sides.

The source used was Vibroseis, with four trucks operated simultaneously. The Vibroseis method requires cross-correlating; this involves taking data recorded during the Vibroseis sweep and cross-correlating it with the sweep to give a quantitative estimate of the degree of similarity between the two time series. The sweep was 16 s long, with frequency 12-72 Hz, and 20 s of data was recorded with a filter high cut off 128 Hz and roll off of 70 db. Only 4 s of data remained after correlation.

The data was recorded using a DFS-V. instrument on 9 track (800 bpi), 1/2 inch tape, with a multiplexing of 120 data channels.



(c) Source-receiver configuration

- 347 : The first station
- 406 : The station before gap
- 409 : The first shotpoint
- 413 : The station after gap
- 472 : The last station

Distance between the shotpoint and receivers = 140 m
 Distance between the shotpoints = 80 m
 Distance between the receivers = 40 m

Fig. 5.1 Receiver array, Source array, and source-receiver configuration for line U-14.

Refer to the lower part of Fig. 5.1. The first shotpoint is 409, the first station 347, the station before gap 406. The station after gap 413, the last station is 472, the second shotpoint is 411. The first station for this shot is 349, the station before gap 408, the station after gap 415, and the last station 474, and so on.

The shotpoint increment is 2, ordered as odd numbers e.g. 409, 411, 413,etc. But in some lines shotpoints the increment is 1 e.g. 471, 472,etc.

Most of the shotpoints are offset from the surveyed station position by 15 m, except one shotpoint (503) is offset (60 m) and three shotpoints 477, 478, and 479 are offset (10 m).

The number of traces in a CMP gather is the fold of the stack.

The general equation for calculating the fold is :

$$\text{Fold} = 0.5 (\text{number of channels} * \text{channel spacing} / \text{shot spacing}) \dots\dots\dots 5.1$$

In our case the maximum fold is 36, and this decreases away on both sides. Because of the asymmetrical shot interval, the fold is not 30, as calculated by the equation 5.1.

5.2.2 Seismic processing sequence

The following processing sequence (Fig. 5.2), starts with

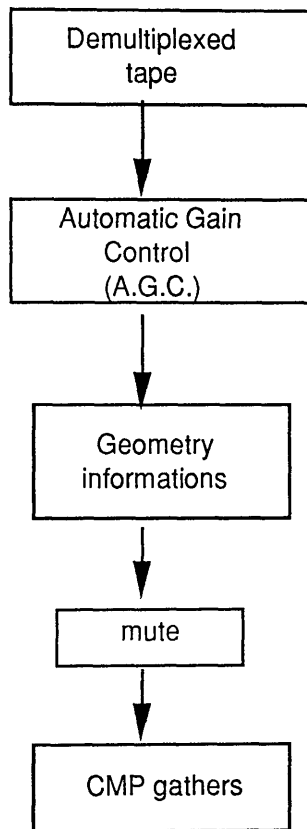


Fig. 5.2 The preliminary seismic processing sequence.

reading the demultiplexed tape (SEG-Y format), in which the data have been reorganised in trace sequential order, that is all the samples of the first trace, followed by all the samples of the second trace and so on. The data, which were read from the tape as shotpoint files (Fig. 5.3) were pre-processed using the SierraSEIS package, starting firstly with the Automatic Gain Control (AGC). This is a method by which the gain function is automatically computed from the data itself on a trace by trace basis.

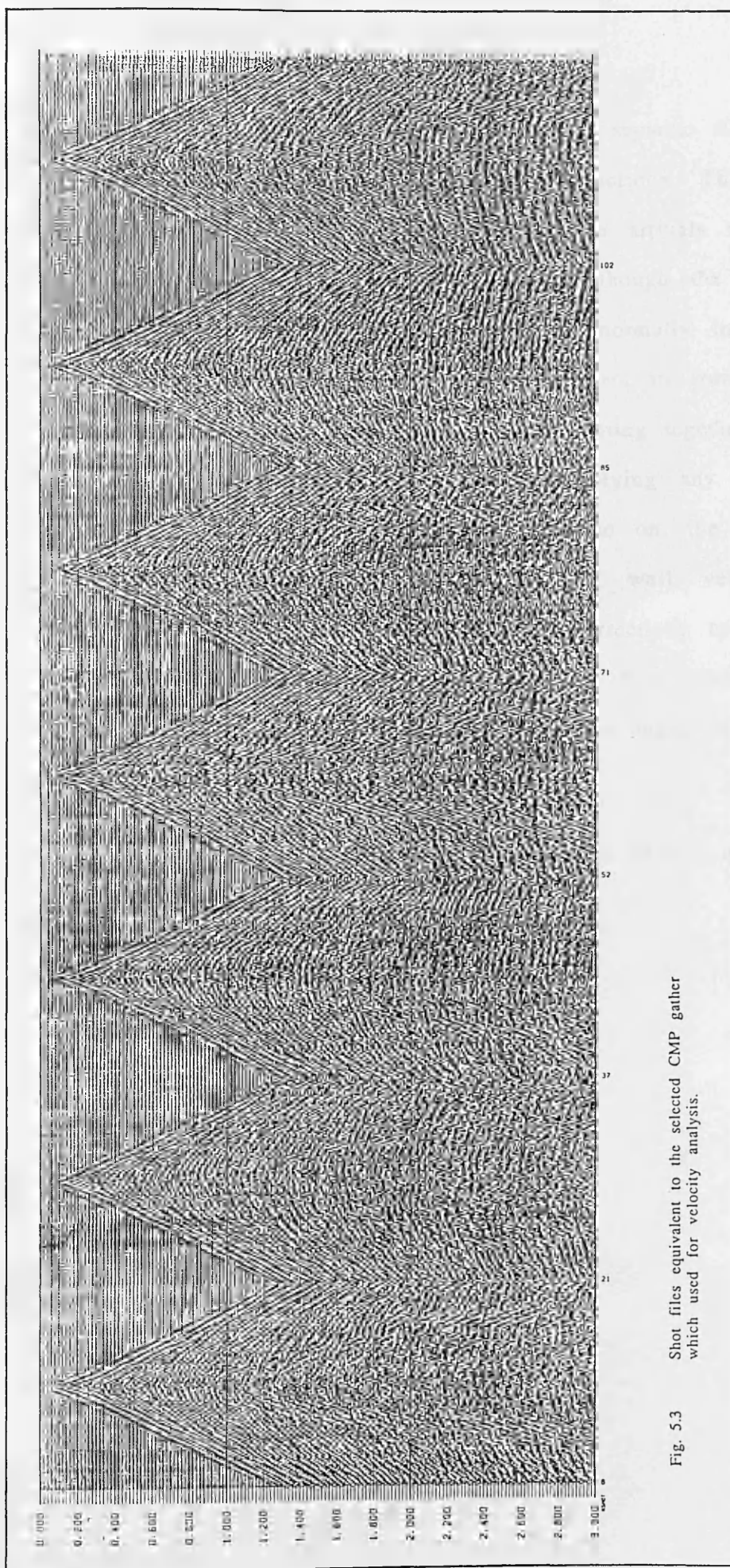


Fig. 5.3 Shot files equivalent to the selected CMP gather which used for velocity analysis.

Secondly, the geometry information is fed in from a separate file in which the field notes are converted to computer instructions. Thirdly, muting is done to eliminate the first breaks and refraction arrivals which have no constructive contribution to the final product. Although the very shallow data are almost uninterpretable, the mute would normally include enough traces for some of the data to stack in. Finally the data are sorted as CMP gathers (Figure 5.4), i.e. the traces are re-ordered to bring together all traces pertaining to one common mid point. Before applying any main processing steps e.g. deconvolution, velocity analysis and so on, the CMP gathers are preliminarily corrected (NMO) using the well velocity information (D1/103; Table 3.2 Chapter 3) with static corrections applied, then stacked. This is called the "raw stack section" (Figure 5.5). From this section we choose the velocity analysis positions for the main detailed velocity analysis.

The main processing sequence from CMP gathers is shown in the following flow chart (Figure 5.6).

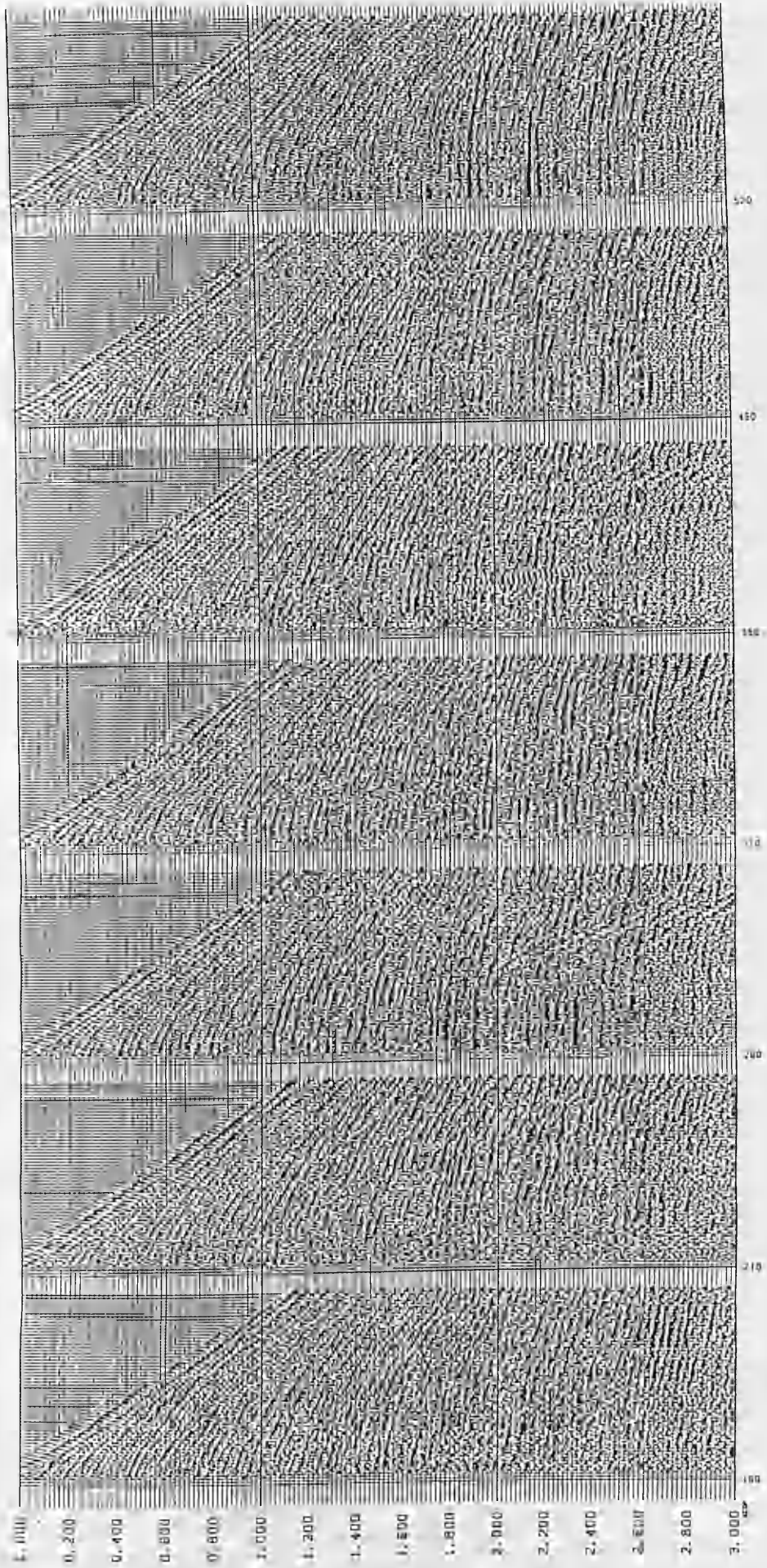


Fig. 5.4 Selected CMP gathers corresponding to the same data as in Figure 5.3.

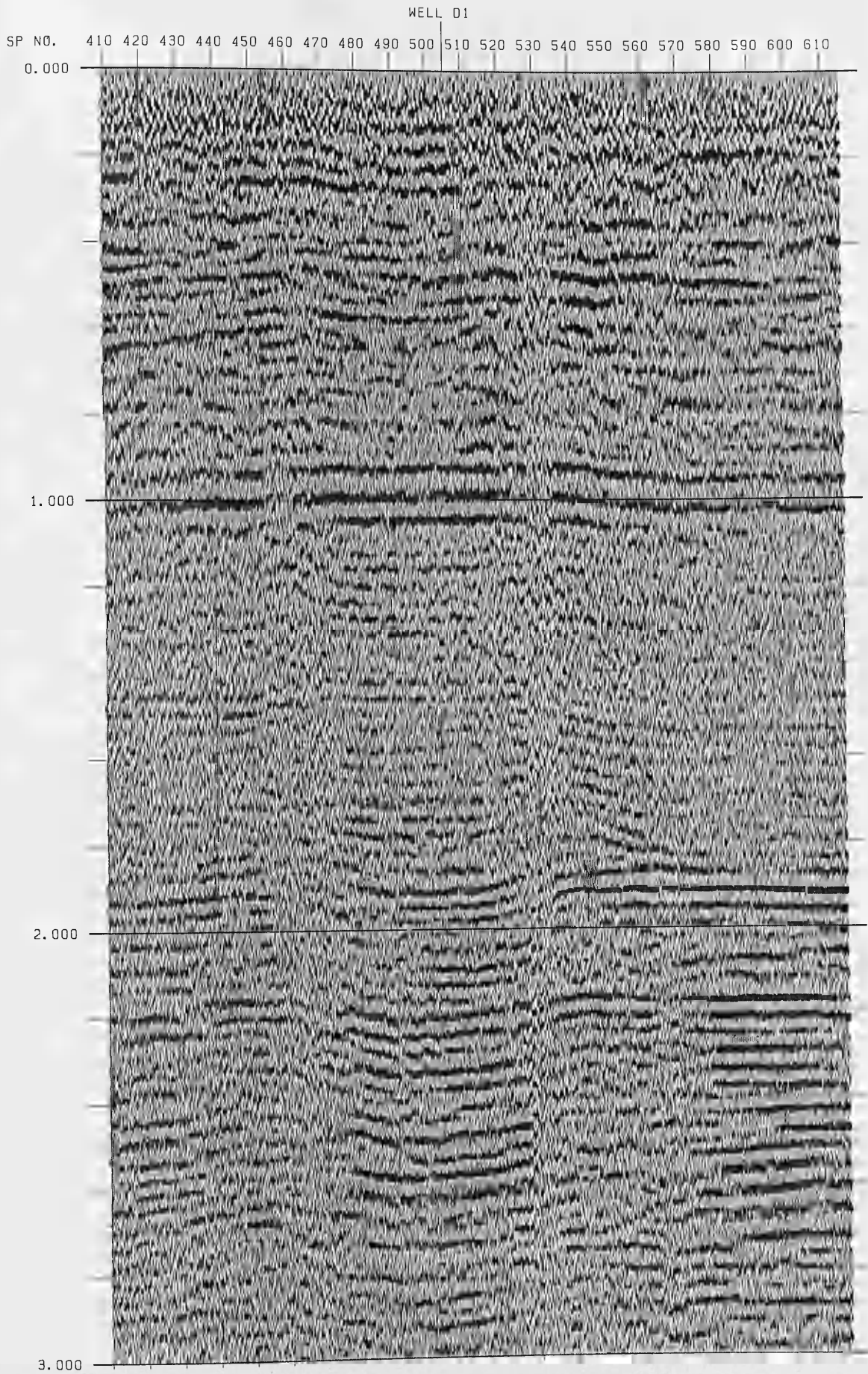


Fig. 5.5 Raw stack section using the well velocity survey (D1/103).

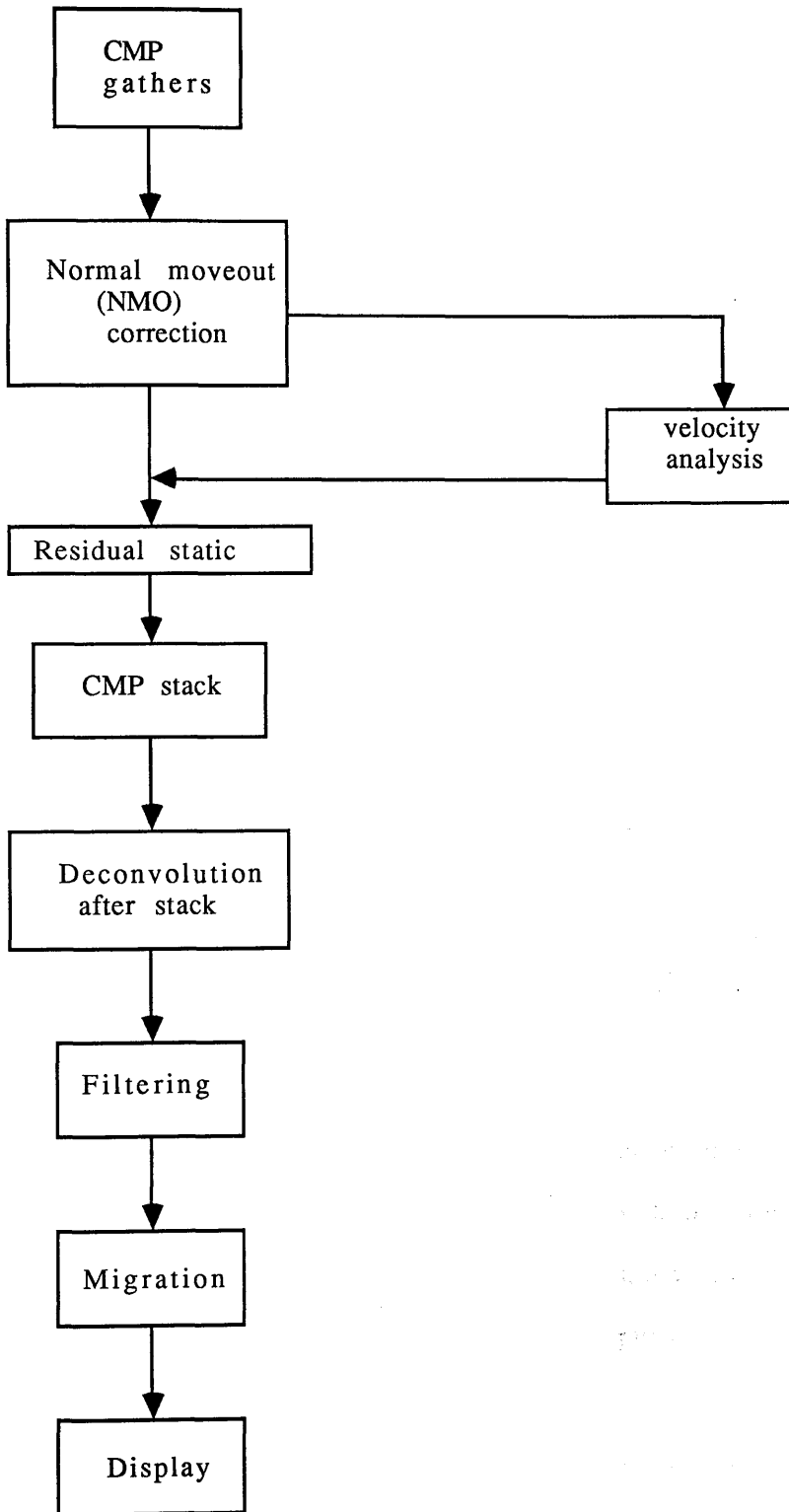


Fig. 5.6 Seismic data processing flow-chart

5.3 *Pre-stack processing*

5.3.1 Static and residual static corrections

The most important processing step for land data is the static correction calculation. It is very difficult to calculate the exact static value due to number of variable factors such as lateral velocity change, changes in low velocity layer thickness, and so on.

Static corrections affect; reflection continuity, structural geometry, resolution, and accuracy of velocity analysis. The purpose of static corrections is to remove the effects of the near surface.

The basic static correction is composed of four parts :

1. LVL (Low Velocity Layer) correction at the source.
2. Datum correction at the source.
3. LVL correction at the geophone.
4. Datum correction at the geophone.

The most significant factor in static calculations is the knowledge on the weathering phenomena. Therefore, it is vital to know the weathering thickness and the velocity of the weathering and sub-weathering layers to calculate the static corrections accurately. The purpose of the static correction is to overcome the effects of changes in the elevation of the source and receiver points due to terrain differences and shot or receiver depths, and variations in velocity and thickness of the weathered zone on land.

A static correction consists of the application of a time shift, to an entire trace. In other words, a constant time correction term is subtracted from all reflection times. The elevation static correction (field static) ranges from -76 to -82 ms.

According to the static calculation in the geometry stage there is no problem static in the area. This because the topography is very flat. The minimum total static is -164 ms, and the maximum total static is -148, so the difference is quite small (16 ms). Figure 5.7 is part of the stacked section with only the field statics applied, which removes a significant part of traveltimes distortions from the data.

The residual static corrections are needed on the other hand because field statics and datum corrections almost never totally compensate for the effects of near surface velocity variations. This is because the near-surface velocity variations are not known (therefore exact corrections cannot be made), and to remove long wavelength static errors. (Yilmaz, 1985). But before we apply the residual static corrections, we must select the optimum correlation windows. The optimum correlation window was found to be 800-2300 ms, suitable for the shallow as well as the deep data. Figure 5.8 shows the same section in Figure 5.7 after using the optimum correlation window and applied residual static corrections some events are adversely affected.

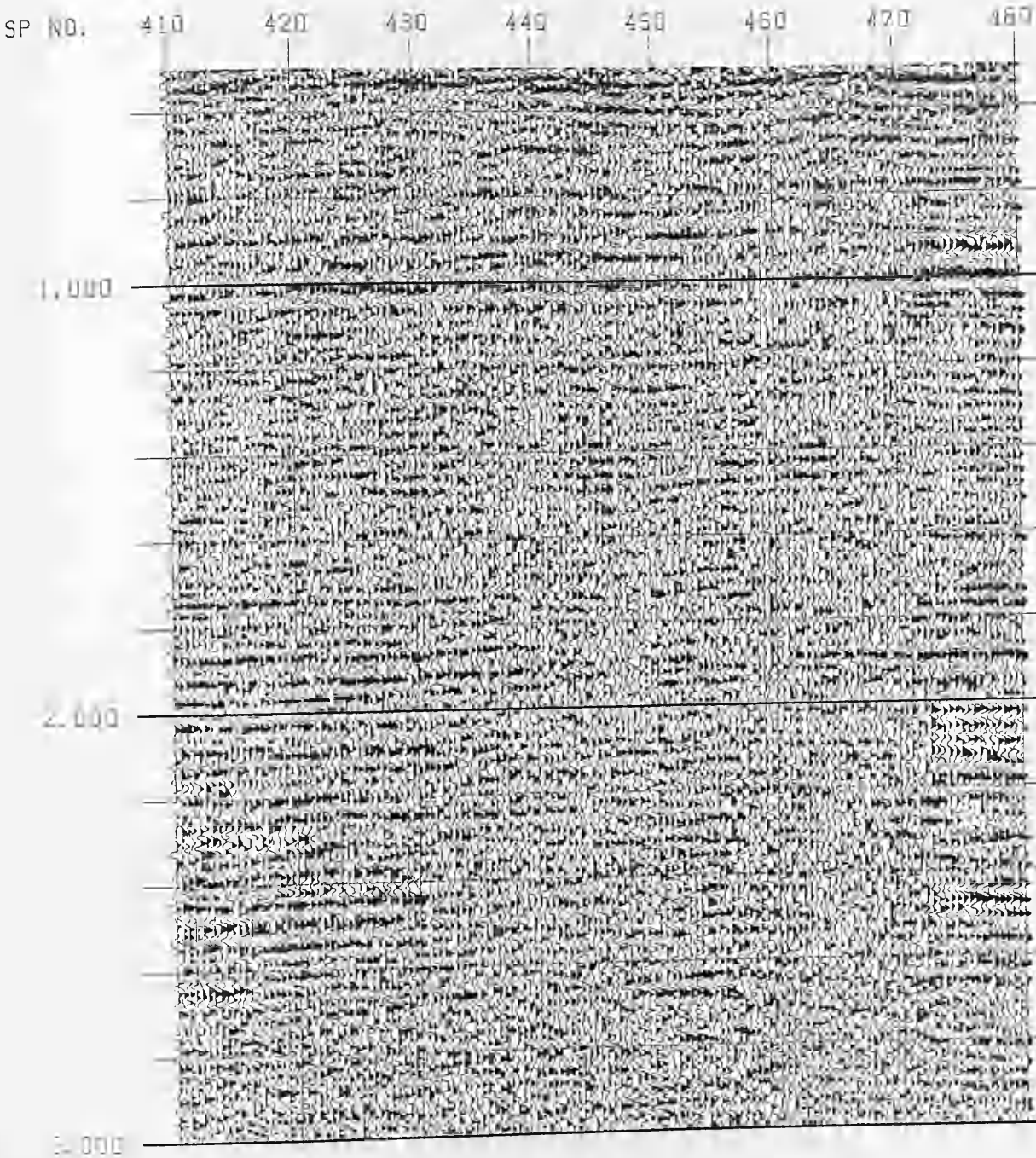


Fig. 5.7 A CMP stack with field statics applied.

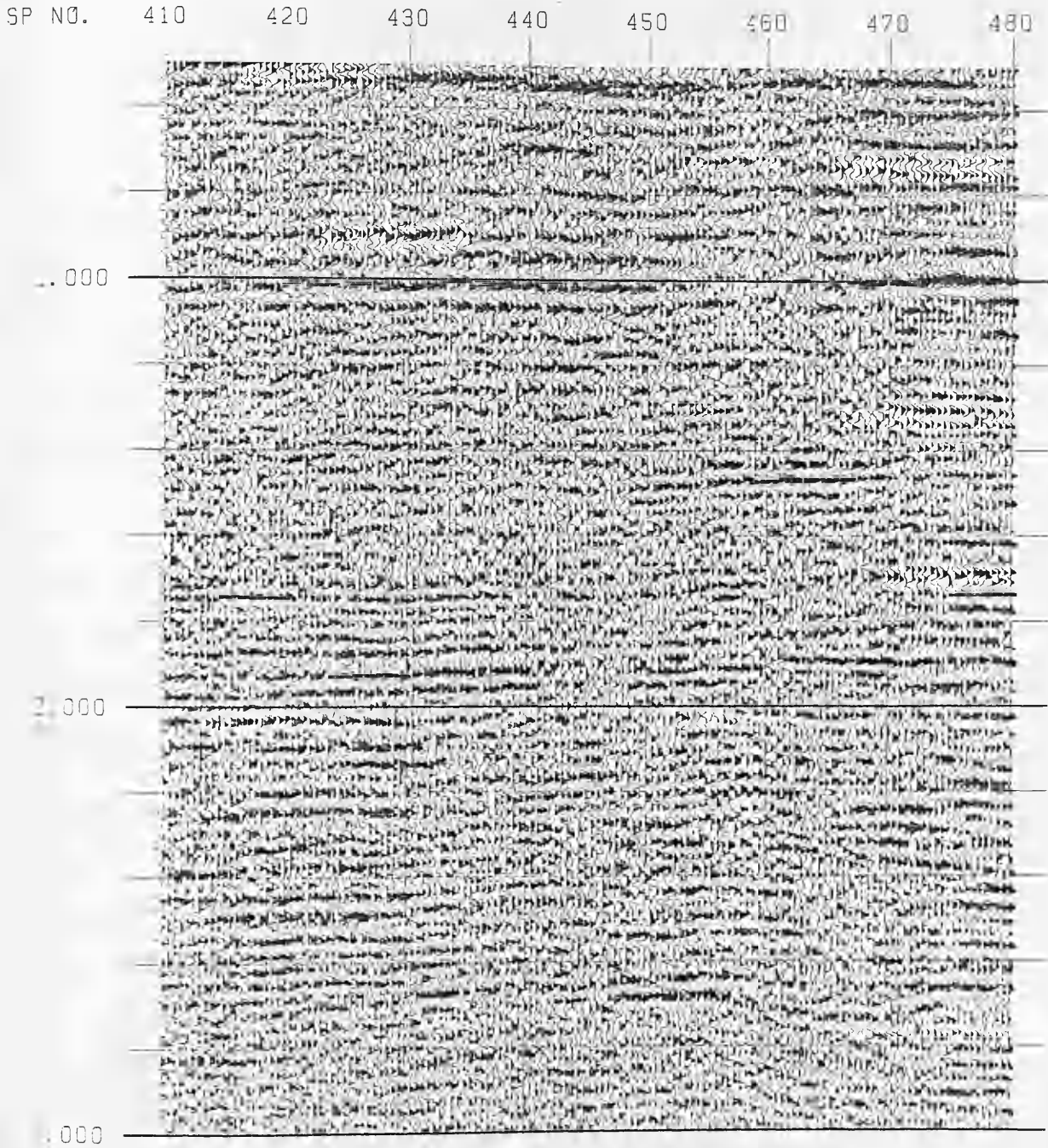


Fig. 5.8 The same section in Figure (5.7) after residual statics corrections.

5.3.2 Deconvolution before stack

Deconvolution is a process which enhances our ability to see detail in our seismic data. This is called increasing the vertical resolution of the data.

The deconvolution process is simply the reverse of the convolution procedure and consists of removing the wavelet shape to reveal the reflection coefficients, and it is used to attenuate multiples.

The deconvolution operation includes the input data, the operator and the final result. This operation is called "spiking deconvolution" since it involves changing the wavelet into a spike.

The deconvolution procedure is perhaps better understood in the frequency domain. Notice that the deconvolution procedure has increased the high frequency content of the input. This is called "whitening" the spectrum and is thus another name for this type of deconvolution. An application of bandpass filtering is the spectral whitening or balancing of seismic data. This process involves balancing the various frequency components so that no component dominates the spectrum of the seismic trace. In the method of application, however, the technique is more closely allied to seismic filtering.

The effective way of selecting between types of operators is to run a set of test panels to observe the result on the data, trying the following operators length, 60, 80, 100, 120, 140, and 160 ms. After testing the operator length, the most suitable was found 160 ms. It is the same operator length used in the section processed by the company, and the operator gap was 24 ms.

Seismic velocity information is used for normal moveout correction, and for time-to-depth conversion. Before performing velocity analysis, the data must have been :

- (1) Filtered, to keep the coherent energy within a limited frequency band and to eliminate the random noise which produces many spurious events in the absence of good reflection events.
- (2) Deconvolved, to suppress undesired coherent energy, and to shape the individual pulses within a gather. This ensures that all data has a somewhat uniform pulse shape.

A crucial step in the processing of seismic data is the determination of the velocities of in subsurface. This is normally done by analyzing the change in the seismic traces as a function of offset. There are actually a number of different ways to define velocity and that it is important to always be aware of the definition being used.

The major objective of velocity analysis is to ascertain the amount of normal moveout which should be removed, to optimise the stacking of events which are considered to be primaries (*Sheriff, 1981*).

The velocity analysis are performed every kilometre along the seismic line by using the more effective one of the following two methods:

- (i) Velocity scans, or
- (ii) Velocity spectrum

Both methods are ordinarily programmed for automatic computation from reflection data recorded in the field. Before the velocity spectra have

Both methods are ordinarily programmed for automatic computation from reflection data recorded in the field. Before the velocity spectra have been made at the following selected CMP gathers, a selection is made with regard to the geology of the area.

The plots are interpreted by observing which velocity provides the best fit to the traces for a particular reflector. Noise in seismic data has a direct effect on the quality of a velocity spectrum. To improve the quality of a velocity spectrum is to use several neighbouring CMP gathers in the analysis.

Figure 5.9 show velocity spectrums for the selected CMPs along the line. Note that several of the contour closures, which another has deemed primary events, have been marked.

It is well known that abrupt lateral changes in subsurface lithology distort stacking velocities determined for reflections at depths below them, making the relation of stacking velocities to interval velocities quite complex. Zones of greater porosity (possibly hydrocarbon-filled porosity) are likely to have a lower stacking velocity as picked from such an analysis for the reflectors below each such zone, than would be seen if little or no lateral velocity change occurs.

Anomalous low velocity zones could indicate possible porosity and even hydrocarbons in appropriate circumstances. Even if low velocity is indicated, porosity represents only one of the possible explanations for its occurrence. Lithological changes can, in fact, also cause lowered velocities and these are most troublesome, particularly if they are unanticipated.

COPS 160 TO 160

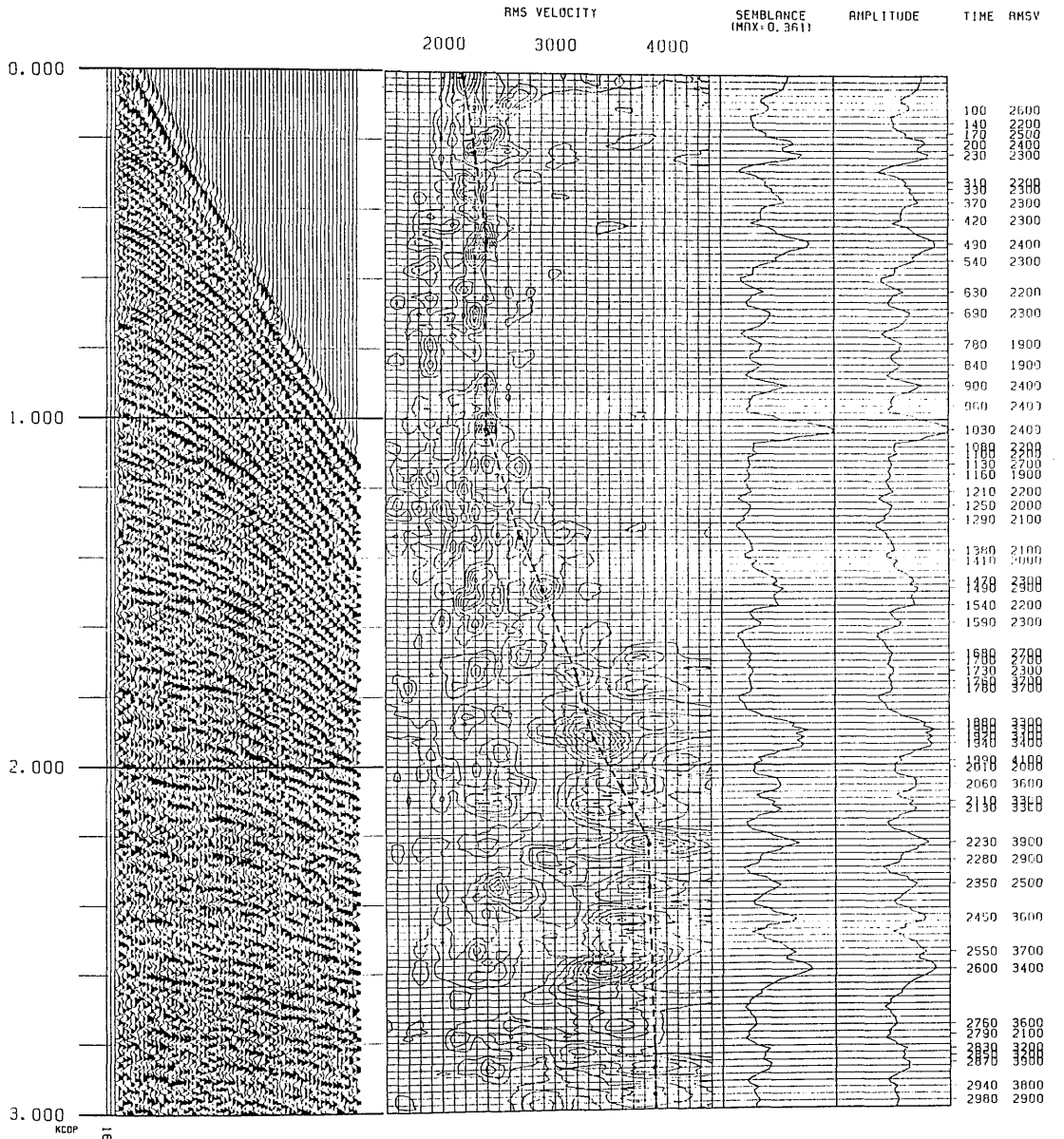


Fig. 5.9 (a) Velocity spectra derived from the CMP gathers in Figure 5.4. The display mode is contour (CDP 160).

COPS 210 TO 210

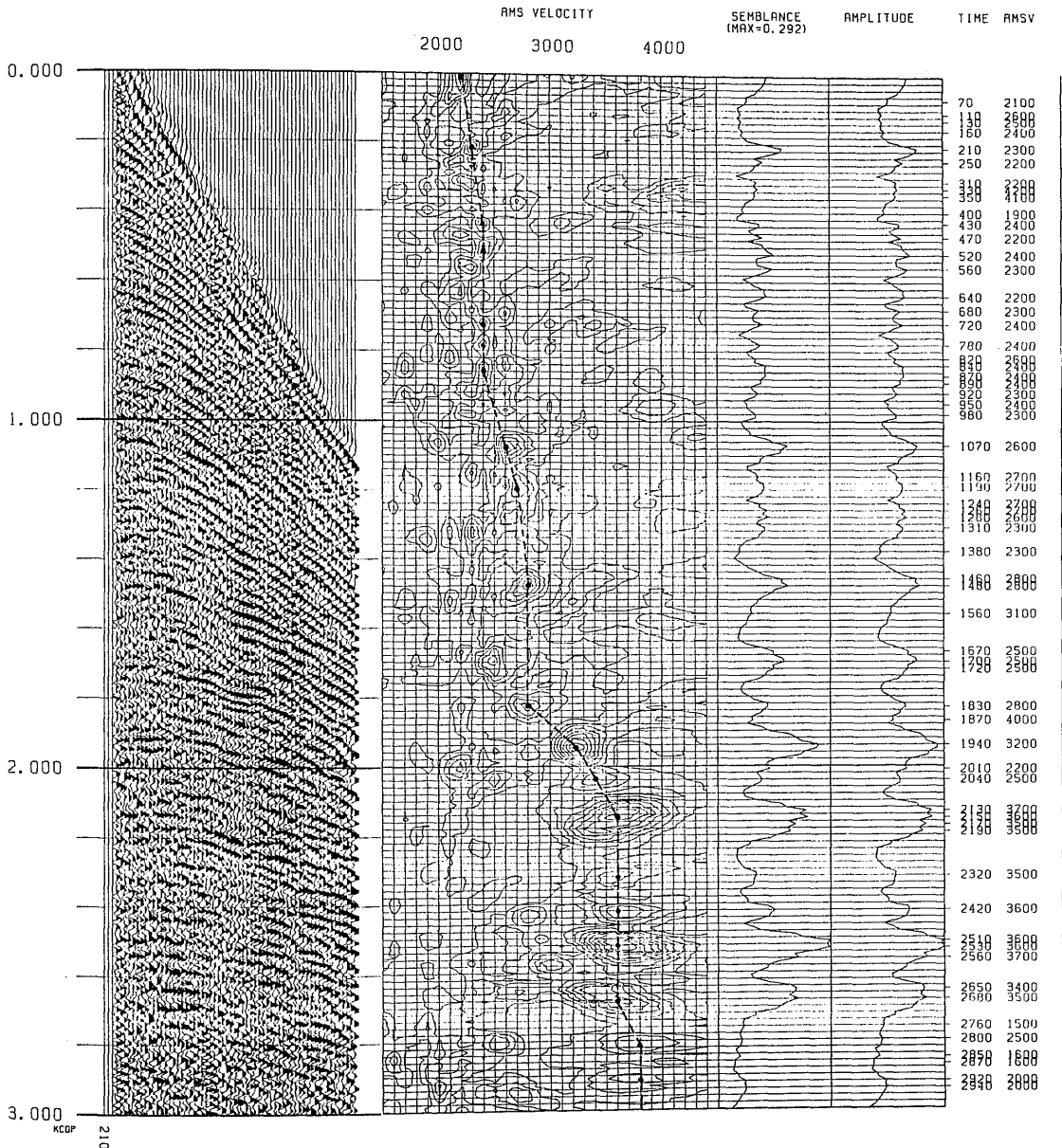


Fig. 5.9 (b) Velocity spectra derived from the CMP gathers in Figure 5.4. The display mode is contour (CDP 210).

COPS 260 TO 260

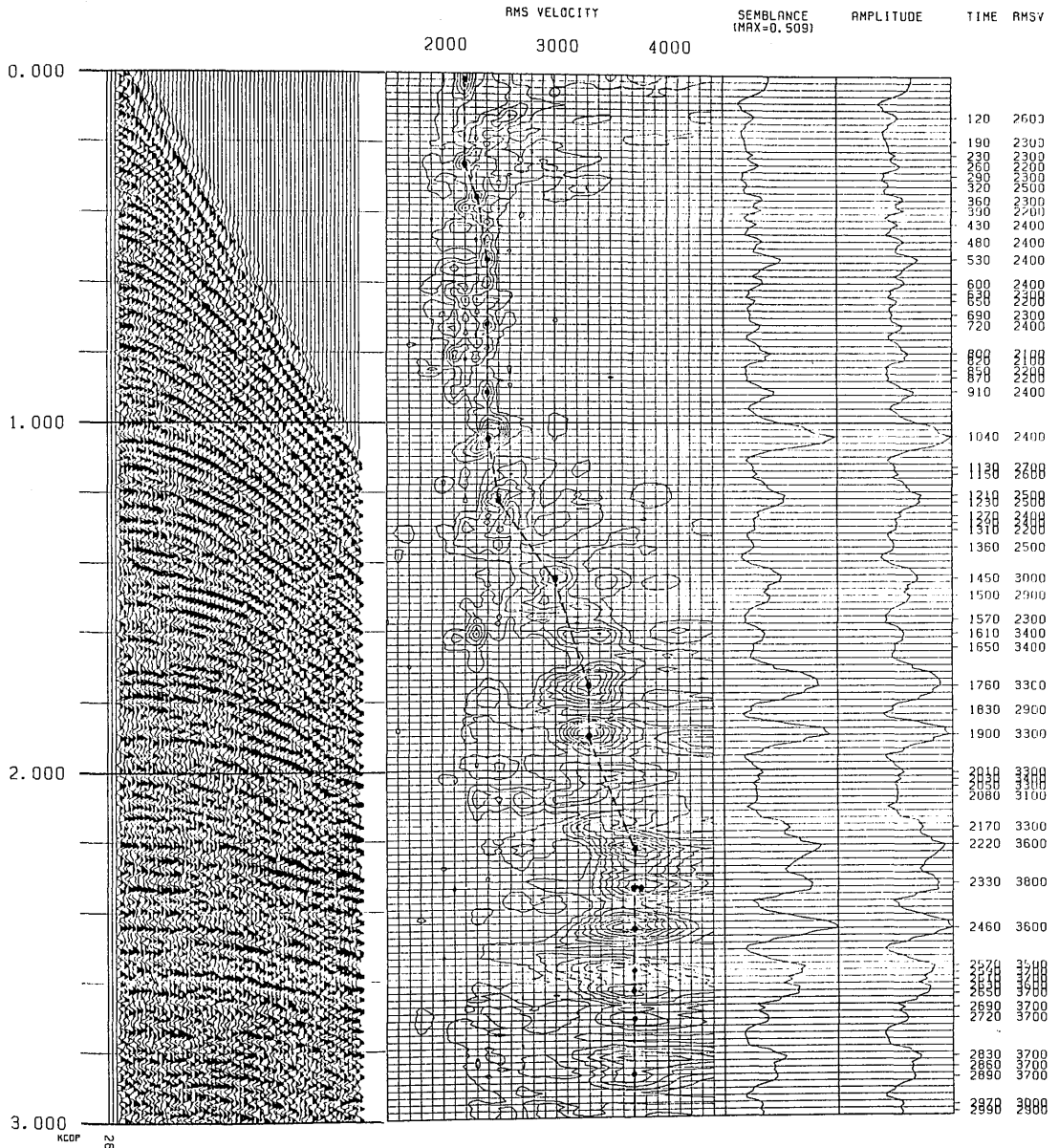


Fig. 5.9 (c) Velocity spectra derived from the CMP gathers in Figure 5.4. The display mode is contour (CDP 260).

COPS 310 TO 310

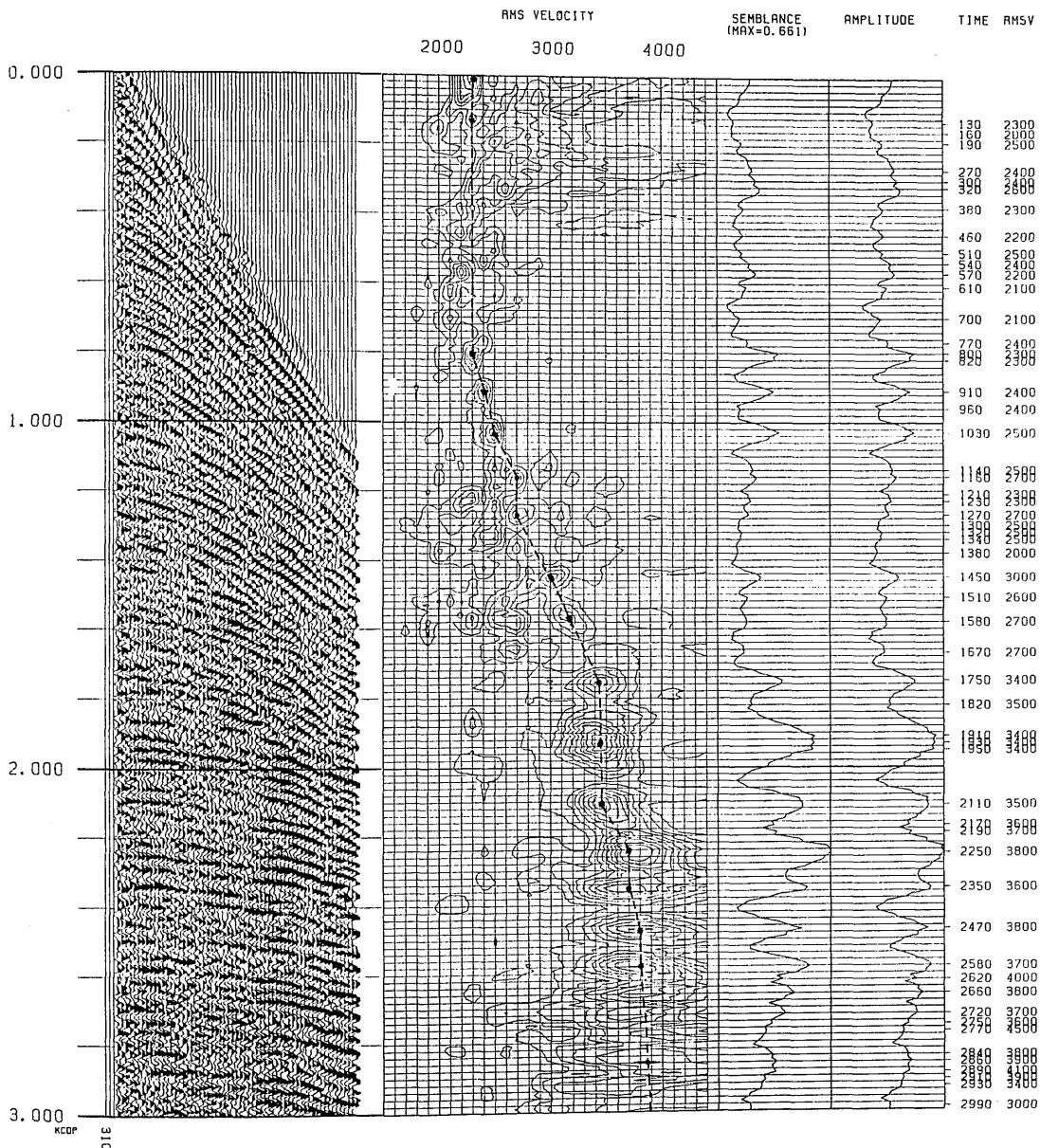


Fig. 5.9 (d) Velocity spectra derived from the CMP gathers in Figure 5.4. The display mode is contour (CDP 310).

COPS 360 TO 360

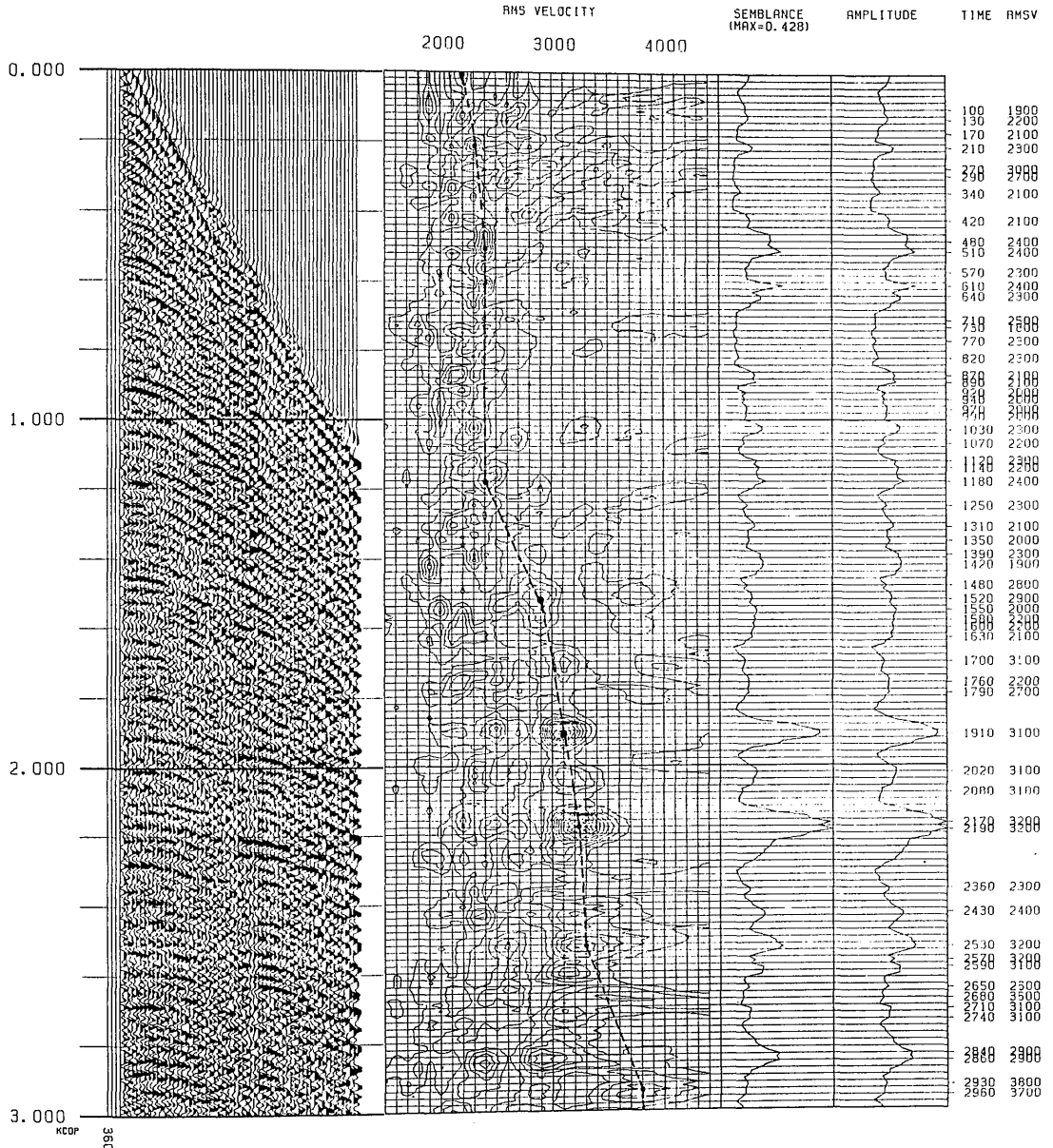


Fig. 5.9 (e) Velocity spectra derived from the CMP gathers in Figure 5.4. The display mode is contour (CDF 360).

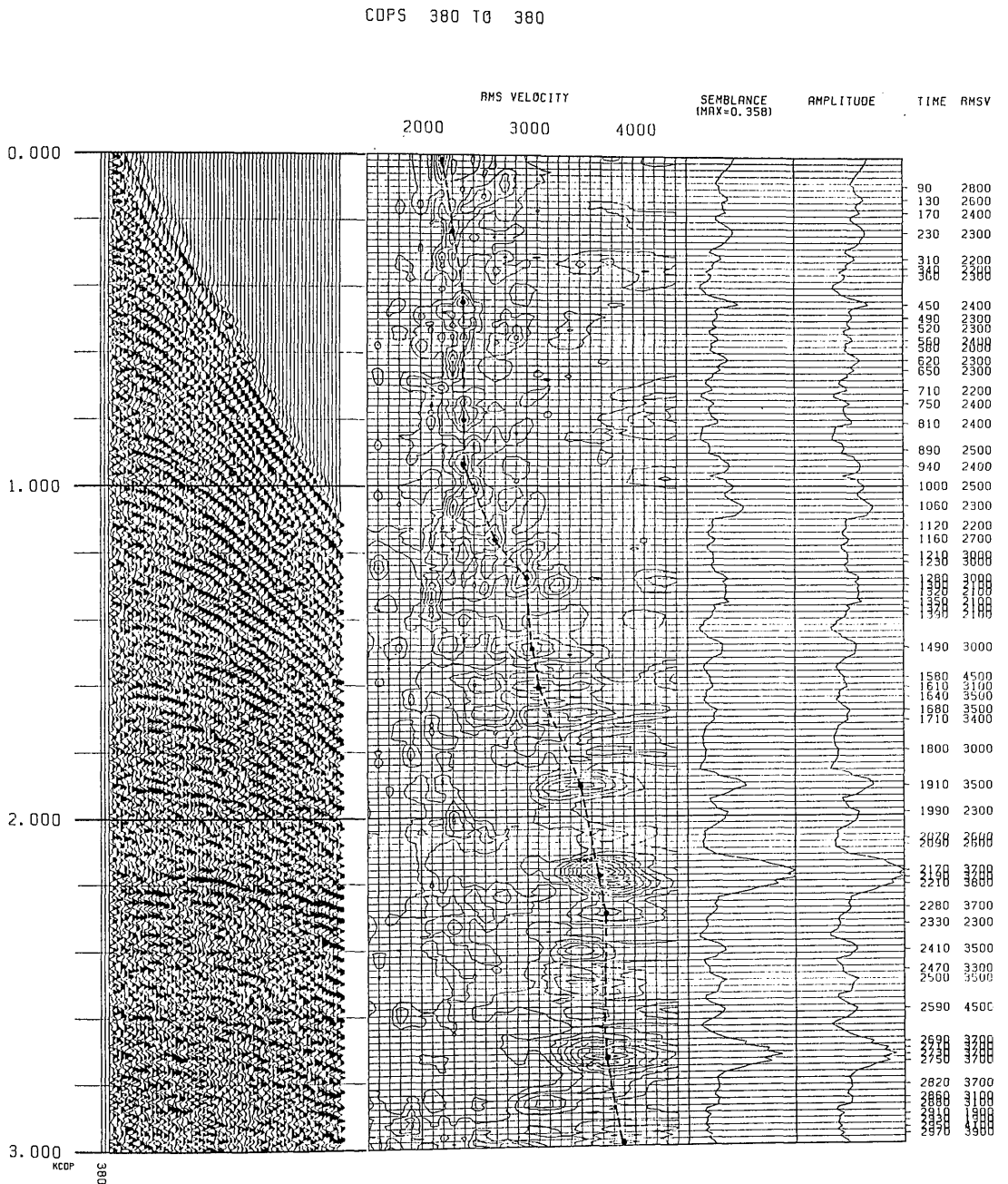


Fig. 5.9 (f) Velocity spectra derived from the CMP gathers in Figure 5.4. The display mode is contour (CDP 380).

COPS 450 TO 450

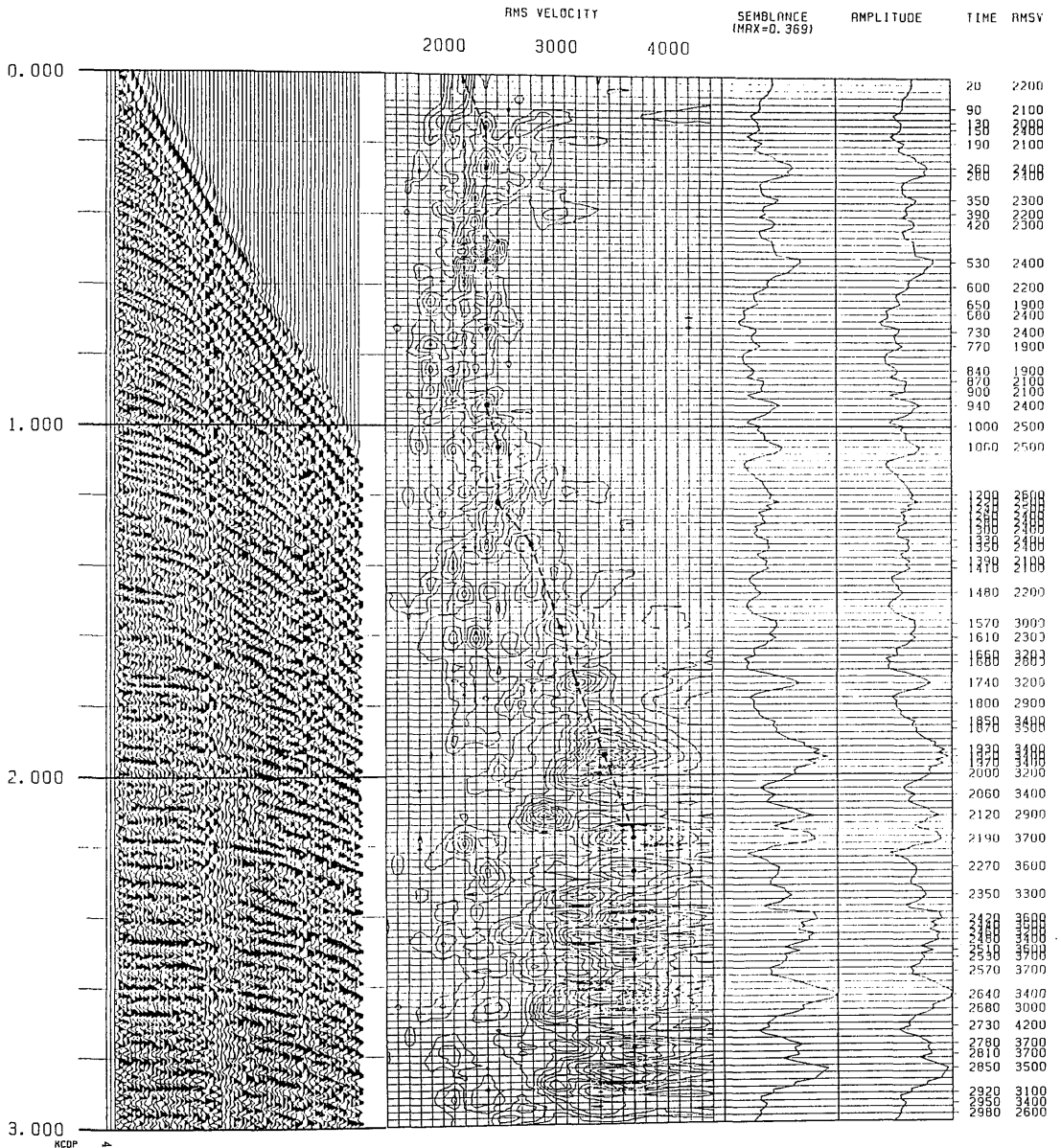


Fig. 5.9 (g) Velocity spectra derived from the CMP gathers in Figure 5.4. The display mode is contour (CDP 450).

CDPS 520 10 520

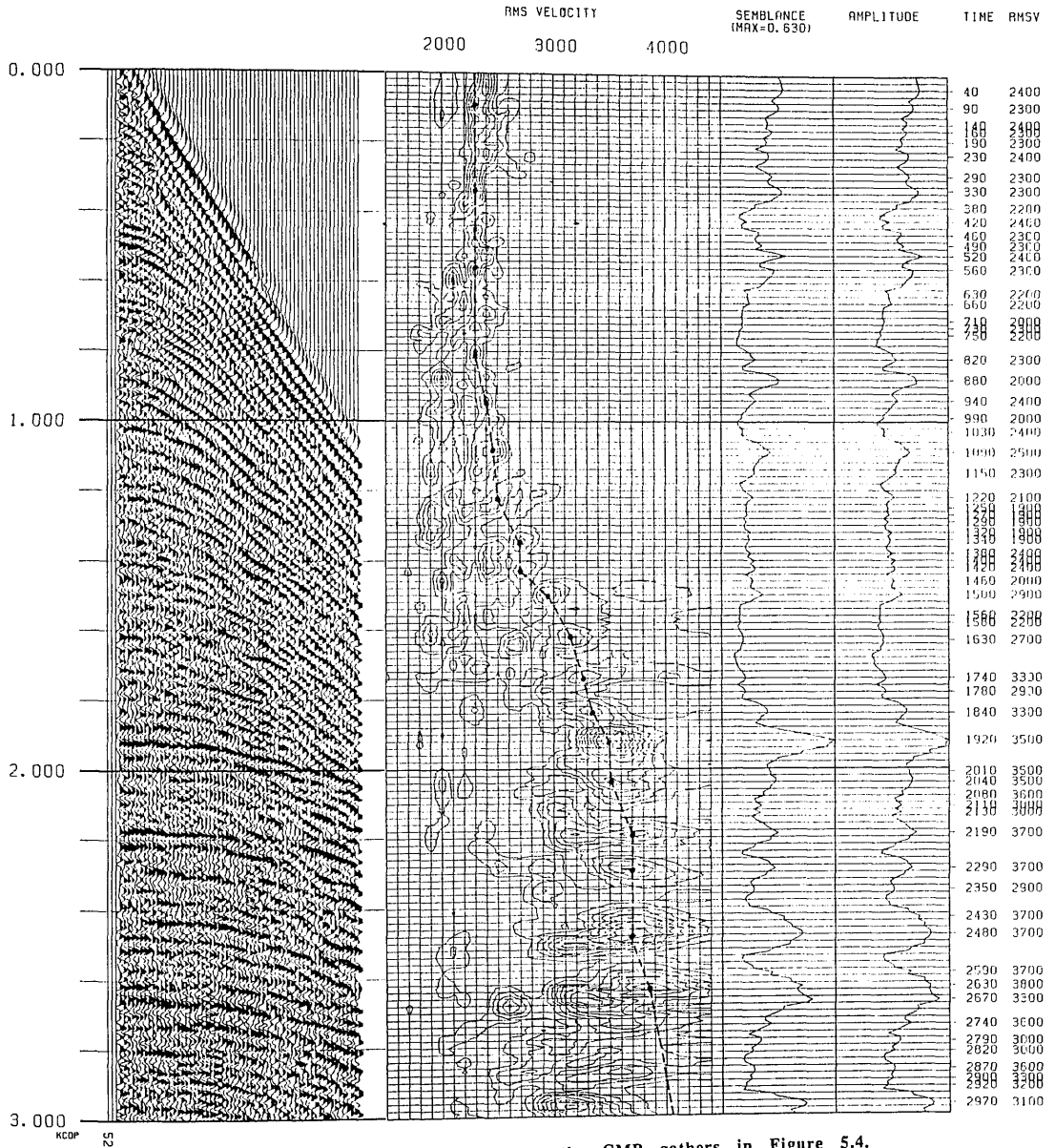


Fig. 5.9 (h) Velocity spectra derived from the CMP gathers in Figure 5.4. The display mode is contour (CDP 520).

The following are important steps for velocity spectrum interpretation (Badley, 1985):

- (i) Checking that the marked velocity breaks also occur in the velocity-log (D1/103), as illustrated in Chapter 3, Section 3.2.1.
- (ii) Assuming that velocity increase with depth.
- (iii) Avoiding picking the semblance peaks of multiples, and other noise. The picking must be on the high-side of the contoured values.
- (iv) Pick the strong reflections.
- (v) Check the velocities for geological sense by computing Dix interval velocities.
- (vi) Correct velocities of dipping reflectors by dividing by the cosine of the dip.

Table 5.1 in the Appendix shows the RMS velocity from the velocity spectra in Figure 5.9, which will be used later in the final stack section.

5.3.4 Normal move-out correction

Normal move out (NMO) is a simple expression for the change in two-way traveltimes with offset. The following equation:

$$T^2 = T_0^2 + \left(\frac{X^2}{V^2} \right) \dots\dots\dots 5.2$$

where :

T_x : is the time at offset X.

T_0 : is the time at zero offset.

X : is the offset of the trace.

V : is the velocity at time T.

is called the NMO equation, and represents a hyperbola. Thus, the events will appear to be hyperbolic on shot gathers, common geophone gathers and also on CMP gather profile. There is only one velocity value which flattens out this hyperbolic curve. The NMO processor applies a normal move out correction to seismic traces. The corrected traces are computed by applying a two-dimensional interpolation to the time-velocity pairs. After a proper NMO correction, the primary reflections will appear as if each trace resulted from the source and geophone being side by side, that is NMO converts the oblique incidence reflection to the normal incidence reflection.

Figure 5.11(a) shows the NMO correction of the previous CMP gathers, and Fig. 5.11(b) with applied mute. Both Figures are for the same CMP gathers as shown in Fig. 5.4.

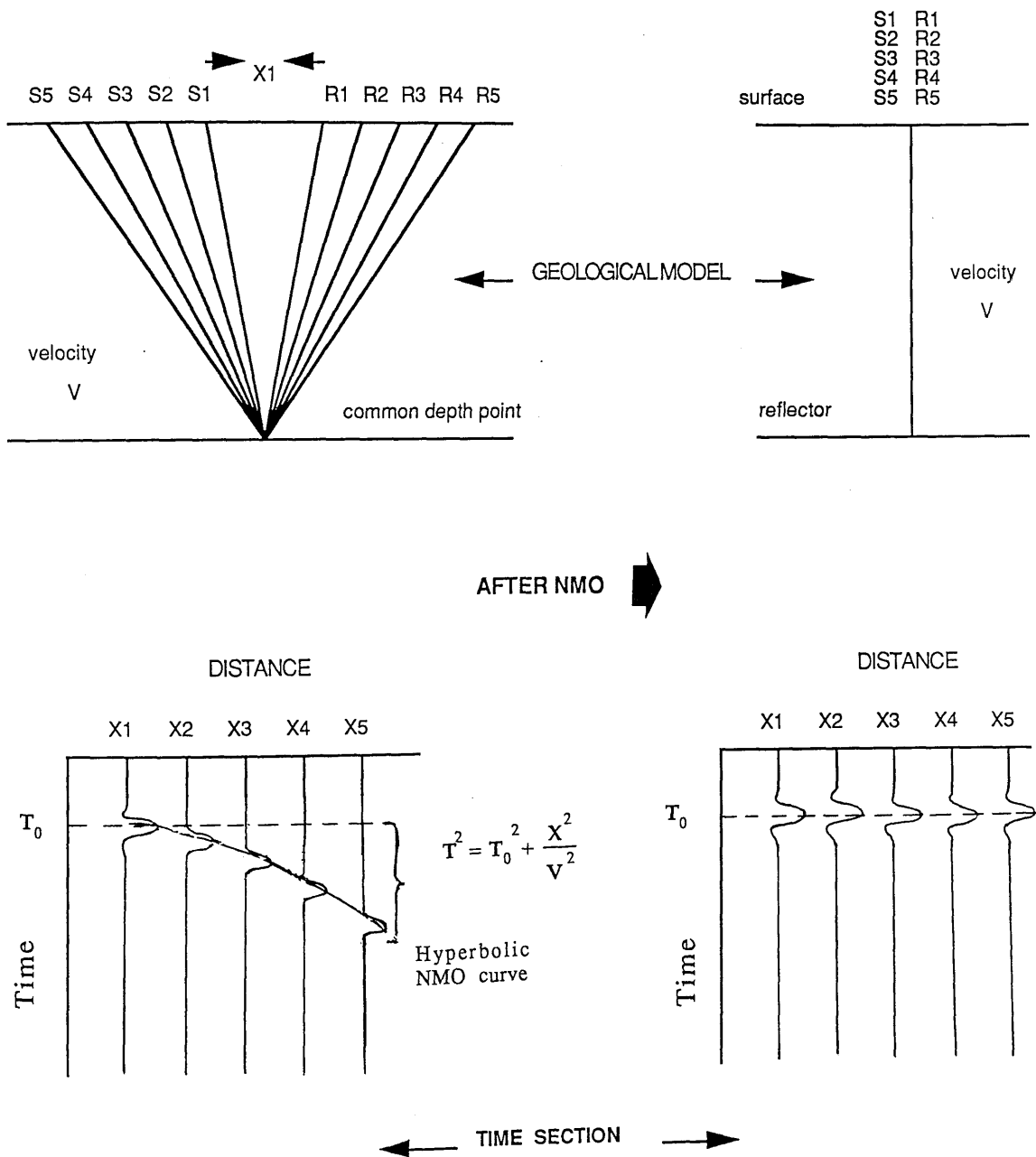


Fig. 5.10 Definition of Normal Move-Out (NMO).

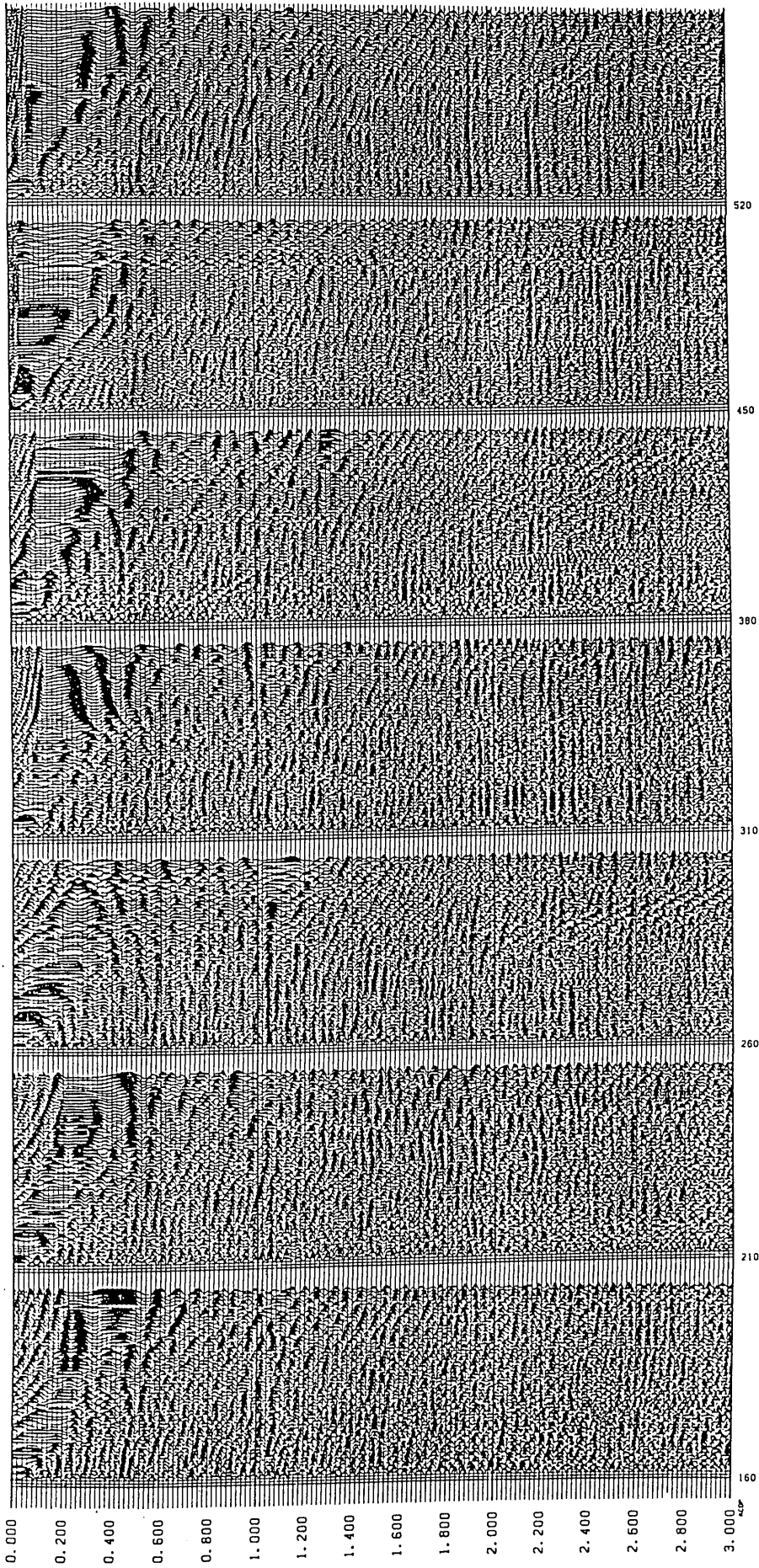


Fig. 5.11 (a) The CMP gathers of Figure 5.4 after NMO correction using the velocity picks derived from Figure 5.7.

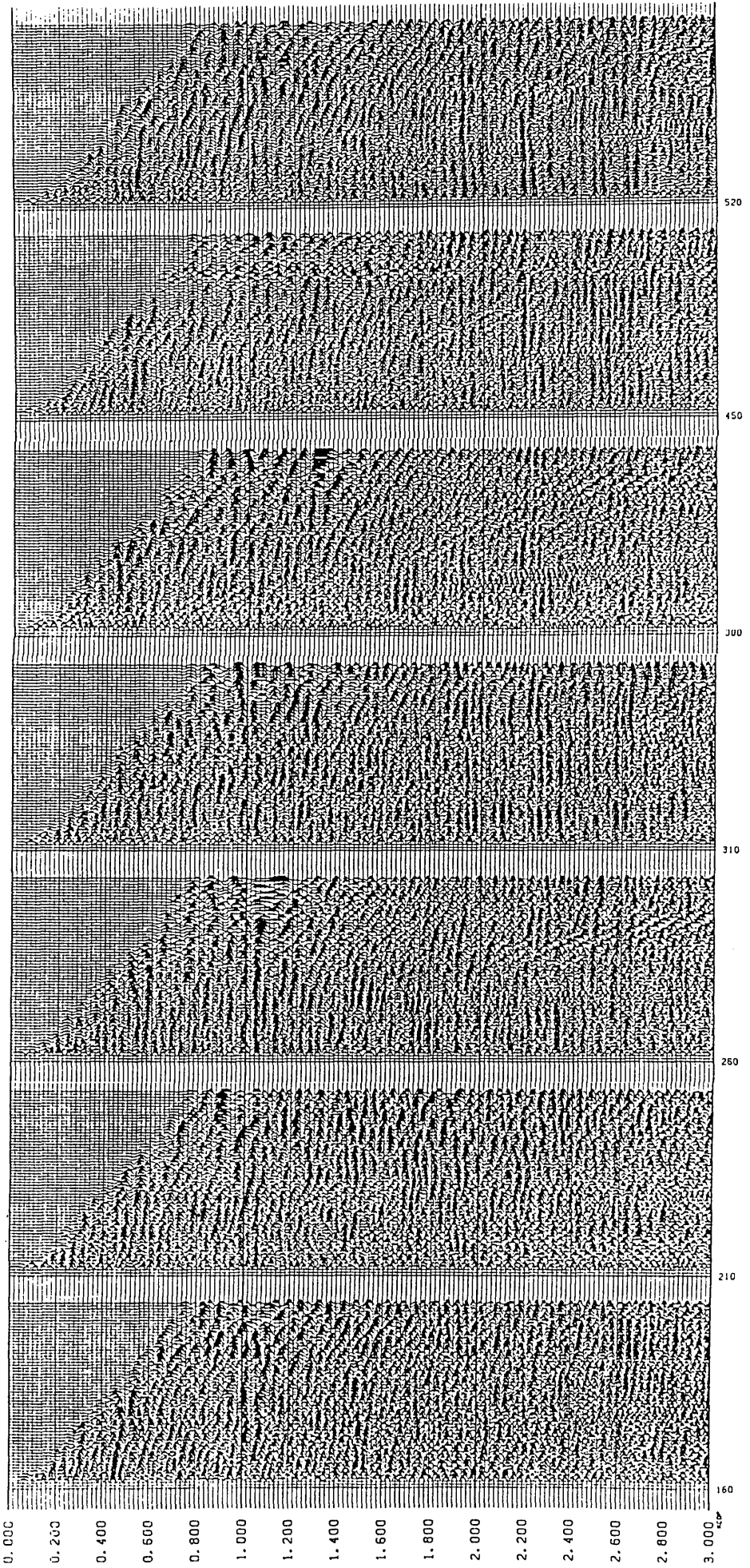


Fig. 5.11 (b) The CMP gathers of Figure 5.13(a) after muting the stretched zones (the very low frequency zones).

5.3.5 Stacking

In the previous sections, we discussed all techniques to correct the raw data. These corrections may be placed in four categories :

- i) Gain corrections
- ii) Static corrections
- iii) Resolution improvement and noise cancellation
- iv) NMO correction

After the application of above corrections, each trace theoretically represents a zero offset recording (that is the shot and receiver were at the same location). The final step now is to sum these traces together.

The main reason for stacking is to increase the signal to noise ratio of our data and to attenuate the multiple reflections. In the stacking process, the signal adds constructively and the noise adds destructively. Thus, the amplitude of the signal is increased and the amplitude of the noise is decreased. Stacking is a very effective method of reducing random noise. Figure 5.12 shows the stack section without deconvolution and without filtering.

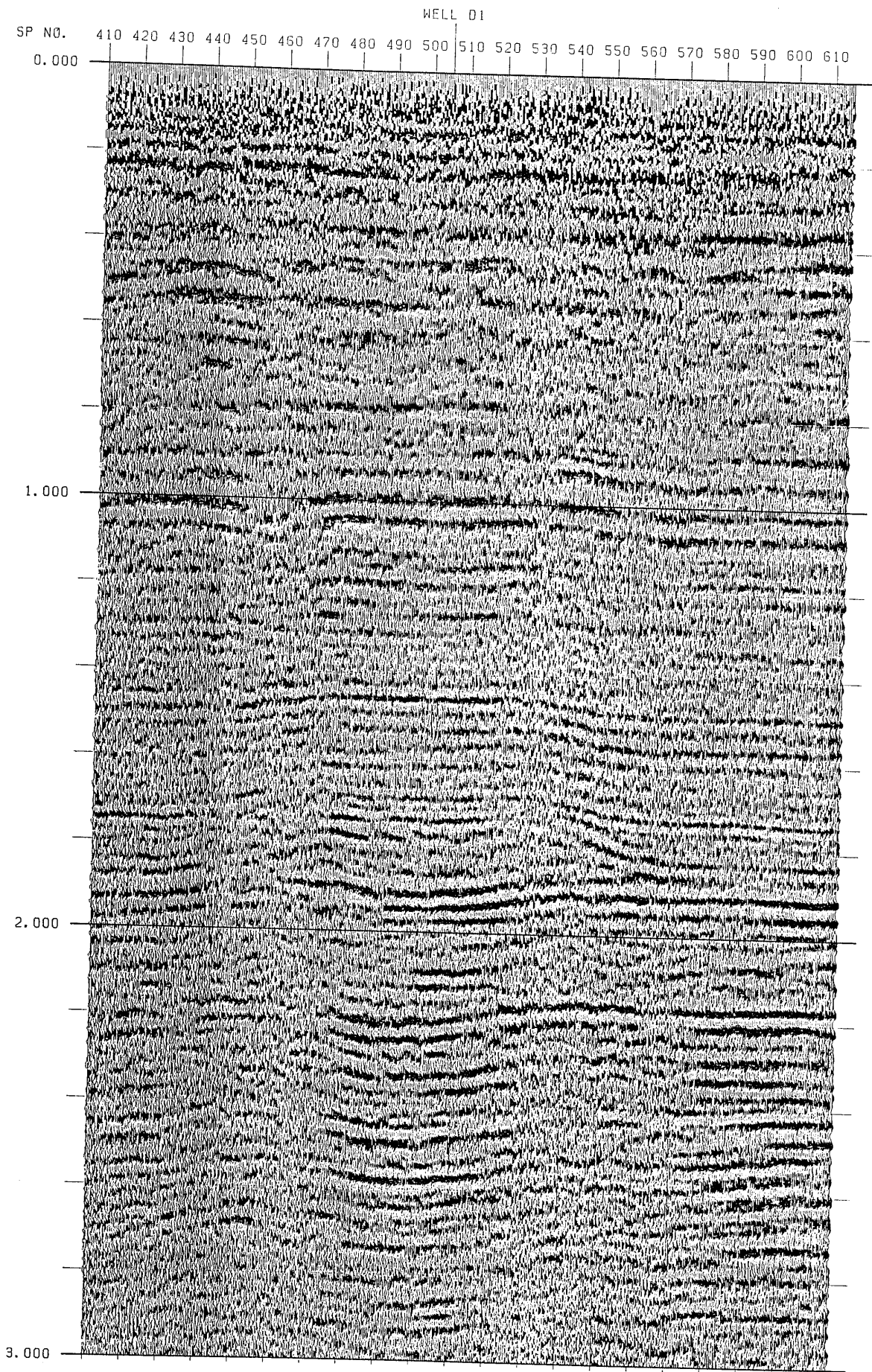


Fig. 5.12 Stack section without deconvolution and without filtering.

5.4 *Post-stack processing*

5.4.1 Deconvolution after stack

In post stack deconvolution of the data we wish to :

- (i) Increase the frequency content of the data.
- (ii) Improve the signal to noise ratio.
- (iii) Remove multiples.

As seen in the previous section, the relevant type of deconvolution is selected and applied to the stacked data to achieve the above goals. Depending upon the requirements we may apply :

- (i) Spiking deconvolution or spectral whitening to increase the frequency content of the data.
- (ii) Predictive deconvolution to improve the signal to noise ratio.

The spiking and predictive operators are often effective in correcting for absorption and to attenuate multiples. Figure 5.13 shows an example of the effect of predictive deconvolution on the stacked section which was shown in Figure 5.12.

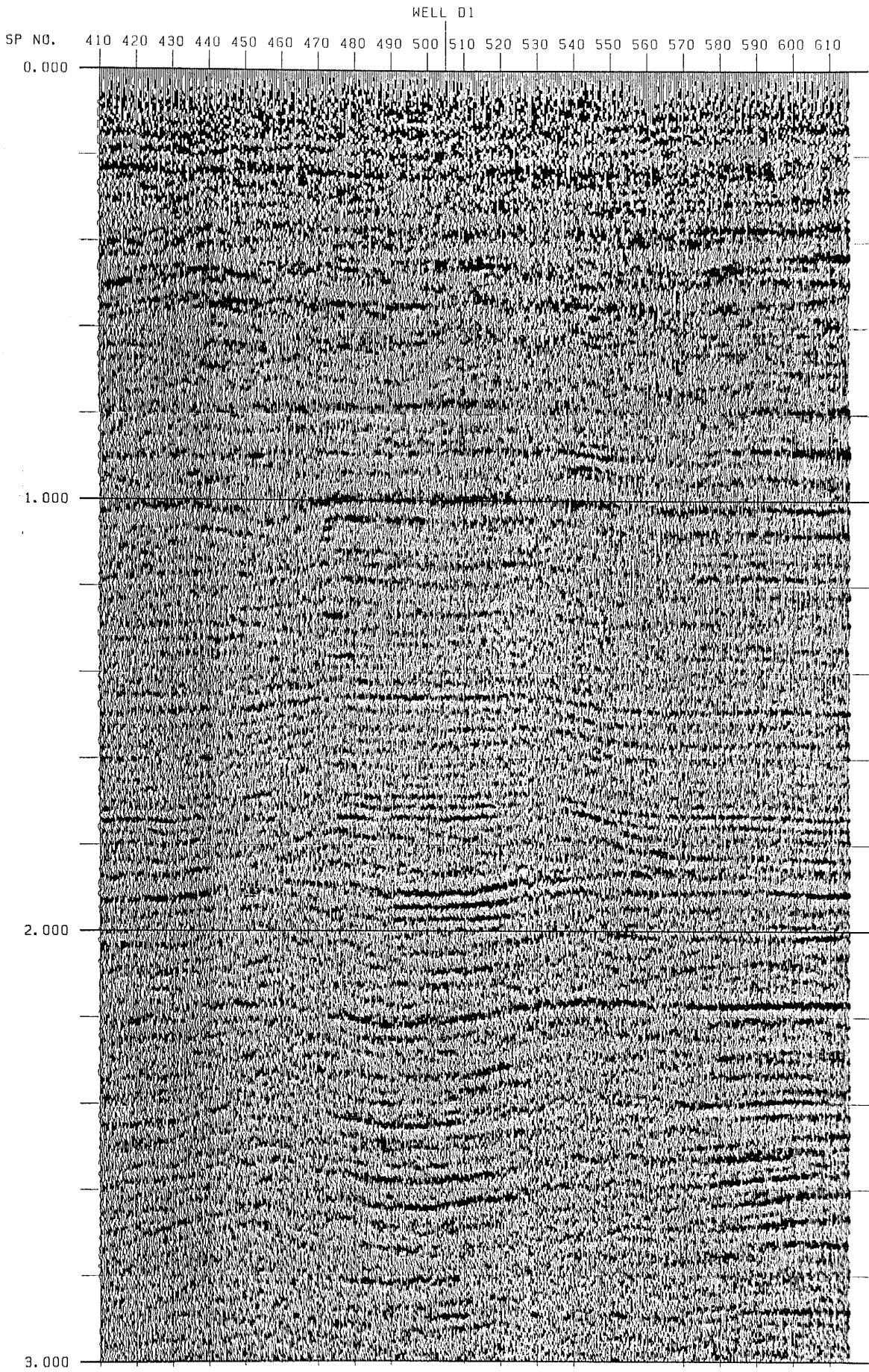


Fig. 5.13 Effect of predictive deconvolution on the stacked data.

5.4.2 Filtering

It is well known that the recorded seismic traces are a mixture of signal and noise. The problem is to separate the signal from the noise. This is done by filtering. In the previous Section (5.3.5) we discussed the attenuation of noise from individual seismic traces using the stacking technique. However, some noise will persistently resist our attempts to "stack out" and will appear as steeply dipping events on the final section. One way to remove this noise is the use of bandpass filters. A frequency analysis of the CMP 309 gather, shows that the dominant frequency is 14-50 Hz, Figure 5.14. A filter with a pass-band of 25-60 Hz used in the shallower part of the section, corresponding to two-way times of less than 1 s.

Obviously, the most important point which we are interested in is how filtering affects the seismic data. Figure 5.15 shows a sequence of bandpass filter tests, before the data has been stacked. In this figure the original record is shown together with eight different band pass filters. The effect of the low cut is to remove the low frequency noise component. The filter range is 14-45 found suitable. It is the same range was used by Western Geophysical Company.

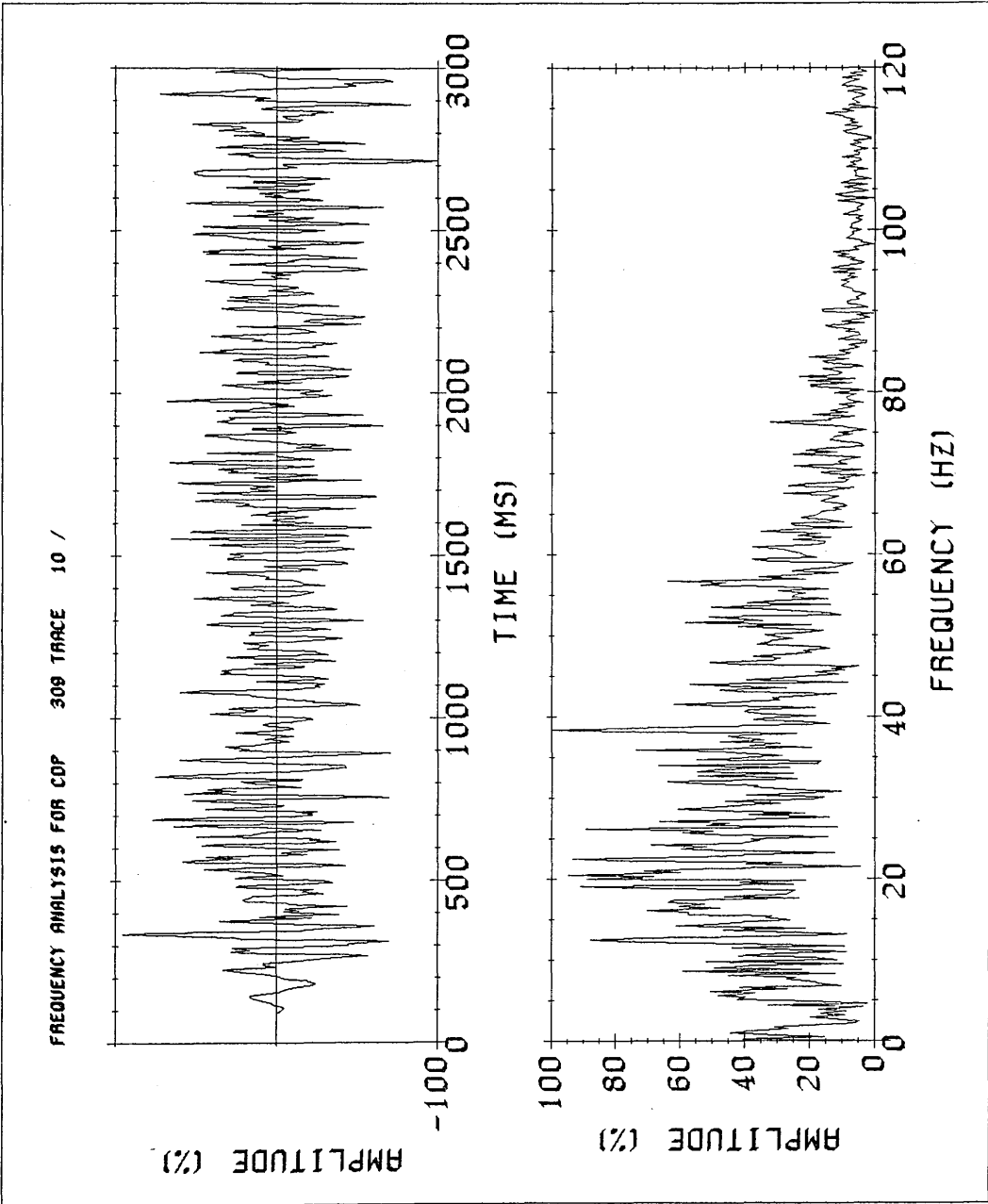


Fig. 5.14 Frequency analysis in the CMP gather (309).

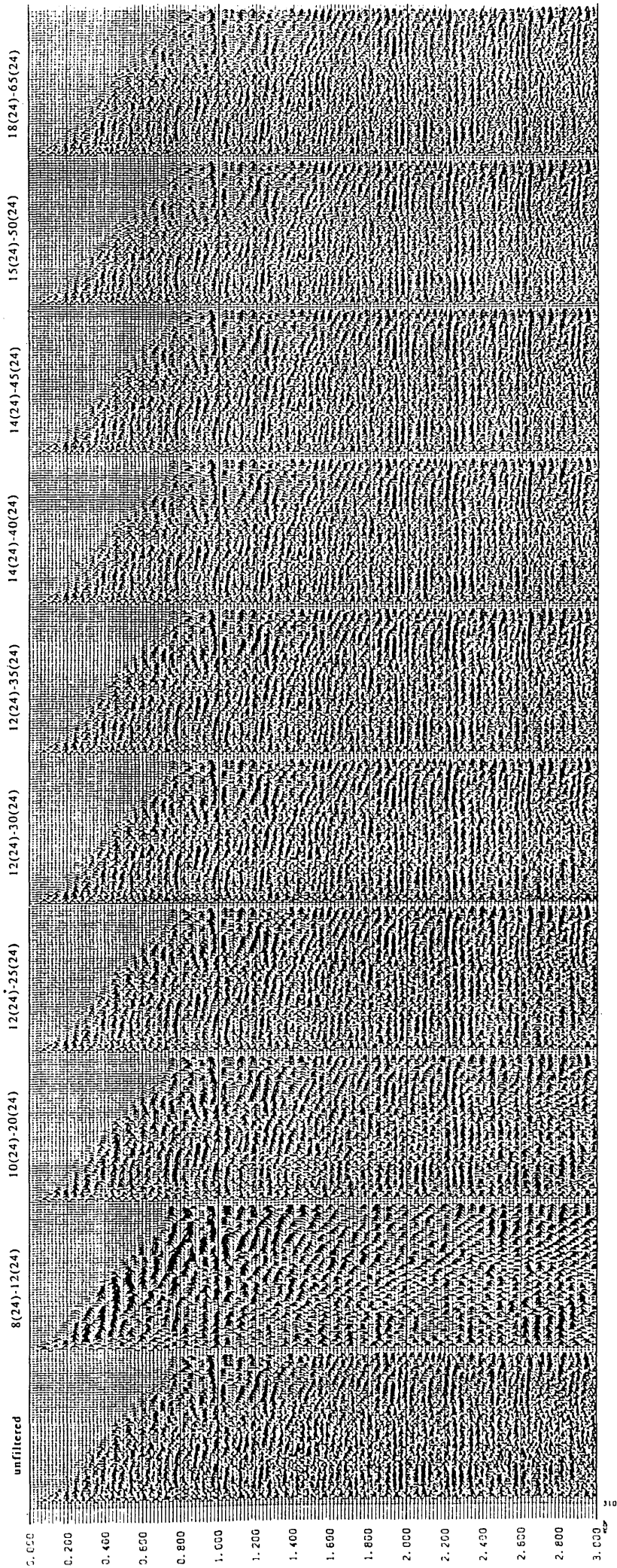


Fig. 5.15 A sequence of bandpass filter tests, for CMP gather (310). Low and high frequency cut-offs in Hz are annotated with respective db/octave slopes in parentheses.

5.5 Results

In final stage of processing, the final stacked section was plotted at a suitable scale. Figure 5.16(a) is the original 36-fold conventional final stack of our section of line U-14 Intisar "D" field data. It was plotted using variable-area plus wiggle (VAW). In this presentation, positive peaks are plotted solid black and negative troughs as a continuous line or 'white'.

The reprocessed version of the same section is plotted using VAW in Figure 5.16(b), and just variable-area (VA) in Figure 5.16 (c). Peaks are solid black, troughs are left unrepresented.

The horizontal scale used is 20 traces per centimetre, and the vertical scale (two-way time) is 12 centimetre per second.

Comparison between the final section processed by the Western Geophysical Company, and the same section reprocessed using the SierraSEIS software package, shows that the latter section has significant improvement, especially at around 1.0 s two-way time. Western's section shows a low-frequency reflector with a smooth anticlinal shape, whereas the new section shows much more detailed structure at SPs 460 and SPs 560 above the reef flanks. The difference between the two sections could be the result of static correction effect, in particular the residual static correction, which has probably removed real structure from the Western version.

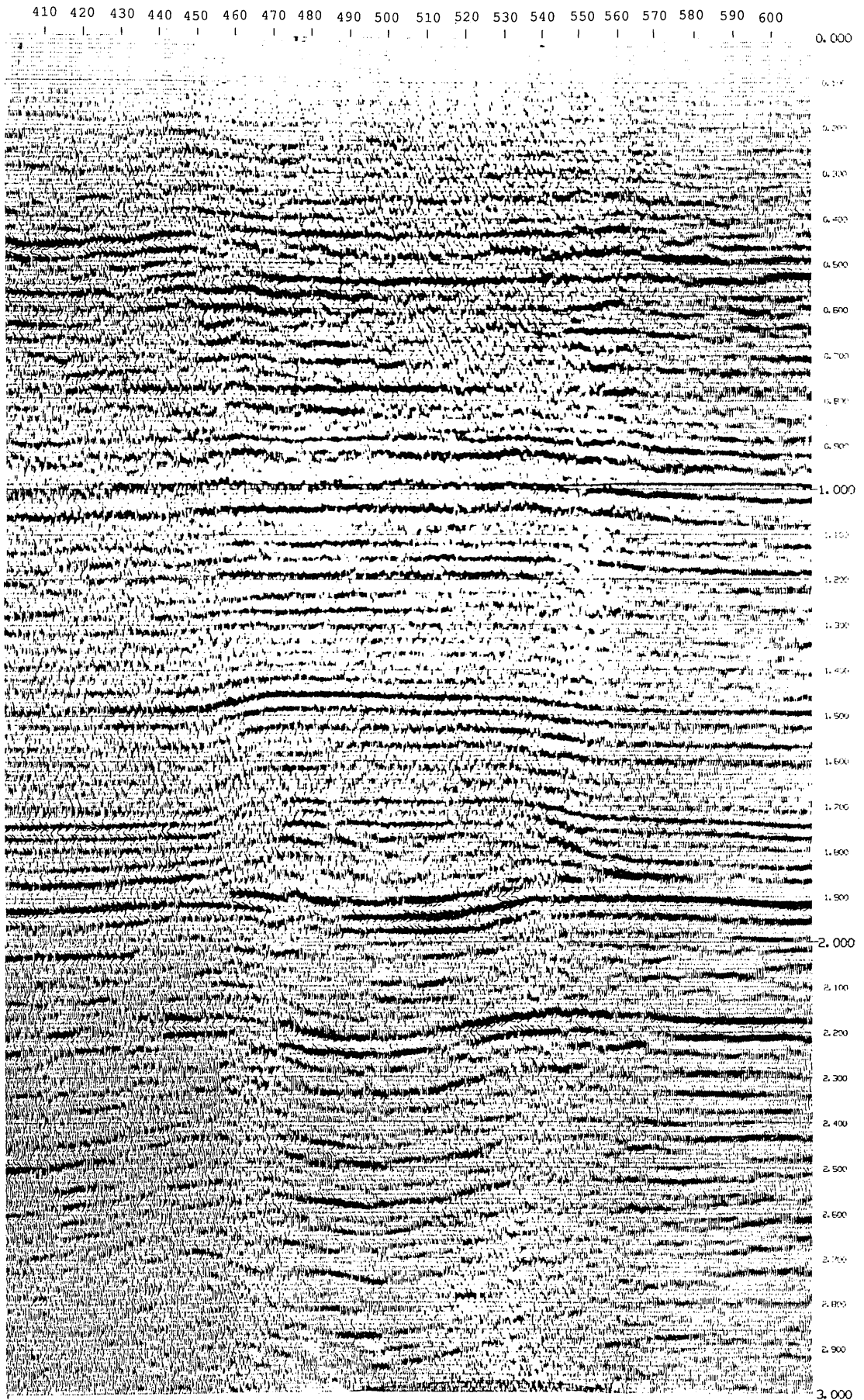


Fig. 5.16 (a) The original seismic section, processed by Western Geophysical Company in 1986.

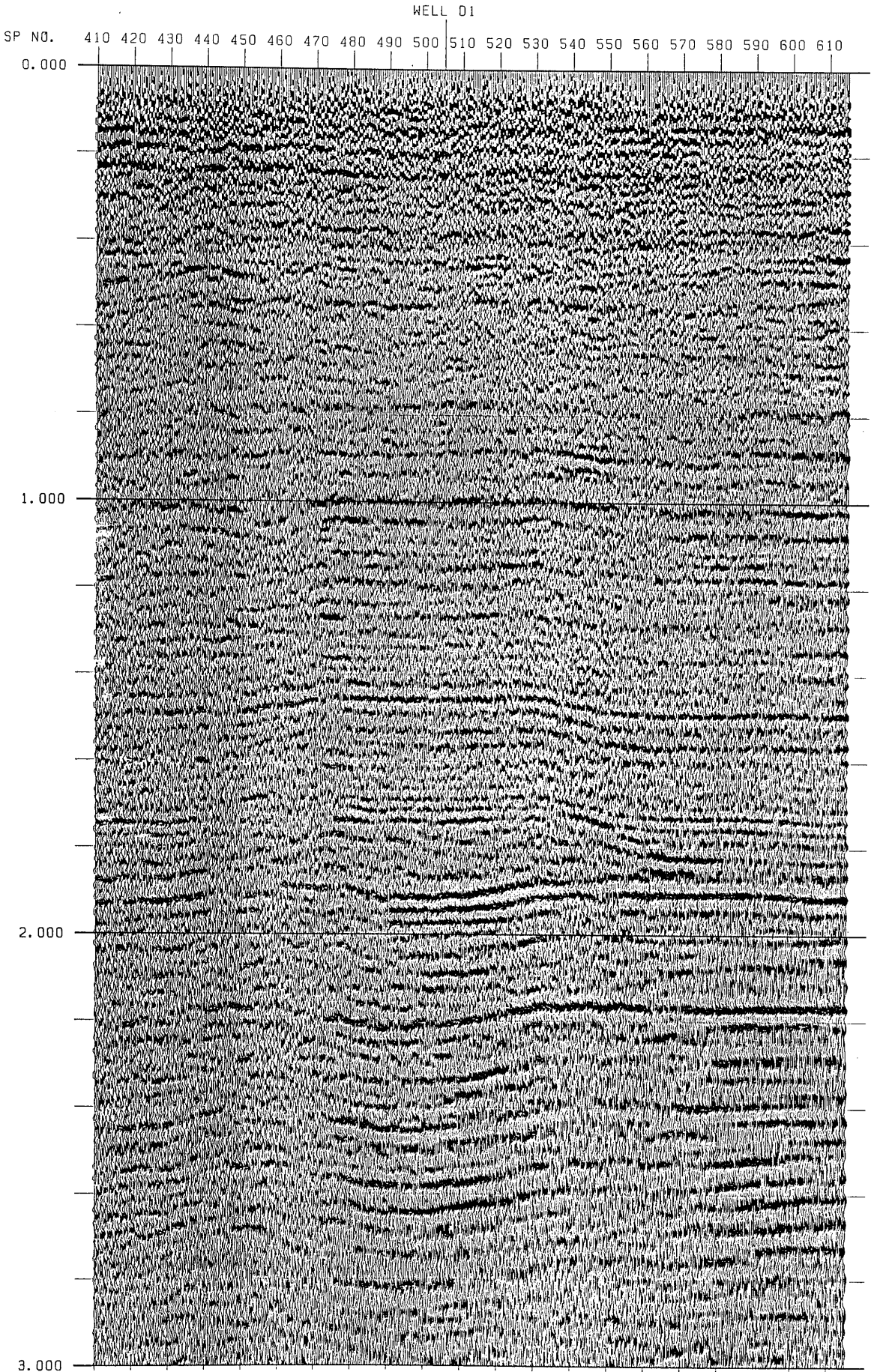


Fig. 5.16 (b) Reprocessed seismic section (final stack section, variable-area and wiggle).

WELL D1

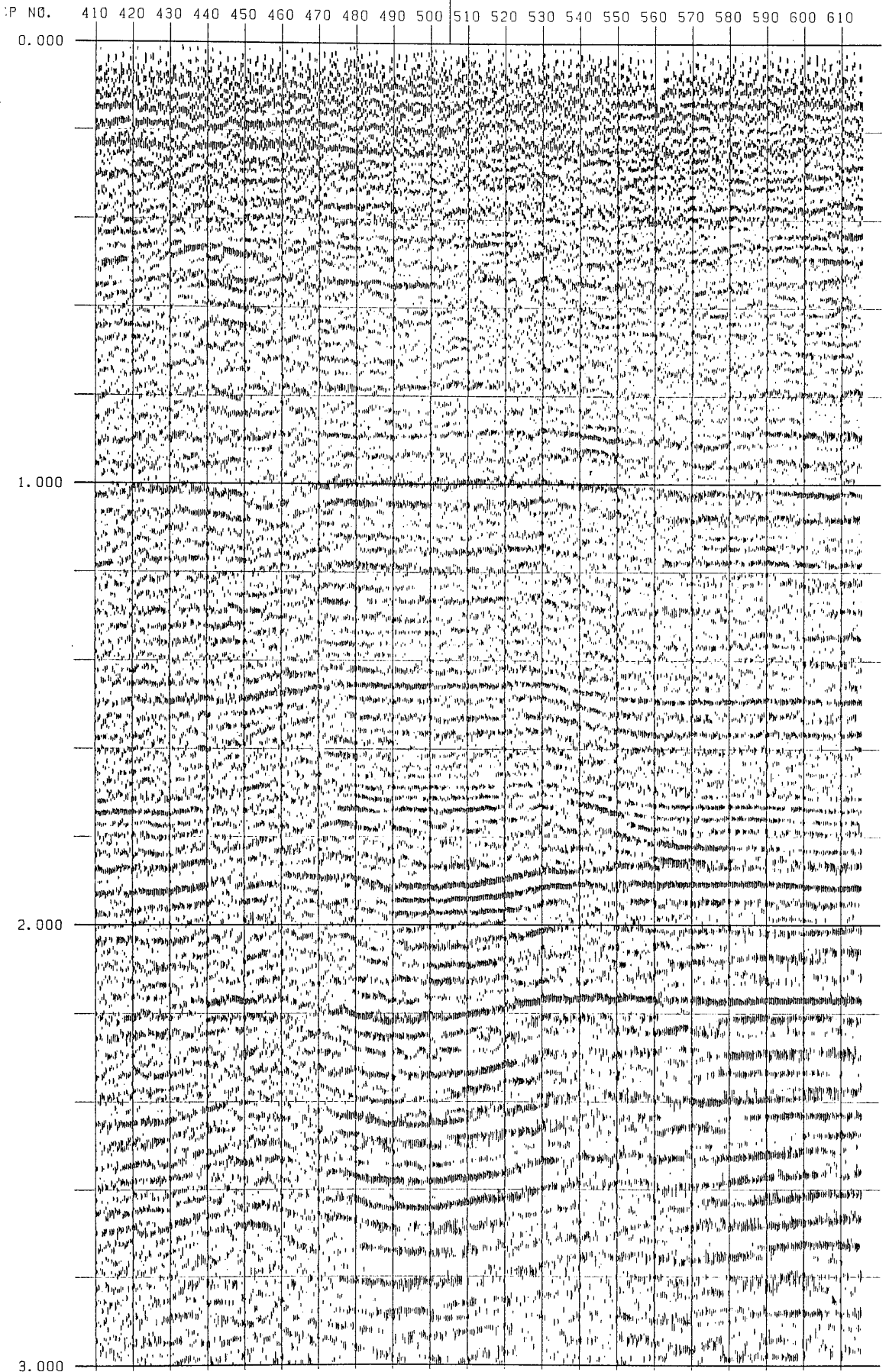


Fig. 5.16 (c) The same seismic section as in Figure 5.16(a) with variable-area display only.

5.6 Migration

Figure 5.17 represents the final stack section after FK migration, using the Stolt FK migration algorithm, to investigate the effect of decreasing or increasing the velocities for migration. Values of $\pm 10\%$ of the original stacking velocities were tested and compared (Figures 5.17 (a), (b) and (c)). The migration results are similar in all three cases. The migration was carried out on the unfiltered deconvolved data, and then passed through the filtering and display processes, as detailed for the unmigrated stacks. Note that migration doesn't displace horizontal events; rather, it moves dipping events in the updip direction and collapses diffractions.

The seismic record section converted to depth is helpful in interpretation of the results in geological terms. The goal of migration is to make the stacked section appear similar to the geologic cross-section along the seismic line. Our objective is to get a depth section from the stacked section. Figure 5.18 shows the seismic section in depth.

The flow-chart in Figure 5.19 summarises in detail the seismic processing steps, together with the figure numbers. More details of the processing steps and the different parameters that have been used are given in the Appendix.

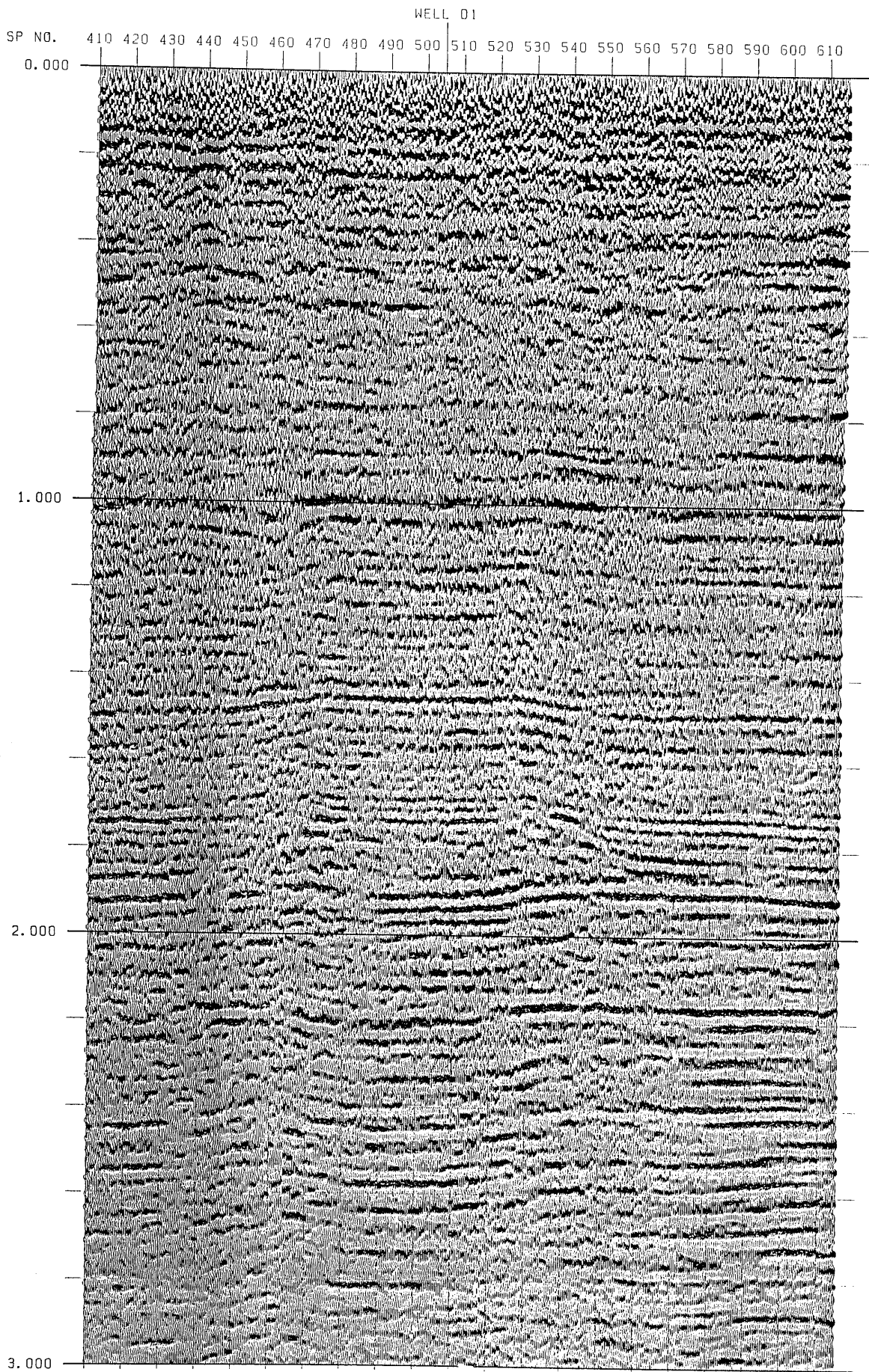


Fig. 5.17(a) Final stack section shown in Fig. (5.16 (b)) after FK-migration using velocity lower 10% than the stacking velocity.

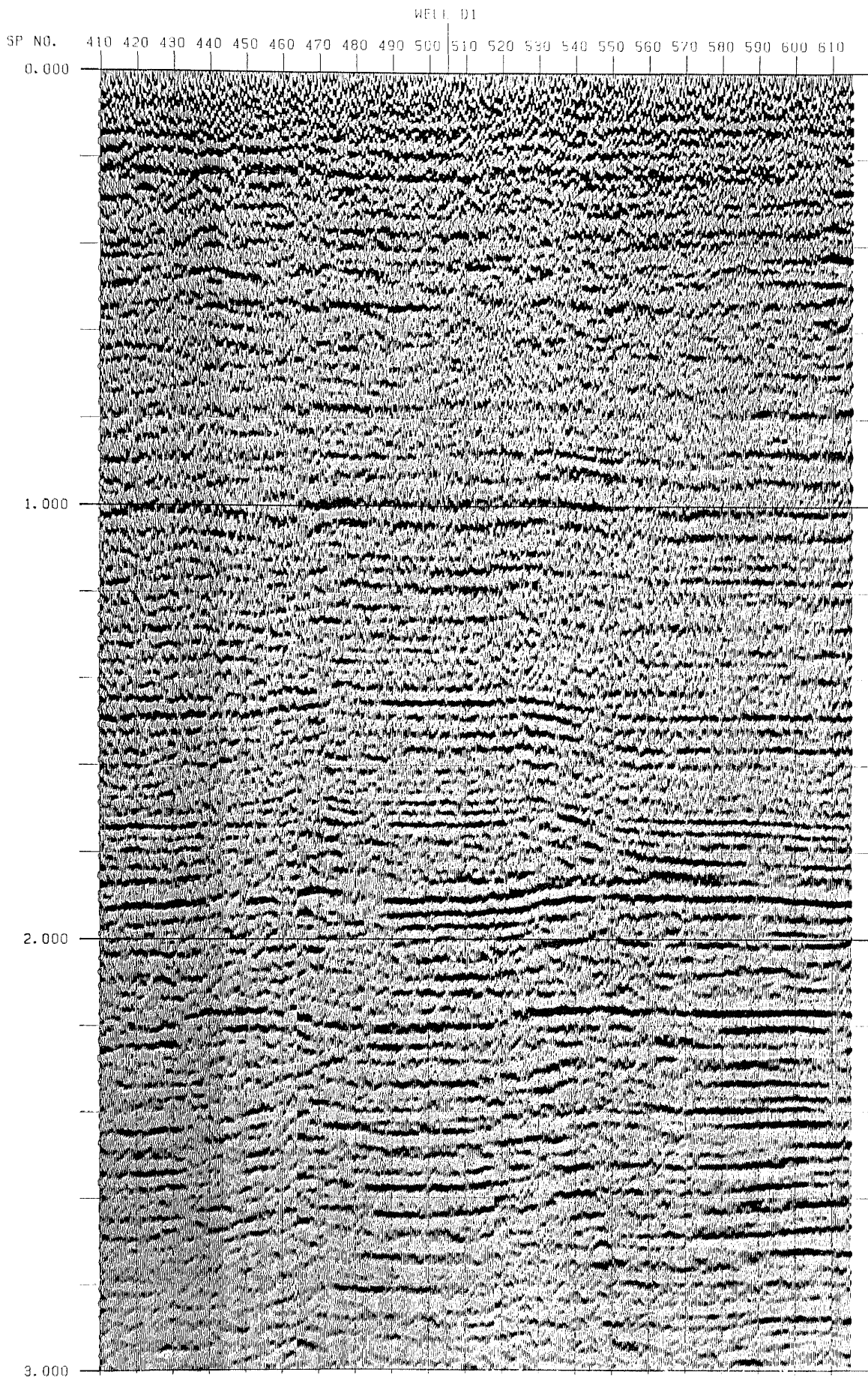


Fig. 5.17(b) Final stack section shown in Fig. (5.16 (b)) after FK-migration using the stacking velocity.

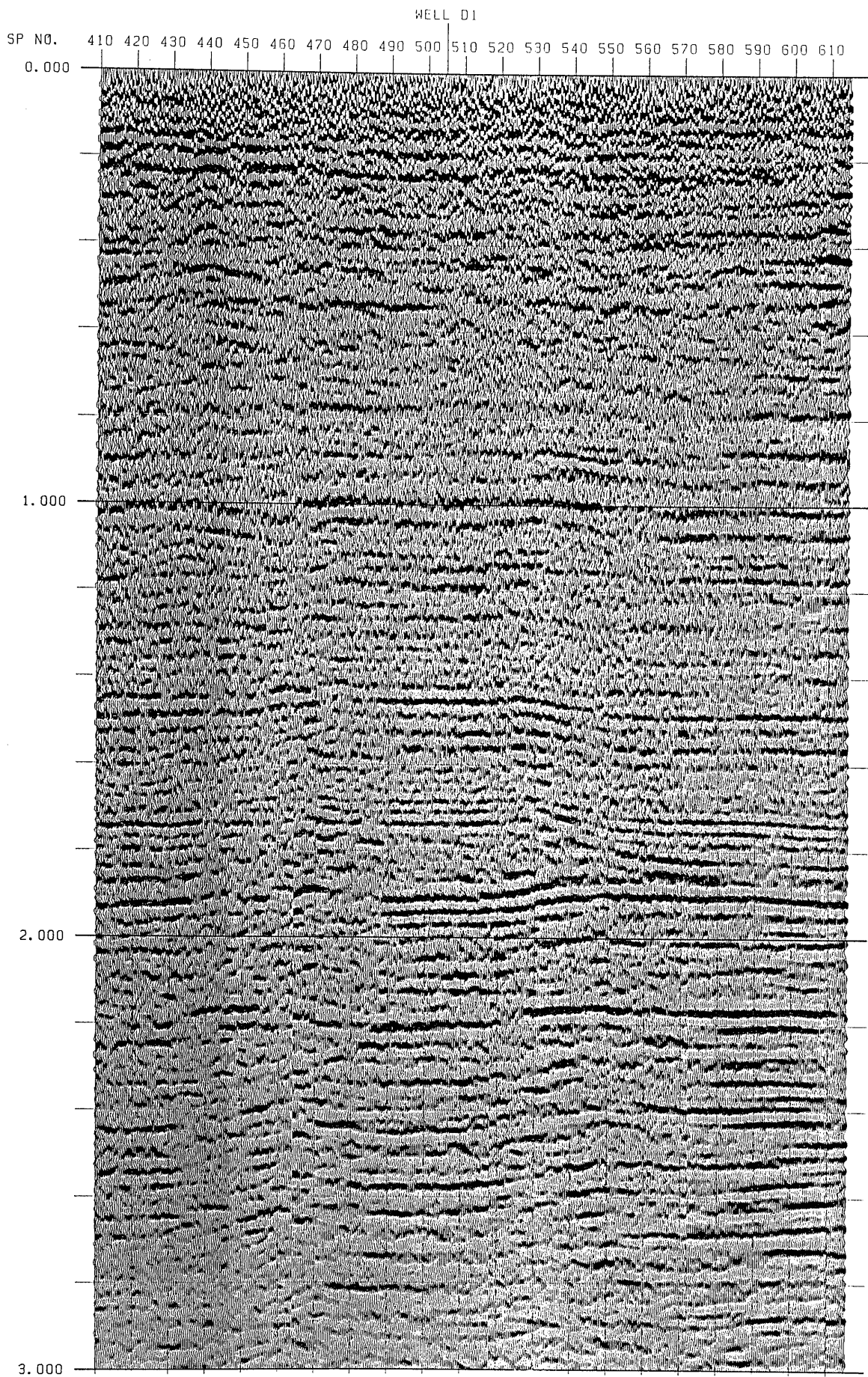


Fig. 5.17(c)

Final stack section shown in Fig. (5.16 (b)) after FK-migration using velocity higher 10% than the stacking velocity.

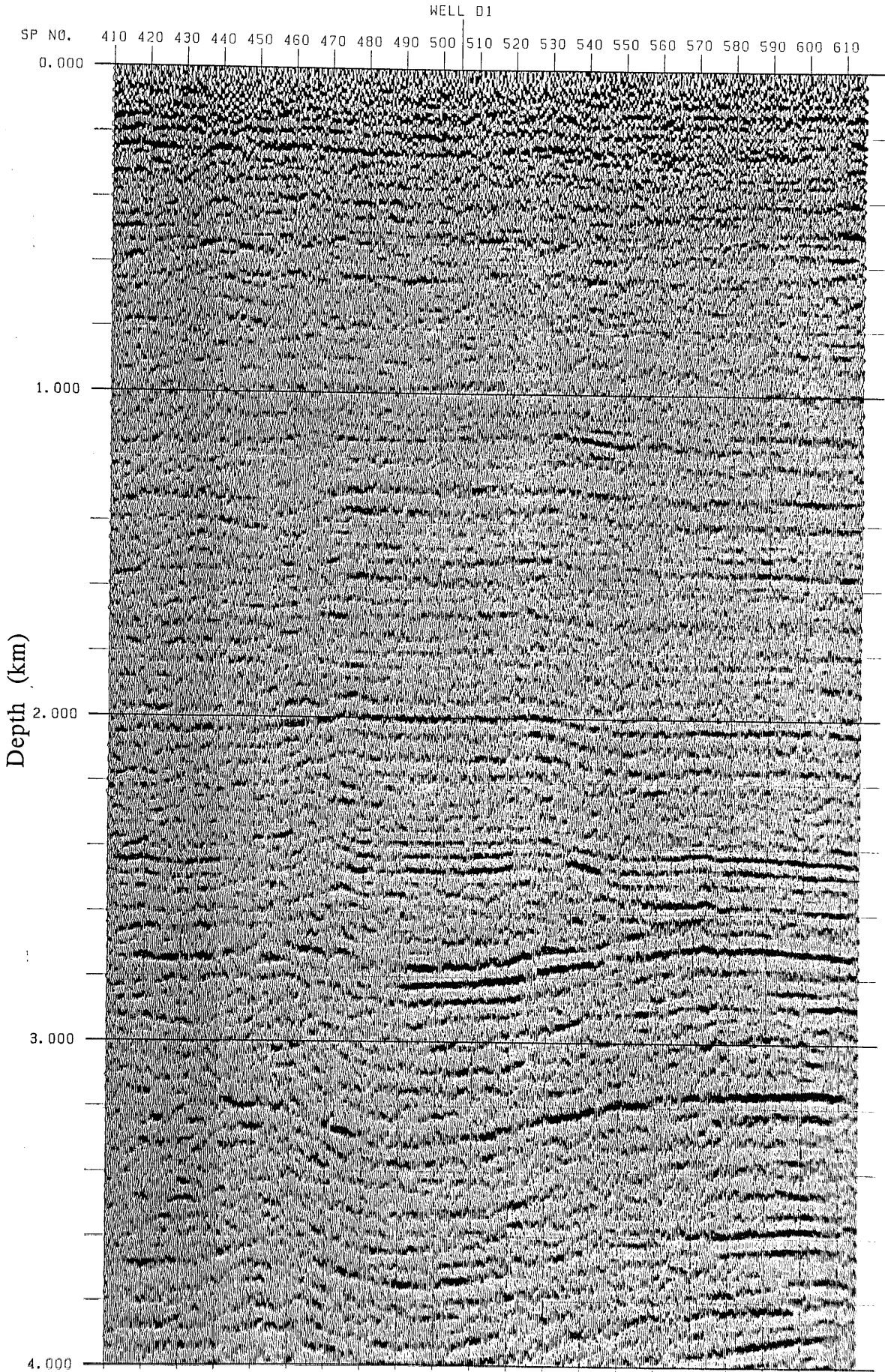


Fig. 5.18 Final stack section after depth migration.

5.7 Summary of Processing

- (1) The spectra indicate that the section contains mostly primary energies down to 1.8 to 2.6 s, and also shows a velocity gradient.
- (2) The residual static correction was a major improvement to the data.
- (3) The final section processed by the Western Geophysical Company, and the same section reprocessed using the SierraSEIS software package, shows that the latter section has significant improvement, especially at around 1.0 s two-way time. Western's section shows a low-frequency reflector with a smooth anticlinal shape, whereas the new section shows much more detailed structure at SPs 460 and SPs 560 above the reef flanks.

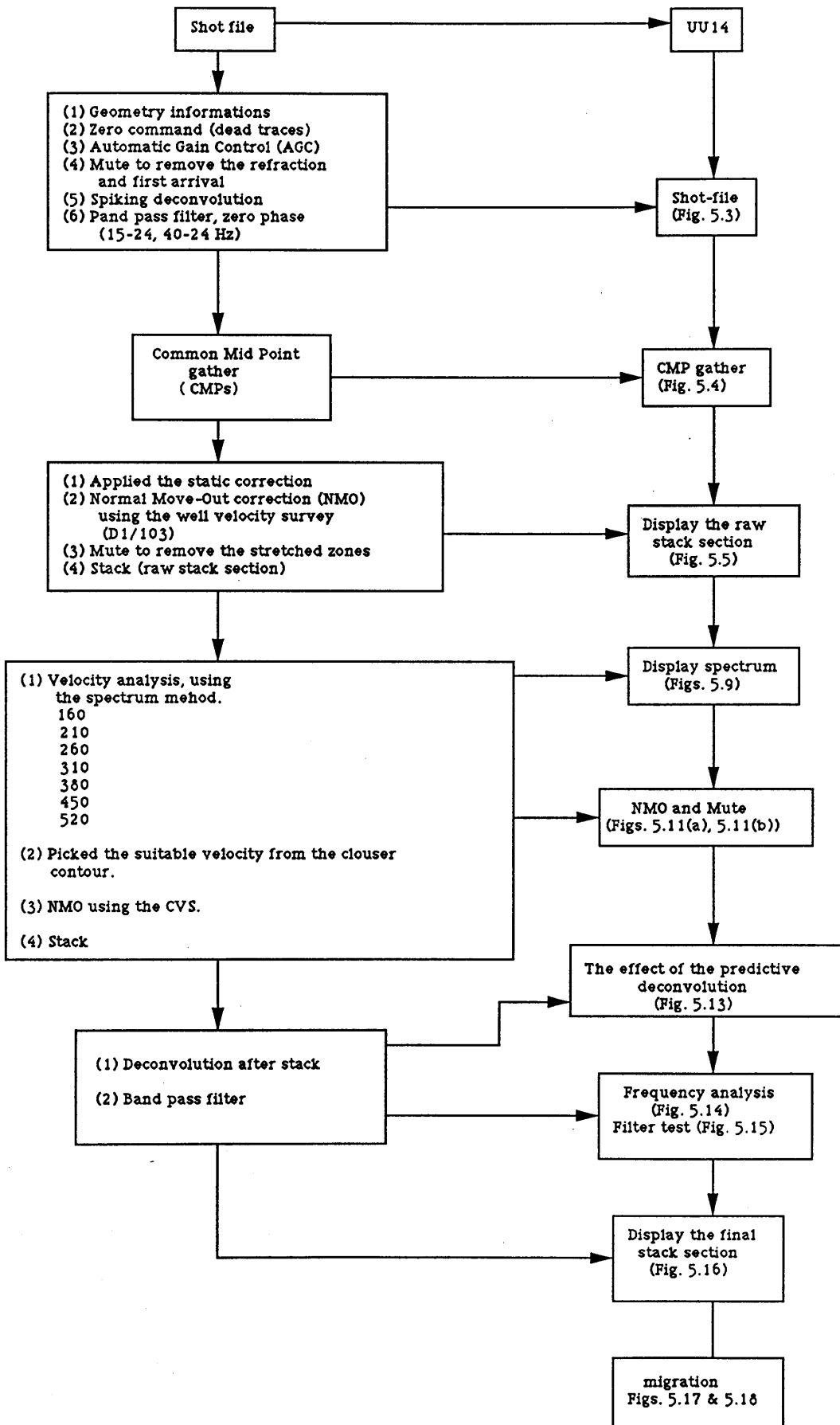


Fig. 5.18 Flow-chart summarizing the seismic processing

Chapter 6

6.0 Conclusions and recommendations for further work

6.1 Conclusions

6.2 Suggestions for further work

6.1 Conclusions

The Palaeocene of the Sirte Basin is characterized by carbonate rocks and shales deposited in an epeiric sea. There is a great thickness of shales in the Agedabya Trough, which are believed to be important source rocks for oil and gas. The Sheterat shale is the most likely candidate for the origin of the oil in the Upper-Sabil in Concession 103, though the Kheir marl and Rakb shale may have contributed.

The "D" reef grew at the same time as the Upper-Sabil platform carbonates were being deposited. At the end of reef growth time near the end of the Palaeocene, the reefs stopped growing with the introduction of the Lower Kheir shales. The "D" reef was in a high energy zone, and as a result post reef shoals grew around and over the "D" reef.

The well to seismic tie matches reasonably closely, particularly at the Lower Eocene and Upper Palaeocene levels. The mis-ties are small. The horizons interpreted are the Upper-Sabil (Upper Palaeocene) at 1910 ms, Kheir (Upper Palaeocene - Lower Eocene) at 1630 ms, Gir (top of Lower Eocene) at 1410 ms, and El-giza (Middle Eocene) at 1140 ms. The figures are two-way travel times near the well D1/103; they increase slightly away from the well (Figure 1.2).

Reflectors in the sediments are mostly parallel bedded and vary laterally in intensity and continuity, with strongly contrasting acoustic impedances between layers. The sequences vary from shale to limestone (e.g. Kheir shale and Upper-Sabil limestone) where the reflection coefficient is positive, and a reflecting boundary appears as a trough (white) on the seismic

sections. when the limestone overlies shale (Upper-Sabil limestone and Shetrat shale) the reflection coefficient is negative and a reflecting boundary appears as a peak (black).

According to the sonic logs generated in wells D2, D1, D5, D12, and D16, (Figures 4.3 and 4.4) the interval velocity increases in the El-giza to Gir and Gir to Kheir intervals from WSW to the centre around well D1/103, where it is 4100 m/s and 4600 m/s respectively, and decrease towards the ENE.

Table 6.1 Summary of interval velocity according to the sonic logs

Formations	South	Centre	North-East
Top El-giza to Top Gir	4000 m/s	4100 m/s	4110 m/s
Top Gir to Top Kheir	4400 m/s	4600 m/s	4900 m/s
Top Kheir to Top reef	3680 m/s	3800 m/s	3900 m/s
Top reef to Top Upper-Sabil		3800 m/s	

Table 6.2 Summary of the interval velocity according to the sonic logs

Formations	W-SW	Centre	E-NE
Top El-giza to Top Gir	4100 m/s	4100 m/s	4150 m/s
Top Gir to Top Kheir	4650 m/s	4600 m/s	4700 m/s
Top Kheir to Top reef	3900 m/s	3800 m/s	4000 m/s
Top reef to Top Upper-Sabil	3800 m/s	3780 m/s	3900 m/s

The seismic interval velocity is lower than the sonic log velocity. The distribution of the seismic interval velocity over the area is shown in the maps. (Figures 4.13, 4.14, and 4.15), where the interval velocity is high on the periphery and low in the centre.

After changing the velocity a long line U-14 and enter the new velocity which is picked from the spectrum, the differences between the well and the seismic velocity for the interpreted horizons become small, which means that the new seismic velocity more accurate.

The reprocessing of part of line U-14, has resulted in a better defined seismic section, displayed both in migrated time and in depth. The improvement results mainly as a result of the good picking of the spectrum.

The new velocity analysis have been picked carefully, avoiding multiples, which gave a high resolution section. A typical velocity spectra display computed from 0.0 s to 3.0 s for velocities varying from 1500 m/s to 4500 m/s at 100 m/s intervals. The velocity function is obtained by connecting the interpreted primary energy arrivals as indicated on the Figure (5.9). These spectra also show some multiple energy around 2.4 to 2.8 s with 2000 to 3200 m/s velocity. Since the spectra are computed for overlapping time gates and very close velocity intervals, the final display will contain the results of analysis of all the reflections, primaries, multiples, and other types of coherent energy. Changes of character of primaries on velocity spectra displays serve as a good indicator that changes have taken place in the stratigraphy. Spectra in Figure 5.9 indicate that the section contains mostly primary energies down to 1.8 to 2.6 s, and also shows a gentle velocity gradient. For example, the rms velocity at 1.820 s on the northwest side of the section is 3300 m/s, on the southeast side it is 3450 m/s.

6.2 *Suggestions for further work*

- (1) Extended mapping, to tie other reefs in the Concession 103 area e.g. "A", "B", "C", and "E" with the "D" reef, to present additional ideas and interpretations.
- (2) Additional seismic coverage is necessary in the area, in particular lines with North-South and West-East directions.
- (3) Re-picking other seismic lines in the area to improve depth maps away from well control.
- (4) The interpretation of the 3-D seismic reflection, covering essentially the eastern part of the field, could provide a means of investigating the reef in greater detail.
- (5) More well-velocity surveys are important, to give accurate velocity information over the field.
- (6) Reprocessing of additional interesting seismic lines with more accurate parameters (e.g. velocity analysis).

References

- AL-CHALABI, M.*, 1974. An analysis of stacking, RMS, average, and interval velocities over a horizontally layered ground. *Geophysical Prospecting* v. 22, p. 458-475.
- AL-SADI, N. H.*, 1980.. Seismic exploration technique and processing. Birkhauser Verlag Basel. P. 161-183.
- ANDERSON, N. L., BROWN, R. J., and HINDS, R. C.*, 1989. Low-and high-relief Leduc formation reefs : analysis. *Geophysics* v. 54, p. 1410-1419.
- ANDERSON, N. L., BROWN, R. J., HINDS, R. C., and HILLS, L. V.*, 1989. Seismic signature of a Swan Hills (Frasnian) reef reservoir, Snipe Lake, Alberta. *Geophysics* v. 54, p. 148-157.
- ANSTEY, N. A.*, 1980. Simple seismics. International Human Resources Development Corporation (IHRDC), p. 21-43, 104-129.
- BADLEY, M. E.*, 1985. Practical Seismic interpretation. International Human Resources Development Corporation (IHRDC), p. 5-27, 71-110.
- BALLY, A.W.*, 1987. Atlas of seismic stratigraphy , Volume (1). AAPG studies in Geology / 27.
- BARR, F. T. and WEGER, A. A.*, 1972. Stratigraphic nomenclature of the Sirte Basin, Libya : Grafiche Trevisan, Italy.
- BERG, O.R. and WOOLVERTON, D.G.*, 1985. Seismic Stratigraphy (II): An Integrated Approach to Hydrocarbon Exploration. AAPG Mem. 39.
- BRADY, T. J., CAMPBALL, N. D. J., and MAHER, C. E.*, 1979. Intisar "D" oil field, Libya. *Bull. Am. Ass. Pet. Geol.*, Mem 30, P. 543-564.
- BRAITHWAITE, C.J.R.*, 1973. Reefs : just a problem of semantics ?. *Bull. Am. Ass. Pet. Geol.*, v. 57, p. 1100-1116.

- BRAITHWAITE, C.J.R.**, 1987. The origins and growth of Recent reefs. *Geology Today*, v. 3, p. 16-21.
- BRAITHWAITE, C.J.R.**, 1987. The structure and history of Recent reefs. *Geology Today*, v. 3, p. 197-201.
- BUBB, J.N. and HATLELID, W.G.**, 1977. Seismic stratigraphy and global changes of sea level, part 10 : Seismic recognition of carbonate build-ups. *Bull. Am. Ass. Pet. Geol. Mem* 26, p.185-204.
- CLIFFORD, H.J., GRUND, R and MUSRATI, H.** 1979. Geology of a stratigraphic Giant : Messla oil field, Libya. *Bull. Am. Ass. Pet. Geol., Mem* 30, P. 507-524.
- CONANT L., C. and GOUDARZI, G. H.**, 1967. Stratigraphic and tectonic framework of Libya. *Bull. Am. Ass. Pet. Geol.*, V.51, P. 719-730.
- DOBRIN, M. B.**, 1976. Introduction to geophysical prospecting. Mc Graw-Hill, p. 201-253, 254-291
- DOBRIN, M. B.**, 1976. Seismic Exploration for stratigraphic traps. *Bull. Am. Ass. Pet. Geol.*, Mem 26, P.329-351.
- FITCH, A. A.**, 1976. Seismic reflection interpretation. Gebruder Borntraeger, Berlin-Stuttgart, P. 47-53, 56-65.
- GARDNER, G.M.F., GARDNER, L.W. and GREGORY, A.R.**, 1974. Formation velocity and density-the diagnostic basis for stratigraphic traps : *Geophysics* v.39, p. 770-780.
- GARDNER, G.M.F., GARDNER, L.W. and GREGORY, A.R.**, 1974. Formation velocity and density-the diagnostic basis for stratigraphic traps : *Geophysics* v.39, p. 770-780.
- HATTON, L., WORTHINGTON, M. H., and MAKIN, J.**, 1986. *Seismic Data Processing: Theory and practic.* Oxford Blackwell Scientific. P. 47-104.
- HEA**, 1969. Symposium on the geology of Libya. Faculty of science, Tripoli, Libya, p.110.

- HUSTON, D. C. and BACKUS, M. M.**, 1989. Offset-dependent mis-tie analysis at seismic line intersections. *Geophysics* v. 54, p. 962-972.
- JANKOWSKY, W.** 1969. Empirical investigation of some factors affecting elastic wave velocities in carbonate rocks. *Geophysical Prospecting* v. 19, p. 103-118.
- KLEYN, A. H.**, 1977. On the migration of reflection time contour maps. *Geophysical Prospecting* v. 25, p. 125-140.
- KLITZSCH, E.**, 1968. Outline of the geology of Libya in geology and archaeology of northern Cyrenaica : Petroleum Exploration Society of Libya, p. 71-78.
- KLITZSCH, E.**, 1969. The structural development of parts of North Africa since Cambrian time. Symposium on Geology of Libya (abstract).
- McQUILLIN, R., BACON, M., and BARCLAY, W.**, 1984. An introduction to Seismic interpretation. Graham & Trotman Limited. p. 67-89, 102-114, 115-132, and 174-194
- MIKE, BADLEY**, 1989. Practical seismic interpretation. Badley Ashton, London.
- MITCHUM, R.M., J.R., VAIL, P. R., and SANGREE, J. B.**, 1977. Seismic stratigraphy and global changes of sea level, part 6 : Stratigraphic interpretation of seismic reflection patterns in depositional sequences. *Bull. Am. Ass. Pet. Geol.*, Mem 26, p. 117-133.
- MITCHUM, R.M., J R., and VAIL, P.R.**, 1977. Seismic stratigraphy and Global changes of sea level, part 7 : Seismic stratigraphic interpretation procedure. *Bull. Am. Ass. Pet. Geol.* Mem 26, p. 135-143.
- MONTALBETTI, J. F.**, 1971. Computer determination of seismic velocities-a review. *Journal of Canadian Society of Exploration Geophysics*, v. 7, p. 32-45.
- NEIDELL, N. S., BEARD, J H., AND ERNEST, E. COOK**, 1985. Use of seismic-derived velocities for stratigraphic exploration on land: seismic and direct gas detection. *Bull. Am. Ass. Pet. Geol.* Mem 39, p. 49-77.

- NEIDELL, N. S.*, 1984. Improve prospect picks with moveout velocity analysis. World Oil (January), p. 129-142.
- PALLISTER, A.E.*, 1960. The preparation of seismic depth maps in oil exploration: Alberta Soc. Petroleum Geologists Jour., v. 8, no. 9, P. 235-246 incl. sketch maps and diagrams, sept.
- PATURET, D.*, 1971. Different methods of time-depth conversion with and without migration. Geophysical prospecting, v. 19, P. 27-41.
- PAYTON, C. E.*, 1977. Seismic Stratigraphy -Applications to hydrocarbon exploration. AAPG Mem. 26.
- ROBERT, E. SHERIFF*, 1978. A first course in Geophysical Exploration and interpretation. Stratigraphic interpretation, p. 275-287.
- ROBERTS, J. M.*, 1968, Amal Field, Libya. Bull. Am. Ass. Pet. Geol., Mem 14, P.438-448.
- ROBINSON, E.A., and DURRANI, T.S.*, 1986. Geophysical signal processing. Cambridge University Press-Cambridge, p. 167-189.
- ROKSANDIC, M. M.*, 1978. Seismic facies analysis concepts. Geophysical Prospecting v. 26, p. 383-398.
- SANGREE, J.B., and WLDMIER, J.M.*, 1979. Interpretation of depositional facies from seismic data. Geophysics. v. 44 no. 2, p.131-160.
- SAVIT, C. H.*, 1982. Geophysical characterization of lithology application to subtle traps. Bull. Am. Ass. Pet. Geol., Mem 32, p. 11-30.
- SHERIFF, R.E. and GELDART, L.P.*, 1983. Exploration Seismology, Volume (2), Data processing and interpretation. Cambridge University Press-Cambridge, p. 81-117.
- SHERIFF, R.E.*, 1976. Inferring stratigraphy from seismic data : Bull. Am. Ass. Pet. Geol., v. 60, p. 528-542.

- SHERIFF, R.E.**, 1980. Seismic stratigraphy. International Human Resources Development Corporation (IHRDC), p. 85-116.
- SHERIFF, R.E.**, 1982. Structural interpretation of seismic data. Education course note series. AAPG # 23, p. 20-48.
- SILVERMAN, DANIEL**, 1967. The digital processing of seismic data. *Geophysics*, v. 32, p. 988-1002.
- TANER, T. M., COOK, E.E., and NEIDELL, N.S.**, 1970. Limitations of the reflection seismic method; lessons from computer simulations. *Geophysics*, v. 35, p. 551-573.
- TANER, T.M. and KOEHLER, F.**, 1969. Velocity spectra-digital computer derivation and applications of velocity functions. *Geophysics*, v. 34, no. 6, p. 859-881.
- TELFORD, W. M., GELDART, L. P., SHERIFF, R. E., and KEYS, D. A.**, 1976. *Applied Geophysics*. Cambridge University Press-Cambridge, p. 396-414.
- TERRY, C. E., and J. J., WILLIAMS**, 1969. The Idris "A" bioherm and oil field, Sirte Basin, Libya - its commercial development, regional Paleocene geologic setting and stratigraphy; in *Exploration for Petroleum in Europe and North Africa J.*: London, Inst. Petroleum, P. 31-68.
- THOMAS, L. DAVIS AND GEOFFERY, M. JACKSON**, 1988. Seismic stratigraphy study of algal mound reservoirs, Patterson and Nancy fields, Paradox basin, San Juan County, Utah. *Geophysics* v. 53, p. 875-880.
- THOMAS, L. DAVIS**, 1969. Velocity variations around Leduc reefs, Alberta. *Geophysics* v. 37, p. 584-604.
- WILLIAM, A. SCHNEIDER**, 1971. Developments in seismic data processing and analysis. *Geophysics*, v. 36, p. 1043-1073.
- YILMAZ, O.**, 1988. Seismic data processing. (*Investigation in Geophysics*, Volume 2), Society of Exploration Geophysicists. P. 155-203, 241-353.

YILMAZ, O., 1989. Velocity-stack processing. *Geophysical prospecting* 37, p. 357-382.

- S.P.: Shot-points.
- T(El.): Two-way time of El-giza horizon (msec).
- T(Gir) : Two-way time of Gir horizon (msec).
- T(Kh.) : Two-way time of Kheir horizon (msec).
- T(U.-S.) : Two-way time of Upper-Sabil horizon (msec).
- D(El.) : Depth of El-giza horizon (m).
- D(Gir) : Depth of Gir horizon (m).
- D(Kh.) : Depth of Kheir horizon (m).
- D(U.-S.) : Depth of Upper-Sabil horizon (m).
- Vi (El.) : El-giza to Gir seismic interval velocity (m/sec).
- Vi (Gir) : Gir to Kheir seismic interval velocity (m/sec).
- Vi (Kh.) : Kheir to Upper-Sabil seismic interval velocity (m/sec).
- Va (El.): Average velocity in the top El-giza horizon (m/s).
- Va (Gir): Average velocity in the top Gir horizon (m/s).
- Va (Kh.): Average velocity in the top Kheir horizon (m/s).
- Va (U.-S.): Average velocity in the top Upper-Sabil horizon (m/s).
- $\Delta Vi(1)$: The difference between the interval velocity in the well (D1/103) and the seismic velocity trough the El-giza to Gir interval (m/sec).
- $\Delta Vi(2)$: The difference between the interval velocity in the well (D1/103) and the seismic velocity trough the Gir to Kheir interval (m/sec).
- $\Delta Vi(3)$: The difference between the interval velocity in the well (D1/103) and the seismic velocity trough the Kheir to Upper-Sabil interval (m/sec).

Table 3.5 : Showing the shot-points, the two-way time in El-giza, Gir, Kheir, and Upper-Sabil horizons, and their depths (line U-14).

S.P.	T(El.) (msec)	T(Gir) (msec)	T(Kh.) (msec)	T(U.-S.) (msec)	D(El.) (m)	D(Gir) (m)	D(kheir.) (m)	D(Upper-Sabil) (m)
320	1190	1420	1705	1930	1550	2075	2654	3040
326	1190	1420	1705	1935	1550	2075	2654	3048
330	1190	1420	1705	1935	1550	2075	2654	3048
340	1190	1420	1710	1940	1550	2075	2662	3056
350	1190	1420	1715	1940	1550	2075	2669	3056
356	1190	1420	1715	1940	1550	2075	2669	3056
360	1190	1420	1715	1940	1550	2075	2669	3056
370	1190	1420	1715	1940	1550	2075	2669	3056
380	1190	1425	1720	1940	1550	2083	2677	3056
390	1190	1430	1725	1945	1550	2090	2685	3063
391	1190	1430	1725	1945	1550	2090	2685	3063
400	1190	1430	1730	1945	1550	2090	2693	3063
410	1190	1440	1730	1945	1550	2105	2693	3063
420	1180	1440	1730	1945	1537	2105	2693	3063
426	1180	1440	1730	1940	1537	2105	2693	3056
430	1180	1440	1730	1940	1537	2105	2693	3056
440	1180	1440	1720	1935	1537	2105	2677	3048
450	1145	1420	1690	1935	1491	2075	2630	3048
451	1145	1420	1690	1935	1491	2075	2630	3048
460	1135	1410	1640	1940	1478	2061	2553	3056
470	1140	1400	1630	1935	1485	2046	2537	3048
476	1140	1400	1630	1930	1485	2046	2537	3040
480	1140	1400	1630	1925	1485	2046	2537	3032
490	1140	1400	1625	1930	1485	2046	2529	3040
500	1140	1410	1625	1930	1485	2061	2529	3040
505	1140	1410	1630	1930	1485	2061	2537	3040
510	1140	1410	1630	1925	1485	2061	2529	3032
520	1140	1410	1630	1910	1485	2061	2529	3008
530	1140	1420	1630	1900	1485	2075	2537	2993
536	1140	1425	1630	1895	1485	2083	2537	2985
540	1140	1430	1640	1890	1485	2090	2553	2977
550	1150	1440	1660	1885	1498	2105	2584	2969
560	1155	1445	1670	1880	1504	2112	2599	2961
570	1160	1445	1690	1890	1511	2112	2630	2977
571	1160	1445	1690	1890	1511	2112	2630	2977
580	1165	1445	1690	1890	1517	2112	2630	2977
590	1170	1450	1690	1890	1524	2119	2630	2977
600	1170	1450	1700	1900	1524	2119	2646	2993
606	1165	1445	1700	1900	1517	2112	2646	2993
610	1165	1445	1700	1900	1517	2112	2646	2993
620	1165	1440	1700	1890	1517	2105	2646	2977
630	1165	1440	1700	1890	1517	2105	2646	2977
636	1165	1440	1700	1890	1517	2105	2646	2977
640	1165	1440	1700	1890	1517	2105	2646	2977
650	1165	1440	1700	1890	1517	2105	2646	2977

Table 3.6 : Showing the shot-points, the two-way time in El-giza, Gir, Kheir, and Upper-Sabil horizons, and their depths (line U-25).

S.P.	T(El.) (msec)	T(Gir) (msec)	T(Kh.) (msec)	T(U.-S.) (msec)	D(El.) (m)	D(Gir) (m)	D(kheir.) (m)	D(Upper-Sabil) (m)
270	1200	1460	1715	1920	1563	2134	2669	3024
280	1200	1450	1710	1910	1563	2119	2662	3008
290	1195	1440	1690	1890	1556	2105	2630	2977
295	1195	1440	1685	1890	1556	2105	2623	2977
300	1195	1440	1680	1890	1556	2105	2615	2977
310	1190	1430	1680	1900	1550	2090	2615	2993
320	1180	1430	1695	1910	1537	2090	2638	3008
330	1180	1435	1700	1915	1537	2097	2646	3016
340	1190	1445	1710	1920	1550	2112	2662	3024
350	1195	1445	1715	1930	1556	2112	2669	3040
360	1190	1445	1720	1930	1550	2112	2677	3040
370	1190	1445	1720	1925	1550	2112	2677	3032
375	1185	1440	1720	1925	1543	2105	2677	3032
380	1180	1440	1720	1925	1537	2105	2677	3032
390	1160	1430	1680	1925	1511	2090	2615	3032
400	1140	1410	1645	1920	1485	2061	2560	3024
410	1140	1405	1635	1930	1485	2053	2545	3040
415	1140	1405	1635	1935	1485	2053	2545	3048
420	1140	1405	1630	1940	1485	2061	2537	3040
430	1140	1415	1630	1945	1485	2068	2537	3063
440	1160	1430	1665	1945	1511	2090	2592	3063
450	1180	1450	1685	1950	1537	2119	2623	3071
455	1185	1460	1700	1950	1543	2134	2646	3071
460	1190	1470	1715	1950	1550	2148	2669	3071
470	1200	1475	1740	1940	1563	2156	2708	3056
480	1200	1470	1740	1940	1563	2148	2708	3056
490	1200	1455	1730	1935	1563	2126	2693	3048
495	1200	1450	1730	1930	1563	2119	2693	3040
500	1200	1445	1725	1925	1563	2112	2685	3032
510	1195	1440	1720	1920	1556	2105	2677	3024
520	1190	1440	1715	1915	1550	2105	2669	3016
530	1190	1440	1715	1910	1550	2105	2669	3008

Table 3.7 : Showing the shot-points, the two-way time in El-giza, Gir, Kheir, and Upper-Sabil horizons, and their depths (line U-51).

S.P.	T(El.) (msec)	T(Gir) (msec)	T(Kh.) (msec)	T(U.-S.) (msec)	D(El.) (m)	D(Gir) (m)	D(kheir.) (m)	D(Upper-Sabil) (m)
400	1190	1490	1740	1945	1550	2178	2708	3063
405	1190	1490	1735	1940	1550	2178	2700	3056
410	1190	1490	1735	1940	1550	2178	2701	3056
420	1190	1485	1735	1940	1550	2170	2701	3056
430	1190	1485	1735	1940	1550	2170	2701	3056
440	1190	1490	1730	1940	1550	2177	2693	3056
445	1190	1490	1730	1940	1550	2177	2693	3056
450	1190	1490	1730	1940	1550	2177	2693	3056
460	1190	1485	1730	1940	1550	2170	2693	3056
470	1190	1480	1730	1940	1550	2163	2693	3056
480	1180	1475	1730	1950	1537	2150	2693	3071
485	1175	1470	1720	1950	1537	2156	2677	3071
490	1170	1465	1720	1950	1530	2148	2677	3071
500	1165	1460	1700	1950	1524	2141	2646	3071
510	1160	1460	1675	1950	1417	2134	2607	3071
520	1155	1440	1670	1950	1504	2105	2599	3071
530	1150	1435	1660	1940	1498	2097	2584	3056
535	1145	1430	1655	1940	1491	2090	2576	3056
540	1145	1430	1650	1940	1491	2090	2568	3056
550	1140	1420	1630	1930	1485	2075	2537	3040
560	1140	1415	1625	1930	1485	2061	2537	3040
570	1140	1410	1625	1930	1485	2061	2529	3040
580	1140	1410	1625	1930	1485	2061	2529	3040
585	1145	1410	1625	1920	1491	2061	2529	3024
590	1150	1410	1630	1920	1498	2061	2537	3024
600	1150	1420	1635	1910	1498	2075	2545	3008
610	1160	1430	1650	1910	1511	2090	2568	3008
620	1160	1440	1665	1920	1511	2105	2592	3024
630	1160	1440	1690	1925	1511	2105	2630	3023
635	1165	1440	1690	1930	1517	2105	2630	3040
640	1165	1440	1695	1930	1517	2105	2638	3040
650	1170	1440	1695	1935	1524	2105	2638	3048
660	1170	1440	1695	1940	1524	2105	2638	3056
670	1185	1440	1700	1930	1543	2105	2646	3040
680	1180	1440	1700	1930	1537	2105	2646	3040
685	1180	1445	1700	1935	1537	2112	2646	3048
690	1180	1450	1700	1935	1537	2119	2646	3048
700	1180	1450	1700	1945	1537	2119	2646	3063
710	1180	1445	1700	1945	1537	2112	2646	3063
720	1180	1445	1700	1945	1537	2112	2646	3063

Table 3.8 : Showing the shot-points, the two-way time in El-giza, Gir, Kheir, and Upper-Sabil horizons, and their depths (line U-53).

S.P.	T(El.) (msec)	T(Gir) (msec)	T(Kh.) (msec)	T(U.-S.) (msec)	D(El.) (m)	D(Gir) (m)	D(kheir.) (m)	D(Upper-Sabil) (m)
300	1190	1440	1680	1890	1550	2105	2615	2977
310	1190	1440	1685	1890	1550	2105	2623	2977
320	1190	1440	1685	1900	1550	2105	2623	2993
326	1190	1435	1695	1905	1550	2097	2638	3000
330	1190	1435	1700	1905	1550	2097	2646	3000
340	1185	1435	1700	1910	1543	2097	2646	3008
350	1185	1440	1700	1910	1543	2105	2646	3008
360	1185	1445	1700	1910	1543	2112	2646	3008
366	1185	1445	1700	1915	1543	2112	2646	3016
370	1185	1440	1700	1915	1543	2105	2646	3016
380	1185	1445	1700	1920	1543	2112	2646	3024
390	1185	1460	1700	1920	1543	2134	2646	3024
400	1185	1450	1700	1925	1543	2119	2646	3032
406	1185	1450	1700	1930	1543	2119	2646	3040
410	1185	1460	1700	1930	1543	2134	2646	3040
420	1185	1460	1710	1940	1543	2134	2662	3056
430	1185	1450	1720	1940	1543	2119	2677	3056
440	1185	1450	1720	1940	1543	2119	2677	3056
446	1185	1460	1720	1940	1543	2134	2677	3056
450	1185	1460	1720	1940	1543	2134	2677	3056
460	1185	1450	1710	1930	1543	2119	2662	3040
469	1170	1445	1710	1920	1524	2112	2662	3024
470	1170	1445	1710	1920	1524	2112	2662	3024
480	1150	1435	1690	1910	1498	2097	2630	3008
486	1140	1420	1670	1910	1485	2075	2599	3008
490	1140	1420	1660	1910	1485	2075	2584	3008
500	1140	1410	1650	1910	1485	2061	2568	3008
510	1140	1410	1650	1910	1485	2061	2568	3008
520	1140	1410	1630	1930	1485	2061	2537	3040
526	1140	1410	1630	1935	1485	2061	2537	3048
530	1140	1410	1630	1935	1485	2061	2537	3048
540	1140	1410	1630	1935	1485	2061	2537	3040
550	1140	1410	1630	1930	1485	2061	2537	3040
560	1140	1420	1630	1940	1485	2075	2537	3056
566	1145	1420	1640	1930	1491	2075	2553	3040
570	1140	1420	1640	1930	1485	2075	2553	3040
580	1150	1420	1640	1935	1498	2075	2553	3048
590	1160	1425	1655	1930	1511	2083	2576	3040
596	1165	1435	1660	1940	1517	2097	2584	3056
600	1165	1435	1660	1940	1517	2097	2584	3056
610	1170	1450	1680	1940	1524	2119	2615	3056
620	1190	1465	1685	1940	1550	2141	2623	3056
630	1185	1475	1695	1940	1543	2156	2638	3056
634	1185	1475	1700	1940	1543	2156	2646	3056
640	1200	1480	1710	1945	1563	2163	2662	3063
650	1200	1470	1710	1935	1563	2148	2662	3048
660	1200	1470	1710	1930	1563	2148	2662	3040
670	1195	1465	1705	1935	1556	2141	2654	3048
671	1195	1465	1705	1935	1556	2141	2654	3048
680	1200	1460	1710	1935	1563	2134	2662	3048
690	1200	1460	1710	1930	1563	2134	2662	3040

Table 3.9 : Showing the shot-points, the two-way time in El-giza, Gir, Kheir, and Upper-Sabil horizons, and their depths (line U-54).

S.P.	T(El.) (msec)	T(Gir) (msec)	T(Kh.) (msec)	T(U.-S.) (msec)	D(El.) (m)	D(Gir) (m)	D(kheir.) (m)	D(Upper-Sabil) (m)
330	1190	1440	1710	1925	1550	2105	2662	3032
340	1190	1445	1715	1925	1550	2112	2669	3032
350	1190	1455	1720	1920	1550	2126	2677	3024
360	1190	1460	1720	1930	1550	2134	2677	3040
367	1195	1460	1720	1930	1556	2134	2677	3040
370	1195	1460	1720	1930	1556	2134	2677	3040
380	1190	1455	1720	1930	1550	2126	2677	3040
390	1190	1455	1700	1920	1550	2126	2646	3024
399	1185	1450	1700	1925	1543	2119	2646	3032
400	1185	1450	1700	1925	1543	2119	2646	3032
410	1185	1460	1720	1930	1543	2134	2677	3040
420	1180	1460	1720	1920	1537	2134	2677	3024
430	1180	1460	1710	1920	1537	2134	2662	3024
436	1180	1445	1710	1925	1537	2112	2662	3032
440	1180	1445	1710	1925	1537	2112	2662	3032
450	1170	1440	1700	1930	1524	2105	2646	3040
460	1165	1430	1690	1930	1517	2090	3630	3040
470	1160	1430	1660	1940	1511	2090	2584	3056
480	1160	1430	1650	1945	1511	2090	2568	3063
482	1160	1430	1650	1945	1511	2080	2568	3063
490	1155	1425	1640	1945	1504	2083	2553	3063
500	1140	1430	1630	1940	1485	2090	2537	3056
510	1140	1420	1630	1940	1485	2061	2537	3040
518	1140	1400	1630	1935	1485	2046	2537	2048
520	1140	1400	1630	1935	1485	2046	2537	3048
530	1140	1400	1630	1930	1485	2046	2537	3040
540	1140	1400	1630	1920	1485	2046	2537	3024
542	1140	1400	1630	1920	1485	2046	2537	3024
550	1140	1410	1635	1920	1485	2061	2545	3024
560	1150	1420	1640	1920	1498	2075	2553	3024
566	1160	1430	1660	1910	1511	2090	2584	3008
570	1160	1430	1660	1910	1511	2090	2584	3008
580	1170	1430	1675	1905	1524	2090	2607	3000
590	1175	1440	1680	1905	1530	2105	2614	3000
596	1175	1450	1685	1910	1530	2119	2623	3008
600	1175	1450	1685	1910	1530	2119	2623	3008
610	1180	1450	1690	1910	1537	2119	2630	3008
620	1185	1450	1690	1910	1543	2119	2630	3008
629	1190	1460	1690	1910	1550	2134	2630	3008
630	1190	1460	1690	1910	1550	2134	2630	3008
640	1185	1460	1690	1910	1543	2134	2630	3008
650	1190	1460	1690	1915	1550	2134	2630	3016
660	1190	1460	1700	1915	1550	2134	2646	3016
670	1190	1460	1700	1915	1550	2134	2646	3016

Table 3.10 : Showing the shot-points, the two-way time in El-giza, Gir, Kheir, and Upper-Sabil horizons, and their depths (line U-9).

S.P.	T(El.) (msec)	T(Gir) (msec)	T(Kh.) (msec)	T(U.-S.) (msec)	D(El.) (m)	D(Gir) (m)	D(kheir.) (m)	D(Upper-Sabil) (m)
210	1180	1450	1685	1900	1537		2623	2993
220	1180	1445	1685	1900	1537	2112	2623	2993
228	1180	1440	1690	1900	1537	2105	2630	2993
230	1180	1440	1690	1900	1537	2105	2630	2993
240	1180	1440	1695	1910	1537	2105	2638	3008
250	1180	1445	1705	1925	1537	2112	2654	3032
258	1190	1450	1715	1925	1550	2119	2669	3032
260	1190	1450	1715	1925	1550	2119	2669	3032
270	1190	1450	1720	1935	1550	2119	2677	3048
280	1185	1460	1725	1940	1543	2134	2685	3056
290	1185	1460	1730	1940	1543	2134	2693	3056
300	1185	1460	1725	1940	1543	2134	2685	3056
308	1180	1460	1720	1935	1537	2134	2677	3048
310	1180	1460	1720	1935	1537	2134	2677	3048
320	1185	1470	1730	1940	1543	2148	2693	3056
330	1185	1470	1730	1940	1543	2148	2693	3056
340	1180	1475	1725	1940	1537	2156	2685	3055
350	1190	1450	1725	1940	1550	2119	2685	3056
353	1190	1480	1725	1940	1550	2163	2685	3056
360	1190	1490	1730	1935	1550	2178	2693	3048
370	1200	1485	1735	1940	1563	2170	2701	3056
380	1200	1485	1735	1935	1563	2170	2701	3048
390	1200	1485	1730	1935	1563	2170	2693	3048
395	1200	1485	1730	1935	1563	2170	2693	3047
400	1200	1485	1730	1935	1563	2170	2693	3048
410	1195	1480	1735	1940	1556	2163	2701	3056
420	1200	1480	1735	1940	1563	2163	2701	3056
430	1200	1480	1735	1930	1563	2163	2701	3040

Table 3.11 : Showing the shot-points, the two-way time in El-giza, Gir, Kheir, and Upper-Sabil horizons, and their depths (line U-6).

S.P.	T(El.) (msec)	T(Gir) (msec)	T(Kh.) (msec)	T(U.-S.) (msec)	D(El.) (m)	D(Gir) (m)	D(kheir.) (m)	D(Upper-Sabil) (m)
340	1180	1430	1700	1925	1537	2090	2646	3032
350	1180	1430	1700	1920	1537	2090	2646	3024
355	1180	1435	1700	1925	1537	2097	2646	3032
360	1180	1440	1705	1925	1537	2105	2654	3032
370	1190	1440	1710	1930	1550	2105	2662	3040
380	1190	1445	1710	1930	1550	2112	2662	3040
390	1190	1445	1710	1930	1550	2112	2662	3040
400	1180	1445	1710	1920	1537	2112	2662	3024
405	1185	1445	1710	1925	1543	2112	2662	3032
410	1190	1445	1710	1925	1550	2112	2662	3032
420	1190	1445	1710	1925	1550	2112	2662	3032
430	1190	1440	1710	1925	1550	2105	2662	3024
440	1185	1445	1705	1910	1543	2112	2654	3008
450	1190	1450	1700	1910	1550	2119	2646	3008
460	1190	1450	1710	1920	1550	2119	2662	3024
470	1200	1460	1715	1920	1563	2134	2669	3024
480	1200	1460	1715	1920	1563	2134	2669	3024
490	1205	1465	1710	1920	1570	2141	2662	3024
500	1200	1455	1710	1920	1563	2126	2662	3024
510	1195	1455	1710	1920	1556	2126	2662	3024
520	1190	1440	1690	1905	1550	2105	2630	3000
525	1195	1440	1690	1900	1556	2105	2630	2993
530	1195	1440	1690	1890	1556	2105	2630	2977

Table 3.12 : Seismic lines, shot-point intersections, two-way time, and mis-tie in the El-giza and Gir horizons.

Lines	Intersection shot-points	El-giza T.W.T (ms)	mis-tie time (El-giza) (ms)	Gir T.W.T (ms)	mis-tie time (Gir) (ms)
U14 - U25	504 - 421	1140 - 1140	-	1410-1405	±5
U14 - U51	504 - 564	1140 - 1140	-	1410-1410	-
U14 - U53	504 - 543	1140 - 1140	-	1410-1410	-
U14 - U54	504 - 514	1140 - 1140	-	1410-1400	±10
U14 - U09	433 - 308	1180 - 1180	-	1440-1460	±20
U25 - U51	421 - 564	1140 - 1140	-	1405-1410	±5
U25 - U53	421 -543	1140 - 1140	-	1405-1410	±5
U25 - U54	421 - 514	1140 - 1140	-	1405-1400	±5
U25 - U06	340 - 481	1190 - 1200	±10	1445-1460	±15
U51 - U53	564 - 543	1140 - 1140	-	1410-1410	-
U51 - U54	564 - 514	1140 - 1140	-	1410-1400	±10
U51 - U09	463 - 353	1190 - 1190	-	1485-1480	±5
U53 - U54	543 - 514	1140 - 1140	-	1410-1400	±10
U53 - U06	379 - 496	1185 - 1200	±15	1435-1455	±20
U06 - U09	426 - 254	1190 - 1190	-	1440-1445	±5

Table 3.13 : Seismic lines, shot-points intersections, two-way time, and mis-tie in the Kheir and Upper-Sabil horizons.

Lines	Intersection shot-points	Kheir T.W.T (ms)	mis-tie time (Kheir) (ms)	U.-Sabil T.W.T (ms)	mis-tie time (U.-Sabil) (ms)
U14 - U25	504 - 421	1630 - 1630	-	1930-1940	±10
U14 - U51	504 - 564	1630 - 1620	±5	1930-1930	-
U14 - U53	504 - 543	1630 - 1630	-	1930-1935	±5
U14 - U54	504 - 514	1630 - 1630	-	1930-1935	±5
U14 - U09	433 - 308	1730 - 1720	±10	1940-1935	±5
U25 - U51	421 - 564	1630 - 1625	±5	1940-1930	±10
U25 - U53	421 - 543	1630 - 1630	-	1940-1935	±5
U25 - U54	421 - 514	1630 - 1630	-	1940-1935	±5
U25 - U06	340 - 481	1710 - 1715	±5	1920-1920	-
U51 - U53	564 - 543	1625 - 1630	±5	1925-1935	±10
U51 - U54	564 - 514	1625 - 1630	±5	1925-1935	±10
U51 - U09	463 - 353	1730 - 1725	±5	1940-1940	-
U53 - U54	543 - 514	1630 - 1630	-	1935-1935	-
U53 - U06	379 - 496	1690 - 1710	±20	1910-1920	±10
U06 - U09	426 - 254	1710 - 1705	±5	1925-1925	-

Table 4.1 : Seismic interval velocity in the El-giza to Gir, Gir to Kheir, and Kheir to Upper Sabil, and the average velocity at the top of each horizon (line U-14)

S.P.	Vi(El.) (m/s)	Vi(Gir) (m/s)	Vi(Kh.) (m/s)	Va(Top El.) (m/s)	Va(Top Gir) (m/s)	Va(Top Kh.) (m/s)	Va(Top U.-S.) (m/s)
320							
326	2877	3579	3793	2364	2733	3014	3537
330							
340							
350							
356	2346	3407	3858	2255	2599	2931	3525
360							
370							
380							
390							
391	2448	3063	4230	2375	2581	3021	3670
400							
410							
420							
426							
430	3770	4442	4676	2505	2722	3025	3244
440							
450							
455	3290	2900	4713	2650	2740	2768	3005
460							
470							
480	4327	4512	4121	2411	2795	3024	3185
490							
500							
505	3841	4969	4257	2616	2832	3127	3280
510							
520							
530	3807	3934	3863	2423	2714	3014	3031
540							
550							
560							
570							
575	4089	4262	4892	2500	2770	2972	3325
580							
590							
600							
610	4142	5586	4200	2481	2779	2997	3317
620							
630							
636	2653	3225	4619	2363	2588	2973	3520
640							
650							

Table 4.2 : Seismic interval velocity in the El-giza to Gir, Gir to Kheir, and Kheir to Upper Sabil, and the average velocity at the top of each horizon (line U-25)

S.P.	Vi(El.) (m/s)	Vi(Gir) (m/s)	Vi(Kh.) (m/s)	Va(Top El.) (m/s)	Va(Top Gir) (m/s)	Va(Top Kh.) (m/s)	Va(Top U.-S.) (m/s)
270							
280							
290							
295	3668	4035	5580	2772	3052	3319	3832
300							
310							
320							
330	3357	4247	4616	2793	3825	3933	4080
340							
350							
360							
370							
375	3380	4364	5289	3314	3911	4881	2224
380							
390							
400							
410							
415	2866	3940	4254	2645	3041	3380	3738
420							
430							
440							
450							
455	3415	4512	5523	3634	3861	4284	4284
460							
470							
480							
490							
495	2955	4594	4814	2935	3409	3740	3619
500							
510							
520							
530	3772	4329	4685	2605	3157	3664	3664

Table 4.3 : Seismic interval velocity in the El-giza to Gir, Gir to Kheir, and Kheir to Upper Sabil, and the average velocity at the top of each horizon (line U-51)

S.P.	Vi(El.) (m/s)	Vi(Gir) (m/s)	Vi(Kh.) (m/s)	Va(Top El.) (m/s)	Va(Top Gir) (m/s)	Va(Top Kh.) (m/s)	Va(Top U.-S.) (m/s)
400							
405	2580	3761	4673	2406	2792	3271	3636
410							
420							
430							
440							
445	3009	3203	4267	2498	2699	3096	3915
450							
460							
470							
480							
485	3293	3419	4011	2673	2936	3254	3731
490							
500							
510							
530							
535	3404	3394	3471	2885	3025	3131	3570
540							
550							
560							
570							
580							
585	3309	3309	4192	2855	2855	3261	3566
590							
600							
610							
620							
630							
635	3496	3388	4891	2795	2986	3504	3419
640							
650							
660							
670							
680							
685	3678	5264	3990	2780	3373	3515	3637
690							
700							
710							
720							

Table 4.4 : Seismic interval velocity in the El-giza to Gir, Gir to Kheir, and Kheir to Upper Sabil, and the average velocity at the top of each horizon (line U-53)

S.P.	Vi(El.) (m/s)	Vi(Gir) (m/s)	Vi(Kh.) (m/s)	Va(Top El.) (m/s)	Va(Top Gir) (m/s)	Va(Top Kh.) (m/s)	Va(Top U.-S.) (m/s)
300							
310							
320							
326	4137	3514	4882	2894	3016	3624	3683
330							
340							
350							
360							
366	3011	4043	4600	2410	2930	3070	3474
370							
380							
390							
400							
406	3549	3731	3840	2593	2850	2917	3154
410							
420							
430							
440							
446	3723	3069	4700	2666	2767	3535	3633
450							
460							
469	2302	5703	4063	2191	2973	3190	3547
470							
480							
486	2284	2748	3188	2233	2340	2509	2844
490							
500							
510							
520							
526	3106	3107	5062	2785	2785	3676	4049
530							
540							
550							
560							
566	2865	4332	4127	2467	3062	3264	3294
570							
580							
590							
596	3690	2706	3700	2839	2810	3366	3483
600							
610							
620							
630							
634	4900	3801	3860	3180	3302	3406	3693
640							
650							
660							
670							
671	2913	3939	3313	2844	3061	3104	3558
680							
690							

Table 4.5 : Seismic interval velocity in the El-giza to Gir, Gir to Kheir, and Kheir to Upper Sabil, and the average velocity at the top of each horizon (line U-54)

S.P.	Vi(El.) (m/s)	Vi(Gir) (m/s)	Vi(Kh.) (m/s)	Va(Top El.) (m/s)	Va(Top Gir) (m/s)	Va(Top Kh.) (m/s)	Va(Top U.-S.) (m/s)
330							
340							
350							
360							
367	3651	4092	4623	3070	3336	3634	3821
370							
380							
390							
399	3335	3452	3790	2614	2854	3088	3187
400							
410							
420							
430							
436	3989	4091	4673	2959	3261	3601	3683
440							
450							
460							
470							
480							
482	3728	4333	4221	2848	3240	3470	3609
490							
500							
510							
518	2670	3405	3974	2386	2627	2881	2942
520							
530							
540							
542	3097	3904	3735	2635	2974	3152	3552
550							
560							
566	2527	3227	4526	2553	2715	3104	3499
570							
580							
590							
596	3421	3642	4729	2865	2913	3252	3417
600							
610							
620							
629	3875	3358	4828	2962	3046	3387	3501
630							
640							
650							
660							
670							

Table 4.6 : Seismic interval velocity in the El-giza to Gir, Gir to Kheir, and Kheir to Upper Sabil, and the average velocity at the top of each horizon (line U-9)

S.P.	Vi(El.) (m/s)	Vi(Gir) (m/s)	Vi(Kh.) (m/s)	Va(Top El.) (m/s)	Va(Top Gir) (m/s)	Va(Top Kh.) (m/s)	Va(Top U.-S.) (m/s)
210							
220							
228	3636	4867	4346	2589	2873	3350	3563
230							
240							
250							
258	3188	4394	4445	2711	3147	3447	3564
260							
270							
280							
290							
300							
308	3205	4297	4306	2653	3151	3151	3441
310							
320							
330							
340							
350							
353	3190	3812	4730	2684	3032	3599	3746
360							
370							
380							
390							
395	3601	4052	4647	2747	3117	3510	3709
400							
410							
420							
430	3240	4528	4855	2717	3262	3760	3823

Table 4.7 : Seismic interval velocity in the El-giza to Gir, Gir to Kheir, and Kheir to Upper Sabil, and the average velocity at the top of each horizon (line U-6)

S.P.	Vi(El.) (m/s)	Vi(Gir) (m/s)	Vi(Kh.) (m/s)	Va(Top El.) (m/s)	Va(Top Gir) (m/s)	Va(Top Kh.) (m/s)	Va(Top U.-S.) (m/s)
340							
350							
355	2538	3326	4570	2279	2574	2863	3452
360							
370							
380							
390							
400							
405	3150	3807	3450	2648	2950	3740	3740
410							
420							
430	2946	3150	6934	2450	2646	3791	3791
440							
450							
460							
470							
480	3360	4225	4604	2610	3064	3458	3661
490							
500							
510							
520							
525	3511	4591	4591	2804	3346	3346	3840
530							

Table 4.8 : Seismic lines, shot-point intersections, seismic interval velocity, and mis-tie in interval velocity for the El-giza horizon.

Lines	Intersection shot-points	Vi (El.) (m/sec)	mis-tie Vi (El.) (m/sec)
U14 - U25	504 - 421	2666 - 2866	±200
U14 - U51	504 - 564	2666 - 3309	±643
U14 - U53	504 - 543	2666 - 2265	±199
U14 - U54	504 - 514	2666 - 2670	±4
U14 - U09	433 - 308	2736 - 3205	±469
U25 - U51	421 - 564	2866 - 3309	±443
U25 - U53	421 - 543	2866 - 2865	±1
U25 - U54	421 - 514	2866 - 2670	±196
U25 - U06	340 - 481	3357 - 3360	±3
U51 - U53	564 - 543	3309 - 2865	±444
U51 - U54	564 - 514	3309 - 2670	±639
U51 - U09	463 - 353	3190 - 3190	-
U53 - U54	543 - 514	2865 - 2670	±195
U53 - U06	379 - 496	3011 - 3420	±409
U06 - U09	426 - 254	2946 - 3188	±242

Table 4.9 : Seismic lines, shot-point intersections, seismic interval velocity, and mis-tie in interval velocity for the Gir horizon.

Lines	Intersection shot-points	Vi (Gir) (m/sec)	mis-tie Vi (Gir) (m/sec)
U14 - U25	504 - 421	3512 - 3940	±428
U14 - U51	504 - 564	3512 - 3309	±203
U14 - U53	504 - 543	3512 - 4332	±820
U14 - U54	504 - 514	3512 - 3405	±107
U14 - U09	433 - 308	2860 - 4297	±1437
U25 - U51	421 - 564	3940 - 3309	±631
U25 - U53	421 - 543	3940 - 4332	±392
U25 - U54	421 - 514	3940 - 3405	±535
U25 - U06	340 - 481	4247 - 4225	±22
U51 - U53	564 - 543	3309 - 4332	±1023
U51 - U54	564 - 514	3309 - 3405	±96
U51 - U09	463 - 353	3203 - 3812	±609
U53 - U54	543 - 514	4332 - 3405	±927
U53 - U06	379 - 496	4043 - 4225	±182
U06 - U09	426 - 254	3150 - 4394	±1244

Table 4.10 : Seismic lines, shot-point intersections, seismic interval velocity, and mis-tie in interval velocity for the Kheir horizon.

Lines	Intersection shot-points	Vi (Kheir) (m/sec)	mis-tie Vi (Kheir) (m/sec)
U14 - U25	504 - 421	4164 - 4254	±90
U14 - U51	504 - 564	4164 - 4192	±28
U14 - U53	504 - 543	4164 - 4127	±37
U14 - U54	504 - 514	4164 - 3974	±190
U14 - U09	433 - 308	4360 - 4306	±54
U25 - U51	421 - 564	4254 - 4192	±62
U25 - U53	421 - 543	4254 - 4127	±127
U25 - U54	421 - 514	4254 - 3974	±280
U25 - U06	340 - 481	4616 - 4604	±12
U51 - U53	564 - 543	4192 - 4127	±65
U51 - U54	564 - 514	4192 - 3974	±218
U51 - U09	463 - 353	4267 - 4730	±463
U53 - U54	543 - 514	4127 - 3974	±153
U53 - U06	379 - 496	4600 - 4604	±4
U06 - U09	426 - 254	6934 - 4445	±2489

Table 4.11 : The difference between the interval velocity in the well (D1/103) and the seismic velocity through the three intervals (El-giza to Gir, Gir to Kheir, and Kheir to Upper-Sabil) in line (U-14).

S.P.	$\Delta V_i(1)$ (m/sec)	$\Delta V_i(2)$ (m/sec)	$\Delta V_i(3)$ (m/sec)
320			
326	+1111	+1270	+36
330			
340			
350			
356	+1642	+1487	+101
360			
370			
380			
390			
391	+1540	+1831	+473
400			
410			
420			
426			
430	+218	+452	+923
440			
450			
455	+698	+1994	+960
460			
470			
480	+339	+382	+368
490			
500			
505	+147	+75	+504
510			
520			
530	+181	+960	+110
540			
550			
560			
570			
575	+101	+632	+1139
580			
590			
600			
610	+154	+692	+447
620			
630			
636	+1335	+1669	+862
640			
650			

Table 4.12 : The difference between the interval velocity in the well (D1/103) and the seismic velocity through three intervals (El-giza to Gir, Gir to Kheir, and Kheir to Upper-Sabil) in line (U-25).

S.P.	$\Delta V_i(1)$ (m/sec)	$\Delta V_i(2)$ (m/sec)	$\Delta V_i(3)$ (m/sec)
270			
280			
290			
295	+320	+859	+1823
300			
310			
320			
330	+631	+647	+859
340			
350			
360			
370	+608	+530	+1532
380			
390			
400			
410			
415	+1122	+95	+497
420			
430			
440			
450			
455	+573	+382	+1766
460			
470			
480			
490			
495	+1033	+300	+1057
500			
510			
520			
530	+216	+565	+928

Table 4.13 : The difference between the interval velocity in the well (D1/103) and the seismic velocity through three intervals (El-giza to Gir, Gir to Kheir, and Kheir to Upper-Sabil) in line (U-51).

S.P.	$\Delta V_i(1)$ (m/sec)	$\Delta V_i(2)$ (m/sec)	$\Delta V_i(3)$ (m/sec)
400			
405	+1408	+1133	+916
410			
420			
430			
440			
445	+979	+169	+510
450			
460			
470			
480			
485	+695	+1470	+254
490			
500			
510			
520			
530			
535	+584	+1500	+286
540			
550			
560			
570			
580			
585	+679	+1585	+435
590			
600			
610			
620			
630			
635	+492	+1506	+1134
640			
650			
660			
670			
680			
685	+310	+370	+233
690			
700			
710			
720			

Table 4.14 : The difference between the interval velocity in the well (D1/103) and the seismic velocity through three intervals (El-giza to Gir, Gir to Kheir, and Kheir to Upper-Sabil) in line (U-53).

S.P.	$\Delta V_i(1)$ (m/sec)	$\Delta V_i(2)$ (m/sec)	$\Delta V_i(3)$ (m/sec)
300			
310			
320			
326	+149	+1380	+1125
330			
340			
350			
360			
366	+977	+851	+843
370			
380			
390			
400			
406	+439	+1163	+83
410			
420			
430			
440			
446	+265	+1825	+943
450			
460			
469	+1686	+809	+306
470			
480			
486	+1704	+2146	+569
490			
500			
510			
520			
526	+882	+1787	+1305
530			
540			
550			
560			
566	+1123	+562	+370
570			
580			
590			
596	+298	+2188	+57
600			
610			
620			
630			
634	+912	1093	+103
640			
650			
660			
670			
671	+1075	+955	+444
680			
690			

Table 4.15 : The difference between the interval velocity in the well (D1/103) and the seismic velocity through three intervals (El-giza to Gir, Gir to Kheir, and Kheir to Upper-Sabil) in line (U-54).

S.P.	$\Delta V_i(1)$ (m/sec)	$\Delta V_i(2)$ (m/sec)	$\Delta V_i(3)$ (m/sec)
330			
340			
350			
360			
367	+337	+802	+866
370			
380			
390			
399	+653	+1442	+33
400			
410			
420			
430			
436	+1	+803	+916
440			
450			
460			
470			
480			
482	+260	+561	+464
490			
500			
510			
518	+1318	+1489	+217
520			
530			
540			
542	+891	+990	+22
550			
560			
566	+1461	+1667	+769
570			
580			
590			
596	+567	+1252	+972
600			
610			
620			
630			
640			
650			
660			
670			

Table 4.16 : The difference between the interval velocity in the well (D1/103) and the seismic velocity through three intervals (El-giza to Gir, Gir to Kheir, and Kheir to Upper-Sabil) in line (U-9).

S.P.	$\Delta V_i(1)$ (m/sec)	$\Delta V_i(2)$ (m/sec)	$\Delta V_i(3)$ (m/sec)
210			
220			
228	+352	+27	+589
230			
240			
250			
258	+800	+500	+688
260			
270			
280			
290			
300			
308	+783	+597	+549
310			
320			
330			
340			
350			
353	+798	+1082	+973
370			
380			
390			
395	+387	+842	+890
400			
410			
420			
430	+748	+366	+1098

Table 4.17 : The difference between the interval velocity in the well (D1/103) and the seismic velocity through three intervals (El-giza to Gir, Gir to Kheir, and Kheir to Upper-Sabil) in line (U-6).

S.P.	$\Delta V_i(1)$ (m/sec)	$\Delta V_i(2)$ (m/sec)	$\Delta V_i(3)$ (m/sec)
340			
350			
355	+1450	+1568	+813
360			
370			
380			
390			
400			
405	+838	+1087	+307
410			
420			
430	+1042	+1744	+3177
440			
450			
460			
470			
480	+628	+669	+847
490			
500			
510			
520			
525	+477	+303	+834
530			

Table 5.1(a): Velocity table. Two-way traveltime, RMS velocities, average velocities, depth, layer thickness, and interval velocities (CDP 160).

TIME (s)	RMS VEL (m/s)	AVE VEL (m/s)	DEPTH (m)	THICKNESS (m)	INT VEL (m/s)
0.000000	2200.000	2200.	0.	0.	2200.
0.020000	2200.000	2200.	22.	22.	2200.
0.152000	2262.264	2262.	172.	150.	2272.
0.232000	2300.000	2299.	267.	95.	2370.
0.272000	2315.385	2315.	315.	48.	2403.
0.492000	2400.000	2398.	590.	275.	2501.
0.532000	2400.003	2398.	638.	48.	2400.
0.720000	2400.003	2398.	863.	226.	2400.
0.900000	2400.000	2399.	1079.	216.	2400.
0.940000	2400.003	2399.	1127.	48.	2400.
1.032000	2400.000	2399.	1238.	110.	2400.
1.060000	2427.273	2422.	1284.	46.	3278.
1.220000	2583.117	2556.	1559.	275.	3442.
1.340000	2700.000	2657.	1780.	221.	3683.
1.492000	2900.000	2822.	2105.	325.	4276.
1.580000	3006.451	2912.	2300.	195.	4438.
1.740000	3200.000	3076.	2676.	376.	4701.
1.920000	3350.000	3215.	3086.	410.	4552.
1.940000	3385.714	3242.	3145.	59.	5879.
2.060000	3600.000	3408.	3511.	366.	6096.
2.180000	3774.418	3553.	3872.	362.	6027.
2.232000	3850.000	3615.	4035.	162.	6243.
2.280000	3850.003	3620.	4127.	92.	3850.
2.352000	3850.000	3627.	4266.	139.	3850.
2.420000	3856.439	3640.	4404.	138.	4073.
2.532000	3867.045	3660.	4633.	229.	4089.
2.780000	3890.530	3701.	5144.	511.	4123.
2.880000	3900.000	3717.	5352.	208.	4155.
2.960000	3900.000	3722.	5508.	156.	3900.
4.000000	3900.000	3768.	7536.	2028.	3900.

Table 5.1(b): Velocity table. Two-way traveltime, RMS velocities, average velocities, depth, layer thickness, and interval velocities (CDP 210).

TIME (s)	RMS VEL (m/s)	AVE VEL (m/s)	DEPTH (m)	THICKNESS (m)	INT VEL (m/s)
0.000000	2200.000	2200.	0.	0.	2200.
0.004000	2200.000	2200.	4.	4.	2200.
0.220000	2300.000	2300.	253.	249.	2302.
0.260000	2318.868	2318.	301.	48.	2420.
0.360000	2366.038	2365.	426.	124.	2484.
0.432000	2400.000	2398.	518.	92.	2563.
0.512000	2400.000	2398.	614.	96.	2400.
0.540000	2400.003	2398.	647.	34.	2400.
0.720000	2400.000	2399.	863.	216.	2400.
0.780000	2400.000	2399.	935.	72.	2400.
0.860000	2400.000	2399.	1031.	96.	2400.
0.920000	2454.545	2447.	1126.	94.	3134.
1.040000	2563.636	2543.	1322.	197.	3282.
1.080000	2600.000	2575.	1391.	68.	3412.
1.200000	2700.000	2665.	1599.	208.	3473.
1.220000	2707.143	2672.	1630.	31.	3106.
1.452000	2790.003	2755.	2000.	370.	3191.
1.480000	2800.000	2765.	2046.	46.	3277.
1.760000	2800.003	2771.	2438.	392.	2800.
1.820000	2800.000	2771.	2522.	84.	2800.
1.900000	3072.727	2940.	2793.	271.	6773.
1.952000	3250.000	3053.	2980.	187.	7177.
2.040000	3400.000	3172.	3235.	255.	5804.
2.140000	3600.000	3324.	3557.	322.	6444.
2.220000	3600.003	3334.	3701.	144.	3600.
2.320000	3600.000	3346.	3881.	180.	3600.
2.340000	3600.003	3348.	3917.	36.	3600.
2.420000	3600.000	3356.	4061.	144.	3600.
2.520000	3600.000	3366.	4241.	180.	3600.
2.580000	3600.003	3371.	4349.	108.	3600.
2.640000	3600.003	3377.	4457.	108.	3600.
2.680000	3600.000	3380.	4529.	72.	3600.
2.720000	3657.143	3425.	4657.	128.	6416.
2.820000	3800.000	3537.	4987.	329.	6589.
2.880000	3800.003	3542.	5101.	114.	3800.
2.912000	3800.000	3545.	5162.	61.	3800.
4.000000	3800.000	3614.	7229.	2067.	3800.

Table 5.1(c): Velocity table. Two-way traveltime, RMS velocities, average velocities, depth, layer thickness, and interval velocities (CDP 260).

TIME (s)	RMS VEL (m/s)	AVE VEL (m/s)	DEPTH (m)	THICKNESS (m)	INT VEL (m/s)
0.000000	2200.000	2200.	0.	0.	2200.
0.004000	2200.000	2200.	4.	4.	2200.
0.132000	2200.003	2200.	145.	141.	2200.
0.260000	2200.000	2200.	286.	141.	2200.
0.360000	2300.000	2295.	413.	127.	2542.
0.540000	2400.000	2393.	646.	233.	2588.
0.720000	2400.000	2395.	862.	216.	2400.
0.800000	2400.003	2395.	958.	96.	2400.
0.912000	2400.003	2396.	1092.	134.	2400.
0.920000	2400.000	2396.	1102.	10.	2400.
1.032000	2400.003	2396.	1236.	134.	2400.
1.040000	2400.000	2396.	1246.	10.	2400.
1.160000	2466.667	2457.	1425.	179.	2983.
1.220000	2500.000	2487.	1517.	92.	3074.
1.272000	2612.069	2570.	1634.	117.	4502.
1.452000	3000.000	2863.	2079.	444.	4938.
1.572000	3116.883	2972.	2336.	257.	4286.
1.752000	3292.208	3133.	2745.	409.	4544.
1.760000	3300.000	3141.	2764.	19.	4705.
1.900000	3300.000	3152.	2995.	231.	3300.
1.932000	3340.003	3186.	3078.	83.	5189.
2.100000	3550.003	3364.	3532.	454.	5408.
2.220000	3700.000	3491.	3875.	343.	5720.
2.240000	3700.003	3493.	3912.	37.	3700.
2.340000	3700.000	3502.	4097.	185.	3700.
2.352000	3700.003	3503.	4119.	22.	3701.
2.480000	3700.003	3513.	4356.	237.	3700.
2.580000	3700.000	3520.	4541.	185.	3700.
2.640000	3700.000	3524.	4652.	111.	3700.
2.720000	3700.000	3530.	4800.	148.	3700.
2.880000	3700.000	3539.	5096.	296.	3700.
4.000000	3700.000	3584.	7168.	2072.	3700.

Table 5.1(d): Velocity table. Two-way traveltime, RMS velocities, average velocities, depth, layer thickness, and interval velocities (CDP 310).

TIME (s)	RMS VEL (m/s)	AVE VEL (m/s)	DEPTH (m)	THICKNESS (m)	INT VEL (m/s)
				0.	2300.
0.000000	2300.000	2300.	0.	5.	2300.
0.004000	2300.000	2300.	5.	18.	2300.
0.020000	2300.003	2300.	23.	129.	2300.
0.132000	2300.000	2300.	152.	101.	2300.
0.220000	2300.003	2300.	253.	322.	2300.
0.500000	2300.003	2300.	575.	138.	2300.
0.620000	2300.003	2300.	713.	207.	2300.
0.800000	2300.000	2300.	920.	169.	3019.
0.912000	2400.000	2388.	1089.	189.	3158.
1.032000	2500.000	2478.	1279.	92.	3849.
1.080000	2575.003	2539.	1371.	161.	4024.
1.160000	2700.000	2641.	1532.	151.	2700.
1.272000	2700.000	2646.	1683.	413.	4592.
1.452000	3000.000	2888.	2096.	168.	4948.
1.520000	3113.333	2980.	2265.	133.	5122.
1.572000	3200.000	3051.	2398.	463.	5140.
1.752000	3450.000	3265.	2860.	255.	3450.
1.900000	3450.003	3280.	3116.	55.	3450.
1.932000	3450.000	3283.	3171.	290.	3450.
2.100000	3450.000	3296.	3461.	251.	6271.
2.180000	3592.857	3405.	3712.	195.	6487.
2.240000	3700.000	3488.	3906.	207.	3700.
2.352000	3700.000	3498.	4113.	340.	5312.
2.480000	3800.000	3591.	4453.	190.	3800.
2.580000	3800.000	3599.	4643.	684.	3800.
2.940000	3800.000	3624.	5327.	2014.	3800.
4.000000	3800.000	3671.	7341.		

Table 5.1(e): Velocity table. Two-way traveltime, RMS velocities, average velocities, depth, layer thickness, and interval velocities (CDP 360).

TIME (s)	RMS VEL (m/s)	AVE VEL (m/s)	DEPTH (m)	THICKNESS (m)	INT VEL (m/s)
0.000000	2200.000	2200.	0.	0.	2200.
0.020000	2200.000	2200.	22.	22.	2200.
0.220000	2300.000	2300.	253.	231.	2310.
0.232000	2304.286	2304.	267.	14.	2381.
0.440000	2378.572	2377.	523.	256.	2459.
0.500000	2400.000	2398.	600.	77.	2552.
0.620000	2400.000	2398.	744.	144.	2400.
0.800000	2400.003	2399.	960.	216.	2400.
0.940000	2400.003	2399.	1128.	168.	2400.
1.080000	2400.000	2399.	1296.	168.	2400.
1.160000	2490.909	2475.	1435.	140.	3494.
1.280000	2627.273	2589.	1657.	222.	3694.
1.492000	2868.182	2793.	2084.	427.	4027.
1.520000	2900.000	2820.	2144.	60.	4265.
1.612000	2948.421	2868.	2312.	168.	3657.
1.900000	3100.000	3015.	2865.	553.	3839.
1.912000	3106.428	3022.	2889.	24.	3996.
2.180000	3250.000	3158.	3442.	554.	4132.
2.292000	3331.053	3230.	3702.	260.	4634.
2.732000	3649.474	3514.	4800.	1098.	4990.
2.940000	3800.000	3647.	5361.	562.	5401.
2.980000	3800.000	3649.	5437.	76.	3800.
4.000000	3800.000	3688.	7375.	1938.	3800.

Table 5.1(f): Velocity table. Two-way traveltime, RMS velocities, average velocities, depth, layer thickness, and interval velocities (CDP 380).

TIME (s)	RMS VEL (m/s)	AVE VEL (m/s)	DEPTH (m)	THICKNESS (m)	INT VEL (m/s)
0.000000	2200.000	2200.	0.	0.	2200.
0.020000	2200.000	2200.	22.	22.	2200.
0.232000	2300.000	2300.	267.	245.	2309.
0.352000	2357.692	2356.	415.	148.	2465.
0.440000	2400.000	2397.	527.	113.	2562.
0.492000	2400.003	2398.	590.	62.	2400.
0.720000	2400.003	2398.	863.	274.	2400.
0.800000	2400.000	2399.	959.	96.	2400.
0.940000	2400.000	2399.	1127.	168.	2400.
1.072000	2580.003	2548.	1366.	238.	3611.
1.160000	2700.000	2649.	1536.	170.	3874.
1.192000	2780.000	2708.	1614.	78.	4860.
1.280000	3000.000	2874.	1839.	225.	5121.
1.460000	3042.453	2930.	2139.	300.	3329.
1.492000	3050.000	2940.	2193.	54.	3376.
1.580000	3086.667	2979.	2354.	161.	3653.
1.612000	3100.000	2994.	2413.	59.	3699.
1.740000	3270.667	3137.	2729.	316.	4939.
1.852000	3420.003	3262.	3021.	292.	5217.
1.912000	3500.000	3330.	3184.	162.	5416.
1.940000	3520.896	3350.	3250.	66.	4734.
2.080000	3625.373	3451.	3589.	339.	4847.
2.180000	3700.000	3522.	3839.	250.	5006.
2.192000	3705.357	3528.	3867.	27.	4576.
2.292000	3750.000	3576.	4098.	231.	4621.
2.420000	3750.003	3585.	4338.	240.	3750.
2.520000	3750.003	3592.	4525.	188.	3750.
2.732000	3750.000	3604.	4923.	397.	3750.
2.800000	3791.129	3642.	5099.	176.	5180.
2.872000	3834.677	3683.	5288.	189.	5255.
2.980000	3900.000	3743.	5577.	289.	5352.
4.000000	3900.000	3783.	7566.	1989.	3900.

Table 5.1(g): Velocity table. Two-way traveltime, RMS velocities, average velocities, depth, layer thickness, and interval velocities (CDP 450).

TIME (s)	RMS VEL (m/s)	AVE VEL (m/s)	DEPTH (m)	THICKNESS (m)	INT VEL (m/s)
0.000000	2200.000	2200.	0.	0.	2200.
0.020000	2200.000	2200.	22.	22.	2200.
0.092000	2309.091	2308.	106.	84.	2338.
0.152000	2400.000	2397.	182.	76.	2533.
0.272000	2400.000	2398.	326.	144.	2400.
0.340000	2400.003	2399.	408.	82.	2400.
0.452000	2400.003	2399.	542.	134.	2400.
0.532000	2400.000	2399.	638.	96.	2400.
0.560000	2400.003	2399.	672.	34.	2400.
0.720000	2400.000	2399.	864.	192.	2400.
0.812000	2400.003	2399.	974.	110.	2400.
0.940000	2400.000	2400.	1128.	154.	2400.
1.060000	2500.000	2487.	1318.	191.	3176.
1.080000	2500.003	2488.	1343.	25.	2500.
1.220000	2500.000	2489.	1518.	175.	2500.
1.340000	2800.000	2705.	1812.	294.	4899.
1.352000	2812.500	2716.	1836.	24.	3968.
1.432000	2895.833	2791.	1998.	162.	4053.
1.500000	2966.667	2854.	2141.	142.	4189.
1.580000	3050.000	2929.	2314.	173.	4325.
1.620000	3087.500	2963.	2400.	86.	4316.
1.740000	3200.000	3065.	2667.	267.	4448.
1.840000	3325.003	3172.	2918.	251.	5025.
1.920000	3425.003	3257.	3127.	209.	5221.
1.940000	3450.000	3279.	3180.	53.	5329.
2.040000	3554.167	3372.	3439.	259.	5176.
2.180000	3700.000	3502.	3817.	378.	5395.
2.192000	3700.003	3503.	3839.	22.	3701.
2.280000	3700.000	3510.	4002.	163.	3700.
2.292000	3700.003	3511.	4024.	22.	3701.
2.420000	3700.000	3521.	4261.	237.	3700.
2.480000	3700.003	3526.	4372.	111.	3700.
2.532000	3700.000	3529.	4468.	96.	3700.
2.640000	3700.003	3536.	4668.	200.	3700.
2.780000	3700.000	3544.	4927.	259.	3700.
4.000000	3700.000	3592.	7184.	2257.	3700.

Table 5.1(h): Velocity table. Two-way traveltime, RMS velocities, average velocities, depth, layer thickness, and interval velocities (CDP 520).

TIME (s)	RMS VEL (m/s)	AVE VEL (m/s)	DEPTH (m)	THICKNESS (m)	INT VEL (m/s)
0.000000	2300.000	2300.	0.	0.	2300.
0.092000	2300.000	2300.	106.	106.	2300.
0.160000	2300.000	2300.	184.	78.	2300.
0.332000	2300.000	2300.	382.	198.	2300.
0.572000	2300.000	2300.	658.	276.	2300.
0.720000	2300.000	2300.	828.	170.	2300.
0.820000	2300.000	2300.	943.	115.	2300.
0.940000	2400.000	2389.	1123.	180.	2995.
1.092000	2450.000	2438.	1331.	208.	2739.
1.220000	2500.000	2485.	1516.	185.	2892.
1.340000	2800.000	2701.	1810.	294.	4899.
1.500000	2950.000	2839.	2129.	319.	3991.
1.740000	3300.000	3131.	2724.	595.	4956.
1.920000	3500.000	3310.	3177.	454.	5040.
2.192000	3700.000	3505.	3842.	664.	4884.
2.300000	3700.000	3514.	4041.	200.	3700.
2.480000	3700.000	3528.	4374.	333.	3700.
2.640000	3800.000	3623.	4783.	408.	5105.
4.000000	3800.000	3683.	7367.	2584.	3800.

/JOB ACCT 'YASAD'

- (1) DIN processor to read seismic data from DOUT created disk files into the processing buffer for use by subsequent processors.

```
/DIN
FILENAME 'UU6'
BI 255 EI 334
BI 338 EI 363
RESEQIT 1
```

- (2) GEOMETRY processor to define the geometry information needed to process our seismic data.

```
/GEOMETRY
GEOMFILE 'GEOM'
PRST
PRRANGES
PRINTALL
PRINFOLD
SURVEY
STBASE 347
SPLIST D 255,334,1 D 338,363,1
XYBASE 0, 0
DISTDIR 347 40 0, 348
SHOT 255 AT 409 INTO D347, 406, 1 D413, 472, 1
INC 2 TO SHOT 286 INC 1 TO SHOT 287 INC 3 TO SHOT 288
INC 1 TO SHOT 292 INC 2 TO SHOT 299 INC 1 TO SHOT 301
INC 2 TO SHOT 302 INC 1 TO SHOT 304 INC 2 TO SHOT 307
INC 1 TO SHOT 309 INC 2 TO SHOT 310 INC 1 TO SHOT 311
INC 3 TO SHOT 312 INC 1 TO SHOT 314 INC 2 TO SHOT 318
INC 1 TO SHOT 319 INC 4 TO SHOT 320 INC 1 TO SHOT 321
INC 2 TO SHOT 325 INC 1 TO SHOT 326 INC 2 TO SHOT 327
INC 1 TO SHOT 328 INC 2 TO SHOT 334 INC 8 TO SHOT 338
INC 2 TO SHOT 363
PROF
SPELX 255 101 256 101 257 100 258 100 259 100 260 99 261 98 262 96
263 96 264 94 265 93 266 92 267 91 268 91 269 92 270 94 271 95
272 96 273 98 274 99 275 100 276 101 277 101 278 101 279 101
280 102 281 101 282 101 283 102 284 102 285 103 286 102 287 103
288 103 289 103 290 103 291 103 292 103 293 102 294 102 295 103
296 104 297 105 298 104 299 105 300 105 301 105 302 106 303 106
304 106 305 106 306 106 307 107 308 107 309 107 310 106 311 106
312 106 313 106 314 106 315 105 316 104 317 103 318 102 319 102
320 103 321 104 322 105 323 105 324 107 325 107 326 106 327 106
328 106 329 105 330 104 331 104 332 104 333 105 334 105 338 106
339 106 340 106 341 106 342 106 343 107 344 107 345 106 346 107
347 105 348 105 349 106 350 106 351 106 352 106 353 105 354 106
355 106 356 107 357 106 358 106 359 106 360 106 361 106 362 107
363 106
DATUM 0
SPDX 255 0 256 0 257 0 258 0 259 0 260 0 261 0 262 0 263 0 264 0
265 0 266 0 267 0 268 0 269 0 270 0 271 0 272 0 273 0 274 0 275 0
276 0 277 0 278 0 279 0 280 0 281 0 282 0 283 0 284 0 285 0 286 0
287 0 288 0 289 0 290 0 291 0 292 0 293 0 294 0 295 0 296 0 297 0
298 0 299 0 300 0 301 0 302 0 303 0 304 0 305 0 306 0 307 0 308 0
309 0 310 0 311 0 312 0 313 0 314 0 315 0 316 0 317 0 318 0 319 0
320 0 321 0 322 0 323 0 324 0 325 0 326 0 327 0 328 0 329 0 330 0
331 0 332 0 333 0 334 0 338 0 339 0 340 0 341 0 342 0 343 0 344 0
345 0 346 0 347 0 348 0 349 0 350 0 351 0 352 0 353 0 354 0 355 0
356 0 357 0 358 0 359 0 360 0 361 0 362 0 363 0
DVEL 2000
```

```

TUH 0, 0, 0, 0, 0, 0, 0, 0, 0, 0, 0, 0, 0, 0, 0, 0, 0, 0, 0, 0, 0, 0,
0, 0, 0, 0, 0, 0, 0, 0, 0, 0, 0, 0, 0, 0, 0, 0, 0, 0, 0, 0, 0, 0,
0, 0, 0, 0, 0, 0, 0, 0, 0, 0, 0, 0, 0, 0, 0, 0, 0, 0, 0, 0, 0, 0,
0, 0, 0, 0, 0, 0, 0, 0, 0, 0, 0, 0, 0, 0, 0, 0, 0, 0, 0, 0, 0, 0,
0, 0, 0, 0, 0, 0, 0, 0, 0, 0, 0, 0, 0, 0, 0, 0, 0, 0, 0, 0, 0, 0,
SPST -79, -79, -78, -78, -78, -78, -77, -76, -76, -75, -75, -74, -74,
-74, -74, -75, -76, -76, -77, -77, -78, -78, -78, -78, -78, -78, -78,
-78, -78, -78, -79, -78, -78, -78, -78, -78, -78, -78, -78, -77, -78,
-78, -79, -78, -79, -79, -79, -79, -79, -79, -79, -79, -79, -79, -79,
-78, -78, -78, -78, -78, -78, -77, -76, -76, -76, -76, -77, -77, -77,
-78, -78, -77, -77, -77, -77, -76, -76, -76, -77, -77, -78, -78, -79,
-79, -79, -80, -80, -79, -80, -79, -79, -80, -80, -80, -80, -81, -81,
-81, -82, -81, -81, -82, -82, -82, -82, -82

```

- (3) AGC processor to apply balancing scalars to a seismic trace to equalize the amplitudes within the trace.

```
/AGC WINDOW 400
```

- (4) MUTE processor to set the ends of seismic traces to zero.

```

/MUTE
FMUTE 1,1 1220,60 0,61 0,120 1220
BYTRACE

```

- (5) DECONV processor to generate single channel, time and space-varying, pulse-shaping, deconvolution operators.

```

/DECONV
PULSDCON
ZONE 1
OPERATOR 1 1500 160 24
OPERATOR 106 1500 160 24
DESIGN 1 120 500 2480 3000
DESIGN 106 120 500 2480 3000
APPLY 1 500 12 3000 12
APPLY 106 500 12 3000 12
BYFILE

```

- (6) GATHER processor to sort the seismic data from one data order to another data order.

```

/GATHER OUTSORT 2
/DOUT
FILENAME 'GATH1'

```

- (7) STATAPLY to apply a static field corrections. The statics computed by the geometry processor are automatically applied.

```
/STATAPLY
```

- (8) TDCOFILT processor provides traces with an enhanced signal for subsequent input into the velocity analysis (VELS).

```

/TDCOFILT
NAJ 11 BANDPASS FILT 12 24 45 24
DISTANCE D0 2480 40
DIPAPPLY 160 250 -2 2 2000 -3 3
DIPAPPLY 210 250 -2 2 2000 -3 3
DIPAPPLY 260 250 -2 2 2000 -3 3
DIPAPPLY 310 250 -2 2 2000 -3 3
DIPAPPLY 360 250 -2 2 2000 -3 3
DIPAPPLY 380 250 -2 2 2000 -3 3
DIPAPPLY 450 250 -2 2 2000 -3 3
DIPAPPLY 520 250 -2 2 2000 -3 3

```

- (9) VELS processor to generate a velocity spectrum contour plot. Also included in the plot is a curve of the maximum semblance and a curve of the average amplitude computed for each specified time step.

```

/VELS
VELRANGE 1, 0 1500 4500
VELINC 100
TIMEINC 10
PROCESS 0, 3000
LEVEL 10, 100, 10
TIMELINE 20 100 1000
BALANCE ON HILBFILT ON
HORZ 1000
VERT 3

```

- (10) VELOCITY processor to specify the RMS velocity distribution as a function of time, CDP, and shot locations.

```

/VELOCITY
UNITS M MSEC'
CMP 160 20 2200, 230 2300, 490 2400, 900 2400, 1030 2400, 1340 2700,
1490 2900, 1740 3200, 1920 3350, 2060 3600, 2230 3850,
2350 3850, 2880 3900, 2960 3900
CMP 210 4 2200, 220 2300, 430 2400, 510 2400, 720 2400, 780 2400,
860 2400, 1080 2600, 1200 2700, 1480 2800, 1820 2800,
1950 3250, 2040 3400, 2140 3600, 2320 3600, 2420 3600,
2520 3600, 2680 3600, 2820 3800, 2910 3800
CMP 260 4 2200, 260 2200, 360 2300, 540 2400, 720 2400, 920 2400,
1040 2400, 1220 2500, 1450 3000, 1760 3300, 1900 3300,
2220 3700, 2340 3700, 2580 3700, 2640 3700, 2720 3700,
2880 3700
CMP 310 4 2300, 130 2300, 800 2300, 910 2400, 1030 2500, 1160 2700,
1270 2700, 1450 3000, 1570 3200, 1750 3450, 1930 3450,
2100 3450, 2240 3700, 2350 3700, 2480 3800, 2580 3800
CMP 360 20 2200, 220 2300, 500 2400, 620 2400, 1080 2400, 1520 2900,
1900 3100, 2180 3250, 2940 3800
CMP 380 20 2200, 230 2300, 440 2400, 800 2400, 940 2400, 1160 2700,
1280 3000, 1490 3050, 1610 3100, 1910 3500, 2180 3700,
2290 3750, 2730 3750, 2980 3900
CMP 450 20 2200, 150 2400, 270 2400, 530 2400, 720 2400, 940 2400,
1060 2500, 1220 2500, 1340 2800, 1580 3050, 1740 3200,
1940 3450, 2180 3700, 2280 3700, 2420 3700, 2530 3700,
2780 3700
CMP 520 90 2300, 340 2300, 450 2300, 560 2300, 810 2300, 940 2400,
1080 2450, 1220 2500, 1350 2700, 1430 2700, 1500 2950,
1620 3150, 1740 3250, 1840 3350, 1920 3500, 2040 3500,
2190 3700, 2290 3700, 2480 3700, 2640 3850

```

- (11) NMO processor to apply normal moveout (dynamic) correction to seismic traces. The correction is computed by applying a two-dimensional interpolation to the time-velocity pairs given for the velocity processor.

```
/NMO
/MUTE
FMUTE 160, 120 20, 320 140, 720 220, 1600 500, 2360 700
```

- (12) RSESTIM processor to compute nonsurface-consistent residual statics.

```
/RSESTIM
FILENAME 'REF.300'
WINDOW 120 800 2300 530 800 2300
/RSSAVE
STATFILE 'DD.103'
DELETE
```

- (13) Stack processor to add traces within a gather and scale the stacked trace after summing.

```
/STACK
```

- (14) DECONV processor to generate single channel, time and space-varying, predictive, deconvolution operators, and apply the operators to seismic data.

```
/DECONV
ZONE 1
OPERATOR 120, 1500, 160, 24
DESIGN 120, 120 300, 2480 1800
DESIGN 530, 120 900, 2480 1800
ZONE 2
OPERATOR 120, 1500, 160, 24
OPERATOR 530, 1500, 160, 24
DESIGN 120, 120 1500, 2480 2500
DESIGN 530, 120 1500, 2480 2500
```

- (15) STVF processor to compute and apply space and time-varying digital filters to seismic data.

```
/STVF
LOWPASS ZERO
FILT 1 25 60
APPLY 1 2 120 800 530 4
/STVF
BANDPASS ZERO
FILT 1 14 24 45 24
FILT 2 15 24 50 24
APPLY 1 2 120 1800 530 800
APPLY 2 2 120 3000 530 1800
```

- (16) FKMIG processor to migrate stacked data using the stolt FK migration algorithm.

```
/FKMIG
SPACING 40
```

(17) DISPLAY processor to create plots of our seismic data.

```
/DISPLAY
METRIC
HORZ 20
VERT 12
WINDOW 0, 3000
TIMELINE 200,1000
TPAORG 119
TPATRACE D120,520,20
TPAVALUE D410,610,10
TPATITLE 'SP NO.'
TPAHGT 0.254
TICKO 119
TICKT D120,520,20
TICKL
TEXTO 119
TEXTT 310
TEXTH 0.254
TEXT 'WELL D1'
```

